Metabolic phenotyping applied to pre-clinical drug induced liver injury and acute liver failure

Thesis submitted by

Michael Kyriakides

For the degree of Doctor of Philosophy of Imperial College London

Supervisors: Dr. Muireann Coen & Prof. Elaine Holmes

Section of Computational Systems Medicine

Department of Surgery and Cancer

Faculty of Medicine

Imperial College London

2014

Statement of originality

I certify that this thesis and the research to which it refers are the product of my own work, and that any ideas, contributions or quotations from the work of other people, published or otherwise, are fully acknowledged in accordance with the standard referencing practices of the discipline.

Copyright declaration

The copyright of this thesis rests with the author and is made available under a Creative Commons Attribution Non-Commercial No Derivatives licence. Researchers are free to copy, distribute or transmit the thesis on the condition that they attribute it, that they do not use it for commercial purposes and that they do not alter, transform or build upon it. For any reuse or redistribution, researchers must make clear to others the licence terms of this work.

Abstract

Liver disease is a prevalent clinical challenge caused by a variety of factors including viral infections and xenobiotic overdose. Improving our mechanistic understanding of disease development will lead to an improved stratification of patients and ultimately a better prognosis. This thesis addresses the role of metabonomics in providing insight into a variety of preclinical models and a clinical study. The metabolic phenotype of preclinical models of paracetamol (APAP) and methotrexate (MTX) toxicity were characterised, together with the study of clinical samples from decompensated cirrhosis, acute on chronic liver failure (ACLF) and acute liver failure (ALF) patients. A comparative metabonomic approach was applied to study the metabolic consequences following administration of APAP and its non-hepatotoxic isomer; N-acetyl-m-aminophenol (AMAP), in mice. The analysis revealed an APAP-induced hepatotoxicity through mitochondrial dysfunction which was characterized by an upregulation of glycolysis as well as the inhibition of beta-oxidation and the Krebs cycle. The metabolic and toxic effects of MTX were investigated in healthy rats and in a model of non-alcoholic steatohepatitis (NASH; as modelled by the methionine choline deficient diet). MTX was shown to have an enhanced toxicity in the context of NASH, which was associated with unique metabolic changes. The clinical work revealed that the serum metabolic phenotypes of clinical decompensated cirrhosis, ACLF and ALF patients were also each characterized by unique metabolic perturbations. The ALF phenotype was associated with the most metabolic changes and consisted of markers of oxidative and energetic stress, as well as markers of amino acid metabolism dysfunction. Subsequently, the novel serum metabolic profiling of the hepatic vein, hepatic portal vein and peripheral artery of patients during liver transplantation aimed to characterize the hepatic disease microenvironment, which was discovered to mainly consist of a perturbed amino acid metabolism.

Table of contents

Statement of originality 2
Copyright declaration 3
Abstract 4
Table of contents 5
Acknowledgements 10
Contributions of others 11
Abbreviations 12
List of figures 19
List of tables 22
Chapter 1: Liver disease and drug induced liver injury 23
Liver and liver disease 24
Non-alcoholic steatohepatitis 25
Non-alcoholic steatohepatitis and the methionine choline deficient diet 30
Drug induced liver injury 33
Paracetamol 34
Mitochondrial dysfunction 40
Apoptosis versus necrosis 42
Glutathione and N-acetylcysteine 43
N-acetyl-m-aminophenol 44
Methotrexate 46
Acute liver failure 51
Cirrhosis and acute on chronic liver failure 53
Thesis hypothesis 55
Chapter 2: Metabonomics analytical background 56
Metabonomics 57
Analytical platforms employed by metabonomics 58
Nuclear Magnetic Resonance spectroscopy 58
Pulse sequences used in NMR experiments 64
Mass spectrometry 66
Chromatography 69
Liquid chromatography 70
Gas chromatography 70

Chemometrics 71
Unsupervised methods 72
Supervised methods 73
Complementary statistical tools 75
Application of the metabonomics approach 76
Metabonomic studies of APAP metabolism and hepatotoxicity 76
Metabonomic studies involving MTX 78
Metabonomic studies of NASH and the MCD diet 78
Metabonomic studies of decompensated cirrhosis and ACLF 80
Metabonomic studies of ALF 80
Chapter 3: Systems level metabolic phenotype of N-acetyl-p-aminophenol and its non-toxic isomer, N-acetyl-m-aminophenol 82
Introduction 83
Study details and aims 83
Materials and methods 84
Animal handling and treatment 84
Liver histopathology 85
Measurement of serum ALT activity 85
Sample preparation and ^{1}H-NMR spectroscopy of hepatic aqueous-soluble component 85
Sample preparation and ^{1}H-NMR spectroscopy of urine 87
Sample preparation and ^{1}H-NMR spectroscopy of serum 87
Processing of ^{1}H-NMR spectra 88
GC-MS analysis of hepatic aqueous-soluble component 89
UPLC-MS analysis of hepatic aqueous-soluble component 92
Statistical analysis 95
Results 96
Serum clinical chemistry and liver histopathology 96
APAP and AMAP metabolism 96
^{1}H-NMR spectroscopic detected endogenous changes in hepatic extracts after APAP and AMAP administration 100
Serum O-PLS-DA of APAP and AMAP administration 105
HILIC-UPLC-MS analysis of hepatic extracts and carnitine 108
GC-MS analysis of hepatic extracts 110
Discussion 113

APAP and AMAP metabolism in C57BL/6 mice 113
APAP administration leads to hepatotoxic endpoint characterized by oxidative and energetic stress 114
AMAP administration leads to a reversible non-hepatotoxic endpoint 118
Study limitations 120
Chapter 4: Metabolic characterization of a model of non-alcoholic steatohepatitis 122
Introduction 123
Study details and aims 123
Methods 124
Animal handling and treatment 124
Liver histopathology and imaging 125
Sample preparation and ^{1}H-NMR spectroscopy of urine 125
Sample preparation and ^{1}H-NMR spectroscopy of faecal water 125
Sample preparation and ^{1}H-NMR spectroscopy of hepatic aqueous-soluble extracts 126
^{1}H-NMR spectral data processing 126
Statistical analysis 127
Results 128
Liver histopathology 128
Animal body weight 128
Hepatic metabolic phenotype of the NASH model 129
Urinary metabolic phenotype of the NASH model 129
Faecal water metabolic phenotype of the NASH model 130
Discussion 132
Histopathology of the MCD diet baseline 132
Hepatic metabolic phenotype of NASH 133
Urinary metabolic phenotype of the MCD diet 135
Potential perturbation of microbial populations 135
Other models of non-alcoholic steatohepatitis 136
Study limitations and future work 138
Chapter 5: Systems level metabolic phenotype of methotrexate administration in non-alcoholic steatohepatitis in the rat 140
Introduction 141
Study details and aims 141
Methods 142

Dosing of MTX 142
Quantification of urinary excretion of MTX 142
Statistical analysis 144
Results 145
Histopathology 145
Animal weight 146
Hepatic metabolic phenotype after MTX administration in the control diet group 146
Hepatic metabolic phenotype after MTX administration in the MCD diet group 149
Phenylalanine elevation 151
Faecal water metabolic phenotype after MTX administration in the control diet 152
Faecal water metabolic phenotype following MTX administration in the MCD diet. 153
Urinary metabolic phenotype following MTX administration in the control diet 155
Urinary metabolic phenotype following MTX administration in the MCD diet 156
Urinary quantitation of MTX 158
Discussion 159
Metabolic and toxic effect of MTX administration in healthy rats 159
The MCD diet affects the disposition and toxicity of MTX 162
Effect of MTX on gut microbial co-metabolites 165
Study limitations and future work 166
Chapter 6: Cross liver metabolic characterization of decompensated cirrhosis, acute on chronic liver failure and acute liver failure 168
Introduction 169
Study details and aims 169
Methods 170
Patient selection and sample collection 170
Sample preparation and ^{1}H-NMR spectroscopy of serum 171
^{1}H-NMR spectral data processing 171
Statistical analysis 172
Results 173
Clinical characteristics of decompensated cirrhosis, ACLF and ALF 173
Serum metabolic phenotype of decompensated cirrhosis, ACLF and ALF 176
Metabolic characterization of APAP-induced ALF 178
Decompensated cirrhosis and ACLF survival PLS analysis 179
Clinical characteristics of the “cross liver” sample set 182

"Cross liver" metabolic profiling 184
"Cross liver" metabolite comparison of decompensated cirrhosis and ACLF relative to ALF in serum metabolic profiles 185
Discussion 188
Pattern of metabolic perturbations associated with decompensated cirrhosis, ACLF and ALF 188
APAP-induced ALF 193
Survival rate PLS analysis 194
"Cross liver" metabonomic analysis 195
Study limitations and future work 198
Chapter 7: Concluding thoughts 201
References 206
Chapter 8: Appendix 230
Publication 238

Acknowledgements

It has been a very enjoyable past few years and I am very thankful to my two supervisors, Dr. Muireann Coen and Prof. Elaine Holmes, collaborators in the UK and USA, as well as everyone else in the section of Computational and Systems Medicine for being very welcoming, helpful and pleasant to work with. I would like to especially thank Dr. Muireann Coen for her constant supervision and for conveying the values of the scientific method. I am also very grateful to Prof. Nigel Gooderham for all of his help at the very beginning and to Prof. Andy Smith for organizing the MRC ITTP program which provided my funding.

I believe that my degree would have been a lot less enjoyable hadn't it been for the help of quite a few friends, which I have listed in (approximate) chronological order (please excuse me if I have forgotten someone): Mr. Chung-Ho Lau and Dr. Olaf Beckonert for their time and help on the NMR instruments, Dr. Panagiotis Vorkas, Mr. Matthew Lewis, Dr. Alexandros Pechlivanis, Dr. Konstantina Spagou, Dr. Alexis Siskos and Dr. Maria Gomez-Romero for sharing their time and mass spectrometry expertise, Dr. Paul Benton for sharing his R knowledge, Dr. Claire Boulange for her invaluable use of MetaSpectra, Miss Andia Redpath for providing mouse liver samples on demand, Dr. Gregory Tredwell and Dr. Volker Behrends for their help with GC-MS, Dr. Mark McPhail for his clinical expertise and finally, Dr. Anthony Dona for putting up with all of my NMR (and non-NMR) related questions. I would also like to separately thank Miss Lea Maitre for her help on our favourite project.

Furthermore, I would like to thank friends from the 4th floor for all the daily distractions (especially Mr. Abdullah Alkandari, Mr. Gabriel Valbuena, Mr. Tsz-Hong Law and Miss Sabrina Lamour) and a very special thanks to Mr. Michael Osborne for "crazy Wednesdays".

Finally, I am also very grateful to my family for their support throughout the years.

Contributions of others

I would like to thank collaborators at the University of Washington (Dr. Brenan Stamper, Dr. Isaac Mohar and Prof. Sid Nelson) and at the University of Arizona (Dr. Rhiannon Hardwick and Dr. Nathan Cherrington) for conducting the animal *in-vivo* experiments presented in Chapters 3, 4 & 6 and for sending the samples to Imperial College London. Likewise, I would like to thank Dr. Vishal Patel for conducting the clinical study presented in Chapter 6 and compiling all of the relevant clinical information, as well as Dr. Mark McPhail for his valuable advice concerning the overall analysis. Finally, I would also like to express my gratitude to Miss Lea Maitre for acquiring the NMR spectra presented in Chapter 3 and to Mr. Zhaosheng Jin and Miss Wei Han for assisting with analysis presented in Chapters 4 & 5.

Abbreviations

1D	One-dimensional
^{1}H	Proton
1hr	1 hour
12hr	12 hours
2D	Two-dimensional
24hr	24 hours
^{2}H	Deuterium
3hr	3 hour
3-PG	3-phosphoglycerate
48hr	48 hours
6hr	6 hour
7-OH-MTX	7-hydroxy methotrexate
ACLF	Acute on chronic liver failure
ACQ	Acquisition
ADR	Adverse drug reaction
AICAR transformylase	phosphoribosylaminoimidazolecarboxamide formyltransferase
ALF	Acute liver failure
ALT	Alanine aminotransferase
AMAP	N-acetyl-m-aminophenol

AMAP-G	AMAP-glucuronide conjugate
AMAP-S	AMAP-sulphate conjugate
AMDIS	Automated Mass Spectral Deconvolution and Identification System software
AMP	Adenosine monophosphate
AP-1	Activator protein 1
APAP	N-acetyl-p-aminophenol
APAP-Cys	APAP-cysteinyl conjugate
APAP-G	APAP-glucuronide conjugate
APAP-NAC	APAP-N-acetyl-cysteinyl conjugate
APAP-Methoxy	APAP methoxylated conjugate
APAP-S	APAP-sulphate conjugate
APAP-SG	APAP-glutathionyl conjugate
ARF	Acute renal failure
ASK1	Apoptosis-signal regulating kinase 1
ATP	Adenosine triphosphate
BMRB	Biological magnetic resonance bank
CAMERA	Collection of annotation related methods for Mass spectrometry data
CLASSY	Cluster analysis statistical spectroscopy
COMET	Consortium for metabonomic toxicology

COSY	Correlation spectroscopy
COX	Cyclooxygenase
CPMG	Carr-Purcell-Meiboom-Gill
Ctrl	Control
CYP	Cytochrome P450
D-3-HB	D-3-hydroxybutyrate
DAMPA	Diamino-2,4-N-10-methylpteroic acid
DHA	Dihydroxyacetone
DHFR	Dihydrofolate reductase
DILI	Drug induced liver injury
DNA	Deoxyribonucleic acid
DRC	Drug related compound
EI	Electron impact
ER	Endoplasmic reticulum
ESI	Electrospray ionisation
FAB	Fast atom bombardment
FBP	Folate binding protein
FDA	Food and drug administration
FFA	Free fatty acid
FID	Free induction decay
FIGLU	Formiminoglutamic acid

GC-MS	Gas chromatography mass spectrometry
GI	Gastrointestinal
G-phosphocholine	Glycerophosphocholine
GSH	Reduced glutathione
GSSG	Oxidized glutathione
GST	Glutathione transferase
H & E	Haematoxylin and eosin
HE	Hepatic encephalopathy
HILIC	Hydrophilic interaction liquid chromatography
HMDB	Human Metabolome Database
HPLC	High performance liquid chromatography
hr	Hour
I	Spin quantum number
IBD	Irritable bowel disorder
iNOS	Inducible nitric oxide synthase
IV	Intravenous
JNK	C-Jun-N-terminal kinase
LC-MS	Liquid chromatography mass spectrometry
LDL	Low density lipoprotein
LPS	Lipopolysaccharide
m/z	Mass to charge ratio

MALDI	Matrix assisted laser desorption ionization
MAS	Magic angle spinning
MCD	Methionine choline deficient
MELD	Model for End-Stage Liver Disease
MLK3	Mixed lineage kinase 3
MPT	Mitochondrial membrane permeability
mRNA	Messenger ribonucleic acid
MS	Mass spectrometry
MSD	Mass selective detector
MSTFA	N-Methyl-N-(trimethylsilyl) trifluoroacetamide
MTX	Methotrexate
MTX-$(Glu)_n$	Methotrexate polyglutamate conjugate
NAD	Nicotinamide adenine dinucleotide
NALFD	Non-alcoholic fatty liver disease
NaN_3	Sodium azide
NAPQI	N-acetyl-p-benzoquinone
NAPSQI	N-acetyl-p-semiquinone imine
NAS	NAFLD Activity Score
NASH	Non-alcoholic steatohepatitis
NMR	Nuclear magnetic resonance
NOE	Nuclear Overhauser Effect

NRES	National Research Ethics Service
NSAID	Non-steroidal anti-inflammatory drug
O-PLS-DA	Orthogonal partial least squares discriminant analysis
p	Spin vector
PCA	Principal component analysis
PEP	Phosphoenolpyruvate
pKC	Protein kinase C
PLS-DA	Partial least squares discriminant analysis
PLS-RA	Partial least squares regression analysis
ppm	Parts per million
PUFA	Polyunsaturated fatty acid
Q	Quadruple
Q^2Y	Predictive ability parameter of PLS-DA/O-PLS-DA model
QC	Quality control
QCcv	Quality control coefficient of variance
Q-TOF	Quadruple and Time of Flight
R	Pearson correlation value
R^2Y	"Goodness of fit" parameter of PLS-DA/O-PLS-DA model
RD	Relaxation delay
RNA	Ribonucleic acid
RP	Reverse phase

SFA	Saturated fatty acid
SIRS	Systemic inflammatory response syndrome
SOFA	Sequential Organ Failure Assessment
STD	Standard deviation
STOCSY	Statistical total correlation spectroscopy
SULT	Sulfotransferase
T_1	Spin-lattice relaxation time
T_2	Spin-spin relaxation time
T2DM	Type 2 Diabete Mellitus
Tcv	Predictive component of PLS-DA/O-PLS-DA Scores plot
THF	Tetrahydrofolate
TMAO	Trimethylamine-*N*-oxide
TOF	Time of Flight
TQ	Triple quadruple
TSP	Trimethylsilyl-[2',2',3,3'-$^2H_4$]-propionic acid sodium salt
TYosc	Orthogonal component of PLS-DA/O-PLS-DA scores plot
UGT	UDP-glucuronosyl transferase
UFA	Unsaturated free fatty acid
UPLC	Ultra performance liquid chromatography
Veh	Vehicle
vLDL	Very low density lipoprotein

List of figures

Chapter 1

Figure 1.1: The structural units of the liver 25

Figure 1.2: The two hit hypothesis and the role of FFAs in NASH 29

Figure 1.3: The proposed mechanism of the MCD diet 33

Figure 1.5: An overview of the hepatic metabolic pathways of APAP metabolism 39

Figure 1.5: Effects of NAPQI 41

Figure 1.6: An overview of the hepatic metabolic pathways of AMAP metabolism 46

Figure 1.7: Summary of known MTX metabolism 50

Figure 1.8: Overview of ALF and ACLF development 55

Chapter 2

Figure 2.1: The components of an NMR spectrometer superconducting magnet 59

Figure 2.2: The effect of a 90^{o} radiofrequency pulse on aligned magnetic vectors 63

Figure 2.3: A representative 1D ^{1}H-NMR urine spectrum 65

Figure 2.4: The components of an ESI-Q-TOF MS instrument 69

Figure 2.5: The reversed phase chromatographic total ion current of a serum sample 71

Figure 2.6: A demonstration of the dimension reduction achieved by PCA 73

Figure 2.7: A ^{1}H-NMR urine O-PLS-DA model comparing a control and treated group 74

Chapter 3

Figure 3.1: The three steps of the normalization procedure employed for GC-MS normalization 94

Figure 3.2: Log serum ALT activities and histology necrosis scores 96

Figure 3.3: Representative ^{1}H-NMR spectra of the hepatic extract metabolic profiles 97

Figure 3.4: Representative ^{1}H-NMR spectra of the serum metabolic profiles 98

Figure 3.5: Representative ^{1}H-NMR spectra of the urinary metabolic profiles 99

Figure 3.6: ^{1}H-NMR DRC ratios relative to APAP or AMAP in the hepatic extracts and urine 100

Figure 3.7: Total glutathione ^{1}H-NMR integrals from the hepatic extracts 103

Figure 3.8: ^{1}H-NMR hepatic extract O-PLS-DA models after APAP administration 104

Figure 3.9: ^{1}H-NMR serum O-PLS-DA models after APAP and AMAP administration 107

Figure 3:10: Summary of hepatic extract and serum O-PLS-DA discriminatory metabolite 108

Figure 3.11: PCA trajectory plot of HILIC-UPLC-MS hepatic extract analysis 109

Figure 3.12: UPLC-MS hepatic extract O-PLS-DA of APAP administration 111

Figure 3.13: Summary of APAP-induced mitochondrial dysfunction 118

Figure 3.14: The interpreted APAP-induced hepatic metabolic changes 120

Chapter 4

Figure 4.1: Histopathology of control and MCD diet groups 128

Figure 4.2: Average weight of control and MCD diet groups 129

Figure 4.3: ^{1}H-NMR hepatic extract, urinary and faecal water O-PLS-DA models of the MCD diet 131

Figure 4.4: Overview of the folate cycle related pathways 133

Chapter 5

Figure 5.1: Histopathology after MTX administration in both diets 145

Figure 5.2: Average weight after MTX administration in both diets 146

Figure 5.3: ^{1}H-NMR hepatic extract O-PLS-DA after MTX administration in the control diet 148

Figure 5.4: ^{1}H-NMR hepatic extract O-PLS-DA after MTX administration in the MCD diet 150

Figure 5.5: Summary of hepatic extract O-PLS-DA discriminatory metabolites 151

Figure 5.6: Biliary hyperplasia and liver fibrosis scores PLS regression models 152

Figure 5.7: ^{1}H-NMR faecal water O-PLS-DA after MTX administration in both diets 154

Figure 5.8: Summary of faecal water O-PLS-DA discriminatory metabolites 155

Figure 5.9: ^{1}H-NMR urinary O-PLS-DA after MTX administration in both diets 157

Figure 5.10: Summary of urinary O-PLS-DA discriminatory metabolites 158

Figure 5.11: Urinary quantity of excreted MTX (per kg) in both diets 158

Figure 5.12: Summary of MTX-induced pathology and metabolic effects in both diets 162

Figure 5.13: Summary of the unique effects of MTX in the MCD diet group 165

Chapter 6

Figure 6.1: Clinical parameters of ACLF, ALF and decompensated cirrhosis 175

Figure 6.2: ^{1}H-NMR serum O-PLS-DA of ACLF, ALF and decompensated cirrhosis..... 177

Figure 6.3: Summary of serum O-PLS-DA discriminatory metabolites 178

Figure 6.4: Summary of serum O-PLS-DA discriminatory metabolites of APAP-induced ALF 180

Figure 6.5: ^{1}H-NMR serum survival PLS regression analysis of ACLF and decompensated cirrhosis. 181

Figure 6.6: Summary of serums survival PLS regression discriminatory metabolites 182

Figure 6.7: Clinical parameters of liver transplant patients..... 185

Figure 6.8: ^{1}H-NMR serum inter-blood vessel metabolic changes of liver transplant patients 187

Figure 6.9: Summary of underlying mechanism of ACLF and decompensated cirrhosis..... 190

Figure 6.10: Overview of transsulfuration pathway and glutathione synthesis..... 191

Figure 6.11: Summary of underlying mechanism of ALF 192

Figure 6.12: Summary of inter-blood vessel metabolic perturbations in liver transplant patients .. 198

Appendix

Figure 8.1: TOCSY and COSY of urine spectra post-APAP administration 231

List of tables

Chapter 3

Table 3.1: ^{1}H-NMR APAP/AMAP DRC assignments in the serum, urine and hepatic extracts 101

Table 3.2: Hepatic extract GC-MS analysis summary after APAP/AMAP administration 112

Chapter 4

Table 4.1: MCD diet induced perturbations in faecal water, urine and hepatic extracts 130

Chapter 5

Table 5.1: ^{1}H-NMR MTX and DRC assignments in the urine and hepatic extracts 143

Chapter 6

Table 6.1: Clinical parameters of ACLF, ALF and decompensated cirrhosis 174

Table 6.2: Clinical parameters of liver transplant patients 183

Table 6.3: ^{1}H-NMR serum inter-blood vessel metabolic perturbations of liver transplant patients. 184

Table 6.4: ^{1}H-NMR serum inter-blood vessel discriminatory metabolites of ALF patients 186

Appendix

Table 8.1: Summary of ^{1}H-NMR experiment parameters of all studies 232

Table 8.2: List of ^{1}H-NMR metabolite assignments 233

Table 8.3: Summary of ^{1}H-NMR O-PLS-DA parameters of MTX urinary analysis 237

Chapter 1: Liver disease and drug induced liver injury

Liver and liver disease

The liver is a vital organ responsible for the metabolism of a vast number of lipid and water soluble molecules and consequently is the most metabolically active organ. In addition to its function as an important source of metabolites for organs, it also possesses a significant array of enzymes responsible for the detoxication and chemical modification of xenobiotic compounds. It is a very vascular organ which can receive up to a quarter of cardiac output through the hepatic artery (30 %) and the hepatic portal vein (70 %) (Abdel-Misih and Bloomston, 2010). The hepatic portal vein also transports the products of digestion directly from the gastrointestinal (GI) tract to the liver, before they are transported to the rest of the body. As a result of its functions, the liver has a critical role in preserving homeostasis, either through supporting other organs or through the processing of potentially harmful compounds, including foreign compounds such as xenobiotics. A diagrammatic representation of the functional unit of the liver, the hepatic lobule, centred on the hepatic vein is presented in Figure 1.1. The hepatic lobule consists of the periportal (outer) region which is specialized for oxidative reactions including gluconeogenesis and β-oxidation, the midzonal (transitional) region, and the centrilobular (inner) region which has the lowest concentration of oxygen and contains the highest concentration of xenobiotic metabolizing enzymes, including the cytochrome P450 (CYP) enzymes (Thoolen et al., 2010).

A dysfunctional liver can lead to severe health complications and even death. Therefore it is important to understand the underlying mechanisms of various liver diseases in order to improve our prognostic and diagnostic capabilities, as well as treatment efficacy and safety. There is a vast spectrum of liver diseases covering a variety of aetiologies, timescales and severities, all of which affect the metabolic capability and function of the liver to a different

extent. According to the office of National Statistics, the incidence of liver disease has almost tripled in the past four decades, while liver disease was repsonsible for approximately 16,000 deaths in 2008 in the UK alone, revealing a 4.5 % increase per annum.

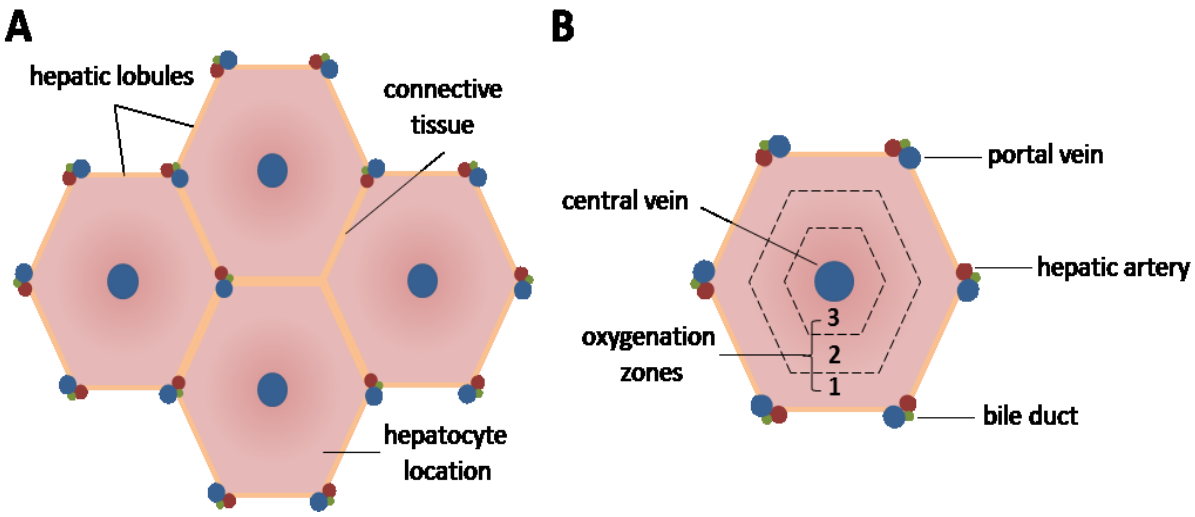


Figure 1.1: The structural units of the liver are depicted. The arrangement of the hepatic lobules within the liver is shown in A. The organization of the blood vessels and the oxygenation zones in each hepatic lobule is presented in B. 1 – 3 represent the periportal, midzonal and centrilobular zones respectively, as well as the relative extent of oxygenation in each zone. The periportal zone is the most oxygenated region while the centrilobular zone is the least oxygenated region.

This thesis is focused on characterizing the metabolic phenotype arising from the underlying mechanisms of different liver conditions, as well as investigating the mechanism of drug induced liver injury, in healthy and disease-compromised livers. More specifically, the liver conditions relevant to this thesis are non-alcoholic steatohepatitis, decompensated cirrhosis, acute liver failure and acute on chronic liver failure, while the drug induced liver toxicities caused by paracetamol and methotrexate were also characterized.

Non-alcoholic steatohepatitis

Non-alcoholic fatty liver disease (NAFLD) is a chronic liver disease that is increasingly recognized as a significant health issue in the modern world. It is generally characterized by

hepatic fat accumulation (steatosis) and insulin resistance, while Type 2 Diabetes Mellitus (T2DM) is also present in many cases. NAFLD is a condition comprising of many different stages that can range from simple steatosis to non-alcoholic steatohepatitis (NASH), fibrosis, cirrhosis and hepatocellular carcinoma (Ali and Cusi, 2009, Nseir and Mahamid, 2013, Larter and Yeh, 2008). Its prevalence is estimated to be ~30 – 40% in the USA population (Ali and Cusi, 2009), while another study has reported that this disease affects ~ 27% of the Japanese adult population (Jimba et al., 2005). There are several risk factors associated with the development of NAFLD, including ethnicity, family history, as well as conditions such as T2DM, gut microbe activity and obesity, which are thought to double the likelihood of disease development and progression (Ali and Cusi, 2009, Farrell and Larter, 2006, Miele et al., 2013).

NASH, first described by Ludwig et al., is a severe form of NAFLD whose main pathological characteristics include lobular inflammation, hepatocyte injury steatosis, macrovesicular steatosis, hepatocyte ballooning (resulting from the accumulation of intracellular fluid) and insulin resistance (Ludwig et al., 1980, Leamy et al., 2013, Farrell and Larter, 2006, Larter and Yeh, 2008). The most accurate method of diagnosing NASH is by histological examination of hepatic tissue following liver biopsy and determining the presence of fibrosis, as well as using the recently developed NAFLD Activity Score (NAS), which consists of a scoring system of 14 histological features. However, it is important to note that liver biopsies are associated with a significant health risk to the patient (Sanyal and American Gastroenterological, 2002). Other diagnostic tests include imaging techniques or inflammation tests can also be employed but it is difficult to distinguish between steatosis, NASH and cirrhosis through imaging, while clinical markers such as alanine aminotransferase (ALT) are not always reliable (Farrell and Larter, 2006). Even though NASH was originally considered to be primarily a disease of the

"West", affecting around 8% of the USA population (McCullough, 2007, Farrell and Larter, 2006), it is increasingly diagnosed in other parts of the world (Farrell and Larter, 2006). If left untreated, it can progress to cirrhosis in up to 15% of patients (Cheng et al., 2012) and a study has reported that NASH might account for ~13% cases of hepatocellular carcinoma (Adams and Angulo, 2005). The link between hepatocellular carcinoma and NASH is thought to lie primarily on the extent of the systemic metabolic disturbance and not the actual fibrotic physiological state of the liver. Furthermore, the importance of the systemic metabolic disturbance present in NASH was highlighted by a study which reported that NASH recurrence was detected after liver transplantation (Farrell and Larter, 2006).

The exact mechanism by which NASH is developed has not been characterized yet but it is understood to be multifaceted. A popular model for NASH development is the "two hit hypothesis", first proposed by *Day and James* (Day and James, 1998, Leamy et al., 2013). It proposes that NASH develops after a first hit which is the result of an imbalanced fat metabolism and a second hit that involves the metabolic and oxidative stress resulting from the response of the cells (Day and James, 1998, Day, 2002). The imbalance in fat metabolism is linked to the fat accumulation in myocytes and the visceral adipose tissue, primarily because of obesity, which has been reported to lead to the release of adipocytokines that cause inflammation and also promote free fatty acid (FFA) synthesis and accumulation in the liver (Figure 1.2). FFA accumulation can be counteracted in the cell by incorporating FFAs in triglyceride molecules which would consequentially lead to an elevation of liver triglycerides, which is a characteristic of NAFLD (Schaffer, 2003). This is thought to be a protective mechanism of dealing with and disposing of excess FFAs, and studies have shown that an elevation of triglycerides is only associated with minimal liver injury (Leamy et al., 2013).

However, this solution might only apply to unsaturated FFAs (UFAs) since saturated fatty acid (SFA) molecules are less efficiently incorporated into triglyceride molecules (Leamy et al., 2013). Previous experiments have revealed that the inhibition of an enzyme responsible for desaturating SFAs, stearoyl-coenzyme A desaturase-1 (SCD-1), led to a reduction in hepatic triglyceride content and a higher sensitivity to palmitate induced apoptosis (Li et al., 2009). This reaffirms that FFA triglyceride incorporation might protect against apoptosis and suggests that SFA molecules need to be desaturated before being used for triglyceride synthesis.

A potential accumulation of SFAs in the liver is thought to have many detrimental effects, including hepatic insulin resistance. The proposed underlying mechanism involves the activation of protein kinase C which would impair the tyrosine phosphorylation that is required for physiological signalling of insulin receptors (Farrell and Larter, 2006). Other effects of SFA accumulation include endoplasmic reticulum (ER) and mitochondrial stress which have been observed in the livers of clinical patients suffering from NASH (Farrell and Larter, 2006, Sharma et al., 2008, Sanyal et al., 2001). Mitochondrial dysfunction is a hallmark in the development of NASH (Pessayre and Fromenty, 2005) and evidence for this include decreased amounts of hepatic mitochondrial DNA (Kawahara et al., 2007) and a drop in mitochondrial activity (Perez-Carreras et al., 2003, Fromenty et al., 2004). A resulting disturbance to the ER structure can affect its functionality, which involves the correct folding of proteins (Borradaile et al., 2006). In NASH, ER dysfunction is thought to be caused by the deposition of SFAs in the ER membrane, which primarily consists of unsaturated phosphatidylcholine (Deguil et al., 2011, Leamy et al., 2013). Finally, the disruption of mitochondria and the ER is also linked to an upregulation of C-Jun-N-terminal kinase (JNK)

signalling which can lead to the assembly of the activator protein-1 (AP-1) complex, a family of pro-apoptotic transcription factors that bind to the AP-1 DNA binding site, leading to apoptosis (Cazanave et al., 2009). A summary of the effects of SFAs is presented in Figure 1.2.

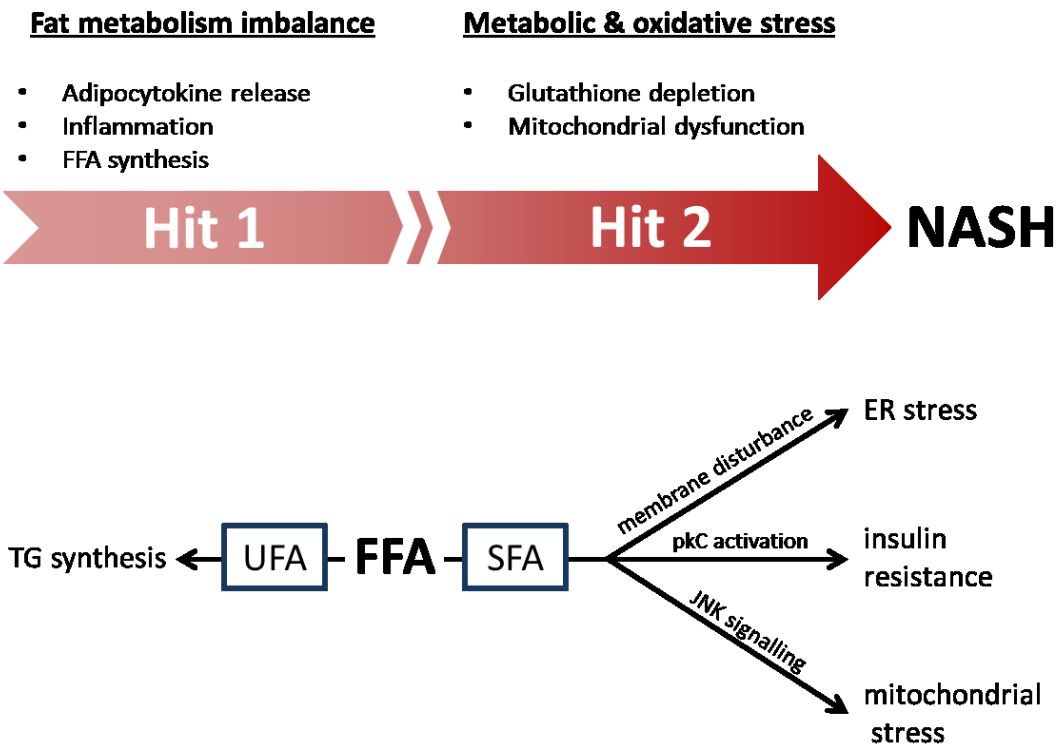


Figure 1.2: The two hit hypothesis and the role of FFAs in NASH. Fat metabolism imbalances, together with metabolic and oxidative stress, are thought to be the two hits that lead to NASH development. The proposed mechanism by which SFAs contribute to NASH development is also presented. FFA – free fatty acid; UFA – unsaturated fatty acid; SFA – saturated fatty acid; NASH – non-alcoholic steatohepatitis; pkC – protein kinase C; ER – endoplasmic reticulum.

Apart from the health risk imposed by NAFLD and NASH, it is important to appreciate the potential effect of these conditions on drug biotransformation, clearance and transport (Fisher et al., 2009), which can lead to adverse drug reactions (ADRs). More specifically, drugs that are known to cause type A (predictable) ADRs might have a different effect when the pre-existing background of the liver reveals NAFLD or NASH (Hardwick et al., 2011, Wooten, 2010). Previous investigations have demonstrated that general hepatic gene expression in the presence of NAFLD and NASH is altered (Rubio et al., 2007, Younossi et al., 2005), while gene

expression changes specific to ADME have also been observed in clinical studies (Lake et al., 2011). Furthermore, other clinical studies have revealed changes in the activity and expression of enzymes that are important for xenobiotic metabolism. These include changes in the activity of hepatic CYP enzymes (Fisher et al., 2009), changes in the activity and mRNA levels of glutathione transferase (GST) enzymes (Hardwick et al., 2010), together with changes in the mRNA of efflux transport proteins (Hardwick et al., 2011). Any effects on the cytochrome P450 system are very important because of their involvement in biotransformation and ability to create reactive metabolites, including the CYP450 mediated metabolism of paracetamol (Miner and Kissinger, 1979). Additionally, a decline in GST activity would compromise the cell's capability to detoxify electrophilic reactive species through the conjugation with glutathione, which could result in hepatotoxicity.

Non-alcoholic steatohepatitis and the methionine choline deficient diet

Due to the significant prevalence of NASH and its potential effect on liver function, it is frequently the subject of investigations in *in-vivo* rodent studies (Tilg and Diehl, 2000, Kamada et al., 2007, Larter and Yeh, 2008). There are several proposed NASH models that can be used for such investigations, including the use of hepatotoxins, promoting physical inactivity and dietary or genetic models (Romestaing et al., 2007, Xu et al., 2010, Larter and Yeh, 2008, Rinella et al., 2008). However, it has proven difficult to create an accurate model of this condition since it would require the replication of both the liver pathology and general metabolic environment of NASH. More specifically, a NASH model should ideally cause liver cell injury, steatosis, fibrosis, inflammation, in addition to insulin resistance, obesity and hyperglycemia (Larter and Yeh, 2008). Therefore, it is important to consider the limitations of

the existing NASH models for a more accurate interpretation of the results and the clinical translational relevance.

A popular diet-based model is the methionine choline deficient (MCD) diet, which is the choline and methionine deficient analogue of a normal diet. Methionine is an essential amino acid that is involved in the biosynthesis of other metabolites including cysteine, S-adenosylmethionine, taurine and phosphatidylcholine (Mato et al., 2008). Choline has many important physiological functions including the synthesis of phospholipids and acetylcholine, as well as cholesterol transport (Zeisel, 2004). The metabolisms of choline and methionine are inter-linked because betaine, an oxidation product of choline, can be used to methylate homocysteine to methionine (Selhub et al., 1991). Alternatively, methionine can also be formed through the methylation of homocysteine by methyl-tetrahydrofolate (Zeisel and Blusztajn, 1994).

Mouse studies have shown that methionine free diets do not induce severe health complications despite the important physiological function of methionine, potentially because of an intracellular methionine conservation response (Tang et al., 2010). Furthermore, dietary methionine restriction has also been reported to have positive effects such as increasing the lifespan of rats and mice, rendering mice more resistant to drug induced oxidative stress, and controlling mouse cancer growth (Cavuoto and Fenech, 2012, Miller et al., 2005). In contrast to methionine, *in-vivo* studies investigating the effect of choline deficiency have observed decreased hepatic concentrations of choline, phosphatidylcholine, betaine and methionine (Pomfret et al., 1990). Intracellular efforts to replenish the choline pools have been previously suggested to lead to the breakdown of membrane lipids such as phosphatidylethanolamine (Pomfret et al., 1990). Such lipids have important roles in the

formation of lipid rafts, including their interaction with cholesterol, therefore a potential breakdown could also affect the cholesterol composition of membranes which would in turn have many negative knock on effects (Musso et al., 2013).

The MCD diet has been traditionally employed to model NASH and its pathology has been well documented (Larter and Yeh, 2008, Pelz et al., 2012, Mu et al., 2010, Rinella and Green, 2004). This diet leads to a condition similar to NASH which is characterized by steatosis, mitochondrial dysfunction, inflammation and oxidative stress (Caballero et al., 2010). Moreover, elevated levels of ALT and aspartate aminotransferase enzymes have been reported in rodent models (Li et al., 2011, Pelz et al., 2012), together with ER stress (Mu et al., 2012), increased CYP 2E1 expression (Weltman et al., 1996), altered drug transporter localization (Hardwick et al., 2011) and downregulation of SCD-1 (Miyazaki et al., 2001), all of which are in line with NASH. However, ER stress might not be essential for the formation of MCD diet induced steatohepatitis since it has been observed that reducing ER stress does not improve the condition in mice (Henkel et al., 2012).

The exact mechanism by which the MCD diet causes a NASH like condition has not been described yet but impaired hepatic vLDL secretion is thought to play an important role (Rinella et al., 2008, Yao and Vance, 1988). This is supported by the role of methionine and choline as precursors to phosphatidylcholine, the main phospholipid coating of vLDL particles (Vance and Vance, 1985), through the Kennedy pathway (Gibellini and Smith, 2010). Another effect of the MCD diet is a decrease in the hepatic folate concentrations of rat livers by a factor of two, which would affect other metabolic pathways such as those of the nucleic acids , as well as further impact the formation of phosphatidylcholine (Zeisel and Blusztajn, 1994, Horne,

1989). Figure 1.3 presents the proposed mechanism by which the MCD diet induces a NASH like disease.

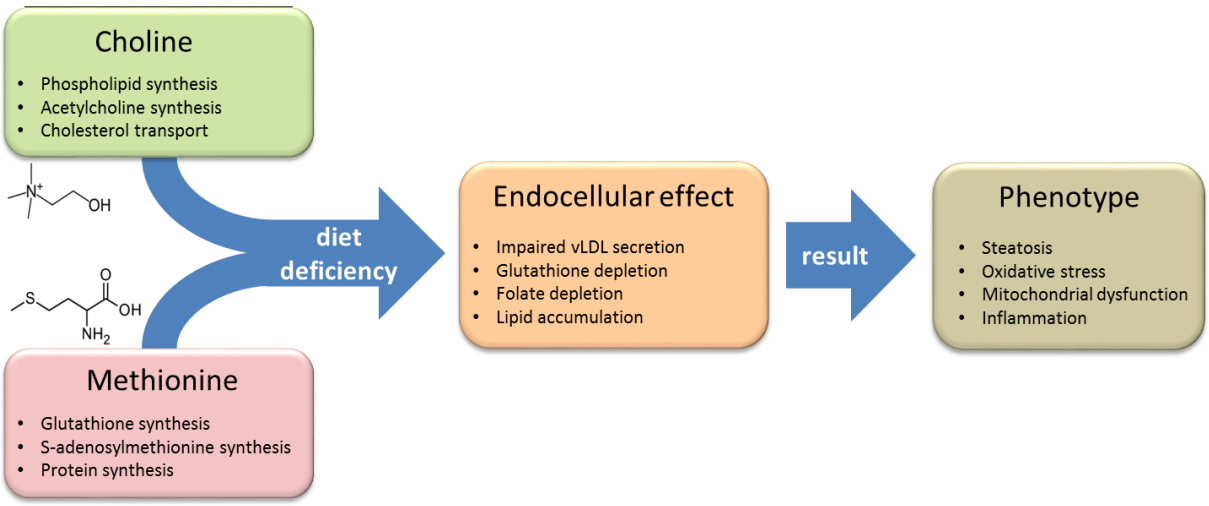


Figure 1.3: The proposed mechanism through which the coupled deficiency of choline and methionine can lead to NASH is shown.

As previously mentioned, it is important to acknowledge that the MCD diet has several limitations and differences from the clinical pathology of NASH. The liver histology induced by the diet resembles that of NASH but the metabolic phenotype is not replicated. More specifically, the MCD diet does not induce obesity, insulin resistance, and hyperglycemia (Larter and Yeh, 2008, Larter, 2007). Finally, animals on the MCD diet also suffer from significant weight loss and there is also evidence to suggest that the diet specifically affects male rodents to a greater extent (Rinella and Green, 2004, Kirsch et al., 2003).

Drug induced liver injury

Drug induced liver injury (DILI) refers to abnormalities in liver function tests related to the intake of medicinal compounds (Bleibel et al., 2007). It has been estimated that more than a thousand drugs have been associated with DILI on more than one occasion (Kaplowitz, 2004, Bernal and Wendon, 2013). Unfortunately the potential of a drug to cause DILI is often realised after it has been released onto the market and therefore DILI has been the single

most frequent reason for drug withdrawal from the market (Russmann et al., 2009). Part of the reason why DILI cannot be detected before market release is that there are various risk factors such as age, sex, underlying diseases, environmental factors or genetic predisposition that might not be accounted for during the drug clinical phase 3 trials which typically represent a relatively small individual cohort (Kaplowitz, 2004).

The pathogenesis of DILI is believed to involve the interaction of a toxic drug or a drug metabolite, which either affects endocellular function or leads to an immune response (Kaplowitz, 2004). Furthermore, DILI can be characterised as intrinsic or idiosyncratic and the latter can be further subdivided into allergic or non-allergic. Intrinsic DILI is regarded to be dose-dependent and the symptoms usually develop within a few days due to direct toxicity from the xenobiotic or its metabolites (Pham, 1997). On the other hand, idiosyncratic DILI is more common and it is thought to be independent of the dose, route or duration of drug administration (Bleibel et al., 2007). Such cases are unpredictable, and potentially related to adaptive immune system reactions, as well as risk factors such as genetic predisposition, age, gender and alcohol status. Furthermore, the symptoms might also develop after a period of time (Uetrecht, 2007, Urban et al., 2012, Bleibel et al., 2007). Some intrinsic DILI causing drugs generally create signature diseases such as acute hepatitis (paracetamol, ritonavir, isoniazid), chronic hepatitis (diclofenac), fibrosis (methotrexate) and NASH (tamoxifen) but many drugs are also associated with more than one signature (Kaplowitz, 2004).

Paracetamol

Paracetamol, 4-Hydroxyacetanilide or N-acetyl-p-aminophenol (APAP) is an antipyretic and analgesic drug that was introduced in the USA and UK in the mid-twentieth century (Sneader, 2005). It is very widely used and more than 170 million tablets of paracetamol or paracetamol

containing tablets were prescribed in the UK in June 2011 alone (NHS non-steroidal anti-inflammatory drugs and analgesics national charts October 2011), while 24.6 billion doses were sold in the United States in 2008 (Krenzelok, 2009).

The therapeutic effect of APAP resembles that of non-steroidal anti-inflammatory drugs (NSAIDs) and has been characterized extensively throughout the years (Botting, 2000, Hinz et al., 2008). Its therapeutic properties were believed to be linked to the disruption of prostaglandin synthesis through the inhibition of cyclooxygenases (COX) 1 and 2 in the brain (Flower and Vane, 1972, Mattamal, 1979, Ruud et al., 2013, Botting, 2000). *Flower and Vane* originally showed that the production of prostaglandin is ten times more sensitive in the brain when compared to the spleen (Flower and Vane, 1972) but this result has been disputed since (Warner et al., 2004, Hinz et al., 2008). Even though COX 1 and 2 were thought to be the original targets of APAP, as well as perhaps COX 3 which might be a splice variant of the COX 1 gene, recent investigations suggest that the main effect of APAP is through COX 2 inhibition (Hinz et al., 2008, Botting, 2000).

APAP is generally considered to be safe at therapeutic doses but it can cause hepatocellular damage at excessive doses, as documented approximately 10 years after its release (Davidson and Eastham, 1966, Mitchell et al., 1973). As a consequence of its toxic capabilities and widespread use, it has been the leading cause of acute liver failure in the developed world with respect to both intentional and non-intentional overdose (Lee, 2012b). This has led to an extensive study of its hepatotoxic properties and it is commonly referred to as a "model hepatotoxin". Furthermore, the US Food and Drug Administration (FDA) recommended that physicians should avoid prescribing medication with a high APAP content due to the risk of liver injury (Mitka, 2014). Even though the liver is the main site of APAP toxicity, it can

additionally cause acute renal failure (ARF) (Blakely and McDonald, 1995), or other conditions such as cataractogenicity (Lubek et al., 1988) and lung malaises (Jeffery et al., 1988).

APAP is a weak organic acid (pKa ~ 9.5), which is essentially non-ionised at physiological pH and is therefore rapidly absorbed by the duodenum after ingestion (McGill and Jaeschke, 2013). The main site of APAP metabolism is the periportal region of the liver, where sulphation and glucuronidation are the major phase 2 conjugation reactions, since the conjugates are more soluble than the parent molecule. These reactions are the respective additions of sulphate or glucuronide moieties to the para-hydroxyl group on the aromatic ring and the resulting products are excreted through the urine or bile in most laboratory species and man, with the help of transporters (Bessems and Vermeulen, 2001, Tone et al., 1990, McGill and Jaeschke, 2013). The glucuronidation reaction is catalysed by UDP-glucuronosyl transferases (UGT) while the sulphation reaction is catalysed by sulfotransferase (SULT) enzymes. A human renal excretion study has shown that the majority of the excreted APAP is in the form of the glucuronide conjugate (Prescott, 1980) but there is significant intra- or inter-species, and gender variation in the production of each metabolite (Savides et al., 1984, Chen et al., 2003, Lee et al., 2009). Additionally, higher doses of APAP saturate sulphation capacity leading to a higher relatively proportion of the glucuronide conjugate (Tone et al., 1990, Howie et al., 1977). It is also important to mention that the respective proportion of each metabolite is highly dependent on other factors, such as liver health. It has been reported that obese mice with steatosis had relative higher levels of the APAP-glucuronide conjugate, while microsomal fractions from humans suffering from steatosis had higher SULT enzyme activity and would therefore produce more of the sulphate conjugate (Hardwick et al., 2013).

The critical biotransformation of APAP is catalysed by the CYP enzymes, which are expressed predominantly in the smooth endoplasmic reticulum of hepatocytes in the centrilobular region and in the kidneys to a smaller extent (Mohandas et al., 1981, Wrighton and Stevens, 1992, Omiecinski et al., 1999). Different members of the CYP450 superfamily are thought to be involved but CYP 1A2, CYP 3A4 and CYP 2E1 are amongst the most important enzymes in humans, while CYP 1A2 and CYP 2E1 are most active in mice (Thummel et al., 1993, Hu et al., 1993). This superfamily is responsible for oxidation of APAP to N-acetyl-p-benzoquinone (NAPQI), a metabolite considered to be responsible for toxicity, as first shown by Dahlin and Nelson (Miner and Kissinger, 1979, Dahlin and Nelson, 1982). Other products of CYP450 catalysed reactions include the 3-hydroxyparacetamol and 3-methoxyparacetamol catechols (Forte et al., 1984, Bessems and Vermeulen, 2001), the latter of which has been reported to have a similar toxic potential as APAP (Forte et al., 1984). An overview of APAP metabolism is presented in Figure 1.4.

The exact mechanism by which NAPQI is formed is currently contested by different proposed theories and not much progress has been made in the past decades in terms of discovering the exact mechanism (Bessems and Vermeulen, 2001). Sidney D. Nelson originally presented a summary of the proposed mechanisms, which suggested that the first step involved an oxidation either at the amide nitrogen or hydroxyl oxygen of the paracetamol aromatic ring that would result to the formation of N-acetyl-p-semiquinone imine (NAPSQI) (Nelson, 1995). NAPSQI is a free radical that can have different resonance structures depending on the oxidation mechanism. It was further hypothesized that the oxidation reaction at the amide nitrogen is more likely because of the orientation of the molecule within the active site of the enzyme, since a re-orientation would be required if the oxidation occurred at the oxygen

atom of the phenol (Nelson, 1995). However, Koymans *et al.* used energy calculations and spin distributions to conclude that the formation of the phenoxy radical is more energetically favourable and it is therefore the most likely mechanism of NAPQI and NAPSQI formation (Koymans et al., 1989). In spite of the previously conducted research concerningK the mechanism of NAPQI formation, there is a possibility NAPQI is not formed through the NAPSQI intermediate, since the formation of NAPSQI has not yet been proven experimentally potentially due to its chemical instability (Bessems and Vermeulen, 2001).

There are several different proposed mechanisms by which NAPQI can cause toxicity but the main pathways are considered to be through protein thiol oxidation and protein arylation. The electrophilic properties of NAPQI allow it to form covalent bonds with proteins, leading to protein arylation (Gibson et al., 1996), while it can also oxidise the exposed thiol groups of proteins leading to inter-strand disulphide bridges, cross-linking between proteins or covalent binding between proteins and glutathione (GSH) (Bessems and Vermeulen, 2001). The covalent binding of NAPQI to hepatic proteins was conclusively linked to APAP-induced hepatotoxicity by *Hinson et al.* (Hinson et al., 1996), who revealed that protein adduct formation reached a maximum after one hour and necrotic cells were present by six hours. Protein arylation is disruptive because a change in protein structure can impede the normal function of a protein and lead to loss of cellular homeostasis once proteins with important functions have been affected (Gibson et al., 1996, Cohen and Khairallah, 1997).

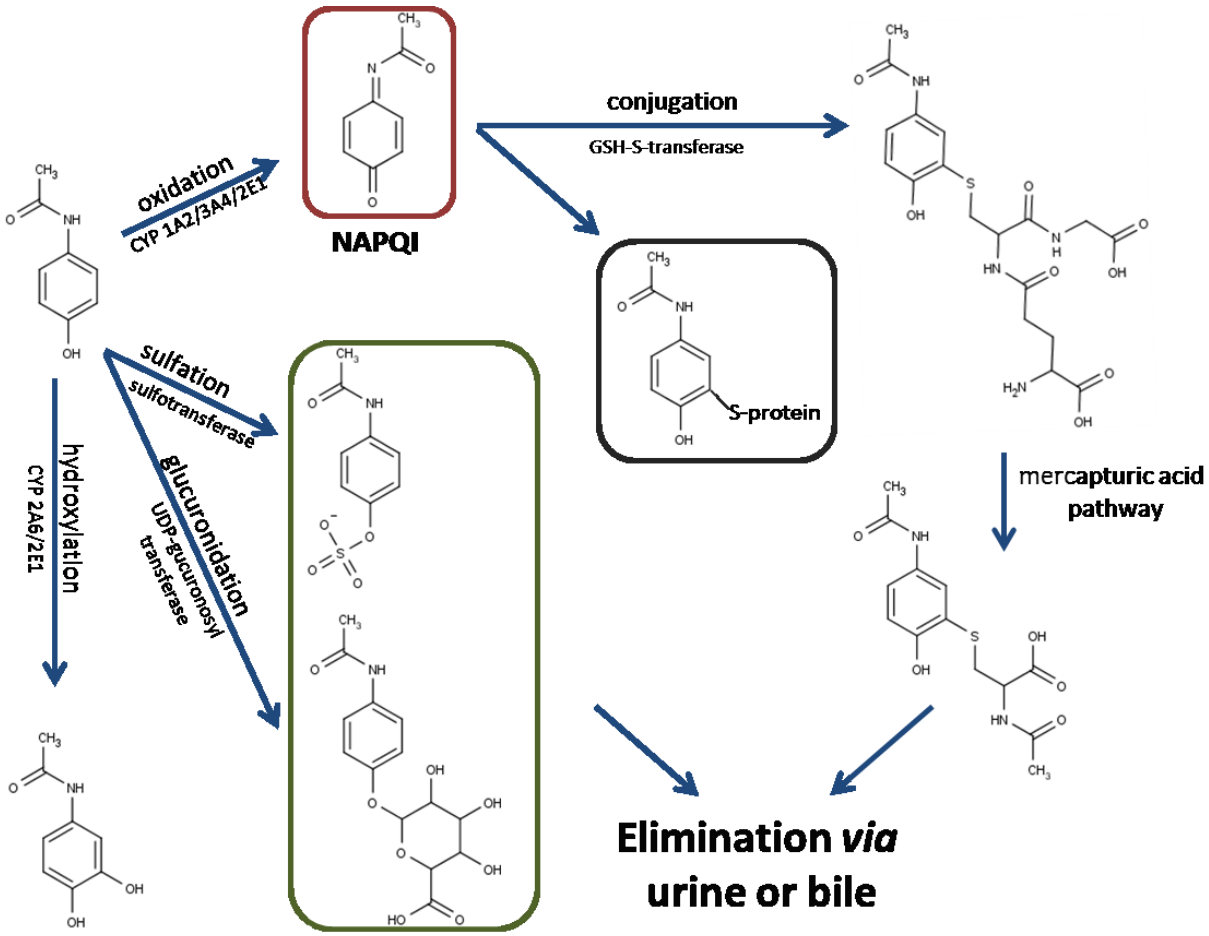


Figure 1.5: An overview of the hepatic metabolic pathways of APAP metabolism are depicted above. The majority of the compound will undergo the glucuronidation and sulphation reactions. A small portion will undergo an oxidation reaction leading to the formation of NAPQI. NAPQI can be neutralized by binding to glutathione and the resulting product is eliminated in the urine via the mercapturic acid pathway. APAP can also undergo a hydroxylation reaction, leading to the catechol.

Further investigations have studied the binding of NAPQI to proteins in specific cellular compartments such as the microsomes, cytosol and mitochondria. In the cytosol, NAPQI was shown to bind to *N*-10-formyltetrahydrofolate dehydrogenase (Pumford and Halmes, 1997), GST (Wendel and Cikryt, 1981) and glyceraldehyde-3-phosphate dehydrogenase (Dietze et al., 1997). NAPQI binds to GST in the microsomes as well, while calreticulin is also another microsomal target protein that was identified in murine liver incubations (Holtzman, 1995). Many mitochondrial proteins have also been identified as targets of NAPQI, including glutamate and aldehyde dehydrogenases (Landin et al., 1996, Halmes et al., 1996) and the

ATP-synthase α subunit (Hinson et al., 2010). It is important to note that currently there isn't any direct evidence that selective inhibition of protein binding will nullify the hepatotoxic effects of APAP (McGill and Jaeschke, 2013).

NAPQI can also affect lipid metabolism by inhibiting β-oxidation and initiating lipid peroxidation. It blocks the transportation of acyl-carnitine molecules (fatty acid and carnitine conjugates) into the mitochondria, which results in an inhibition of mitochondrial β-oxidation (Chen, 2009, McGill et al., 2014a). The initiation of lipid peroxidation is not thought to be directly induced by NAPQI but NAPQI could be involved in the production of superoxide anions through futile redox cycling of CYP450 enzymes (Younes et al., 1986, Mourelle et al., 1990). NAPQI has additionally been reported to have nuclear effects, in mammalian *in-vitro* studies where high doses of APAP interfered with nucleotide excision repair in keratinocytes (Skorpen et al., 1998), as well as inhibiting DNA synthesis by interfering with the function of ribonucleotide reductase (Hongslo et al., 1994). However, it can be argued that the characterised nuclear effects are simply another consequence of NAPQI protein adduct formation and therefore could be classified as an indirect downstream effect. A summary of the mechanisms by which NAPQI can cause endocellular toxicity is presented in Figure 1.5.

Mitochondrial dysfunction

The aforementioned effects of NAPQI, in addition to other unknown mechanisms, lead to a general disruption of cellular processes and especially mitochondrial function. APAP-induced toxicity alters the morphology of mitochondria and leads to mitochondrial oxidative stress, lower respiration rates and depletion of the ATP pool (Katyare and Satav, 1989, Placke et al., 1987). It has been observed that mitochondrial damage can be detected in mice *in-vivo* at an earlier time-point than other signs of toxicity and therefore it has been hypothesized that

mitochondrial dysfunction is an important milestone for APAP-induced toxicity (Meyers et al., 1988, Ramsay et al., 1989, Stamper et al., 2010, McGill et al., 2012a). Moreover, a recently published study suggested that mitochondrial damage was directly correlated to the mortality of acute liver failure in APAP overdose patients (McGill et al., 2014b).

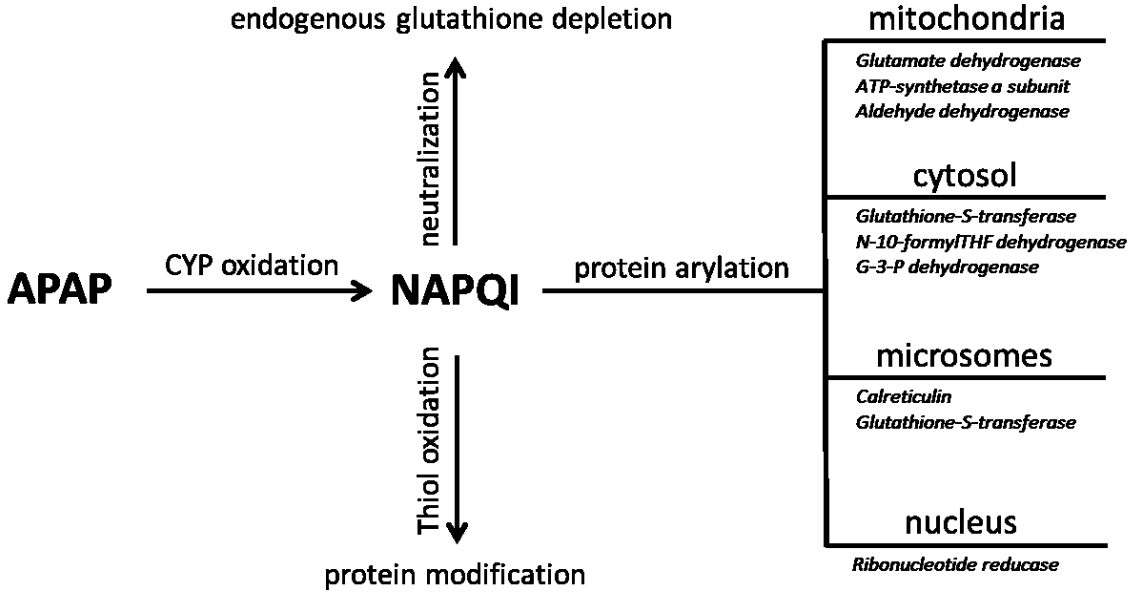


Figure 1.5: The effects of NAPQI are depicted. NAPQI has the ability to modify proteins through thiol oxidation or protein arylation and cause glutathione depletion. Examples of known protein targets of NAPQI and their respective endocellular compartments of NAPQI are also depicted. APAP – N-acetyl-p-aminophenol; NAPQI – N-acetyl-p-benzoquinoneimine. CYP – cytochrome P450 enzyme.

Oxidative stress is considered to be crucial for the induction of mitochondrial dysfunction and mitochondrial death. In addition to protein thiol oxidation by NAPQI, peroxynitrite formation can also lead to the deterioration of mitochondrial function (Jaeschke et al., 2012, Knight et al., 2002). Peroxynitrite is thought to be formed through the reaction of nitric oxide with highly reactive superoxide anions (Radi et al., 2001), while it is also possible that the up-regulation of nitric oxide synthases, such as inducible nitric oxide synthase (iNOS), is also a contributing factor (Gardner et al., 1998). Previous investigations have shown that peroxynitrite is formed inside the mitochondria of hepatocytes after APAP administration (Cover et al., 2005) and that it can cause extensive damage by binding to mitochondrial

proteins, leading to the formation of nitrotyrosine adducts (Agarwal et al., 2011), as well as damaging mitochondrial DNA (Cover et al., 2005). Furthermore, additional oxidative stress is thought to be caused by the translocation of activated JNK into the mitochondria, through the activation of mixed lineage kinase 3 (MLK3) and apoptosis-signal regulating kinase 1 (ASK1) (McGill and Jaeschke, 2013, Saito et al., 2010a).

An important detrimental effect of oxidative stress is the formation of the mitochondrial permeability transition (MPT), which is a significant and abrupt increase in the mitochondrial membrane permeability that allows molecules of smaller than 1500 Da to enter the mitochondrion. This leads to loss of membrane potential, uncoupling of oxidative phosphorylation and increase of mitochondrial volume (Masubuchi et al., 2005). MPT also causes the collapse of the mitochondrial membrane and the subsequent release of mitochondrial pro-apoptotic intra-membrane proteins, such as apoptosis inducing factor, cytochrome C, and endonuclease G, which are responsible for the characteristic nuclear DNA fragmentation seen after APAP hepatotoxicity (Jaeschke, 2008, Bajt et al., 2006).

Apoptosis versus necrosis

There used to be a discrepancy in the literature whether apoptosis, necrosis or a combination of the two is the predominant mechanism of hepatocyte death following APAP induced injury. It was initially reported that both necrosis and apoptosis (3:2 ratio) were observed after APAP toxicity (Ray et al., 1996), while other investigations also reported that mild APAP toxicity leads to apoptosis (Hu and Colletti, 2010). Apoptosis is thought to be promoted by the release of mitochondrial pro-apoptotic factors, such as cytochrome C and caspase enzymes. However, the current general consensus is that the predominant mechanism of cell death is necrosis (Gujral et al., 2002, Schulze-Osthoff and Bantel, 2011, Hinson et al., 2010). Apoptosis

is an energy dependent process, while APAP-induced toxicity is characterized by a depletion of ATP, which suggests that apoptosis would have a smaller role during APAP-induced hepatotoxicity (Antoine et al., 2010, Schulze-Osthoff and Bantel, 2011). The reliance of apoptosis on the energy status of the cell during APAP-induced toxicity has been previously demonstrated in fasted mice after APAP administration, where the majority of the hepatocytes were undergoing necrosis and not apoptosis (Antoine et al., 2010).

Glutathione and N-acetylcysteine

Endogenous GSH, a tri-peptide consisting of glycine, glutamate and cysteine, is the cell's defence mechanism against oxidative stress agents and its depletion is a classic marker of oxidative stress. GSH can bind to NAPQI to form an APAP-SG conjugate or reduce NAPQI back to its original form, which will lead to the oxidation of GSH to oxidized glutathione (GSSG) (Rashed et al., 1990). APAP-SG undergoes several reactions in the intestine and kidney before its excretion (Newton et al., 1986). Initially the glutamate group is removed, followed by the removal of the glycine molecule, leading to the production of APAP-cysteinyl (APAP-Cys). This molecule can be further metabolized by microsomal N-acetyltransferase to from the mercapturate; APAP-N-acetyl-cysteinyl (APAP-NAC) (Tate, 1980). An overdose of APAP will lead to the irreversible depletion of hepatic GSH stores, leading to incomplete neutralization of NAPQI molecules (Mitchell et al., 1973).

Cysteine availability is the rate-limiting step in GSH formation and therefore N-acetyl cysteine (NAC) is given to APAP overdose patients clinically in order to promote GSH synthesis and NAPQI neutralization, even though the exact mechanism for its therapeutic action has yet to be elucidated (Saito et al., 2010b). NAC has been reported to attenuate the expression of pro-inflammatory cytokines (Bemeur et al., 2010) and reduce renal inflammation (Ucar et al.,

2013); therefore its therapeutic effects extend beyond GSH regeneration. However, a previous study in mice has demonstrated that NAC supplementation leads to an elevation of hypotaurine, instead of GSH, levels and has therefore questioned the usage of NAC for replenishing endocellular GSH stocks (Zwingmann and Bilodeau, 2006). Moreover, administration of NAC is also associated with adverse effects such as vomiting and as a result anti-emetics have to be co-administered, but these effects might be minimized by changing its dose regimen (Bateman et al., 2013). Finally, it is also important to note that other treatments that can be used to replace cysteine, such as methionine and S-adenosylmethionine, have also been shown to have a similar effect to NAC in rodents (Pratt and Ioannides, 1985, Michael et al., 2012).

N-acetyl-m-aminophenol

N-acetyl-m-aminophenol (AMAP) is a structural isomer of APAP, with a 3' hydroxyl group. It was originally reported to have similar therapeutic properties in mice and cause significantly less toxicity to mice and hamsters *in-vivo* as well as hepatocytes *in-vitro* (Nelson, 1980, Roberts, 1978, Salminen et al., 1997). Unlike APAP, AMAP is metabolized to a methoxylated molecule or two different catechols before the CYP catalyzed formation of quinone reactive molecules. The methoxylated molecule is also a metabolite of APAP but it is postulated that not enough is formed during AMAP metabolism for severe hepatotoxicity to occur (Rashed and Nelson, 1989b, Rashed et al., 1990, Streeter et al., 1984, Hamilton and Kissinger, 1986). It has not yet been elucidated which CYP enzymes catalyse the oxidation of AMAP but it is believed that there are at least two different enzymes in mice (Forte et al., 1984), including CYP 2E1 (Halmes et al., 1998). A summary of AMAP metabolism is presented in Figure 1.6.

Reactive metabolites resulting from AMAP metabolism have been demonstrated to be as potent as NAPQI in terms of their ability to covalently bind to proteins (Holme et al., 1991). It is believed that they bind to proteins close to the point of formation away from the mitochondria (Pumford and Halmes, 1997) as supported by evidence that AMAP derived reactive metabolites form adducts with cytosolic and microsomal proteins to a much greater extent than mitochondrial proteins *in-vivo* (Tirmenstein and Nelson, 1989, Myers et al., 1995). Additionally, AMAP has been shown to decrease cytosolic GSH levels but it had no effect on mitochondrial GSH levels, further suggesting that its reactive metabolites do not enter the mitochondria and do not cause mitochondrial dysfunction (Tirmenstein and Nelson, 1991, Myers et al., 1995, Roberts et al., 1990).

Several investigations have recently focused on the contrasting toxicities and effect of these two compounds. *In-vivo* gene expression studies have revealed that AMAP had a smaller effect on gene expression when compared to APAP, and APAP uniquely affected genes associated with the cell cycle, protein kinase cascades, cell death, inflammation and biopolymer metabolism (Beyer et al., 2007, Priyadarsiny et al., 2008). These results are in line with the hypothesis concerning the contrasting underlying mechanisms of toxicity of the two compounds. However, there have also been studies which question the hypothesis concerning the contrasting toxicity of AMAP. An *in-vitro* study revealed that AMAP was more toxic in rat and human liver slices than APAP and have therefore questioned whether AMAP should be considered as a non-toxic isomer (Hadi et al., 2013). Furthermore, a recent computer simulation (DILIsym) suggested that the contrasting toxicities of these two is due to the different amounts of reactive metabolite produced by each compound and not due to mitochondrial binding (Howell et al., 2014). The decreased burden of AMAP reactive

metabolites, relative to APAP, may arise from the reported inhibition of CYP 2E1 enzymes by the reactive metabolites of AMAP (Halmes et al., 1998).

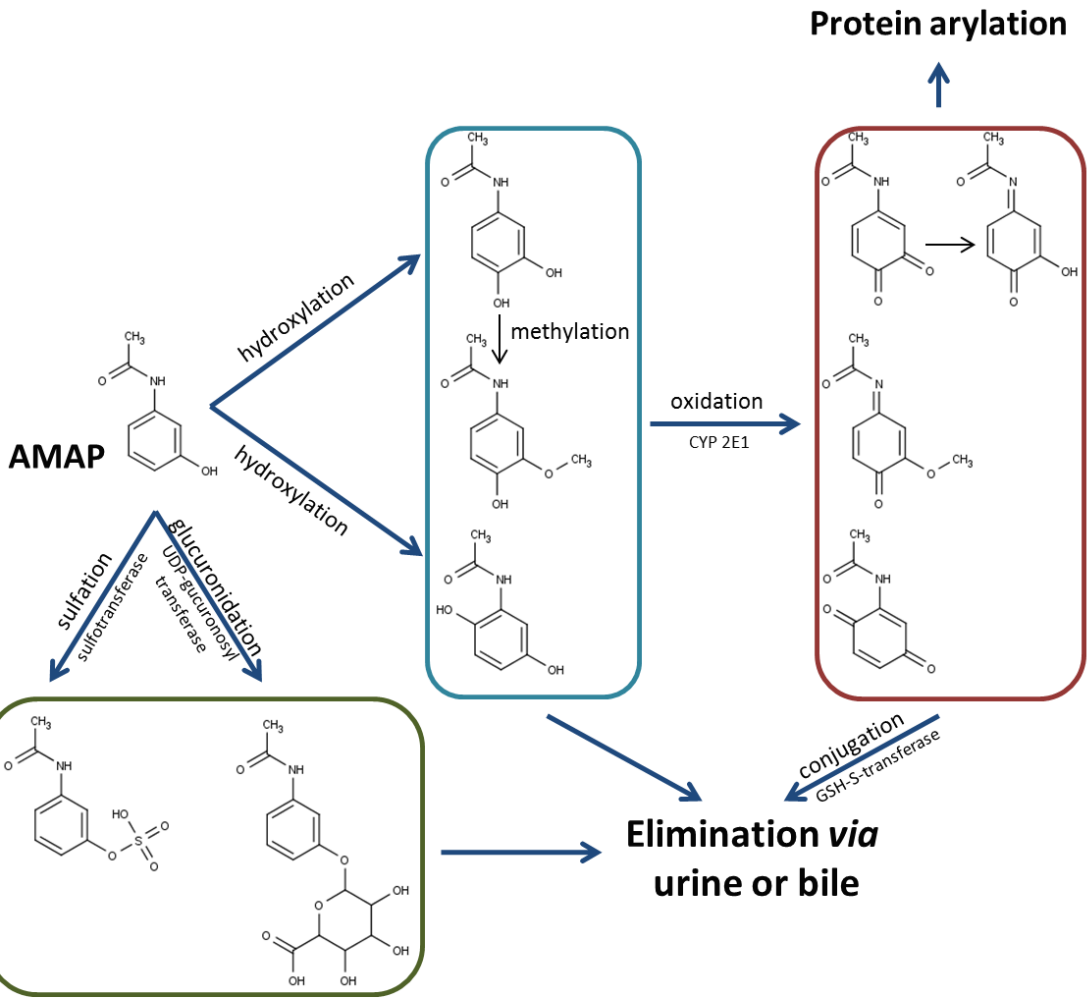


Figure 1.6: An overview of the hepatic metabolic pathways of AMAP metabolism are depicted above. The majority of the compound will undergo the glucuronidation and sulphation reactions and a portion will also undergo hydroxylation and subsequent oxidation reactions leading to the formation of reactive quinones that can cause protein arylation. AMAP – n-acetyl-m-aminophenol; CYP – cytochrome P450 enzyme.

Methotrexate

The folate cycle has a very important role in endocellular metabolism and in particular the one carbon, amino acid and nucleotide metabolic pathways. It involves the reduction of the pyrazine ring constituent of the folate pterin ring to its active tetrahydro form, the addition of glutamate moieties by gamma linkage and the oxidation or reduction of one carbon metabolites (Bailey, 2009). There are three tetrahydrofolate (reduced) molecules which have

an important role as one carbon donors in the formation of DNA precursors through the donation of their methyl groups; 10-formyltetrahydrofolate, 5,10-methylenetetrahydrofolate and 5-methyltetrahydrofolate (Kremer, 2004). Since mammals lack the capability of synthesizing the constituents of the folate cycle *de novo* they rely on dietary sources (Bailey, 2009).

Amethopterin, 4-amino-*N*-10-methylpteroylglutamic acid or methotrexate (MTX) is a folate analogue that inhibits folate metabolism. It was originally used as a replacement to aminopterin for the treatment of acute lymphoblastic leukemia by disrupting the function of dihydrofolate reductase (DHFR) (Meyer et al., 1950, Farber et al., 1956) through competitive inhibition. DHFR catalyzes the reduction of dihydrofolate to tetrahydrofolate, which is an integral component of the folate cycle. Due to the potency of MTX in leukemia treatment through the inhibition of DHFR, it was tested with other forms of cancer and other diseases (Khan et al., 2012) and was discovered to also inhibit other enzymes such as phosphoribosylaminoimidazolecarboxamide formyltransferase (AICAR transformylase) and amidophosphoribosyltransferase (Fairbanks et al., 1999, Schroder, 2003). Currently, it is widely used for the treatment of malaises such as neoplastic malignancies, rheumatoid arthritis, psoriasis or as a general immunosuppressant and anti-inflammatory drug (Genestier et al., 2000, Khan et al., 2012). It was the most popular prescribed anti-rheumatic drug in the UK in the period of 2006-2011, according to NHS statistics (NHS NSAIDS and Analgesics National Charts October 2011).

MTX is a weak acid with two carboxylic acid groups located on its glutamate moiety. It has a pKa value of approximately 5.0, a low membrane permeability and a low aqueous solubility (0.01 mg/ml) (Kasim et al., 2004) and as a result it primarily relies on carrier proteins to enter

the cell (Genestier et al., 2000, Khan et al., 2012). There are at least two different folate transporter receptors; a low affinity reduced folate carrier or a glycoprotein known as the folate-binding protein (FBP), which can transport MTX into the cell. Even though FBP is a more efficient transporter of MTX, it has a much higher affinity for reduced folates (Genestier et al., 2000). At high concentrations MTX can also diffuse passively through the cell membrane (Jansen et al., 1990, Goldman and Matherly, 1985). The ability of MTX to undergo passive diffusion is important in the case of mutant cells which do not have active transporters (Genestier et al., 2000). Removal of MTX from cells is believed to be primarily an active process and it relies on transporter proteins classified as the multidrug resistance-associated proteins, such as p-glycoprotein or the ATP-binding cassette proteins (more specifically Abcc2 and Abcc3) (Kremer, 2004, Wang et al., 2011). Crucially, the expression of these proteins can vary in cells and is therefore one of the most important mechanisms of tumour resistance to MTX (Wang et al., 2011, Genestier et al., 2000).

Tumour cell experiments have shown that once inside the cell, MTX can undergo polyglutamation reactions in the cytosol. These involve the sequential addition of glutamate molecules to the terminal glutamate moiety through a gamma linkage, catalysed by the enzyme folypolylglutamyl synthetase (Figure 1.7) (Barrueco et al., 1992). This leads to accumulation of MTX molecules since the conjugated product cannot be as easily transported out of the cell (Fry et al., 1983). There is a direct relationship between the number of conjugated glutamate residues and the resulting conjugate's cell membrane permeability (Genestier et al., 2000). It has been demonstrated that the polyglutamate conjugate of MTX that consists of five glutamate moieties can remain within cells for at least twenty four hours after the removal of the circulating drug (Genestier et al., 2000). Hydrolase enzymes can

cleave the glutamate residues so that MTX can be more easily transported out of the cell (Kremer, 2004). The polyglutamate conjugates of MTX also have inhibitory capabilities and were discovered to inhibit AICAR transformylase (Allegra et al., 1985b), as well as thymidylate synthase (Allegra et al., 1985a). The endocellular accumulation of the polyglutamate conjugates, coupled to their ability to inhibit enzymes, are both very important factors in the disruption of endocellular folate metabolism (Genestier et al., 2000).

In humans, the majority of MTX seems to undergo a hydroxylation reaction at the 7-position of the pterine ring in the liver to form the 7' hydroxyl derivative (7-OH-MTX) (Figure 1.7) (Jacobs et al., 1976). This reaction is either catalysed by aldehyde oxidase or xanthine oxidase and there is a significant inter-species variability in the role played by these phase 1 enzymes (Moriyasu et al., 2006, Jordan et al., 1999). The hydroxylation reaction is considered to be a detoxication step and the resulting product is not as potent an inhibitor as the polyglutamation conjugates. However, 7-OH-MTX can also be converted to a polyglutamate conjugate at a higher rate than the parent molecule and could therefore inhibit enzymes in its polyglutamate form (Genestier et al., 2000, Fabre et al., 1983). Finally, MTX can also be excreted *via* the bile to the intestinal tract where it is converted to diamino-2,4-N-10-methylpteroic acid (DAMPA) by bacterial carboxypeptidases, before DAMPA is reabsorbed again (Widemann et al., 2000). Studies have shown that DAMPA is a less potent inhibitor of DHFR than the parent molecule, so this reaction might be a detoxication pathway (Valerino et al., 1972). Excretion of MTX and its metabolites occurs primarily through the urine through active tubular secretion or glomerular filtration (Reich et al., 1977). This process can be affected by other factors including the use of non-steroidal anti-inflammatory drugs (NSAIDs),

which can interfere with MTX excretion and lead to a rise in serum levels (Schroder, 2003). An overview of MTX metabolism is presented in Figure 1.7.

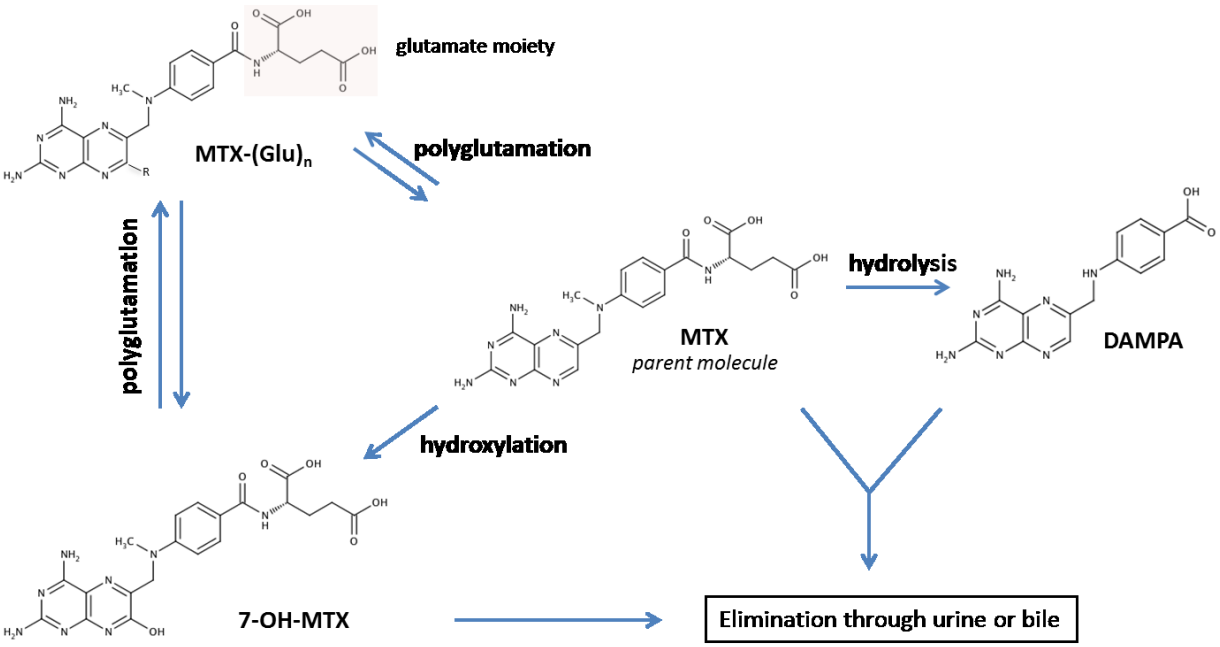


Figure 1.7: Summary of known MTX metabolism. MTX can undergo hydroxylation reactions to form the 7-hydroxy derivative (7-OH-MTX) or polyglutamation reactions to form the polyglutamate conjugate (MTX-$(Glu)_n$). MTX can also be excreted to the intestine where its glutamate moiety is cleaved by bacterial enzymes to form DAMPA. R_1 = H, R_2 = OH.

As a result of its potency in disrupting folate metabolism MTX has a variety of adverse effects including nausea, vomiting and diarrhoea (Khan et al., 2012), while it can also cause hepatic injury and hematological disturbances (Feagan et al., 1995), as well as intestinal epithelium damage that can eventually lead to weight loss (Lobo and Balthasar, 2003). Chronic use of MTX can lead to more severe effects on the liver such as fibrosis or cirrhosis, while it is also not administered to pregnant women due to its teratogenic properties (Rosenberg et al., 2007, Khan et al., 2012, Moisa et al., 2006). Because of the severity of the aforementioned potential toxicity, MTX is often administered with folate supplements. There have also been efforts to improve its delivery and to control its release by creating pro-drugs or using delivery systems such as lipid nanoparticles or liposomes (Khan et al., 2012).

It is also important to appreciate that the development of many side effects depends on the rate of MTX clearance and the underlying health of the patient. Reduced renal clearance of MTX could be the cause of MTX-induced renal dysfunction and would significantly enhance the risk of toxicity (Ries and Klastersky, 1986, Flombaum and Meyers, 1999). An example of a disease that can enhance MTX-induced toxicity is inflammatory bowel disease (IBD). Patients who are receiving low dose MTX and are also suffering from IBD can have diarrhoea, fever and a higher risk of infection (Schroder, 2003). Other conditions that are risk factors for MTX toxicity include diabetes mellitus, fasting or NASH. Finally, potentially dietary supplements can also have an effect, such as the root of *Pueraria lobata* herb which can enhance MTX toxicity by reducing MTX elimination (Chiang et al., 2005). Due to the variety of conditions that can influence the pharmacology and toxicology of MTX, formal guidelines for MTX administration were drafted (Roenigk et al., 1982, Langman et al., 2001).

Acute liver failure

Acute liver failure (ALF) is a rare severe condition that occurs in patients without a pre-existing liver disease (Bernal and Wendon, 2013). It is associated with a sudden significant hepatocyte cell death and general liver dysfunction, while it is commonly described as the onset of coagulopathy, as well as encephalopathy in advanced stages (Lee, 2012a, Friedman and Emmet, 1998). The presence of ALF can lead to further complications including cerebral oedemas, neurological conditions, renal failure, infection and hypoglycaemia, while it may also progress to multiple organ failure or death in approximately half of ALF cases (Lai, 2004, Bernal and Wendon, 2013, Friedman and Emmet, 1998).

ALF was originally divided to two subgroups: a) fulmimant hepatic failure where encephalopathy (brain dysfunction) develops within eight weeks of illness onset and b)

subfulminant hepatic failure where encephalopathy develops between eight weeks and six months (Friedman and Emmet, 1998). Modern classifications vary depending on the system that is used but they generally attempt to reflect differences in clinical features more accurately by quantifying the interval between the onset of the initial symptoms and the development of encephalopathy (Bernal and Wendon, 2013, O'Grady et al., 1993). There can be hyperacute cases, with encephalopathy developing in less than a week, and subacute cases, where encephalopathy requires a longer period to develop. Subacute cases can be easily confused with chronic liver diseases and generally have a worse outcome than hyperacute cases (Bernal and Wendon, 2013).

The majority of the cases of ALF are due to viral infections including hepatitis A, B and E, and consequently ALF is more common in the developing world. Other important causes include drug induced liver injury, which is responsible for approximately 50 % of the cases of ALF in the USA, Wilson's disease, autoimmune hepatitis and mushroom ingestion (Bernal and Wendon, 2013, Friedman and Emmet, 1998). However it should also be noted that Wilson's disease, hepatitis B and autoimmune hepatitis are also commonly recognized as chronic liver conditions rather than being categorised as ALF (Stravitz and Kramer, 2009).

The specific cause of ALF is also thought to determine the mechanism of hepatic cell death. The extent of apoptosis and necrosis in ALF is currently a controversial topic but it is generally thought that cells undergo necrosis when there is a severe disruption to endocellular function or when the ATP stores have been depleted. Recent data suggest that the presence of necrosis is associated with poor outcome, therefore the distinction of these two processes is potentially very important (Bantel and Schulze-Osthoff, 2012).

The outcome and pathogenesis of ALF is also thought to depend on the activation of systemic immune responses (Antoniades et al., 2008). The presence of the systemic inflammatory response syndrome (SIRS), a severe malfunction of the immune system, has been associated with a poor prognosis and can have infectious and non-infectious causes (Rolando et al., 2000). SIRS is described as the clinical manifestation of an abnormal systemic inflammatory reaction which is distant from the initiating insult and its severity correlates positively with the extent of organ dysfunction and mortality/morbidity. It is characterized by elevated levels of pro- and anti- inflammatory cytokines (Antoniades et al., 2008). The mechanism by which SIRS develops is thought to be due to the "spill over" of a localized inflammatory response. The resulting elevated systemic levels of pro-inflammatory cytokines trigger the release of anti-inflammatory cytokines in an attempt to control the immune response. This leads to a generally unbalanced immune system that can cause multiple organ failure and death (Antoniades et al., 2008). SIRS is an important risk in ALF patients who have several immunological defects, while a third of the patients fail to raise an immune response after an infection (Rolando et al., 2000). For example, the occurrence of SIRS after a fungal infection has been estimated to raise the mortality from 70 % to 100 % (Rolando et al., 2000).

Cirrhosis and acute on chronic liver failure

Liver fibrosis is characterized by the replacement of injured tissue by collagen fibres. Liver cirrhosis is an advanced condition of liver fibrosis triggered by the distortion of hepatic circulation, which can lead to the clinical consequence of portal hypertension (Schuppan and Afdhal, 2008). Liver cirrhosis can be further categorized to compensated and decompensated cirrhosis depending on the clinical outcome. Decompensated cirrhosis is characterized by more severe portal hypertension, ascites, GI bleeding and encephalopathy, while bacterial

translocation is also considered to have a key role in the progression of compensated cirrhosis to decompensated cirrhosis (Jalan et al., 2012, Garcia-Tsao et al., 2010, Moreau et al., 2013). If left untreated, liver cirrhosis can regress to a hepatocellular carcinoma and is estimated to affect 0.15 % of people in the USA (Schuppan and Afdhal, 2008).

Acute on chronic liver failure (ACLF) is another type of liver failure syndrome that was initially described as a condition where an acute insult takes places on a liver suffering from a chronic condition (Ohnishi et al., 1995). Currently it is increasingly recognized as a condition encompassing a critical deterioration of liver function in patients most commonly suffering from cirrhosis, but an evidence based definition is still lacking (Jalan et al., 2012, Pinzani et al., 2011). ACLF is characterized by a rapid progression and a high short-term mortality rate of 50 – 90 % (Jalan and Williams, 2002). Improved understanding of this condition will improve treatment outcome and answer questions such as whether ACLF patients should be admitted to intensive care or not (Das et al., 2010, Moreau et al., 2013).

Several acute insults have already been identified to be responsible for the acute deterioration of chronic liver disease patients to ACLF but these can vary depending on the geographical region (Sarin et al., 2009). Alcoholic hepatitis, drug toxicity, bacterial infections and viral infections have all been commonly identified as precipitating events. However, the acute insult might also not be easily identifiable and it is estimated to be unknown in approximately 40 % of patients (Jalan et al., 2012, Ikeda et al., 1990, Moreau et al., 2013). Knowledge of the acute episode is important because it might be enable personalized treatment which could possibly reverse liver deterioration and avoid the need for transplantation (Sarin et al., 2009). Finally, SIRS, commonly triggered through bacterial translocation, is also thought to be an important determinant of disease severity in ACLF

patients. Furthermore, it can pre-dispose ACLF patients to further infections which would in turn further aggravate a pro-inflammatory response and create a vicious cycle (Jalan et al., 2012). Similarly to ALF, there is a direct positive correlation between the severity of SIRS and ACLF mortality (Jalan et al., 2012). An overview of ACLF and ALF development is presented in Figure 1.8.

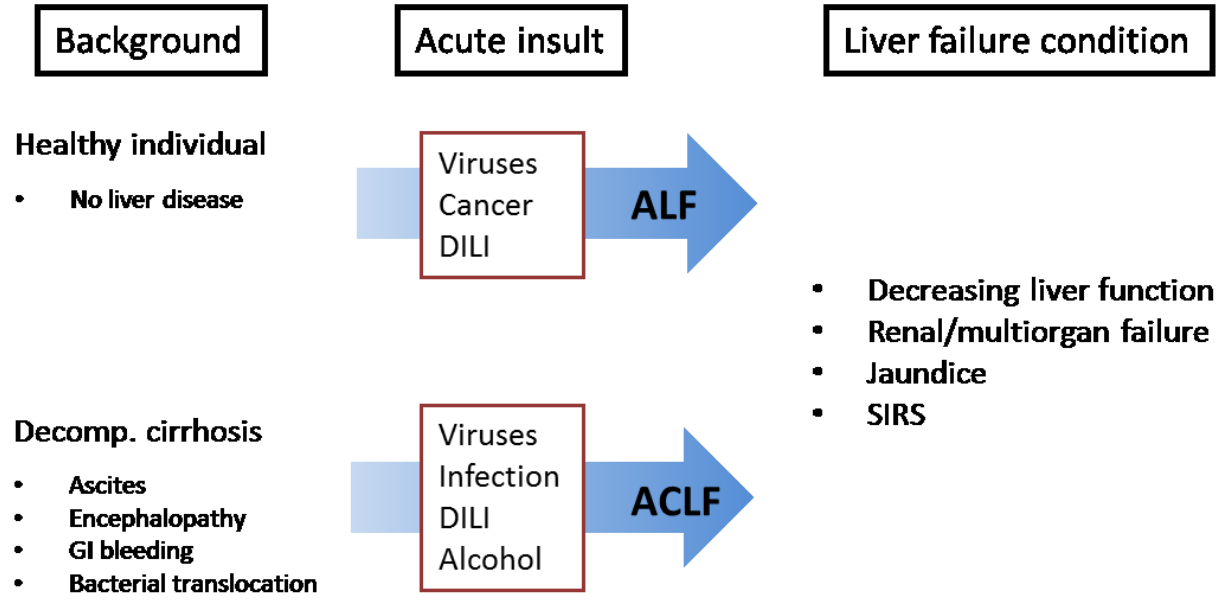


Figure 1.8: Overview of ALF and ACLF development. ALF normally develops in individuals who don't suffer from a background liver disease while ACLF develops in people suffering from a background disease, typically decompensated cirrhosis. Both conditions require an acute insult to develop. SIRS – systemic inflammatory response syndrome; DILI – drug induced liver injury; ALF – acute liver failure; ACLF – acute on chronic liver failure.

Thesis hypothesis

The aforementioned liver conditions are hypothesized to be characterized and driven by endocellular metabolic perturbations. The aim of this thesis is to determine whether the approach of metabonomics, which is introduced in Chapter 2, can be a useful tool in the elucidation of the underlying metabolic perturbations that accompany liver diseases through the identification of mechanistic or diagnostic markers. This methodology was applied to two DILI animal model studies (Chapters 3 and 5) and one liver disease animal model (Chapter 4), before concluding with the metabonomic analysis of a clinical liver disease study (Chapter 6).

Chapter 2: Metabonomics analytical background

Metabonomics

There is a pressing need for the development of novel technologies that would enable the mechanistic bases of liver disease such as DILI to be elucidated and ultimately lead to prediction of susceptibility to DILI and of prognosis following an adverse event (Watkins et al., 2008). The development of technologies such as metabonomics and its subsequent application to the prediction of the response of individuals following drug administration, pharmacometabonomics, have shown promise in enhancing our understanding of the underlying mechanisms of DILI and potentially identifying markers of idiosyncratic hepatotoxicity (Lindon et al., 2006).

Metabonomics is a top-down systems approach that involves the generation of information-rich metabolic profiles of biological samples and studies the dynamic response of these metabolic profiles following a perturbation due to a toxic insult, genetic changes or external stimuli (Nicholson et al., 1999, Lindon et al., 2006). A non-targeted approach can be employed to profile the metabolic complement of tissues and biofluids and investigate the effect of the stimulus of interest such as a toxin, (Nicholson and Lindon, 2008, Coen et al., 2008). In addition, targeted approaches are often applied which enable focus on specific classes of metabolites or metabolic pathways that are hypothesised to be affected (Chen et al., 2009, Want et al., 2010).

Metabonomics is a rapidly growing, versatile and dynamic approach which is currently used in many fields, including toxicological (Coen, 2010, Robertson, 2005, Robertson et al., 2011), environmental (Viant et al., 2003), nutritional (Claus and Swann, 2013) and clinical studies (Andrew, 1984, Ladep et al., 2014, Lindon and Nicholson, 2014). Recently, metabonomics has also been employed to improve our understanding of the important role of the gut

microbiome and its metabolic interactions with the host and how it is affected by several disease states (Nicholson et al., 2012).

Analytical platforms employed by metabonomics

Metabonomic investigations typically rely on two different analytical platforms to acquire the metabolic profiles; nuclear magnetic resonance (NMR) spectroscopy and mass spectrometry (MS) coupled to different types of chromatography (Nicholson et al., 2002). These analytical platforms can analyse a wide range of compounds (<1000 Daltons), known as metabolites (Nicholson et al., 1999, Beckonert et al., 2007). Estimates suggest that there are approximately 2000 main metabolites in the human metabolome (Beecher, 2003), while 2651 compounds have been identified in total in human urine (Bouatra et al., 2013). Each analytical technique has advantages and disadvantages, and a complimentary use of both techniques ensures maximal coverage of the metabolome and recovery of information.

Due to the versatility of NMR and MS, they can be used to analyse many different sample matrices including urine, serum/plasma and tissue extracts, which are most commonly examined (Bollard et al., 2005, Beckonert et al., 2007, Dona et al., 2014). Both techniques can also be used to study solid tissue samples, such as the magic angle spinning (MAS) application of NMR (Beckonert et al., 2010) and the matrix assisted laser desorption ionization (MALDI) method of MS (Fagerer et al., 2013).

Nuclear Magnetic Resonance spectroscopy

NMR spectroscopy is a non-destructive analytical technique that can be used to profile the metabolic composition of complex fluid or solid biological samples (Beckonert et al., 2007, Beckonert et al., 2010, Dona et al., 2014). Modern NMR instrumentation consists of a

superconducting electromagnet cooled to temperatures close to absolute zero (-273.15 ^{o}C) in order to achieve a strong magnetic field. The NMR spectrometer also utilizes a probe which is responsible for generating and transmitting the radiofrequency pulse to the sample, a pulse programmer and radiofrequency transmitter and finally, a signal receiver. Figure 2.1 presents the general layout of the superconducting magnet of an NMR spectrometer.

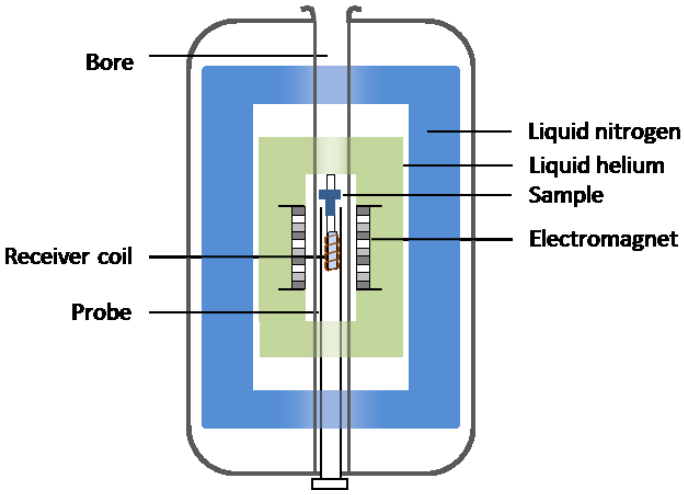


Figure 2.1: The components of an NMR spectrometer superconducting magnet are depicted above. Inside the casing of the magnet there is an outer storage tank of liquid nitrogen which is acting as an insulator to the inner liquid helium store. The liquid helium cools the superconducting coils sufficiently in order to reach a superconducting state. The bore is the space in the centre of the magnet where the sample is inserted and the probe is located. The probe holds the sample and has the circuitry required to excite the sample, as well as detect the resulting signal (through the receiver coil).

The theory of NMR relies on the basic physical properties of atomic nuclei, mass quantity and spin, which lead to an intrinsic angular momentum, a vector, defined as *spin* (p) and whose absolute value is derived by the following formula:

$$p = \hbar[I(\mathrm{I}+1)]^{1/2}$$

I - spin quantum number; ħ - reduced Planck's constant

The spin quantum number of each atomic nucleus depends on its number of protons and neutrons, and can range from 0 (including ^{12}C and ^{16}O), to 1/2 (including ^{1}H, ^{13}C and ^{19}F), 1 (including 2H and ^{14}N), 3/2 (^{15}N) and so on.

Another important physical property of nuclei is known as magnetic moment ($\underline{\mu}$), which is another vector arising from the spin and positive charge of the nucleus. This property is related to the angular momentum through the gyromagnetic ratio (γ), which is a proportionality constant unique to each different nucleus. It is important to note that the spin quantum formula reveals that if a nucleus has a spin quantum number value equal to zero, it will not have an intrinsic angular momentum or a magnetic moment and therefore it will not be detectable by NMR. The proton nucleus (^{1}H), which is the most commonly studied nucleus in the context of metabonomics and most relevant to this thesis, has a spin quantum number of ½. Nuclei with a spin equal to ½ can have two different directions, ±½ħ, and therefore the vectors of the proton nuclei can have either of the two possible orientations (Hore, 2011).

When protons are placed in an external magnetic field, such as that created by a superconducting magnet, their nuclei move from a random to an ordered orientation and precess about the axis of the magnetic field. This precession and its frequency are defined as the Larmor precession and frequency respectively, as first described by Landau and Lifshitz (Landau and Lifshitz, 1935). The external magnetic field causes a separation of the nuclei to separate energy levels, depending on their spin orientation and spin quantum number. In the case of ^{1}H-NMR, protons can have two different orientations, leading to nuclei with spin -½ħ to be located at the higher energy level and vice versa. The population of nuclei at each energy level is predicted by the Boltzmann distribution. At thermal equilibrium, more nuclei will be located at the lower energy state and therefore some high energy state nuclei will give off energy to the lattice in order to transition to the lower energy state. This phenomenon is known as spin-lattice relaxation and it occurs exponentially with time, with a time constant known as the spin-lattice relaxation time (T_1). Nuclei can also undergo spin-spin relaxation as

a result of inter-nuclei interactions and this is characterized by the spin-spin relaxation time (T_2). The energy difference between the two energy levels for the nuclei in a magnetic field is determined by the strength of the external magnetic field and it can be calculated with the following formulae:

$$\Delta E = \gamma \hbar Bo \qquad \Delta E = \nu h$$

Bo - strength of the external magnetic field; v - frequency of electromagnetic radiation; h - Planck's constant

The second formula reveals that electromagnetic radiation, equal to the resonance (Larmor) frequency can be used to increase the probability of nuclei transitioning, flipping, between energy levels and therefore allowing us to perform NMR spectroscopy (Gutowsky, 1954). It is important to note that in order for maximum net absorption to take place thermal equilibrium between the two energy levels must be first established, which is dependent on T_1. Only at this point will the population difference will be maximized, which will therefore permit the maximum net absorption (Hore, 2011).

An important property of NMR spectroscopy is that not all nuclei have identical resonance frequencies due to an effect known as chemical shift which is dictated by the electronic environment of each nucleus. The external magnetic field applied to a nucleus will also cause surrounding electrons to circulate within their atomic orbitals which will subsequently generate a smaller opposing magnetic field (due to their mass and charge), known as nuclear shielding. Therefore, the effective magnetic field experienced by each nucleus will be the difference between the two opposing magnetic fields and as a result will be weaker than the external magnetic field. For example, proton nuclei bonded to atoms with high electronegativity, such as oxygen, will have a lower electron density, due to the pulling effect of the highly electronegative oxygen nucleus. This will cause a smaller degree of shielding

against the external magnetic field of the superconducting electromagnet, leading to a greater effective magnetic field and to a higher resonance frequency since the difference between the aforementioned energy levels will be greater (as predicted by the formula). In contrast, proton nuclei in a methyl functional group will have a higher electronic density which will lead to greater shielding, a weaker effective magnetic field and a subsequently lower resonance frequency. Finally, the chemical shift is defined as the difference of the resonance frequency of a nucleus relative to the resonance frequency of a standard nucleus, divided by the operating frequency of the magnet and it is expressed in parts per million (ppm). This is an important effect because it permits the separation of nuclei from different chemical structures within an NMR spectrum (Hore, 2011).

Another important property of NMR spectroscopy which can provide additional molecular structural information arises from spin-spin coupling, also known as J-coupling. Neighbouring nuclei can also have different spin orientations and therefore will occupy different energy levels when the external magnetic field is applied. J-coupling describes the through-bond interaction between nuclei that are separated by three bonds that leads to an effect on the energy level of the each nucleus, depending on the energy level of the neighbouring nucleus. This interaction is expressed in Hz and leads to spectral peak multiplicity and therefore providing useful information concerning the neighbouring nuclei, which can then be converted to structural information (Hore, 2011).

Modern NMR experiments rely on radiofrequency pulses to excite the nuclei from the lower energy state to the higher energy state. Radiofrequency pulses are employed because they permit the excitation of nuclei with different Larmor frequencies, instead of exciting each nucleus individually. The cumulative effect of a radiofrequency pulse can be demonstrated by

using the vector model shown in Figure 2.2. An applied radiofrequency pulse will lead to the rotation of the magnetization of a collection of nuclear spins away from the axis of the external magnetic field (z axis; as shown in Figure 2.2A). The duration of the pulse dictates the extent of the rotation, which is usually 90^0 or 180^0 in experiments relevant to this thesis. When a 90^o degree radiofrequency pulse is applied, the magnetic vectors are rotated to the axis of the pulse (y axis) and precess in the xy plane (Figure 2.2B). A receiver coil located on the y axis detects the magnetic vectors through a change in voltage which is later amplified by the receiver. This detectable signal is known as the free induction decay (FID) and it represents the sum of all the nuclei within the sample. Once the pulse is switched off, the nuclei will precess back to their original position leading to the characteristic decaying FID signal (Figure 2.2C). Fourier transformation of the resulting FID leads to a spectrum with the chemical shift of the nuclei on the x axis and the intensity the resonances on the y axis, as shown in Figure 2.3 (Hore, 2011).

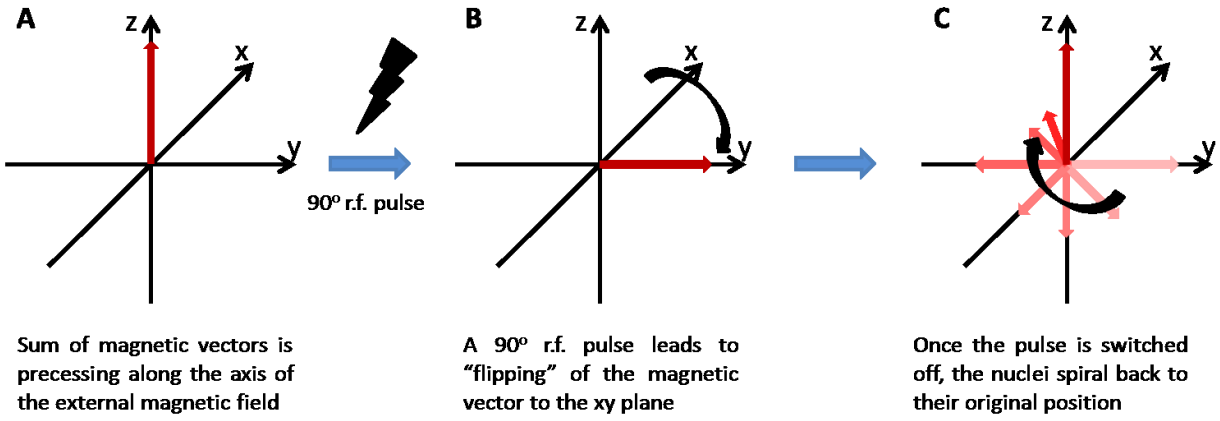


Figure 2.2: The effect of a 90^o radiofrequency pulse on aligned magnetic vectors is shown. The magnetic vectors are precessing around the axis of the external magnetic field (z axis; A). A 90^o degree radiofrequency pulse leads to the flipping of the magnetic vectors from the z plane to the xy plane (B). Once the radiofrequency pulse is switched off, the magnetic vectors will precess back to the original position (C). The resulting decaying signal is known as the FID.

Pulse sequences used in NMR experiments

A diverse array of NMR pulse sequences can be used depending on the sample and analysis. Please note that only the pulse sequences relevant to this thesis will be further discussed.

One dimensional standard solvent suppression pulse sequence (NOESYpr1d pulse sequence)

One dimensional pulse sequences with water pre-saturation are typically used in metabonomics to acquire spectra of samples that are typically of low protein or lipid content, such as urine or tissue aqueous-soluble extracts (Beckonert et al., 2007, Dona et al., 2014). An example is a pulse sequence which is an adaptation of a two dimensional Nuclear Overhauser Effect (NOE) experiment which consists of the following sequence: RD – 90^o – t – 90^o – t_m – 90^o – ACQ; where RD is the relaxation delay, 90^o is a 90^o degree radiofrequency pulse, t is the first increment in a NOESYpr1d sequence, t_m is the mixing time and ACQ is the FID acquisition period (Jeener et al., 1979, McKay, 2011). During relaxation delay (RD) and t_m the water resonance is selectively irradiated with a low power continuous wave in order to pre-saturate and attenuate its resonance by a factor of 10^5 or more before FID acquisition (Nicholson et al., 1995, McKay, 2011). This is advantageous because higher spectrometer receiver gains can then be used in order to achieve an improved signal to noise ratio (Nicholson et al., 1984). A representative urine spectrum acquired with a standard solvent suppression pulse sequence is shown in Figure 2.3.

CPMG pulse sequence

The Carr-Purcell-Meiboom-Gill (CPMG) spin-echo pulse sequence (Carr and Purcell, 1954, Meiboom and Gill, 1958) is used for samples that are expected to have significant macromolecular (protein and lipid) content such as blood plasma or sera samples which are

also typically analysed in metabonomics analyses (Beckonert et al., 2007). This pulse sequence has the form: RD – 90° – (t – 180° – t)$_n$ – 90° – ACQ, where t is defined as the spin echo delay (time delay between the pulses), 180° is a 180° degree radiofrequency pulse and n is the number of loops used (Beckonert et al., 2007). The spin echo experiment uses a 180° degree radiofrequency pulse to restore the phase of the different magnetic vectors in a sample that are precessing at different Larmor frequencies after a 90° degree radiofrequency pulse. The CPMG pulse sequence employs the spin echo experiment multiple times but the amplitude of the received signal decays over time due to T_2 relaxation (Hahn, 1950, Carr and Purcell, 1954, Meiboom and Gill, 1958). Since bigger molecules, macromolecules, have faster T_2 relaxation their signal will be lost first, leading to the attenuation of their resonance.

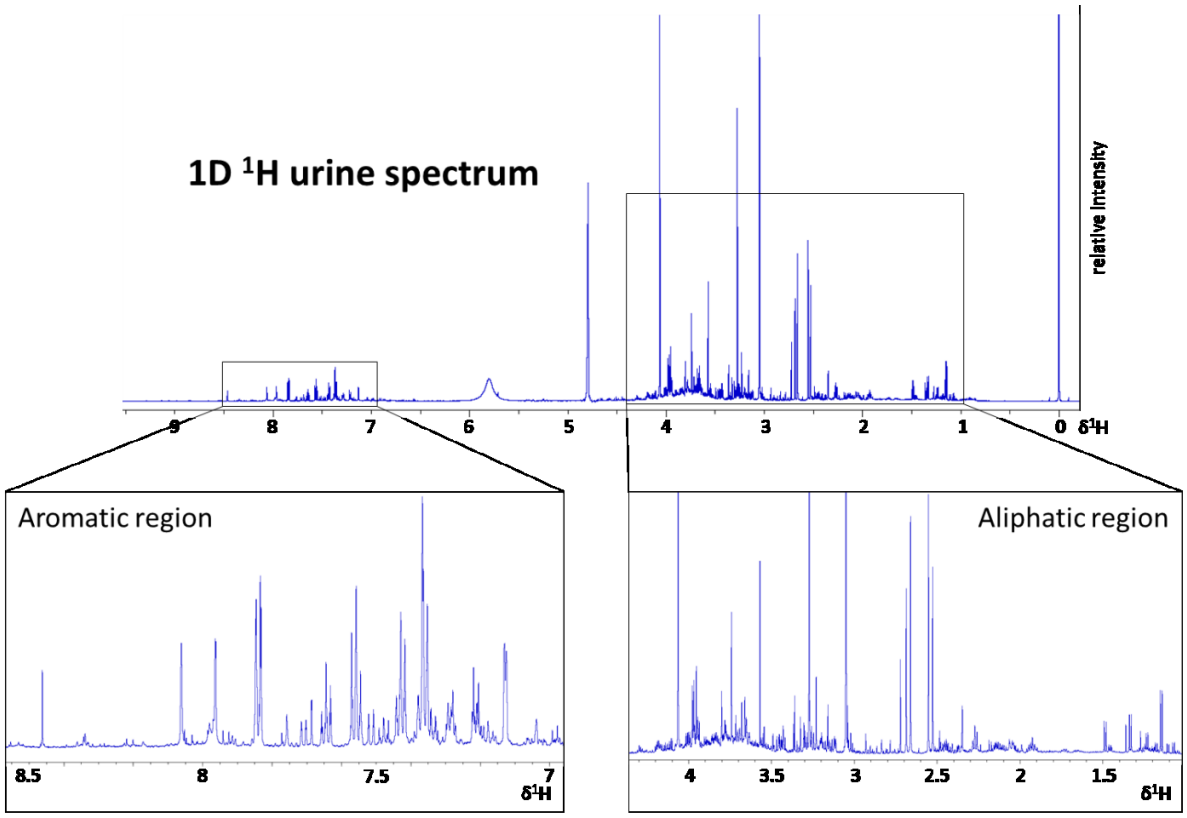


Figure 2.3: A representative 1D ^{1}H-NMR urine spectrum acquired at a frequency of 600 MHz is depicted above. The chemical shift scale is located at the x-axis (δ^1H), while the relative intensity is shown on the y-axis. Magnified versions of the aliphatic and aromatic regions of the spectrum are also depicted above.

Two dimensional NMR experiments

Multi-dimensional NMR experiments can provide further structural information, by plotting the data in multiple frequency axes. Two and three dimensional experiments, which can either be homo- or hetero-nuclear, are typically used in biology (Marion, 2013). The two dimensional homo-nuclear NMR experiments commonly used in metabonomics analyses are correlation spectroscopy (COSY) and total correlation spectroscopy (TOCSY) and are very useful because they reveal structural information concerning adjacent protons in a molecule (Aue et al., 1975, Hore, 2011). The COSY experiment reveals the spin-spin coupling between protons (three bonds apart), while the TOCSY experiment permits the observation of correlation with more distant protons (Hore, 2011). The spectra of both types of experiments are presented with a diagonal line containing the chemical shifts of the nuclei, and cross-peaks on either side of the diagonal that represent the coupling information between the nuclei.

Mass spectrometry

MS is a very sensitive analytical technique which is typically coupled to upstream chromatographic platforms in metabonomic analyses. Unlike NMR, MS is a destructive technique since it requires the ionisation of the samples, a process which can be described by the following equation for positive polarity ionisation:

$$M + e^- \rightarrow M^+ + 2e^-$$

M - molecule to be ionised; e^- - electron used to ionise the molecule; M^+ - ionised molecule

Modern MS instruments require a vacuum and consist of three different main modules: the ion source which ionises molecules and converts them to a gaseous phase, the mass analyser which separates the resulting ions based on their mass to charge ratio (m/z) and finally the detector, where the ions are detected and their relative abundance is calculated. There are

different types of ionisation and analyser modules but only the ones most relevant to metabonomics and this thesis will be further discussed.

Ionisation sources used for organic analyses include electron impact ionisation (EI), chemical ionisation, fast ion or atom bombardment (FAB) ionisation, MALDI and electrospray ionisation (ESI) (De Hoffman et al., 1996, Fenn et al., 1989, Hillenkamp et al., 1990, Nier, 1947). ESI is commonly used in liquid chromatography mass spectrometry (LC-MS) analyses since it is considered to be a "soft" ionization method and leads to mass spectra with reduced ion fragment content. (Dettmer et al., 2007, Fenn et al., 1989, De Hoffman et al., 1996). ESI imposes a strong electric field on the sample passing through a capillary tube and the voltage difference between the capillary exit and counter electrode results in the formation of highly charged droplets (Figure 2.4A). As the solvent in the droplets evaporates with the help of a drying gas, the electrical charges become more dense leading to a cascade of droplet ruptures and ion desorption is achieved when the electrical density becomes large enough (De Hoffman et al., 1996). An advantage of ESI is that it can lead to ions with multiple charges, which aid the separation of the ions in the mass analyser, as well as permit the analysis of bigger molecules. Gas chromatography mass spectrometry analyses utilize hard ionisation methods, such as EI. This ionisation method uses a heated filament to give off electrons which are then accelerated before impact with the gaseous molecules which are injected into the source. This leads to the removal of electrons from molecules and the formation of positive ions only (De Hoffman et al., 1996). It is also important to note that modern MS instruments employ a Z spray system at the ion source in order to avoid direct injection of neutral molecules or contaminants in the mass analyser.

The mass analysers separate the resulting ions according to their mass to charge ratio before they reach the detector. Common mass analysers include the quadrupole (Q), the time of flight (TOF), the fourier transform ion cyclotron resonance and the ion trap analyser, all of which have different upper mass limits, transmission and resolution (De Hoffman et al., 1996). The quadrupole and TOF mass analysers are typically used in metabonomic analyses (Figure 2.4). Quadrupoles are real mass to charge analysers that consist of four parallel poles, where each pair of parallel rods is connected to each other and share the same radiofrequency potential (Figure 2.4B). A direct current is then superimposed on the quadrupoles (Ferguson et al., 1965, De Hoffman et al., 1996) which results in an electric field where only ions of the selected m/z can pass through to the detector without hitting the quadrupoles, and therefore the quadrupole mass analyser is ideal for targeted analyses (De Hoffman et al., 1996). The TOF mass analyser exploits the principle that ions with greater mass to charge ratio will travel more slowly in space than ions with a smaller mass-to-charge ratio (Wiley and McLaren, 1955). They are typically accelerated before reaching the detector by a "pusher" and the longer the distance covered before reaching the detector, the better the separation (Figure 2.4C) (De Hoffman et al., 1996). Different combinations of mass analysers can be used in order to achieve improved ion separation, such as the Q-TOF (Figure 2.4) or the triple quadrupole (TQ) configuration. TQ setups can be used to perform MS/MS fragmentation analyses, where further fragmentation takes place in the middle quadrupole, known as the collision cell. Ions can then be identified based on the pattern of the fragment ions.

Finally, the ions are detected on the detector which can either record a direct measurement of the charges or amplify the signal through several multiplication techniques, such as electron photon multipliers. The resulting difference in potential caused by the ions is

converted to a digital signal by an analogue to digital converter and the computer assigns the detected ions to their respective mass to charge ratios and relative intensities (De Hoffman et al., 1996).

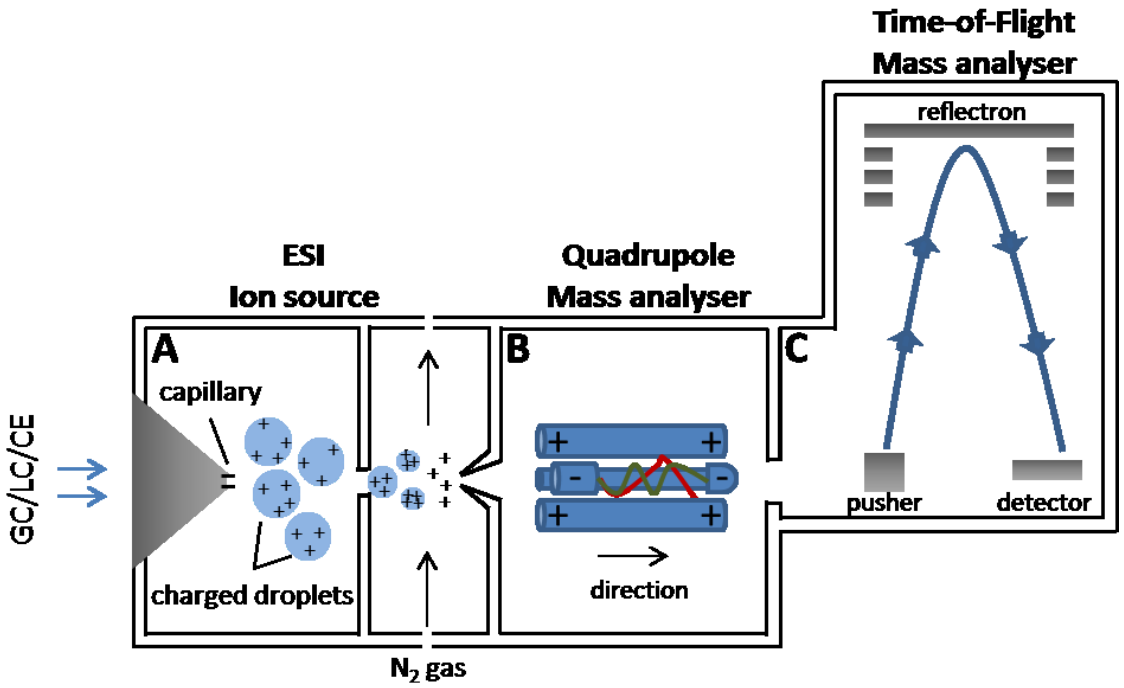


Figure 2.4: The components of an ESI-Q-TOF MS instrument are illustrated above. The ESI source (A) is where the samples are ionised and freed from droplets with the aid of the drying gas (N_2 gas). The first mass analyser (B) is a quadrupole where ions with specific m/z can be selected for analysis. Finally C depicts the time-of-flight mass analyser, with a reflectron which separates ions according to their mass and charge. The ion detector is located in compartment C as well. GC – gas chromatography; LC – liquid chromatography; CE – capillary electrophoresis

Chromatography

Chromatography systems are used upstream of MS instruments to separate or fractionate the sample in order to avoid the complications resulting from a direct sample injection, which include ion suppression and higher background noise. Metabonomics experiments most commonly rely on liquid chromatography (LC), gas chromatography (GC) and capillary electrophoresis (CE) platforms (Dettmer et al., 2007, Dunn et al., 2011).

Liquid chromatography

Liquid chromatography is an aqueous-phase separation technique which relies on columns with different chemical compositions that can be used depending on the chemical nature of the metabolites of interest in the biological sample. Reverse-phase (RP) chromatography typically consists of C-18 bonded silica in narrow bore columns and is used to separate medium polar and non-polar analytes (Dettmer et al., 2007). In RP chromatography, polar metabolites are generally eluted first because they are not well retained by the column, whereas the retention time of non-polar molecules depends on the extent of their non-polarity and the strength of column interaction. For the retention of very polar metabolites, hydrophilic interaction liquid chromatography (HILIC) is preferred in metabonomic analyses (Tolstikov and Fiehn, 2002, Spagou et al., 2011, Dettmer et al., 2010). HILIC uses silica or derivatized silica to retain the polar molecules and requires a significant portion of water in the mobile phase in order for the molecules to be retained on the column (Dettmer et al., 2010). The relative metabolite elution time of molecules in HILIC is opposite to that of RP chromatography, where non-polar metabolites are eluted first and vice versa.

Finally, one of the later methods of liquid chromatography is termed as ultra-performance liquid chromatography (UPLC; Waters Corp., MA, USA) because it uses smaller particles sizes and operates at higher pressures (10,000 – 15 000 psi) in order to increase chromatographic resolution and achieve narrower chromatographic peaks (Wilson et al., 2005). A UPLC-RP chromatographic spectrum of a serum sample is shown in Figure 2.5.

Gas chromatography

Gas chromatography relies on the thermal stability and volatility of molecules and therefore typically uses an EI ion source. In order to increase the proportion of molecules that will fulfil

this requirement derivatization of the sample is performed prior to analysis . The two derivatizing reagents relative to this thesis are: N-Methyl-N-(trimethylsilyl) trifluoroacetamide (MSTFA) which adds a silyl group to active hydrogen functional groups such as –SH or –OH and methoxyamine which reacts with carbonyl groups to form the oxime derivative and forces sugars to adopt an open ring formation (Dettmer et al., 2007).

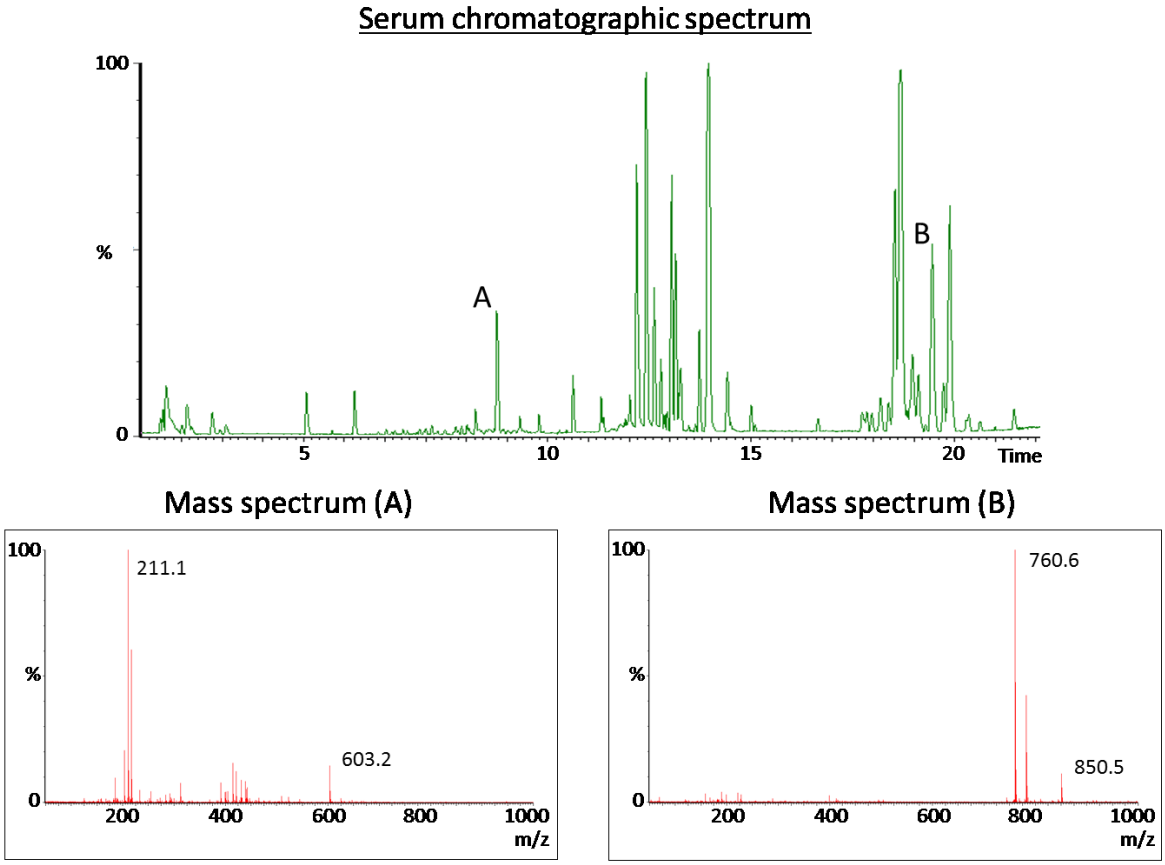


Figure 2.5: The reversed phase chromatographic total ion current of a serum sample is shown above. The peak retention time is indicated on the x axis, while the y axis reveals the relative intensity of each peak. A and B represent the mass spectra associated with two peaks. The m/z of the peaks in the mass spectra are shown on the x axis, while the y axis reveals the relative intensity of each peak.

Chemometrics

The analysis and interpretation of NMR and MS metabonomic data rely on chemometric tools, which primarily include multivariate statistical tools that are employed to deconvolute and maximize the recovery of the information from the complex metabolic profiles, which

will facilitate their analysis (Fonville et al., 2010). Multivariate statistical methods can produce simplified weighted combinations of the tens of thousands of original variables generated by NMR and MS analyses, which would reveal metabolic patterns that would not be easily determined otherwise (Fonville et al., 2010). These tools can be unsupervised (no input of *a-priori* sample class is required) or supervised (sample class is defined) and each type of analysis can be used to extract different information.

Unsupervised methods

Principal component analysis (PCA) is an unsupervised statistical tool that is typically employed at the beginning of the statistical analysis. PCA reduces the number of dimensions in order to improve visualisation and reveal patterns in the data, with minimal loss of information. PCA uses an orthogonal linear transformation which transforms the original data in Euclidean space to a compressed space (characterized by principal components), consisting of fewer dimensions, and thus reducing dimensionality and complexity. The first principal component characterizes the greatest variance in the matrix, while the second principal component is orthogonal to the first and describes the second largest proportion of the variance (Wold et al., 1987). Figure 2.6 (A-C) depicts the underlying principle of the dimension reduction performed by PCA. The first two principal components describe the largest proportion of the variance of the dataset (Figure 2.6A) and define the plane (Figure 2.6B) onto which the samples will be projected, which has reduced dimensionality (Figure 2.6C). All observations will be projected onto the new plane as scores points and the results can be presented in the format of a “scores” (Figure 2.6D) and a “loadings” plot (Figure 2.6E) (Wold et al., 1987). The scores plot illustrates the relationship of samples in multivariate space, while the loadings plot illustrates the weight of each variable in the separation of the whole sample set as observed in the scores plot.

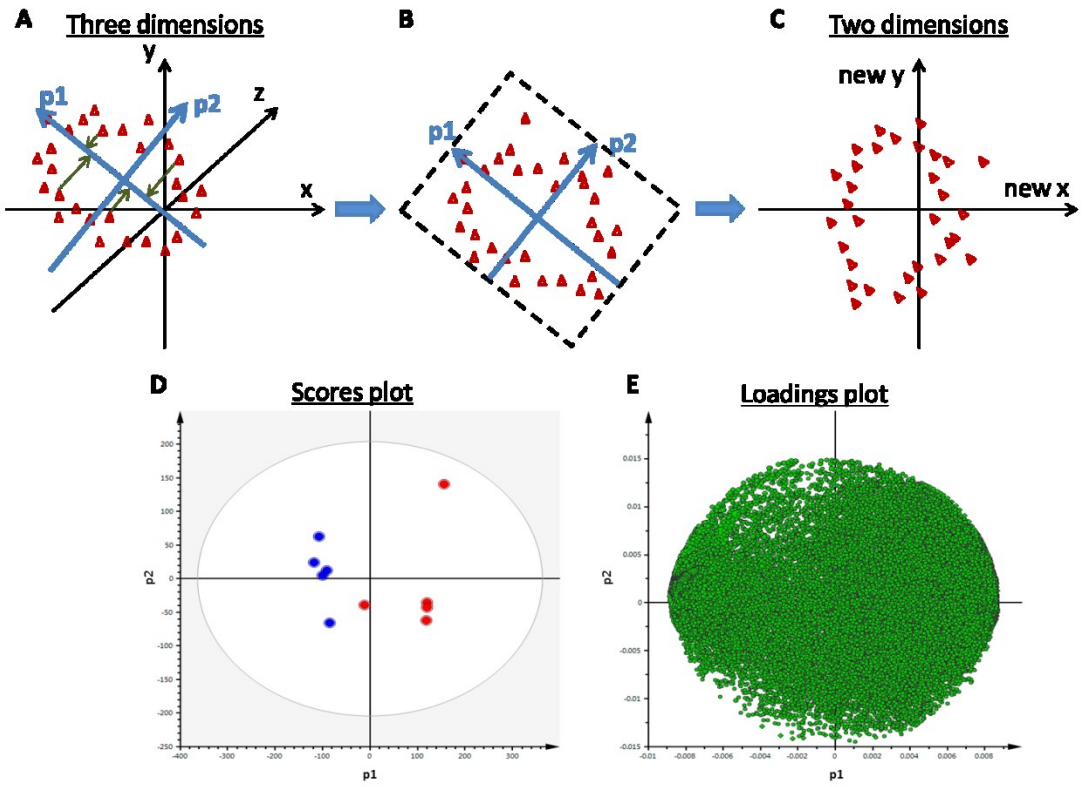


Figure 2.6: A demonstration of the dimension reduction in dataset as achieved by PCA is depicted. The first two principal components (p1 and p2) describe the majority of the variance in the dataset (A). They define a new plane (B) onto which the variables are projected on (C). The results are usually presented in scores plot, which reveals the group separation in multivariate space (D), and loadings plot, which reveals the weight of each variable (E). Univariate scaling was applied to this dataset.

Supervised methods

Supervised statistical tools such as partial least square (PLS) analysis and orthogonal partial least squares discriminant analysis (O-PLS-DA) are employed when more subtle differences between groups are investigated or when we are trying to distinguish between the real differences between groups from variance that is orthogonal to the class membership or "background noise" (Fonville et al., 2010). Background noise is defined as variation not in direct relation to the biological separation of the groups of interest, such as instrument instability. These techniques require a description of the sample classes (Y matrix) in order to derive the components that best describe the classes of the Y matrix (Fonville et al., 2010).

O-PLS-DA is a useful iteration of the PLS-DA statistical tool because it employs one or more orthogonal components in order to account for the variance that is orthogonal to the biological variation (Fonville et al., 2010, Trygg and Wold, 2002). O-PLS-DA is typically applied to both NMR and MS metabonomic datasets. In NMR analyses, the resulting loadings plot can be "back-projected" onto a pseudo-NMR spectrum, which is achieved by back-scaling the unit variance scaled model to a correlation matrix (Fonville et al., 2010, Cloarec et al., 2005b). The pseudo-NMR spectrum, or loadings coefficient plot, is also coloured with a scale which reveals the correlation of each variable and how significantly different it is between the two classes (Figure 2.7).

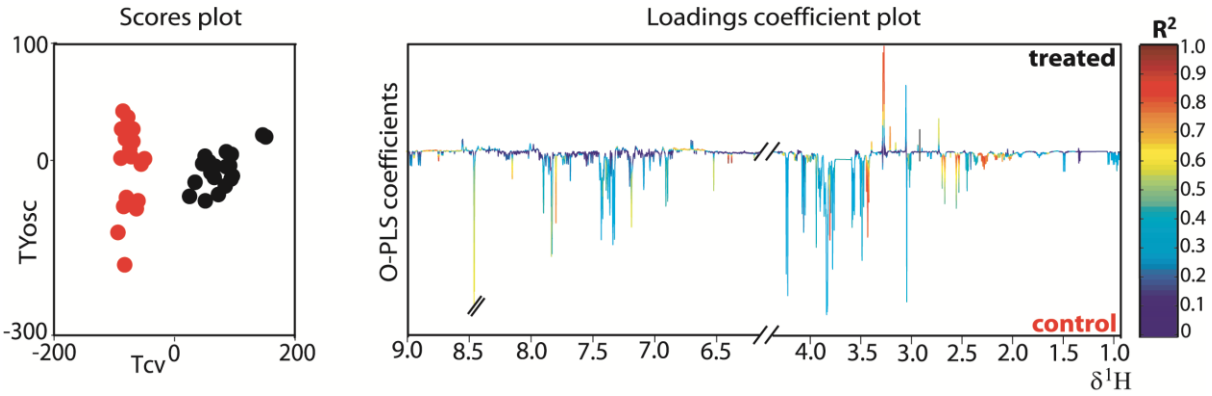


Figure 2.7: A urine O-PLS-DA model comparing a control and treated group is depicted above. The scores plot reveals the separation of the two groups (red, control and black, treated) in multivariate space, while the loadings coefficient plot illustrates the spectral comparison between the two classes. The direction in which each resonance points reveals the relative difference between the two groups. Resonances pointing downwards are higher in the control group and vice versa. Tcv (predictive component) reveals the inter-group separation, while TYosc reveals the intra-group separation. The correlation scale has a range from low correlation (0; blue) to high correlation (1; red) based on the squared Pearson correlation coefficient (R^2).

PLS and O-PLS-DA can produce models with greater predictive ability but require validation since they are prone to over-fitting. A seven fold cross-validation is commonly applied to during the calculation of supervised models, which excludes a seventh of the sample set and rebuilds the model in order to predict the class of the excluded set using the model. Furthermore, model validity can also be evaluated through the use of permutation tests,

which randomize sample class labels and calculate the subsequent predictive ability of each model, before comparing it to the predictive ability of the actual model using biologically meaningful classes. A 95 % significance threshold ($p < 0.05$) to test for statistical significance is commonly used.

Complementary statistical tools

Metabonomic analyses employ an array of multivariate or univariate statistical tools which can facilitate the analysis of the complex spectra but biological interpretation and data recovery remains a significant challenge. Spectra typically contain thousands of metabolites which might be hard to assign because of overlapping or low signal intensities. Therefore, various other useful tools have been developed to improve the recovery of information from the spectra of both NMR and MS analyses.

Statistical total correlation spectroscopy (STOCSY) and cluster analysis statistical spectroscopy (CLASSY) are two useful tools that complement NMR data analysis and peak assignment (Cloarec et al., 2005a, Robinette et al., 2009). STOCSY relies on the correlation patterns that arise from a series of spectra in order to identify which peaks are correlated to each other and potentially belong to the same compound or metabolic pathway (depending on the correlation value). The correlation between peaks to the selected peak of interest is indicated by a colour scale which ranges from low correlation (0) to high correlation (typically 1) (Cloarec et al., 2005a). CLASSY profiles quantitative changes in the metabolic profiles by using a correlation algorithm to simultaneously identify resonances belonging to the same chemical structure, as well as clustering metabolites that behave similarly and could therefore belong to the same metabolic pathway (Robinette et al., 2009). A chemometric tool specific to MS data analysis is “collection of annotation related methods for mass spectrometry data”

(CAMERA) , which facilitates the identification of features (including fragments and adducts) that belong to single compounds (Kuhl et al., 2012).

Application of the metabonomics approach

The metabonomics approach offers a distinct and complimentary view to other –omics approaches and has provided valuable, previously uncharacterized, information in the field of toxicology and liver disease (Robertson, 2005, Beyoglu and Idle, 2013, Lindon et al., 2003, Robertson et al., 2011).

Metabonomic studies of APAP metabolism and hepatotoxicity

Early metabonomic studies employed NMR to characterize APAP related metabolites in human urine (Bales et al., 1984), as well as rat urine and bile (Spurway et al., 1990). LC coupled NMR (LC-NMR) has also been used to characterize APAP metabolites in human urine, rat urine and rat bile (Spraul et al., 1994) and LC-NMR-MS had also been employed to study APAP metabolites in human urine (Shockcor et al., 1996). Other applications of LC-NMR include metabolism studies aiming to identify the glucuronide molecule of an APAP metabolite in human urine (Godejohann et al., 2004), as well as to further study the deacetylation and reacetylation of APAP metabolites in rat and human urine (Nicholls et al., 1997), which was initially reported by NMR in rat urine (Nicholls et al., 1995). Other recent drug assignment studies, include the demonstration of how STOCSY can be used to identify APAP metabolites in human urine ^{1}H-NMR spectra (Holmes et al., 2007), as well as to characterize the prevalence of APAP metabolites in human urine in epidemiological studies (Loo et al., 2012).

Pharmacometabonomic studies have also focused on predicting the metabolism and toxicity of APAP. Initially, urine metabolic profiles were used to predict the extent of liver necrosis

after administration of APAP in an animal model (Clayton et al., 2006). A human pharmacometabonomic study involving the administration of non-hepatotoxic doses of APAP indicated that it was possible to predict its metabolism, in terms of percentage of sulphation and glucuronidation, by looking at the baseline metabolic profiles prior to dosage (Clayton et al., 2009). Another human study focusing on APAP metabolism revealed that the urinary metabolic profiles of individuals receiving the maximum therapeutic dose (4 grams) per day for seven days could predict a sub-clinical rise in ALT activity, indicating the importance of early intervention (Winnike et al., 2010). Finally, a recent clinical study showed that resected livers had a similar capability of producing similar amounts of NAPQI after APAP administration (Galinski et al., 2014).

Metabonomic analyses have also focused on the mechanisms of toxicity of APAP in a variety of species and sample matrices. One of the very first studies revealed that APAP overdose could be linked to the disruption of deamination and transamination processes, due to the higher level of amino acids in patients' blood and urine (Bales et al., 1988). Other, more recent studies have focused on the APAP-induced disturbance of endocellular metabolism in rodent models. APAP intoxication was shown to lead to energy depletion, as indicated by the lower hepatic levels of glycogen and glucose in mice (Coen et al., 2003). Moreover, another recent study performed on rats has shown that increasingly higher doses of APAP have significant effects on the urinary metabolic profiles of rats, such as depletion of hippurate, citrate and succinate (Fukuhara et al., 2011). APAP has also been shown to affect lipid metabolism by inhibiting fatty acid β-oxidation in serum metabonomic studies (Chen et al., 2009, McGill et al., 2014a), while a lipid targeted NMR analysis has shown that APAP intoxication leads to a drop in phospholipids and an increase in triglyceride content in murine liver samples (Coen et

al., 2004). Finally, metabolic profiling studies have also investigated the potential of ophthalmic acid as a marker of APAP-induced oxidative stress and glutathione depletion (Soga et al., 2006), as initially reported by Ghauri *et al.* who characterized oxyprolinuria in rats by NMR (Ghauri et al., 1993).

Metabonomic studies involving MTX

Kumar *et al.* employed a metabonomic approach to identify common markers for liver toxicity between APAP, MTX and carbon tetrachloride by UPLC-MS. Daily administration of MTX (50 mg/kg) was reported to affect urinary levels of bile acids, steroids and amino acids, some of which were proposed as biomarkers of liver toxicity (Kumar et al., 2012). Another biomarker study investigated serum biomarkers for predicting therapeutic efficacy to MTX treatment in rheumatoid arthritis patients who were receiving MTX (10 mg/kg) weekly for 24 weeks. The levels of metabolites including amino acids, nucleic acids and cholesterol were discovered to be discriminatory between responders and non-responders of MTX treatment but the investigators also noted that age, sex, diet and individual health were important confounding factors (Wang, 2012). Finally, another recent investigation characterized the metabolic and toxic effect of MTX on isolated human CD4+ T cells. Even though the levels of 148 metabolites were identified to be significantly altered, it was concluded that the toxic effect of MTX on CD4+ T cells was minimal at clinically relevant doses (Chimenti et al., 2013).

Metabonomic studies of NASH and the MCD diet

There have been a number of metabonomic studies which investigated the human serum metabolic profile differences between patients with NASH, NAFLD and healthy volunteers. UPLC-MS has been previously employed to characterize and compare the serum metabolic

profiles of healthy volunteers versus NAFLD and NASH patients. The results showed that increased lipogenesis characterized both NAFLD and NASH conditions. Furthermore, impaired polyunsaturated fatty acid (PUFA) metabolism and non-enzymatic oxidation in the peroxisomes were associated with the progression to NASH from NAFLD (Puri et al., 2009). Another study also implicated that the progression of NAFLD to NASH was associated with significant metabolic alterations including the levels of certain glycerophospholipids and unconjugated arachidonic acid (Barr et al., 2010). A third clinical study reported that NASH and NAFLD could not be distinguished based on their plasma metabolic profiles but however discovered that NAFLD was characterized by marked alterations in bile salts levels, while NASH had several metabolic alterations, including higher levels of branched chain amino acids and carnitine conjugates (Kalhan et al., 2011b).

There have also been several metabonomic studies investigating the metabolic profiles associated with NASH in *in-vivo* MCD diet rodent models. An NMR based metabonomic study comparing the serum metabolic profiles of healthy C57BL/6 mice and C57BL/6 mice fed with an MCD diet showed that elevations in the levels of glutamate/glutamine, taurine, glucose and lactate could be used to distinguish the two diet groups. When they translated their results to a clinical study with people suffering from NAFLD at various stages versus healthy controls, they observed that the elevations of serum taurine, glutamate/glutamine and lactate were once again predictive of the disease (Li et al., 2011). Another study that employed UPLC-MS to investigate the effect of the MCD diet in mice, observed that LPC molecules were depleted in the serum while taurine conjugates were upregulated, when compared to healthy mice. Furthermore, changes in the gene expression of transporter proteins and lysophosphatidylcholine catabolism enzymes were also observed (Tanaka et al.,

2012). Finally, a recent study also employed a metabolic profiling approach to investigate potential therapeutic agents for NASH through the MCD diet model in mice and concluded that hypotaurine is a potential therapeutic agent for NASH (Yoshihiko et al., 2014).

Metabonomic studies of decompensated cirrhosis and ACLF

The metabolic profiles of serum from patients with decompensated cirrhosis and ACLF have only been recently characterized by metabonomics. An investigation employed ^{1}H-NMR spectroscopy to distinguish between the plasma metabolic profiles of patients suffering from compensated and decompensated cirrhosis. Twelve discriminatory metabolites were identified, including pyruvate, phenylalanine and succinate (Qi et al., 2012). Alcoholic compensated and decompensated cirrhosis have also been compared to ACLF by plasma ^{1}H-NMR spectroscopy, revealing that the progression to ACLF involves an increase in the levels of metabolites such as phenylalanine, lactate, glutamine and pyruvate (Amathieu et al., 2014). Finally, a recent investigation also employed UPLC-MS analysis to compare the serum metabolic profiles of hepatitis B induced ACLF, chronic hepatitis B and cirrhotic patients. Seventeen prognostic metabolites associated with the development of hepatitis B induced ACLF were identified, the majority of which was comprised by lysophosphatidylcholine molecules, while eleven of these metabolites were also correlated with treatment outcome (Nie et al., 2014).

Metabonomic studies of ALF

There has only been a limited application of metabonomics to the study of ALF. Two GC-MS studies have characterized the hepatic and serum metabolic changes associated with D-galactosamine treatment as a model of acute liver failure in mice and rats. They identified

changes in the levels of serum and hepatic markers, including amino acids, ketone bodies and fatty acid molecules that were associated with hepatic failure in mice (Feng et al., 2007, Feng et al., 2013). An LC-MS/MS study identified mainly plasma and hepatic ceramide molecules which were also associated with the development of hepatic failure in the rat (Yamaguchi et al., 2004). Finally, NMR has also been previously utilized to associate metabolite levels in the serum and urine with the therapeutic outcome of ALF treatment (Saxena et al., 2006), as well as to identify early prognostic serum markers of irreversible damage in viral hepatitis patients, which revealed a general disruption in the urea cycle and amino acid metabolism (Bala et al., 2013).

Chapter 3: Systems level metabolic phenotype of N-acetyl-p-aminophenol and its non-toxic isomer, N-acetyl-m-aminophenol

Introduction

Study details and aims

This study employed a comparative metabonomic approach to characterize the systemic metabolic consequences induced by the administration of APAP and its non-hepatotoxic isomer AMAP (Roberts, 1978). APAP toxicity was hypothesized to be mediated through mitochondrial dysfunction and subsequent energetic stress. ^{1}H-NMR spectroscopic analysis was initially used in a 'global' metabolic profiling approach to acquire the metabolic profiles of the aqueous-soluble hepatic extracts, serum and urine. UPLC-MS and GC-MS were subsequently employed to analyse the aqueous-soluble hepatic extracts in a more targeted approach focusing on metabolites indicative of mitochondrial dysfunction. More specifically, the UPLC-MS analysis focused on carnitine metabolism which is an important component of β-oxidation, while the GC-MS analysis was employed to profile glycolysis and Krebs cycle intermediates in an attempt to characterize the APAP-induced energetic stress. Finally, the metabolic effect of AMAP was compared to that of APAP, aiming to isolate the pharmacological, or aminophenol non-specific, metabolic effects from those associated specifically with APAP toxicity. The rationale behind this was that common metabolic effects between the two compounds would not be related to the effects associated with APAP toxicity.

Materials and methods

The animal handling and treatment, clinical chemistry and liver histopathology were conducted by our collaborators at the University of Washington (Seattle, Washington, USA). The ^{1}H-NMR spectroscopic metabolic profiles were acquired by Miss Lea Maitre.

Animal handling and treatment

Male C57BL/6 mice (*n* = 50, average age of 10 weeks) were purchased from Jackson Laboratory (Bar Harbor, Maine, USA) and were kept in a pathogen free environment at the University of Washington. The animals were housed in temperature controlled rooms with a 12 hour light/dark cycle during the duration of the study. Prior to the beginning of the experiments, the animals were acclimated for one week and had access to *ad libitum* rodent chow diet and acidified sterile water (pH = 2.77). After a fasting period which lasted 12 hours, the animals were treated with APAP (300 mg/kg, *n* = 15), AMAP (300 mg/kg, *n* = 15) and sterile saline as a control (*n* = 20) *via* I.P. injections of 15 µL/g body weight. The selected APAP dose has been reported to cause marked liver damage in mice in previous investigations (Masubuchi et al., 2005, McGill et al., 2012b). An equimolar dose of AMAP was selected for comparative purposes and has also been reported to be non-toxic in this strain of mice (Fountoulakis et al., 2000, Priyadarsiny et al., 2008).

Mice from each treatment group were euthanized by carbon dioxide inhalation and cervical dislocation at 1, 3 and 6 hours post treatment (1hr, 3hr and 6hr respectively). At each time-point liver from the left lateral lobe was immediately snap frozen, blood from a cardiac puncture was collected in serum separator tubes (Microtainr, BD Bioscences, San Jose, California, USA) and urine was collected in conical tubes containing sodium azide (1 mL, 1 % w/v water; NaN_3). Sera fractions were collected after the incubation of the collected blood at

room temperature for 30 minutes and subsequent centrifugation at 4000 g for 6 minutes. All samples were stored at -80^{o}C.

Liver histopathology

Tissue sections from the medial lobe of each animal were fixed with 10 % formalin overnight prior to dehydration, paraffin embedding and staining with haematoxylin and eosin (H & E). The liver sections were examined by light microscopy by a blinded board certified pathologist who scored the extent of liver necrosis with the following scoring criteria: 0 (no lesion), 1 (< 10 % lesion – minimal), 2 (10 – 25 % lesion; mild), 3 (25 – 40 % lesion; moderate), 4 (40 – 50% lesion; marked) and 5 (> 50 % lesion; severe).

Measurement of serum ALT activity

Serum ALT activity was calculated with a commercially available assay (Diagnostic Chemicals Limited, Charlottetown, Canada). Sera fractions were diluted with water (1:5) to a final volume of 10 µL. The samples were then placed in duplicate in a 96-well microtiter plate containing 100 µL of "ALT activity determination solution". The optical density at 340 nm of each mixture was measured for 2 minutes by a 96-well microplate reader (Gemini Spectromax, Molecular Devices, Sunnyvale, California, USA). The mean ALT activity from the two replicates was calculated with the following formula: (*conversion factor*) x (*dilution factor*) x (|*gradient*|).

Sample preparation and ^{1}H-NMR spectroscopy of hepatic aqueous-soluble component

Liver tissue metabolite extraction for NMR analysis was performed according to the protocol described by *Beckonert et al.* (Beckonert et al., 2007). Briefly, liver tissue samples (average weight of 41.4 mg and standard deviation (STD) ± 3.1 mg) were added to ice-cold

acetonitrile/water (1.5 mL, 1:1). The samples were homogenised with 5 mm stainless steel beads in a homogenizer (Qiagen Tissue Lyser, Retsch GmBH, Haan, Germany) at 25 Hz for 8 minutes. The samples were then kept on ice for 10 minutes prior to centrifugation at 17,000 g for 15 minutes at 4^{o}C (Biofuge Pico, Heraeus, Hanau, Germany). The supernatant was concentrated and dried overnight in a centrifugal evaporator (SpeedVac, Thermoscientific, Waltham, Massachusetts, United States) at 30^{o}C. The resultant dried supernatant was reconstituted in phosphate buffer (600 µL of a 0.2 M solution containing 99.9% D_2O, 3 mM sodium azide (NaN_3) and 1 mM 3-(trimethylsilyl)-[2',2',3,3'-$^{2}H_4$]-propionic acid sodium salt (TSP)), vortexed for 30 seconds and then centrifuged at 17,000 g for 15 minutes at 4 ^{o}C (Biofuge Pico). The supernatant (550 µL) was placed in 5 mm NMR tubes (NMR Precision tube 507-HP-7, Norell, Landisville, New Jersey, United States). NMR spectral data were acquired on a Bruker Avance-600 spectrometer operating at 600.13 MHz (14.1 T) ^{1}H frequency and at a temperature of 300 K using a Bruker TXI probe (Bruker Biospin, Rheinstetten, Germany) and an automated sample handling carousel (Bruker). A standard one-dimensional solvent suppression pulse sequence (noesypr1d) was used to acquire the FID (RD - 90° pulse- 4 µs delay - 90° pulse - mixing time - 90° pulse - ACQ) (Beckonert et al., 2007). The D_2O present in the buffer provided a field frequency lock, whilst the TSP was used as the chemical shift reference compound. For each experiment, 256 transients were collected into 64,000 data points using a spectral width of 12,000 Hz, with a relaxation delay of 4 seconds, mixing time of 100 ms and an acquisition time of 4.56 seconds. A line-broadening factor of 0.3 Hz was applied to all spectra prior to Fourier transformation (FT).

A summary of the ^{1}H-NMR acquisition parameters is presented in Table 8.1 in the appendix.

Sample preparation and ^{1}H-NMR spectroscopy of urine

Urine samples were prepared for ^{1}H-NMR analysis as previously described (Beckonert et al., 2007). Briefly, urine and phosphate buffer (2:1, 600 µL total volume, 0.2 M as above) were mixed by vortexing for 1 minute and centrifuged at 17,000 g for 15 minutes at 4 ^{o}C (Biofuge Pico). The resulting supernatants (550 µL) were then transferred to 5 mm NMR tubes (507-HP-7). NMR spectral data were acquired on a Bruker Avance-600 spectrometer operating at 600.13 MHz (14.1 T) ^{1}H frequency and at a temperature set at 300 K, using a Bruker TXI probe and an automated sampling handling carousel (Bruker). A standard one-dimensional solvent suppression pulse sequence was employed to acquire the FID of 256 transients, with a relaxation delay of 4 seconds, mixing time of 100 ms, spectral width of 12,000 Hz, 64,000 data points and an acquisition time of 4.56 seconds. A line broadening factor of 0.3 Hz was applied prior to FT. A summary of the ^{1}H-NMR acquisition parameters is presented in Table 8.1 in the appendix.

Sample preparation and ^{1}H-NMR spectroscopy of serum

Sera samples were thawed, vortexed for a period of 15 seconds and allowed to stand for 10 minutes before mixing with saline solution (1:1, 60 µL total volume; 99.9 % D_2O, 0.9 % NaCl and 1 mM TSP). The mixtures were then transferred to 1.7 mm capillary NMR tubes (Match tubes, Bruker). NMR spectral data were acquired on a Bruker Avance-600 spectrometer operating at 600.13 MHz (14.1 T) ^{1}H frequency and at a temperature set at 300 K, using a Bruker TXI probe and an automated sampling handling carousel (Bruker). A CPMG pulse sequence with a fixed spin-spin relaxation delay 2nτ of 64 ms (n = 160, τ = 200 µs), was used to acquire the spectra, with 158 transients, a relaxation delay of 2 seconds, mixing time of 100 ms and an acquisition time of 2.72 seconds. A line-broadening factor of 0.3 Hz was applied

to all spectra prior to FT. A summary of the ^{1}H-NMR acquisition parameters is presented in Table 8.1 in the appendix.

Processing of ^{1}H-NMR spectra

NMR spectra were imported to TopSpin 3.0 NMR software (Bruker) for manual phasing, baseline correction and calibration to the TSP for the aqueous-soluble hepatic extract and urine spectra, or the lactate peak for the serum spectra. Full resolution NMR data were then imported into MATLAB (R2012, Mathworks Inc., Natick, Massachusetts, USA) using an in-house script, for further processing including the removal of the TSP and water resonance regions before performing probabilistic quotient normalization in the aqueous-soluble hepatic extract and serum spectra data (Dieterle et al., 2006). Endogenous metabolite assignments were performed using chemometrics tools such as STOCSY (Cloarec et al., 2005a), COSY experiments, spectral databases (Human Metabolome Database (HMDB) and Biological Magnetic Resonance Bank (BMRB)), software including Chenomx NMR Suite (Chenomx Edmonton, Alberta, Canada) and previously published assignments in the literature (Waters et al., 2005, Nicholson et al., 1995). Finally, the following hepatic metabolites were identified by spike-in experiments with the pure standard compounds: phosphocholine, dimethylamine, GSSG, choline, succinate, 2-aminoadipate and adenosine monophosphate (AMP). Table 8.2 in the appendix presents more detailed assignments of identified metabolites in all matrices from all studies.

The spectral assignments of APAP and AMAP were also based on the existing literature (Bales et al., 1984, Holmes et al., 2007, Nicholls et al., 2006), STOCSY and two dimensional COSY and TOCSY experiments. In-house scripts were used to calculate the integral of resonances belonging to drug related and parent compounds in both groups, in order to estimate their

relative abundance to the parent molecule. The integrated resonances in the aqueous hepatic extract ^{1}H-NMR profiles were: APAP parent (δ^{1}H = 7.26), APAP-glucuronide conjugate (δ^{1}H = 7.15). APAP-glutathionyl conjugate (δ^{1}H = 6.96), APAP-N-acetylcysteinyl conjugate (δ^{1}H = 1.85), AMAP-glucuronide conjugate (δ^{1}H = 7.24) and AMAP parent (δ^{1}H = 7.03). The resonances used in the urine ^{1}H-NMR metabolic profiles were: APAP parent(δ1H = 6.88), APAP-glucuronide conjugate (δ^{1}H = 7.32), APAP-sulphate conjugate (δ^{1}H = 7.31), APAP-cysteinyl conjugate (δ^{1}H = 7.50), APAP-N-acetylcysteinyl conjugate (δ^{1}H = 1.86), AMAP-glucuronide conjugate (δ^{1}H = 7.24), AMAP-sulphate conjugate (δ^{1}H = 7.43), AMAP parent (δ^{1}H = 7.01) and APAP-methoxy conjugate (δ^{1}H = 3.88). Each integral was proton adjusted (divided by the number of protons it consists of) before the ratio to the parent molecule was calculated. Table 3.1 in the appendix presents more detailed assignments of AMAP/APAP DRCs, while Figure 8.1 in the appendix depicts the TOCSY/COSY spectra used to assign APAP metabolites in the urine.

GC-MS analysis of hepatic aqueous-soluble component

Liver tissue samples with an average weight of 25.25 mg and STD ± 0.22 mg were added to ice-cold HPLC grade water/methanol (1:1, 1.2 mL total volume) and homogenized with zirconia beads at 6,500 Hz (Precellys 24-Dual, Precellys, Montigny-le-Bretonneux, France) for two 45 seconds periods with an intermediate 5 minute cooling period on dry ice. The homogenized mixtures were incubated for 45 minutes on ice before centrifugation at 13,000 rpm for 15 minutes at 4 ^{o}C (Biofuge Pico). The resulting supernatants were mixed with ice cold methanol/water (2:1, 0.5 mL) prior to overnight incubation at -4 ^{o}C. The following day the samples were centrifuged again at 17,000 g for 15 minutes at 4 ^{o}C (Biofuge Pico).

Quality control (QC) samples were prepared by collecting 5 µL aliquots from each sample prior to drying overnight in a centrifugal concentrator (SpeedVac) at room temperature. The dried supernatants were then derivatized using the methoximation/silylation protocol described by Fiehn *et al*. (Fiehn, 2008). Briefly, U-^{13}C-D-Glucose (20 µL of a 1 mM solution in anhydrous pyridine) and myristic d_{27} acid (5 µL of a 6 mM solution in anhydrous pyridine) were mixed with the dried supernatants for quantitation purposes and retention time locking respectively. Methoxyamine hydrocholoride (40 µL of 0.3 M solution in anhydrous pyridine) was then added to each sample prior to incubation at 30 ^{o}C for 90 minutes with shaking at 30 minute intervals. The samples were then incubated with N-methyl-N-(trimethylsilyl) trifluoroacetamide (MSTFA; 90 µL) solution at 37 ^{o}C for 30 minutes. Finally, 2-fluorobiphenyl (10 µL of a 1 mM solution in anhydrous pyridine) was then added as an injection standard.

GC-MS analysis was performed on an Agilent 7890 gas chromatograph coupled to a 5975 mass selective detector quadruple mass spectrometer (Agilent Technologies, Santa Clara, California, USA) in accordance to the protocol described by Fiehn *et al*. (Fiehn, 2008). QC samples were set at the beginning of the run to condition the chromatographic column and at five sample intervals. The acquired GC-MS spectra were initially processed with the Automated Mass Spectral Deconvolution and Identification System software (AMDIS, NIST, Gaithersburg, Maryland, USA) by using the Fiehnlib library of compounds (Kind et al., 2009). An in-house script was used to import the spectra to MATLAB (Mathworks) where the chromatographic peaks of all identified metabolites were manually inspected. Prior to integration, features not consistently present in the QC samples were immediately removed (Behrends et al., 2011).

The GC-MS analysis led to the tentative assignment of 250 different species according to the Fiehn library (Fiehn, 2008), of which 50 were confidently assigned and 38 were statistically analysed. Reasons of further metabolite exclusion prior to analysis include poor chromatographic peak shape and peak overlap.

Initial examination of the raw data by PCA revealed a significant batch effect between the samples and QCs of the two experiments (Figure 3.1A). Furthermore, an exponential decay in signal intensity was observed in the majority of the metabolites in the QC samples over time in both batches (Figure 3.1B). This meant that the signal intensity of a specific metabolite would be significantly lower in the QC samples at the end of the experiment when compared to the QC samples used at the beginning of the experiment. The observed signal intensity decay was attributed to a combination of instrument instability and decay of the derivatization product.

In order to correct for the observed signal decay in the QC samples 3rd order polynomial curves were used (Dunn et al., 2011)(Figure 3.1B1). These functions were used to estimate the fractional change (decay factor) of the metabolite signal intensity as the experiment progressed, in order to project how the intensity of the metabolite would decay with respect to the position of the sample in the experiment. The decay factor for each metabolite in each sample, depending on sample position, was multiplied by the original recorded signal intensity of that metabolite in that sample. This permitted the interpolation of the metabolite intensity to the estimated value of the sample if it was at position one. The resulting PCA scores plot (Figure 3.1B2) revealed that a batch effect remained, which was expected since the QCs of the two batches (on which the polynomials were based on) were not previously clustered in multivariate space.

Following intra-batch normalization, inter-batch normalization was performed to account for the observed batch effect. Due to the significant range of signal intensity for different metabolites in each batch, a logarithmic scale was applied to the data to reduce the variance prior to normalization. The median intensity for each metabolite was then calculated in each batch and the factor difference between the medians of the two batches was calculated individually for each metabolite. The factor of each metabolite was then multiplied with the respective intensities in all of the samples in the second batch, which generally had a lower intensity value for all metabolites. This multiplication step led to an improved clustering of the two batches (Figure 3.1C), as verified by PCA (Wang et al., 2013a).

UPLC-MS analysis of hepatic aqueous-soluble component

Liver tissue samples (average weight of 42 mg and STD ± 2.8 mg) were added to ice-cold HPLC grade water/methanol (1:1, 1.2 mL total volume) and homogenized with zirconia beads at 6,500 Hz (Precellys 24-Dual) for two 45 seconds periods with an intermediate 5 minute cooling period on dry ice. The homogenized mixtures were incubated for 45 minutes on ice before centrifugation at 13,000 rpm for 15 minutes at 4 ^{o}C (Biofuge Pico). The resulting supernatants were mixed with ice cold methanol/water (2:1, 0.5 mL) prior to overnight incubation at -4 ^{o}C. The following day the samples were centrifuged at 17,000 g for 15 minutes at 4 ^{o}C (Biofuge Pico). The samples were then dried overnight in a centrifugal concentrator (SpeedVac) at room temperature. The following day the dried supernatants were reconstituted and mixed in an acetonitrile/water mixture (1:1, 240 µL total volume) and were then centrifuged at 17,000 g for 15 minutes at 4 ^{o}C. The resulting supernatants (170 µL) were then transferred to a 96-well plate. QC samples were prepared by aliquoting 30 µL from all the remaining supernatants into a pooled sample in a glass vial.

An Acquity UPLC instrument with an Acquity UPLC BEH HILIC chromatography column coupled to an ESI-TOF LCT Premier mass spectrometer (Waters Corp., Manchester, UK) was used to acquire the UPLC-MS data. A sample injection volume of 7.50 µL and an elution time of 21 minutes were used (Spagou et al., 2011). The solvent gradient used gradually changed from acetonitrile/water (19:1) to acetonitrile/water (1:1) with a flow rate of 0.4 mL/minute. The capillary voltage of the MS instrument was set at 3200 V and the sample cone was 35 V. Mass accuracy was ensured with a LockSpray interface (Waters Corp.) with leucine enkephalin (556.26 $[M+H]^+$ and 554.26 $[M-H]^-$ for positive and negative ionization modes respectively) as the mass standards. QC samples were set at the beginning of the run to condition the chromatographic column and at seven sample intervals.

An Acquity UPLC instrument with an Acquity UPLC BEH HILIC chromatography column coupled to a Xevo G2-S QTOF (Waters Corp.) was used for metabolite identity verification by MS/MS analysis. The UPLC-MS acquisition parameters were set as previously stated, while the collision cell voltage was set within the range of 10 kV and 40 kV. MS/MS analysis was used to verify the assignments of L-carnitine, acetylcarnitine, propionylcarnitine, adenosine, adenine, hypoxanthine, GSSG and APAP.

The UPLC-MS spectra were processed with MarkerLynx (version 4.1; Waters Corp.) for peak detection and marker collection for both ionization methods. The mass boundaries were set between 50 and 1000 m/z while the intensity threshold was set at 800 for the positive polarity and 600 for the negative mode. The data were normalized by probabilistic quotient normalization (Dieterle et al., 2006). Features with CV coefficient of variation (QVcv) greater than 30 % were removed prior to analysis. TargetLynx (version 4.1; Waters Corp.) was used in a targeted method, with the pure chemical standard, to detect and quantify the positive ion

adduct, $[M+H]^+$, of L-carnitine (m/z = 162.115). A 0.2 min retention time deviation window was used before peak integration.

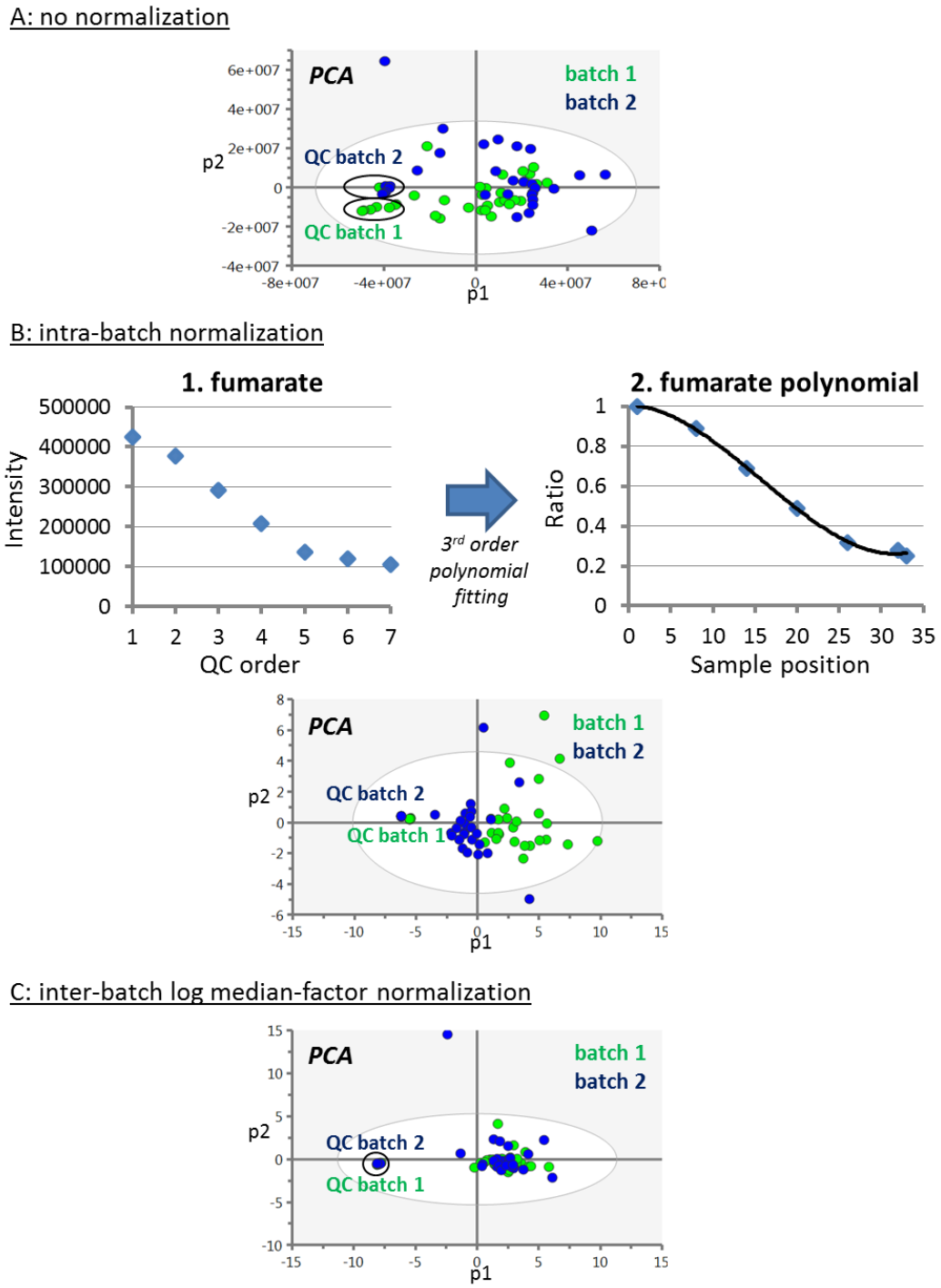


Figure 3.1: The three steps of the normalization procedure employed for GC-MS normalization are depicted above. A detailed description is provided in the following page QC – quality control; PCA – principal component analysis

Statistical analysis

PCA models were initially constructed to obtain an overview of the NMR, UPLC-MS and GC-MS data following pre-processing and normalization (SIMCA 13.0; Umetrics, Umea, Sweden). O-PLS-DA was employed to analyse the NMR (serum and hepatic extract component) and the UPLC-MS data in MATLAB (Mathworks) and SIMCA (Umetrics) respectively. In order to avoid data over-fitting, a seven fold cross validation, R^2Y (goodness of fit) and Q^2Y (predictive ability) were used. All O-PLS-DA models were tested for statistical significance at $p < 0.05$ with permutation testing (*n* = 1000 for class membership). A heatmap presenting the Pearson correlation coefficient values (R) of the identified discriminatory resonances from the serum and hepatic extract NMR O-PLS-DA models was constructed with an R cut-off value of |0.5|. Prism 5.0 (Graphpad, La Jolla, California, USA) was used for non-parametric univariate statistical analysis (Kruskal-Wallis coupled to Dunn's multiple test correction) of the liver histopathology, clinical chemistry, GC-MS derived integrals and UPLC-MS derived carnitine integrals, with a statistical significance threshold set at $p < 0.05$.

Results

Serum clinical chemistry and liver histopathology

Serum ALT activity (U/L) was measured for the APAP, AMAP and control groups at 1hr, 3hr and 6hr post-treatment (Figure 3.2A). APAP administration led to a statistically significant increase of ALT activity at 1hr, 3hr and 6hr ($p < 0.05$), relative to control levels, while AMAP administration did not lead to a statistically significant change at all time-points. At 6hr, the APAP group had an average ALT activity of 2052 U/L (STD ± 1486 U/L), while the average ALT activities of the control and AMAP groups were 14.5 U/L (STD ± 21 U/L) and 11.8 U/L (STD ± 10 U/L) respectively. The histopathological analysis which scored the severity of hepatic necrosis revealed that APAP administration caused minimal and mild necrosis at 3hr and 6hr respectively, relative to the control group. In contrast, the administration of AMAP did not lead to an AMAP-induced lesion in the 6 hour timeframe (Figure 3.2B).

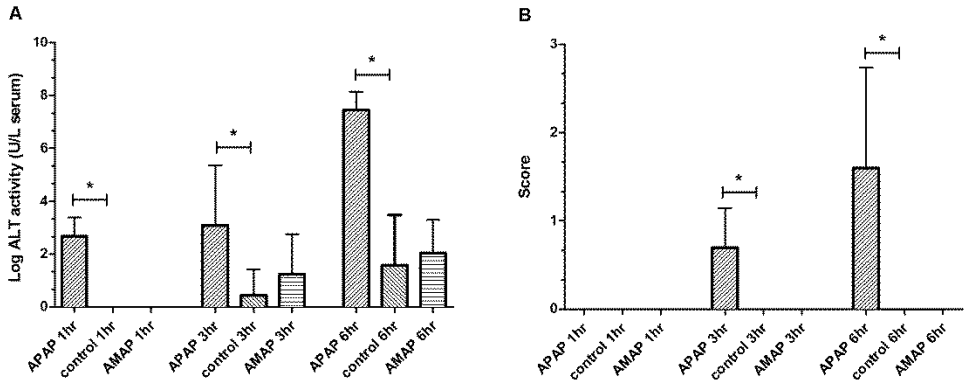


Figure 3.2: The mean and standard deviation of the log serum ALT activities (A) and histology necrosis scores (B) in the three treatment groups (n = 5 for APAP and AMAP and n = 7 for control per time-point) are shown above. Statistical significance is indicated by the asterisk (*; $p < 0.05$). The scoring criteria are: 0 = no significant lesions, 1 = minimal, 2 = mild, 3 = moderate.

APAP and AMAP metabolism

In the hepatic extracts of the APAP treated group, the APAP-glucuronide, glutathionyl conjugates, APAP parent and the N-acetylcysteinyl conjugate were detected at 1hr in order of abundance. Similarly, the AMAP-glucuronide conjugate was the most concentrated drug

related metabolite in the AMAP treated group, while the AMAP parent was also detected at lower levels at the 1hr time-point (Figure 3.3; Figure 3.6A).

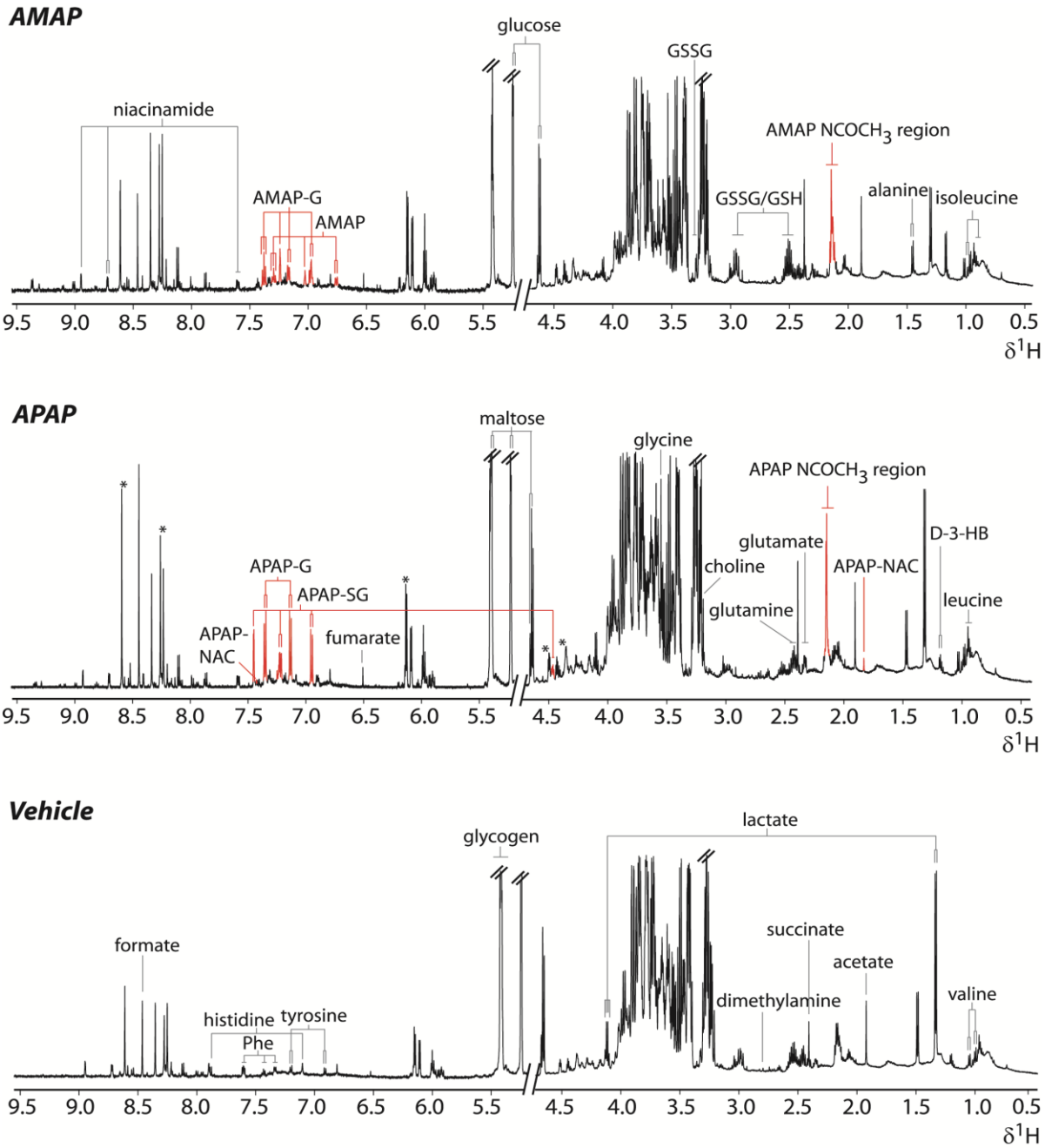


Figure 3.3: Representative ^{1}H-NMR spectra of the hepatic extract metabolic profiles for each treatment group at 1hr. DRC resonances are coloured in red. Please note that the respective intensities of the high and low field regions are not equal. APAP-G – APAP glucuronide conjugate; APAP-SG – APAP glutathionyl conjugate; APAP –NAC – APAP N-acetylcysteinyl conjugate; AMAP-G – AMAP glucuronide conjugate; asterisk – APAP methoxy conjugate; APAP/AMAP $NCOCH_3$ – Overlapped APAP/AMAP and conjugate N-acetyl resonances; D-3-HB – D-3-hydroxybutyrate; Phe – phenylalanine; asterisks – AMP resonances.

In the serum metabolic profiles at 1hr, the APAP parent and APAP-glucuronide conjugate were detected in the APAP treated groups, while the AMAP-glucuronide conjugate was the only detected DRC in the AMAP treated group (Figure 3.4).

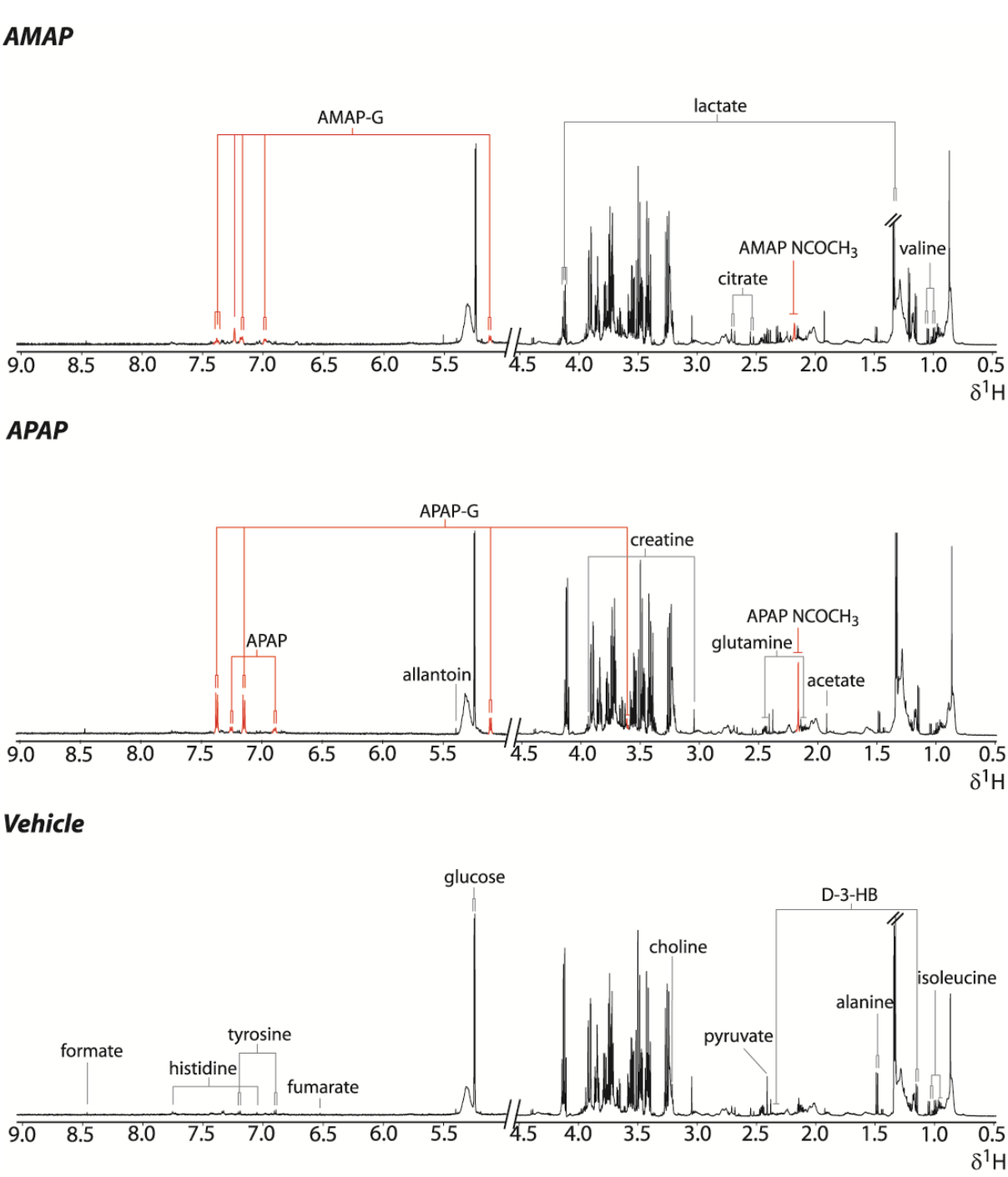


Figure 3.4: Representative ^{1}H-NMR spectra of the serum metabolic profiles for each treatment group at 1hr. Please see legend of Figure 3.3.

In the urinary metabolic profiles of the APAP treated group at 1hr, the APAP-glucuronide conjugate, APAP parent, sulphate, cysteinyl and N-acetylcysteinyl conjugates were detected

in order of abundance. In the respective AMAP treated group, the AMAP-glucuronide, sulphate and APAP-methoxylated conjugates as well as the parent molecule, were detected in order of concentration (Figure 3.5; Figure 3.6B).

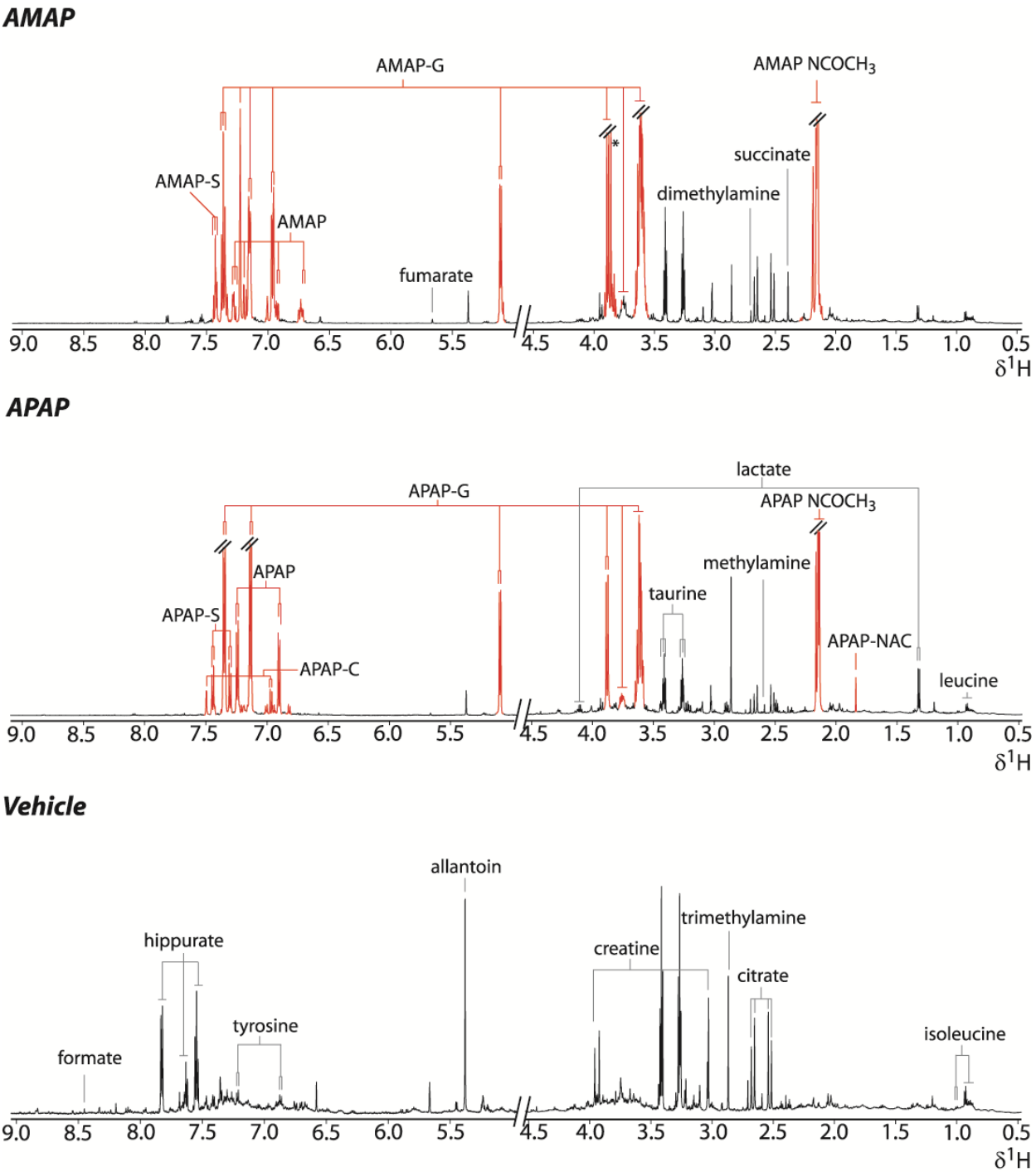


Figure 3.5: Representative ^{1}H-NMR spectra of the urinary metabolic profiles for each treatment group at 1hr. Please see legend of Figure 3.3. APAP-C – APAP cysteinyl conjugate; asterisk – APAP methoxylated conjugate; AMAP-S – AMAP sulphate conjugate

In summary, the glucuronide conjugate was the most abundant metabolite for AMAP and APAP in all sample matrices. There was no evidence of an AMAP-glutathionyl, cysteinyl or N-acetylcysteinyl conjugates in all sample matrices. The assignments of all assigned DRCs are shown in Table 3.1. Please note that due to extensive overlap, it was not possible to assign all of the resonances arising from some compounds.

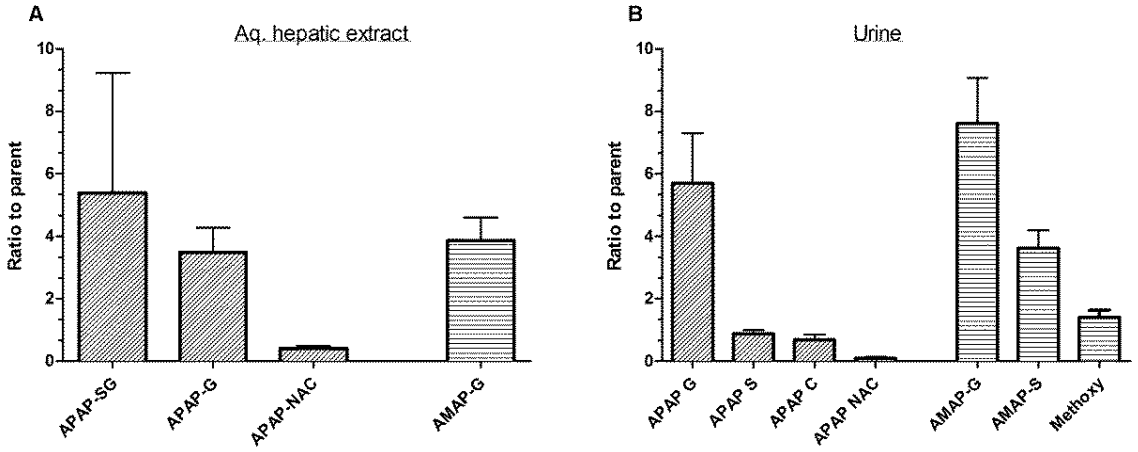
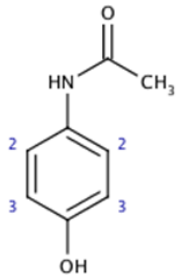


Figure 3.6: The mean and standard deviations of the integral DRC ratios relative to APAP or AMAP (*n* = 5 for each treatment group) in the hepatic extracts (A) and urine (B) metabolic profiles at 1hr are depicted. -G – glucuronide conjugate; -SG – glutathionyl conjugate; NAC – N-acetylcysteinyl conjugate ; -C – cysteinyl conjugate; -S, sulphate conjugate; Methoxy – methoxylated conjugate.

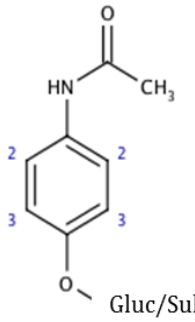
^{1}H-NMR spectroscopic detected endogenous changes in hepatic extracts after APAP and AMAP administration

The ^{1}H-NMR metabonomic analysis of the hepatic extracts revealed that the concentrations of glutathione (reflecting both oxidized and reduced forms – resonance δ 2.54) was statistically significantly lower after the administration of APAP at 1hr (2 fold change) and 3hr (1.4 fold change) post-treatment (Figure 3.7). In contrast, the administration of AMAP did not induce a visible change to glutathione levels at all time-points.

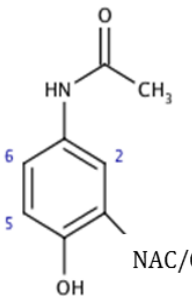
APAP



APAP-G/-S

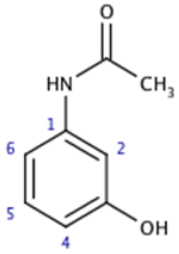


APAP-NAC/-Cys

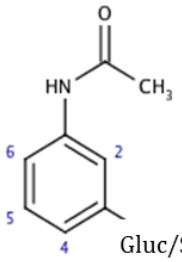


Metabolite	Species	Chemical shift (ppm)	Multiplicity	J-coupling (Hz)
Serum				
APAP	H2	7.26	d	8.44
	H3	6.90	d	8.44
APAP-G	H2	7.37	d	8.90
	H3	7.15	d	8.90
	H1’	5.11	d	7.17
	Ha	2.17	s	-
Hepatic extract				
APAP	H2	7.26	d	8.85
	H3	6.92	d	8.85
	Ha	2.15	s	-
APAP-G	H2	7.37	d	8.93
	H3	7.15	d	8.93
	H1’	5.11	d	7.43
	Ha	2.17	s	-
APAP-SG	H2	7.47	s	-
	H5	6.97	d	8.70
	H6	7.23	dd	8.70
	Ha	2.16	s	-
APAP-NAC	H2	7.44	s	-
	NAC-CH_3	1.85	s	-
Urine				
APAP	H2	7.26	d	8.82
	H3	6.91	d	8.82
	Ha	2.15	s	-
APAP-G	H2	7.37	d	8.89
	H3	7.15	d	8.89
	H1’	5.11	d	7.43
	Ha	2.17	s	-
APAP-S	H2	7.46	d	8.89
	H3	7.32	d	8.89
	Ha	2.18	s	-
APAP-NAC	NAC-CH_3	1.86	s	-
APAP-Cys	H2	7.50	s	-
	H5	6.98	d	8.70

AMAP

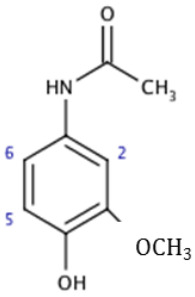


AMAP-G/-S



Gluc/Sulfate

APAP-O-CH_3



Metabolite	Species	Chemical shift (ppm)	Multiplicity	J-coupling (Hz)
Serum				
AMAP-G	H2	7.24	s	-
	H4	6.98	d	8.74
	H5	7.37	t	7.56
	H6	7.18	d	8.74
	H1'	5.13	d	6.96
	Ha	2.17	s	-
Hepatic extract				
AMAP	H2	7.03	s	-
	H4	6.76	d	8.58
	H5	7.29	t	8.16
	H6	6.97	d	8.58
	Ha	2.17	s	-
AMAP-G	H2	7.24	s	-
	H4	6.98	d	8.51
	H5	7.38	t	8.18
	H6	7.17	d	8.51
	H1'	5.13	d	7.19
	Ha	2.18	s	-
Urine				
AMAP	H2	7.02	s	-
	H4	6.75	d	8.48
	H5	7.28	t	8.16
	H6	6.94	d	8.48
	Ha	2.16	s	-
AMAP-G	H2	7.24	s	-
	H4	6.98	d	8.50
	H5	7.36	t	8.29
	H6	7.16	d	8.50
	H1'	5.11	d	7.43
	Ha	2.17	s	-
	H5	7.44	t	7.89
	Ha	2.18	s	-
APAP-O-CH_3	-O-CH_3	3.86	s	-

Table 3.1: The assigned resonances of AMAP and APAP related molecules are depicted above. AMAP/APAP-G – AMAP/APAP glucuronide conjugate; AMAP/APAP-S – AMAP/APAP sulphate conjugate; APAP-NAC – APAP N-acetylcysteinyl conjugate; APAP-Cys – APAP cysteinyl conjugate; APAP-O-CH_3 – APAP methoxylated conjugate; s – singlet; d – doublet; ppm – parts per million; Hα – -$NCOCH_3$ resonance.

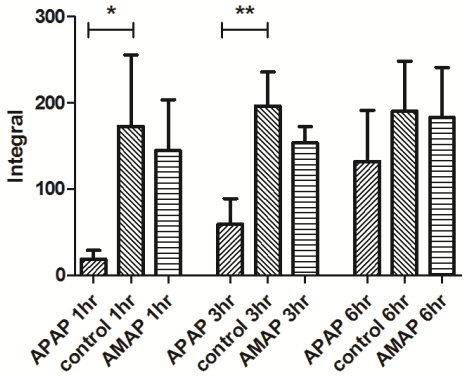


Figure 3.7: The mean and standard deviation of total glutathione integrals from the hepatic extracts metabolic profiles from the three different treatment groups , at all time-points groups (*n* = 5 for APAP and AMAP and *n* = 7 for control per time-point), are shown above. Statistical significance, tested by Kruskal-Wallis analysis coupled to Dunn's multiple test correction, is indicated by the asterisks (*) and (**) representing $p < 0.05$ and $p < 0.01$ respectively.

The hepatic metabolic effect of each xenobiotic at each of the three different time-points relative to the control group was characterized by pair-wise O-PLS-DA models. The O-PLS-DA model describing the metabolic effect of APAP at 1hr relative to control (Figure 3.8A, R^2Y = 0.9955 and Q^2Y = 0.5083) revealed a complete discrimination in the predictive component of the scores plot (Tcv, Figure 3.8A1). The corresponding loadings coefficient plot showed that endogenous metabolite level perturbations included the elevation in the levels of succinate, glycine, fumarate and formate, as well as the depletion of glutathione in the APAP group. The robust O-PLS-DA model of the hepatic extracts NMR profiles characterizing the effect of APAP at 3hr, relative to control, (Figure 3.8B, R^2Y = 0.9820 and Q^2Y = 0.4497; $p < 0.05$) achieved partial discrimination in the scores plot (Tcv, Figure 3.8B1). The equivalent coefficient plot (Figure 3.8B2) revealed that APAP administration led to the elevation of leucine, glutamate, succinate, fumarate and 2-aminoadipate, as well as the depletion of AMP and glutathione. Finally, the O-PLS-DA model describing the effect of APAP at 6hr (Figure 3.8C, R^2Y = 0.9758 and Q^2Y = 0.4716; $p < 0.05$) achieved partial separation between the two groups in the scores plot (Tcv, Figure 3.8C1). The corresponding coefficient plot (Figure 3.8C2) showed that APAP caused an elevation in the levels of glutamate, D-3-hydroxybutyrate (D-3-HB), acetate, 2-

aminoadipate and leucine, as well as depletion in the levels of glucose, glycogen, AMP and glutathione.

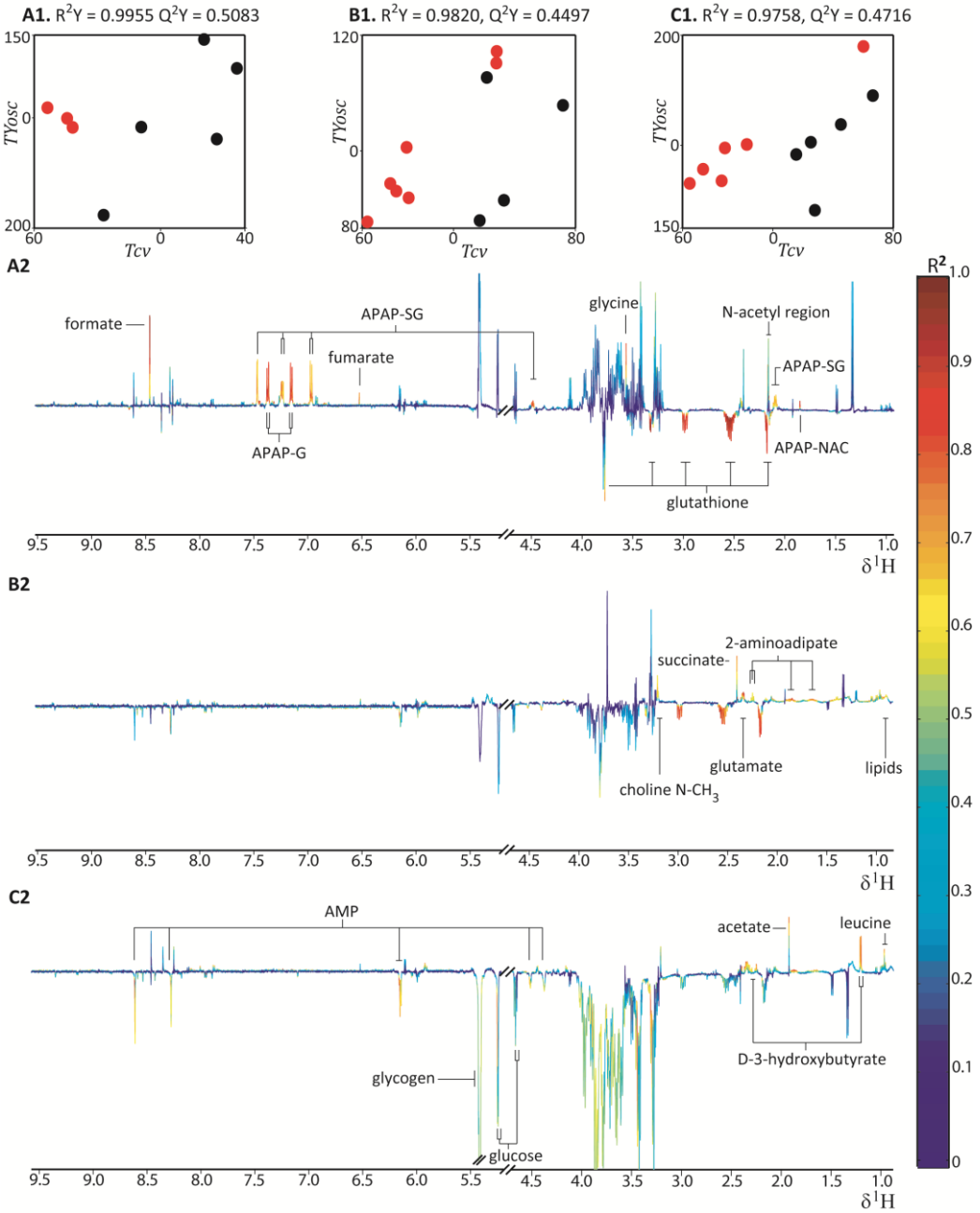


Figure 3.8: O-PLS-DA of the hepatic extract ^{1}H-NMR spectra of the APAP-treated group versus the control group at 1hr (A), 3hr (B) and 6hr (C) post-treatment. The scores plots (A1, B1 and C1) show the separation of the APAP (black) and control (red) samples where Tcv is the predictive component and TYosc is the orthogonal component. The coefficients plots (A2, B2 and C2) illustrate the discriminatory metabolites between the groups. Resonances pointing up indicate an increase in that specific resonance in the APAP group and vice versa. The Pearson correlation scale (R^2) ranges from low (0; blue) to high (red; 1). The models were validated at $p < 0.05$ using 1000 permutations. (*n* = 5 for APAP 1hr and APAP 6hr, while *n* = 4 for APAP 3hr, *n* = 3 for Ctrl 1hr, *n* = 7 for Ctrl 3hr and *n* = 6 for Ctrl 6hr)

The O-PLS-DA models constructed to describe the ^{1}H-NMR hepatic metabolic effect of AMAP relative to the control group at 1hr ($R^2Y = 0.9940$, $Q^2Y = 0.6844$) achieved complete separation between the groups in the predictive component of the scores plot. The equivalent coefficient plot revealed that AMAP administration led to the elevation of D-3-HB and the concomitant depletion of dimethylamine, glucose and glutamine, relative to control levels. The O-PLS-DA models characterizing the effect of AMAP at 3hr and 6hr were of low predictive ability, as deduced by the Q^2Y values, and were therefore not further analysed.

Overall, the O-PLS-DA of the hepatic extracts metabolic profiles revealed that APAP had a progressively more disruptive metabolic effect, as suggested by the increasing amount of metabolic perturbations overtime. In contrast the metabolic effect of AMAP was restricted to 1hr. A summary of the identified metabolic effects of APAP and AMAP can be viewed in the form of a heatmap in Figure 3.10 which displays the Pearson correlation value with a cut off value of |0.5|.

Serum O-PLS-DA of APAP and AMAP administration

Pair-wise O-PLS-DA models were computed to describe the serum metabolic effect of APAP and AMAP relative to the control group at the 1hr, 3hr and 6hr time-points. The O-PLS-DA models of the sera ^{1}H-NMR spectroscopic profiles that discriminated between APAP and the control groups at 1hr and 3hr were of low predictive ability, as deduced by the Q^2Y values and permutation testing, and were therefore not further analysed. The O-PLS-DA model describing the effect of APAP relative to control at 6hr (Figure 3.9A; $R^2Y = 0.8737$ and $Q^2Y = 0.4352$; $p < 0.05$) achieved a degree of discrimination in the predictive component of the scores plot (Figure 3.9A1). The corresponding coefficients plot (Figure 3.9A2) showed that

APAP administration led to the elevation of glutamine and acetate and the concomitant depletion of alanine and pyruvate.

The O-PLS-DA models constructed to reveal the discriminatory metabolites between the AMAP administration group and the control group at 1hr (Figure 3.9B; $R^2Y = 0.9703$ and $Q^2Y = 0.6037$; $p < 0.05$) achieved partial separation between the two groups in the predictive component of the scores plot (Figure 3.9B1. The corresponding coefficients plot (Figure 3.9B2) revealed that AMAP led to an increase in the levels of citrate and D-3-HB and depletion in the levels of alanine, betaine and lactate. The O-PLS-DA model describing the metabolic effect of AMAP administration at 3hr, relative to control, (Figure 3.9C; $R^2Y = 0.8957$ and $Q^2Y = 0.4635$; $p < 0.05$) achieved partial separation between the two groups in the scores plot (Figure 3.9C1). The corresponding coefficients plot (Figure 3.9C2) showed that AMAP administration caused a decrease in the levels of betaine, alanine and creatine. The O-PLS-DA model describing the metabolic effect of AMAP on serum at 6hr was of low predictive ability, as deduced by the Q^2Y and permutation testing, and was therefore not further analysed.

The metabolic effect of APAP in the serum was more pronounced at 6hr, while the metabolic effect of AMAP was restricted to the early time-points of 1hr and 3hr, reflecting the results of the aqueous soluble hepatic extract analysis' results. A summary of the APAP and AMAP induced metabolic effects in the serum can be seen in Figure 3.10.

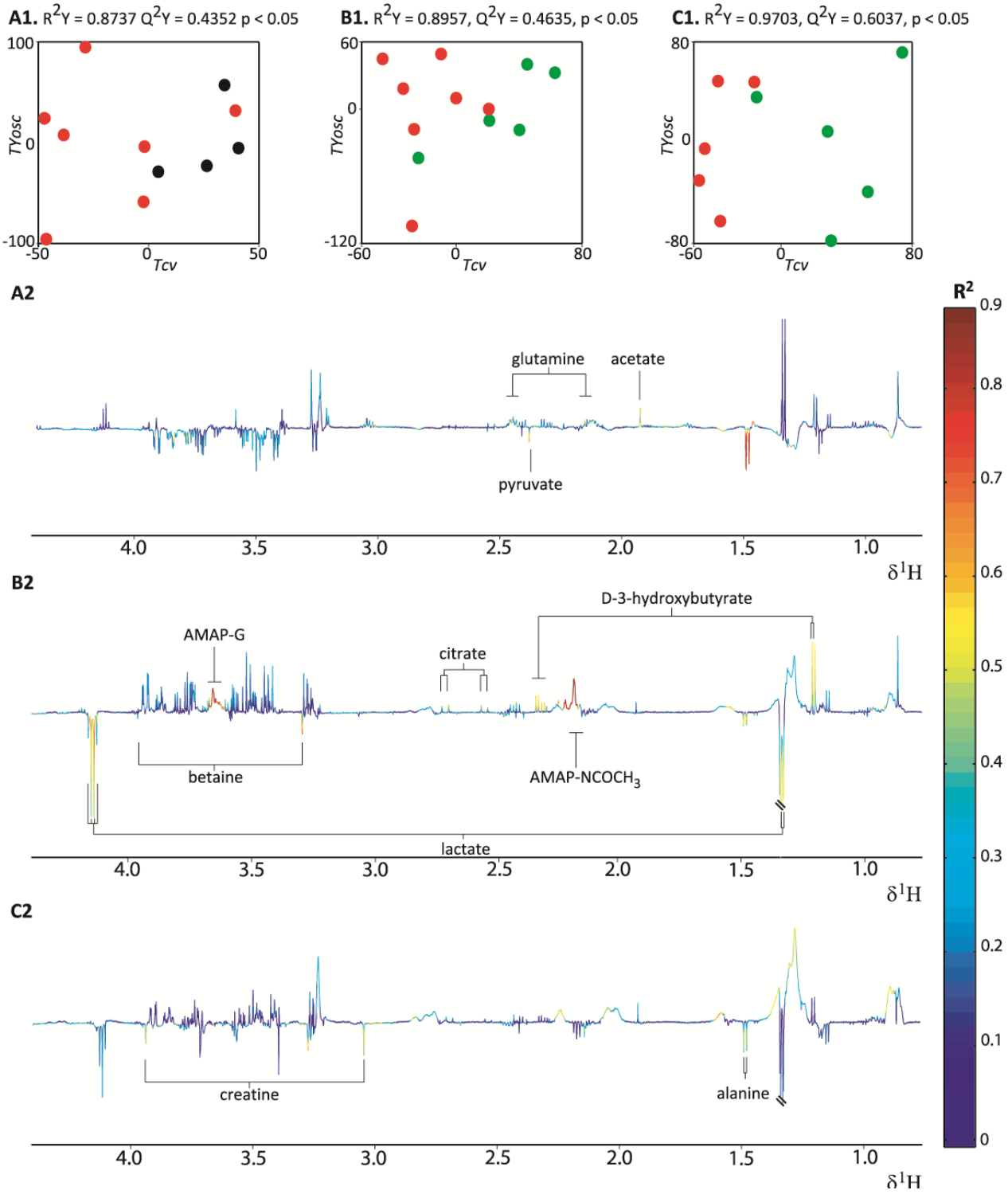


Figure 3.9: O-PLS-DA models of the serum ^{1}H-NMR spectra of the APAP-treated group (*n* =5) versus the control group at 6hr (*n* = 7; A) and AMAP-treated group (*n* = 5) versus the control group at 1hr (*n* = 7; B) and 3hr (*n* = 5 and *n* = 5 for the AMAP treated and control groups respectively; C). The scores plots (A1, B1 and C1) show the separation of the APAP (black) and control (red) samples, as well as AMAP (green) and control (red) samples. Please see legend of Figure 3.8. AMAP-G – AMAP glucuronide conjugate. AMAP-NCOCH3 – AMAP and conjugates N-acetyl resonance.

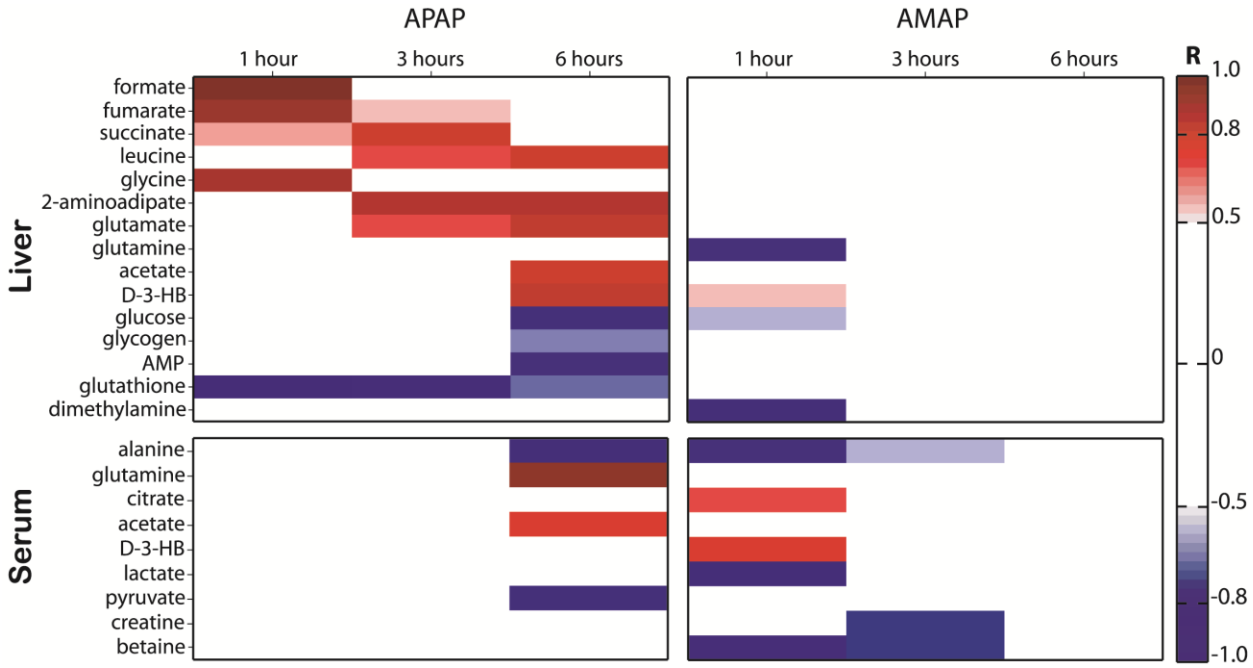


Figure 3.10: A summary of the discriminatory metabolites assigned in the O-PLS-DA models of the hepatic extracts and serum metabolic profiles after APAP/AMAP administration. Positive correlation values (red colour) indicate an increase in the levels of a metabolite and vice versa (blue colour). A |0.5| Pearson correlation (R) value cut-off point was used. D-3-HB - D-3-hydroxybutyrate; AMP – adenosine monophosphate.

HILIC-UPLC-MS analysis of hepatic extracts and carnitine

HILIC-UPLC-MS analysis was used to characterize the hepatic metabolic perturbations associated with AMAP and APAP administration. Initially, a PCA trajectory plot was constructed to map the trajectory of the HILIC-UPLC-MS hepatic metabolic profiles after APAP and AMAP administration overtime, relative to the control groups at each time-point (Figure 3.11; R^2X = 0.5110, Q^2X = 0.4740). The PCA trajectory analysis revealed unique hepatic metabolic trajectories for both AMAP and APAP across time. At the 1hr time-point, the metabolic profiles of the AMAP-treated group were distinct from those of the control and APAP treated groups but at 3hr and 6hr post-AMAP administration, the hepatic extract metabolic profiles clustered with those of the control groups. The hepatic extract metabolic profiles 1hr post-APAP administration were distinct from those of the AMAP and control groups at 1hr. At 3hr and 6hr post-APAP administration, the hepatic metabolic profiles of the

APAP treated groups did not return to control levels (as determined by the multivariate space clustering) revealing a maintained perturbed metabolic homeostasis at 6hr post-treatment and a different trajectory from that of AMAP (Figure 3.11).

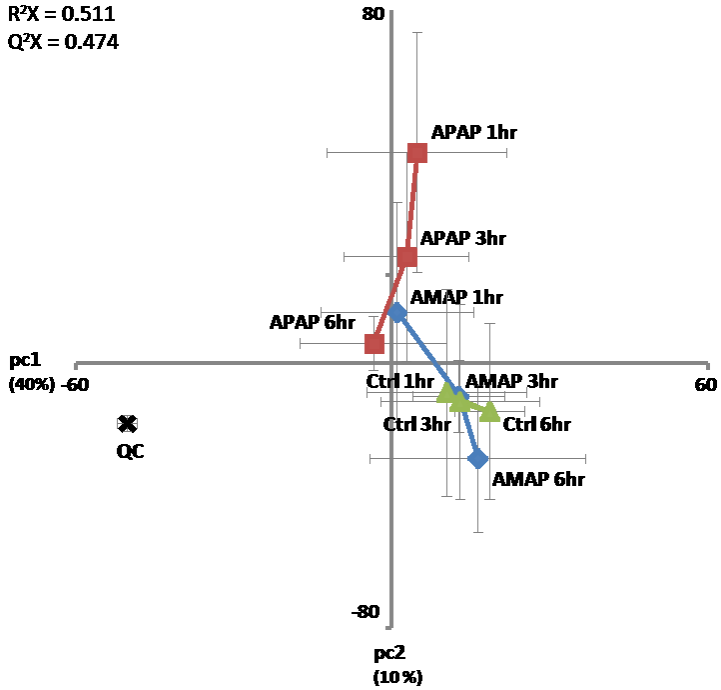


Figure 3.11: PCA trajectory plot of HILIC-UPLC-MS hepatic extract analysis. The first and second principal component (pc1 and pc2 respectively) average values and standard deviations were calculated for each group. The APAP-treated (*n* = 5), AMAP-treated (*n* = 5) and control groups (*n* = 7) at all time-points are shown in red, blue and green respectively, while the QCs are shown in black.

Following the PCA trajectory plot, O-PLS-DA was subsequently employed to discriminate the metabolic profile of APAP and AMAP relative to the control group at each time-point. The O-PLS-DA model (positive polarity) describing metabolic effect of APAP administration relative to control at 1hr (Figure 3.12; $R^2Y = 0.9590$, $Q^2Y = 0.6940$, $p < 0.05$) achieved complete separation in multivariate space (Tcv; Figure 3.12A) and the corresponding S-plot (Figure 3.12B) revealed that the levels of hypoxanthine, GSSG and L-carnitine were depleted after APAP administration, while the levels of adenosine, adenine and the APAP-glucuronide conjugate (tentatively assigned) were at higher levels (Figure 3.12B). Following the discovery that L-carnitine was one of the most significant discriminatory metabolites of the APAP-

treated group at 1hr, it was decided to conduct a targeted analysis on carnitine metabolism since this class of metabolites was not characterized by ^{1}H-NMR spectroscopy.

The targeted analysis of the data acquired in positive polarity showed that free carnitine (L-carnitine; m/z = 162.114) was statistically significantly depleted at 1hr in the APAP cohort, relative to the control cohort as calculated by TargetLynx (Waters Corp.) and tested with the Kruskal-Wallis test coupled to Dunn's multiple test correction (Figure 3.12C). The levels of free carnitine in the APAP-treated cohort were not statistically significantly different at 3hr and 6hr from those of the control group, while AMAP was not observed to have an effect at any time-point. Figure 3.12D illustrates the mass fragmentation pattern of L-carnitine. Other carnitine conjugates were detected during the targeted analysis but were not found to be statistically significantly different between all treated groups at all time-points.

GC-MS analysis of hepatic extracts

The GC-MS analysis of the hepatic extracts revealed that APAP-administration led to the statistically significant elevation of guanosine, xanthine and nicotinamide at 1hr and the depletion of hypotaurine and thymine at 3hr (Table 3.2). At 6hr, APAP administration led to the elevation of phosphoenolpyruvate, 3-phosphoglycerate and uracil, as well as the concomitant depletion of hypotaurine, AMP, inosine monophosphate, adenosine, methionine and aspartate. The respective analysis characterizing the metabolic effect of AMAP revealed a statistically significant elevation of guanosine at 1hr while there were not any observed statistically significant changes at the later time-points. A summary of the xenobiotic-induced statistically significant effects in the aqueous soluble hepatic extracts after GC-MS analysis is presented in Table 3.2. Overall the GC-MS analysis results revealed a similar pattern to that observed in the ^{1}H-NMR spectroscopic analysis.

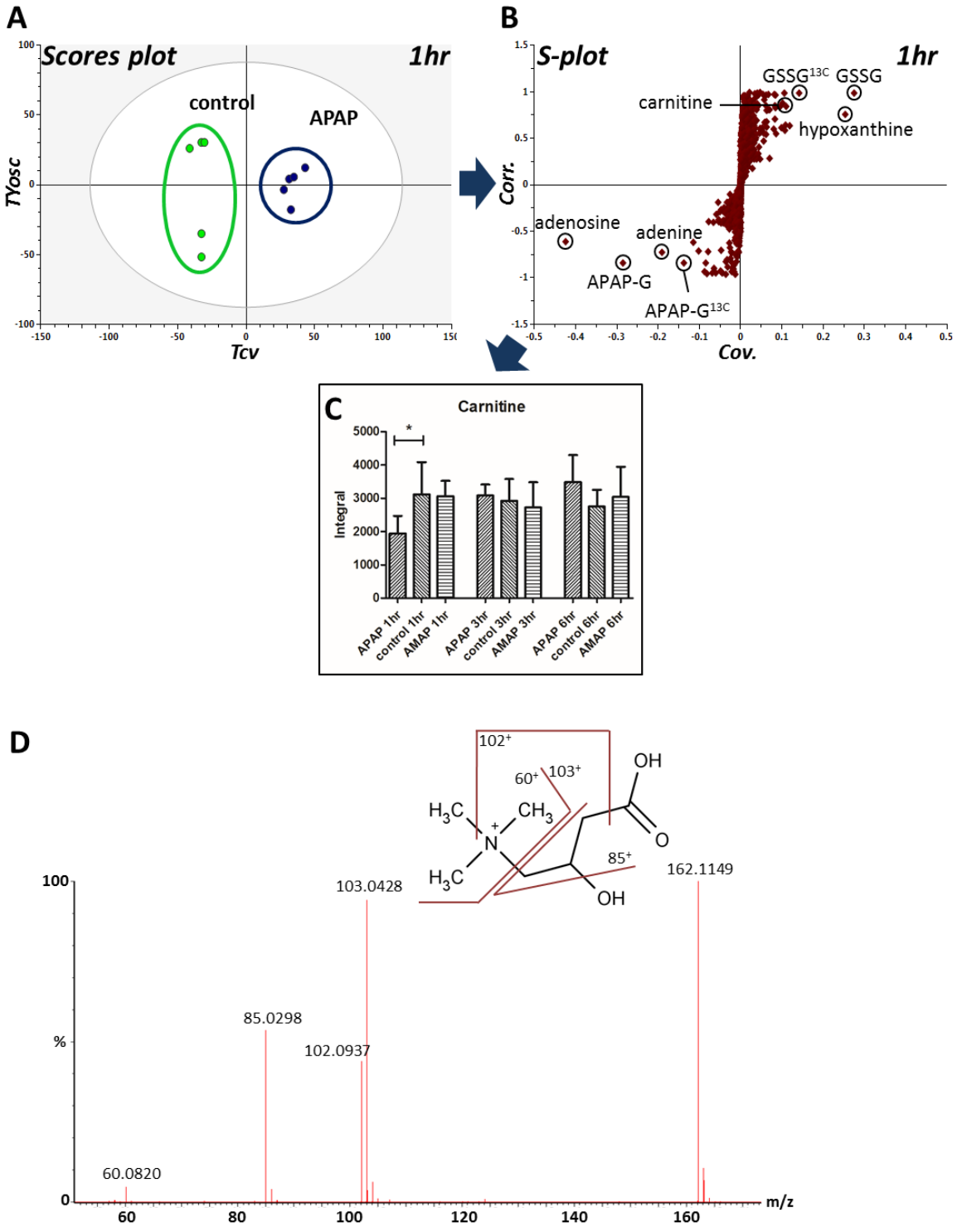


Figure 3.12: The O-PLS-DA hepatic extract model scores and S-plots (positive polarity data) describing the metabolic effect of APAP (*n* =5) relative to the control (*n* = 7) at 1hr are depicted above (A and B respectively). The mean and standard deviation of the L-carnitine integrals (m/z 162.115 $[M-H]^+$) in each treatment group (*n* = 5 for APAP/AMAP and *n* = 7 for control per each time-point) is shown at C and the fragmentation pattern of carnitine by MS/MS is also depicted (D). Kruskal-Wallis tests coupled to Dunn's multiple test correction was used to determine statistical significance which is signified by the asterisk (*), representing $p < 0.05$. GSSG – oxidized glutathione; APAP-G – APAP glucuronide conjugate (tentatively assigned); 13C – molecule isotope with an additional ^{13}C atom (+1 in m/z).

Treatment group	Time-points					
	1hr		3hr		6hr	
	Elevated	Depleted	Elevated	Depleted	Elevated	Depleted
APAP	guanosine* xanthine* nicotinamide*			hypotaurine** thymine*	3-PG* PEP** uracil*	hypotaurine** AMP* IMP* adenosine* methionine* aspartate*
AMAP	guanosine*					

Table 3.2: Summary of the statistically significant discriminatory metabolites from the GC-MS analysis of the hepatic extracts after APAP/AMAP administration (*n* = 5 at each time-point per treatment group) relative to control (*n* = 7 at each time-point). Statistical significance is represented by the asterisks (*) and (**) which signify $p < 0.05$ and $p < 0.01$ respectively. PEP – phosphoenolpyruvate; 3-PG – 3-phosphoglycerate; AMP – adenosine monophosphate; IMP – inosine monophosphate.

Discussion

APAP and AMAP metabolism in C57BL/6 mice

The ^{1}H-NMR spectroscopic profiling of the serum, hepatic extract and urine matrices characterized and contrasted the biotransformation products of the two xenobiotic compounds. The glucuronide conjugate was consistently the most abundant DRC in all three sample matrices for both treatment groups, as also reported in the literature in Swiss-Webster mice (Rashed et al., 1990). The most significant difference between the observed DRCs of the two administered compounds was the absence of glutathionyl conjugate related molecules after in the AMAP administration groups. In contrast, the APAP-glutathionyl and N-acetylcysteinyl conjugates were detected in the hepatic extract metabolic profiles, while the APAP-cysteinyl and APAP-N-acetylcysteinyl were observed in the urine. The presence of glutathione conjugates in the hepatic extract and urinary metabolic profiles post-APAP administration corroborated the observed APAP-induced depletion of hepatic glutathione at 1hr and 3hr, relative to control levels. In contrast, the absence of AMAP glutathionyl conjugates and of an AMAP-induced depletion of hepatic glutathione suggested that the administration of AMAP did not lead to oxidative stress. It is however likely that AMAP metabolism did lead to the formation of reactive quinones and subsequent glutathione conjugates which were simply below the detection limit of NMR or where excreted through the bile, as reported (Rashed and Nelson, 1989a). Moreover, previous studies in the mice have suggested that the majority of AMAP quinones in Swiss-Webster mice are formed through the 3-OH-APAP intermediate (common metabolite with APAP), whose methoxylated derivative was detected in the metabolic profiles of the AMAP treated group at 1hr post-

treatment (Rashed and Nelson, 1989a, Rashed et al., 1990) and therefore further suggesting the formation of undetected AMAP derived reactive quinones.

APAP administration leads to hepatotoxic endpoint characterized by oxidative and energetic stress

Liver histopathology and clinical chemistry inferred that the APAP-induced oxidative stress resulted in hepatocellular cell death at 3hr and 6hr. The metabolic effect of APAP was visible from the early 1hr time-point and was deemed to be, as deduced by the highest number, in terms of metabolic perturbations, maximal at the 6hr time-point in all sample matrices. The progressive nature of the APAP-induced metabolic effect and the histopathological evidence of liver necrosis reveal that the hepatocytes did not recover from the initial toxic insult, which led to oxidative stress (visible from the 1hr time-point) and subsequently resulted in a disruption of homeostasis and eventual cell death.

The depletion of hepatic glutathione at 1hr and 3hr post-APAP administration resulted in other downstream hepatic metabolic effects, such as the consumption of hypotaurine at 3hr and 6hr and methionine at 6hr, as observed by the GC-MS analysis. Glutathione depletion will cause a higher rate of glutathione synthesis, which will lead to a higher rate of utilization and subsequent depletion of cysteine. Lower levels of cysteine would lead to the consumption of other sulphur containing compounds, including methionine and hypotaurine in order to replenish cysteine stocks. Methionine can be converted to cysteine through homocysteine in the transsulfuration pathway (Lu, 1999), while hypotaurine is a downstream metabolite of cysteine. *In*-vitro studies have shown that methionine levels are decreased in response to oxidative stress through the formation of cysteine (Panayiotidis et al., 2009), while liver hypotaurine depletion has also been reported to occur in response to drug-induced oxidative

stress (Jung et al., 2013). Finally, a previous investigation has demonstrated that APAP administration can lead to hepatic hypotaurine and methionine depletion in rats (Yamazaki et al., 2013).

APAP-induced oxidative stress, coupled to the covalent binding of NAPQI to mitochondrial proteins, can cause mitochondrial dysfunction which results in energetic stress (Jaeschke et al., 2012). NAPQI has been reported to bind to mitochondrial proteins such as glutamate dehydrogenase (Halmes et al., 1996), aldehyde dehydrogenase (Landin et al., 1996), succinate dehydrogenase (part of mitochondrial complex II in the electron transport chain) (Dixon, 1984, Katyare and Satav, 1989) and the α-subunit of ATP synthetase (Qiu et al., 1998). Covalent modification of mitochondrial proteins will impair their function and lead to a loss of mitochondrial homeostasis. The perturbation of mitochondrial protein function could explain the elevated hepatic levels of succinate and fumarate at 1hr and 3hr, as well as glutamate at 3hr and 6hr. However, another possible hypothesis for the observed elevations of fumarate and succinate is that the disruption of mitochondrial function led to a decreased rate of utilization of Krebs cycle intermediates, leading to the early elevation in the levels of succinate and fumarate (Burcham and Harman, 1991) (Figure 3.13).

APAP-induced mitochondrial impairment has already been reported to decrease mitochondrial ATP production (Katyare and Satav, 1989), which could trigger an upregulation of glycolysis as a compensatory mechanism. This hypothesis is supported by the observed concomitant depletion of glucose and glycogen coupled with the elevation in the levels of D-3-hydroxybutyrate and acetate at 6hr after APAP administration which could be indicative of energetic stress and a shift to glycolysis, as previously suggested by other metabonomic studies (Coen et al., 2003, Coen et al., 2004). Furthermore, an upregulation of glycolysis and

an increased consumption of glucose would lead to a rise in the levels of glycolytic intermediates such as phosphoenolpyruvate and 3-phosphoglycerate, as observed in the GC-MS analysis of the hepatic extracts at 6hr post APAP-administration (Figure 3.13).

Another class of metabolites that is closely associated with mitochondrial function is free carnitine and the acylcarnitine conjugates. Fatty acid molecules bind to carnitine in order to be transported into the mitochondria for fatty acid β-oxidation to take place (Bremer, 1983). In addition to its role in fatty acid metabolism, carnitine is also known for its anti-oxidative properties during drug-induced oxidative stress (Yapar et al., 2007). The observed depletion of hepatic carnitine at 1hr could therefore be indicative of oxidative stress and early mitochondrial dysfunction through the impairment of β-oxidation impairment (Figure 3.13). Serum carnitine has been reported to be depleted in humans after exposure to APAP (Nowaczyk et al., 2000), while the serum levels of carnitine conjugates have also been reported to be elevated in mice shortly after APAP administration (Chen et al., 2009) and humans (McGill et al., 2014a). It is worth noting that the time scale required by APAP-induced toxicity to affect the levels of carnitine (in the serum or liver) compared to the latter observed metabolic effects, suggests that the inhibition of β-oxidation could be an early milestone of mitochondrial dysfunction as previously hypothesized (Chen et al., 2009).

In addition to the perturbation of energy metabolites, APAP administration was also observed to affect nitrogenous base containing compounds. The NMR and GC-MS analysis revealed that AMP was depleted at the 6hr time-point after post APAP administration while the GC-MS analysis also revealed other perturbations in the levels of nucleobases (uracil and thymine) and nucleosides (adenosine) throughout the duration of the study. The UPLC-MS analysis also showed a general APAP-induced perturbation in the levels of adenosine related molecules,

such as hypoxanthine and adenine. However, since adenosine, adenine and hypoxanthine are all derivatives of AMP it might be possible that the energy associated with molecule ionization in the MS source could lead to the fragmentation of the parent compound and therefore the apparent perturbations of the levels of these metabolites might not be directly linked to the metabolic effect of APAP. This hypothesis is also supported by MS/MS experiments which revealed that the AMP ion ($[M+H]^+$; m/z = 348.064; data not shown) was fragmenting to the smaller nucleosides and nitrogenous bases. APAP has been previously suspected to have a general effect on the levels of nitrogenous base compounds through DNA damage (Bessems and Vermeulen, 2001) and the inhibition of adenosine deaminase (Ataie et al., 2004). Furthermore, it is has also been hypothesized that an APAP-induced degradation of adenine nucleotides is an attempt to produce more energy as a response to the depletion of ATP (Tirmenstein and Nelson, 1990). A summary of the observed hepatic metabolic and toxic effect of APAP is shown in Figure 3.14.

Finally, the general delay observed in the metabolic effect of APAP in the serum metabolic profiles, relative to the liver, was expected since the liver is the primary site of APAP metabolism and would therefore be the first site to develop drug-induced metabolic changes. The lower levels of both pyruvate and alanine at 6hr post-APAP treatment could be linked to the potential up-regulation of gluconeogenesis in response to the aforementioned hepatic glucose depletion (Exton, 1972). However, this observation is in contrast to what has been reported in a different strain of mice (Coen et al., 2003) and the underlying reason for this discrepancy is not clear.

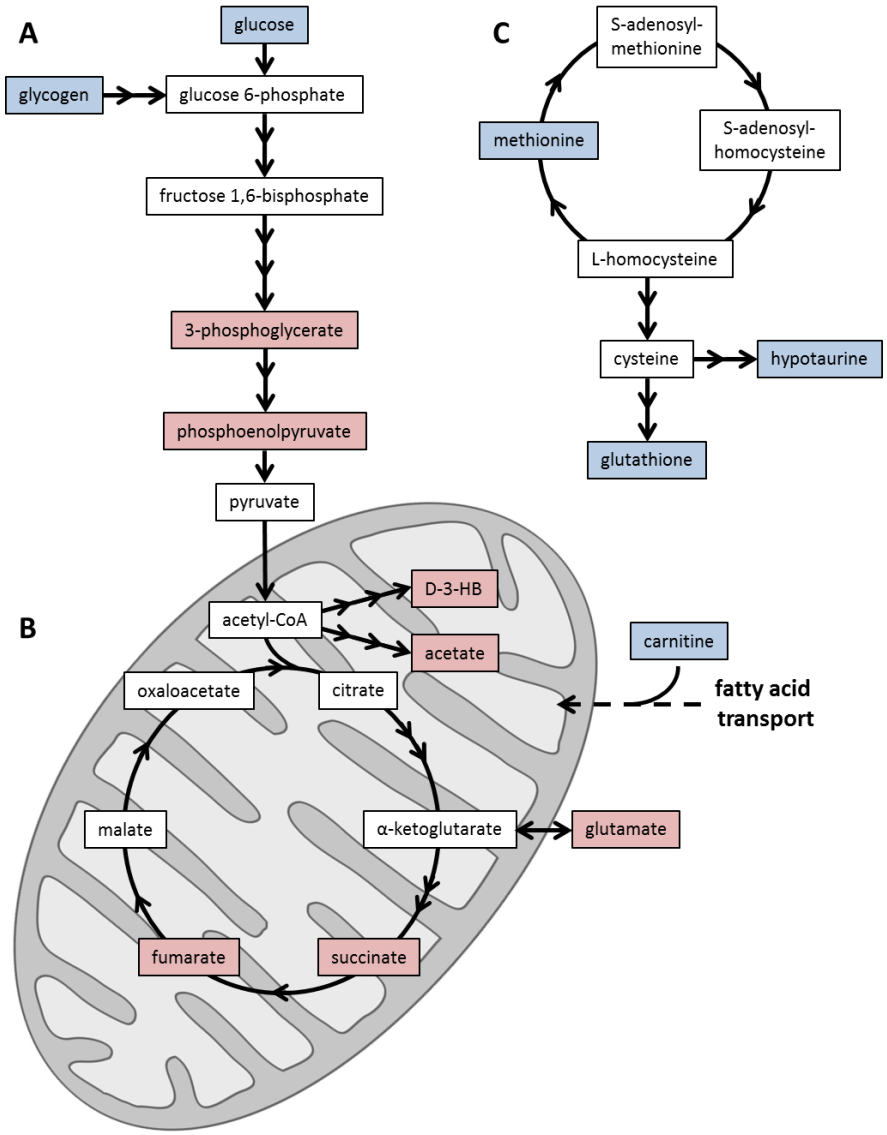


Figure 3.13: Summary of metabolic perturbations associated with APAP-induced mitochondrial dysfunction and oxidative stress. Diagrammatic representations of the glycolysis pathway (A), Krebs cycle (B) and glutathione synthesis (C) are shown. Red shading depicts APAP-induced elevations, while blue shading represents APAP-induced depletions. D-3-HB – D-3-hydroxybutyrate.

AMAP administration leads to a reversible non-hepatotoxic endpoint

The clinical chemistry and histopathology results did not reveal any signs of AMAP-induced liver damage and were therefore in agreement to the drug metabolism analysis, where the reactive metabolites of AMAP were not observed to cause oxidative stress or form glutathione adducts. Relatively lower concentrations of AMAP related quinones have also been reported by previous investigations which noted that the mercapturic acid conjugates

of AMAP in Swiss-Webster mice represented 5% of the dose (600 mg/kg), while the mercapturic and cysteinyl conjugates of APAP comprised of approximately 20 % of the APAP dose (250 mg/kg) (Rashed et al., 1990). Assuming that the administration of APAP and AMAP result in a comparable hepatic exposure, the literature findings coupled to the results of this study, suggest a difference in their propensity for bioactivation or their relative affinity for alternative routes of metabolism, such as glucuronidation or sulphation. Furthermore, this hypothesis is also supported by a recent computer simulation (DILIsym) which suggested that the difference of toxicity between the two compounds exists due to a quantitative difference in the amount of reactive metabolite formed by APAP and AMAP. This is understood to be due to the inability of the AMAP parent molecule to be directly oxidized to a quinone by CYP enzymes, as well as the reported CYP 2E1 inhibition by AMAP-related reactive metabolites (Howell et al., 2014, Halmes et al., 1998).

The interpretation of the metabolic effects of AMAP was difficult because of their transient nature. It is interesting however that AMAP had a more pronounced metabolic effect in the serum at 1hr and 3hr relative to control, in comparison to the metabolic effect of APAP. This could be an indication that the hepatic metabolic effect of AMAP is more immediate, as previously suggested (Potter et al., 1974, Roberts et al., 1990), while it is also indicative of non-critical protein binding since the effect was transient and did not lead to an observable liver damage. Finally, another possible explanation of the early AMAP-induced metabolic effect is that AMAP might be metabolized at other sites other than the liver, but this is less likely since the liver has the highest concentration of CYP enzymes.

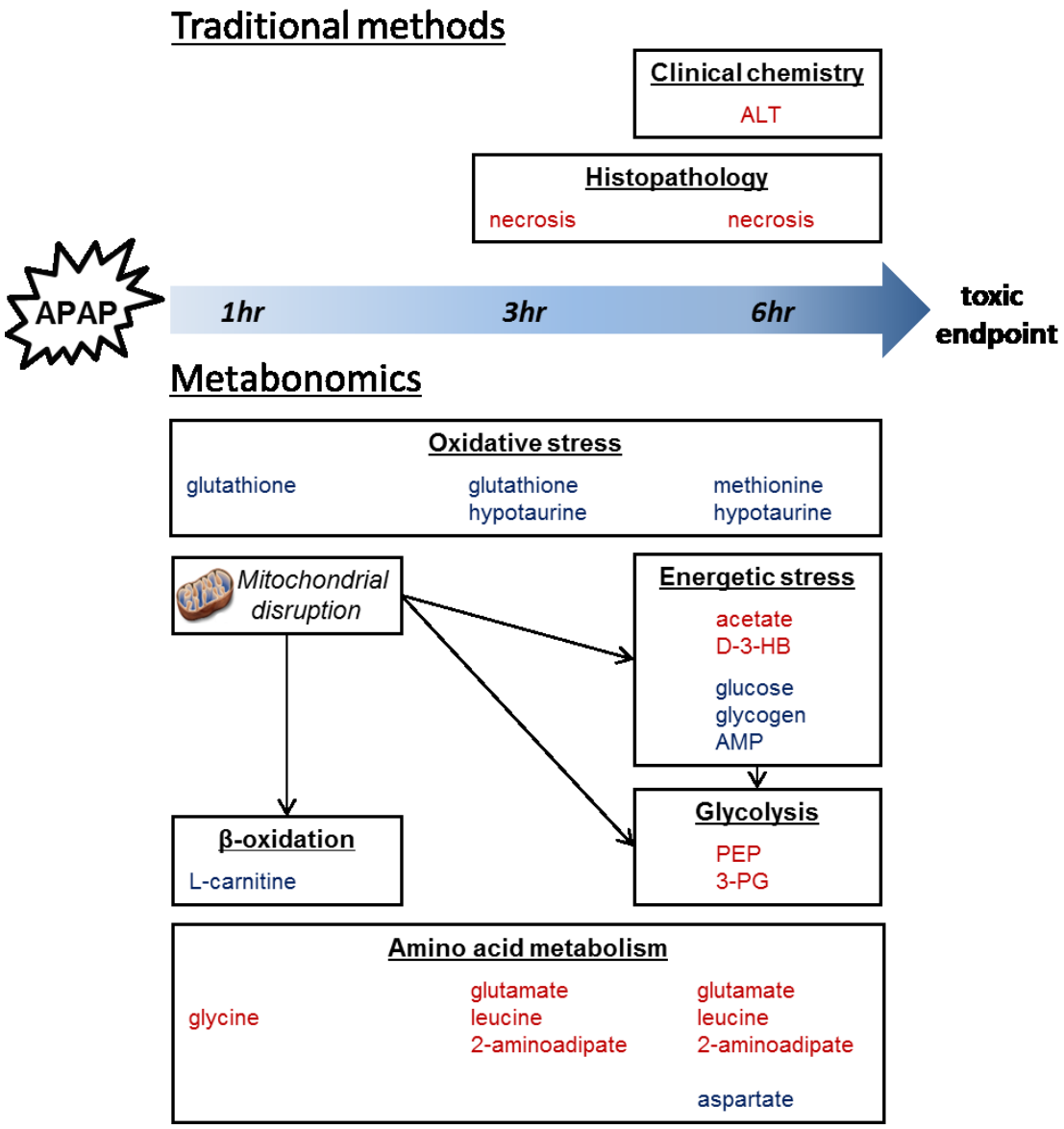


Figure 3.14: The interpreted APAP-induced hepatic metabolic changes at each of the time-points are shown above. Elevated metabolites are shown in red while depleted metabolites are shown in blue. PEP – phosphoenolpyruvate; 3-PG – 3-phosphoglycerate; ALT – alanine amino transferase.

Study limitations

The absence of data revealing the degree of covalent binding of the reactive metabolites of each compound at the selected dose rendered the direct comparison of their metabolic effects more difficult because it was not possible to determine whether the contrasting metabolic differences were simply the result of a smaller amount of AMAP quinones being formed. It is worth noting however that using relative amounts of APAP and AMAP which

result to a similar degree of covalent binding might not be the optimal way of comparing their contrasting toxicities because their reactive metabolites interact with different proteins (Roberts et al., 1990). Ideally, a dose response study with a low non-toxic dose, a mid and a high toxic dose would have facilitated the contextualization of the metabolic effects induced by each compound, as well as the separation of the pharmacological and toxicological effects. This is especially true for AMAP, where higher doses could have led to a greater potential of causing an adverse effect, as reported in rat and human liver slices (Hadi et al., 2012). Finally, another important limitation of this study was the absence of animal food intake records. Energy metabolite levels were expected to be perturbed since APAP is hypothesized to cause toxicity through mitochondrial dysfunction but the extent of contribution of a potential reduced dietary intake to the observed metabolic effect is unknown.

Chapter 4: Metabolic characterization of a model of non-alcoholic steatohepatitis

The hepatic extract and urine analysis presented in this chapter have been previously published (Kyriakides et al., 2014). A copy of the publication is provided in the appendix.

Introduction

Study details and aims

The work in this chapter presents the metabonomic characterization of the MCD diet model in rats. Specifically, hepatic aqueous-soluble extract, faecal water and urine ^{1}H-NMR spectroscopic metabolic profiles of rats fed with either a normal or MCD diet are described. The aim of this investigation was to generally characterize the baseline metabolic profile of the MCD diet model of NASH in order to further understand the metabolic perturbations associated with the hepatic physiological changes, as induced by the MCD diet relative to the control diet. The metabonomic analysis of the three sample matrices would also facilitate the characterization of the systemic metabolic changes hypothesized to be associated with the physiological effects of this condition.

Methods

This study was conducted in parallel to the work presented in Chapter 5, where the metabolic consequences of MTX administration in rats fed with either a control or MCD diet were investigated. The methods relevant to both chapters are presented below. The animal handling and treatment was conducted by our collaborators at the University of Arizona, Tucson, Arizona, USA.

Animal handling and treatment

Male Sprague-Dawley rats (*n* = 44, Harlan Laboratories; Indianapolis, IN) were housed in an AAALAC-accredited animal facility for one week prior to the initiation of the experiments, where they were acclimated to 12-hour light and dark cycles. The rats were then split randomly into the two diet groups (*n* = 20 and *n* = 22 for the control and MCD diet group respectively) and were provided ad libitum tap water and either fed a choline sufficient and amino-acid defined diet or the equivalent methionine-choline deficient diet (Dyets Inc; Bethlehem, PA) for a period of 8 weeks. Each diet group was then randomly split to four different treatment groups which were administered either 10, 40, 100 mg/kg of MTX (0.3 M sodium bicarbonate ;Toronto Chemicals; Toronto, Canada; *n* = 5 per dose group per diet; *n* = 6 for 100 mg/kg in the MCD diet group) or vehicle (*n = 5;* 0.3 M sodium bicarbonate) via a single intra-peritoneal injection.

Faecal samples were collected at two pre-dose time periods, baseline, (-12 to -6 and -6 to 0 hours; 0hr; *n* = 36 and *n* = 42 for the control and MCD diet respectively) and at a single post-dose time period (36 – 48 hours; 48hr). Urine samples were collected at a single pre-dose time period, baseline, (-6 to 0 hour collection; 0hr; *n* = 21 and *n* = 22 for the control and MCD diet respectively) and across the following time periods (*n* = 5 per MTX dose group per diet; *n*

= 6 for 100 mg/kg MTX in the MCD diet): 6 - 12 (12hr), 18 -24 (24hr) and 36 - 48 (48hr) hours post-dose. At 96 hours post-dose, animals were euthanized (*n* = 5 per MTX dose group per diet; *n* = 6 for 100 mg/kg MTX in the MCD diet) via CO_2 asphyxiation and liver samples were collected. All samples were immediately snap frozen after collection and stored at -80 °C.

Liver histopathology and imaging

Histomorphologic examination of the medial lobe from the liver tissue of each animal was carried out by fixing it in 10% neutral-buffered formalin for 24 hours and then placing it in 70% ethanol until paraffin embedding and H & E staining. Liver sections were examined by light microscopy by a board certified blinded veterinary pathologist for liver necrosis, inflammation, fibrosis, lipid accumulation and biliary hyperplasia. The scoring criteria were as follows: 0 (no lesion), 1 (<10% lesion; minimal), 2 (10 - 25 % lesion; mild), 3 (25 - 40 % lesion; moderate), 4 (40 - 50 % lesion; marked) and 5 (>50 % lesion; severe).

Sample preparation and ^{1}H-NMR spectroscopy of urine

The protocol for sample preparation and ^{1}H-NMR spectroscopy of urine was performed as previously described in Chapter 3. NMR spectral data were acquired on a Bruker Avance-600 spectrometer operating at 600.13 MHz (14.1 T) ^{1}H frequency and at a temperature of 300 K using a Bruker TXI probe and an automated sample handling carousel (Bruker). A standard one-dimensional solvent suppression pulse sequence was used to acquire the FID as described previously. The acquisition parameters can be seen in Table 8.1 in the appendix.

Sample preparation and ^{1}H-NMR spectroscopy of faecal water

Faecal samples were prepared for ^{1}H-NMR analysis as previously described in the literature (Saric et al., 2008). Briefly, 50 mg of faecal sample from each rat (average of 49.98 mg and STD ± 2.64) was mixed with phosphate buffer (1.1 ml, 0.2M final concentration, 99 % D_2O)

containing NaN_3 (3.3 mM) and TSP (1 mM). The mixture was homogenized thrice for 40 seconds, each followed by a five minute cooling down period on ice. The resulting homogenate was then centrifuged at 17,000g for 20 minutes and then 700 µl of the supernatant was centrifuged again at 14,000 g for 5 minutes. Finally 550 µl of the final supernatant was then transferred to an NMR tube for spectral acquisition. A standard one-dimensional solvent suppression pulse sequence and CPMG spin-echo pulse sequence were used to acquire the FID. The acquisition parameters can be seen in Table 8.1 in the appendix.

Sample preparation and ^{1}H-NMR spectroscopy of hepatic aqueous-soluble extracts

The general protocol for liver metabolite extraction and ^{1}H-NMR spectroscopy of the hepatic aqueous-soluble extracts was performed as previously described in Chapter 3. The weighed liver tissue samples had a mean weight of 52.5 mg and a standard deviation of ± 0.73 mg. NMR spectral data were acquired on a Bruker Avance-600 spectrometer operating at 600.13 MHz (14.1 T) ^{1}H frequency and at a temperature of 300 K, using a Bruker TXI probe and an automated sample handling carousel (Bruker). A standard one-dimensional solvent suppression pulse sequence and CPMG spin-echo pulse sequence were used to acquire the FID. The acquisition parameters can be seen in Table 8.1 in the appendix.

^{1}H-NMR spectral data processing

The NMR spectra were processed in TopSpin 3.0 NMR software (Bruker) and MATLAB (Mathworks) as described in Chapter 3. Processing prior to alignment and normalization included the removal of the TSP, tartrate, water and glucosan resonances from the hepatic aqueous-soluble component spectra, the removal of the ethanol, methanol, urea, water, glucosan, TSP and tartrate resonances from the urinary spectra and finally the removal of TSP, tartrate, ethanol and water resonances from the faecal water spectra. Spectral assignments

were performed using STOCSY, spectral databases (in-house, Human Metabolome Database and Biological Magnetic Resonance Bank), Chenomx NMR Suite and previously published assignments (Nicholson et al., 1995, Waters et al., 2005, Saric et al., 2008). The assignments of uracil, hypoxanthine, inosine, uridine, maltose, mannose, choline, phosphocholine and glycine in the hepatic aqueous-soluble extracts, sarcosine, propionate, isovalerate and 5-aminovalerate in the faecal water and dimethylamine, methylamine, phenylacetylglycine, putrescine, 3-indoxylsulphate, tartrate, glucosan and taurine in the urine were confirmed by addition of the pure standard compounds ('spike-in' experiments). Please note that the glutathione assignment in the hepatic extracts refers to total hepatic glutathione (sum of oxidized and reduced glutathione), while dihydroxyacetone and choline have been tentatively assigned in the faecal water metabolic profiles.

Statistical analysis

Multivariate statistical tools were employed to analyse the ^{1}H-NMR spectroscopic data of the urine, faecal water and hepatic extracts. O-PLS-DA in MATLAB (Mathworks, using in-house scripts) was subsequently performed, which discriminated between the two diets. The pre-dose time periods (0hr) of the urine and faecal water spectra were compared, while the vehicle groups were compared in the hepatic extracts. Area normalization was used in the faecal extract analysis and probabilistic normalization was used for the urinary and hepatic extract analysis. The models were validated by permutation testing ($p < 0.05$, $n = 1000$) and the results are presented in the form of a heatmap as discussed in Chapter 3. Prism 5.0 (Graphpad) was used for non-parametric univariate analysis (Kruskal-Wallis tests coupled to the Dunn's multiple test correction). A significance threshold value of $p < 0.05$ was set throughout.

Results

Liver histopathology

Liver was histopathology scored for liver necrosis, liver inflammation, lipid accumulation, biliary hyperplasia and liver fibrosis. The MCD diet was observed to be characterized by marked lipid accumulation, mild liver necrosis and moderate liver inflammation, while there were no signs of biliary hyperplasia or liver fibrosis (Figure 4.1). The control diet group did not have any observed histopathology.

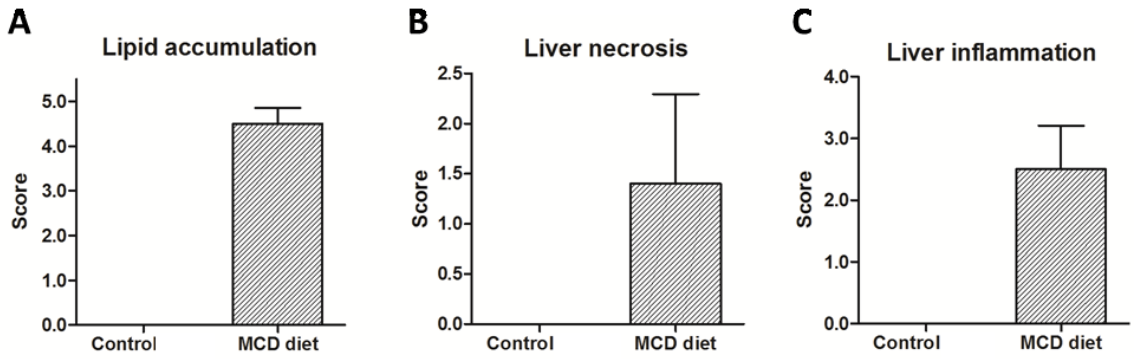


Figure 4.1: Histopathology scores representing lipid accumulation (A), liver necrosis (B) and liver inflammation (C) (mean and standard deviation) of the vehicle groups in both the control and MCD diet groups (*n* = 5 for each) are depicted above. The scoring criteria are: 0 = no significant lesions, 1 = minimal, 2 = mild, 3 = moderate, 4 = marked and 5 = severe. Veh – Vehicle.

Animal body weight

The body weight of the animals was recorded at the beginning and at the end of the study. At the beginning of the study, the control diet animals had an average weight of 391 g (STD ± 40 g) whilst the animals fed with the MCD diet had an average weight of 202 g (± 10 g), while minimal weight loss was recorded by the end of the study (Figure 4.2). The weight difference of the two different diet groups was statistically significant at both time-points ($p < 0.05$).

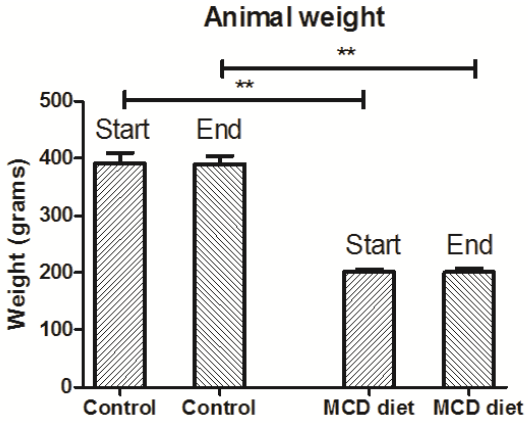


Figure 4.2: The mean and standard deviation of the weight of the animals at the beginning of the study (Start) and at the end (End) for both diet groups (*n* =5 for each group) are shown above. Statistical significance is indicated by the asterisks (**), representing $p < 0.01$.

Hepatic metabolic phenotype of the NASH model

Pair-wise O-PLS-DA models were constructed to identify the discriminatory metabolites between the two diet groups in the hepatic aqueous soluble component. A robust O-PLS-DA model (Figure 4.3A; $R^2Y = 0.9913$, $Q^2Y = 0.9315$ and $p < 0.05$) achieved complete separation between the metabolic profiles of the two diet groups as seen in the scores plot (Tcv; Figure 4.3A1). The corresponding coefficient plot (Figure 4.3A2) inferred that the metabolic signature of the MCD diet group included depleted levels of glucose, glycogen, mannose, maltose, glutathione, lactate, niacinamide, choline, phosphocholine, trimethylamine, tyrosine, 1-methylhistidine, inosine and uridine, together with elevated levels of glycine, lipids, fumarate and formiminoglutamic acid (FIGLU), with respect to the control diet group. A summary of the discriminatory metabolites is presented in Table 4.1.

Urinary metabolic phenotype of the NASH model

The O-PLS-DA model computed to compare the urinary baseline (pre-dose, -6 to 0 hours) metabolic profiles of the two diet groups (Figure 4.3B; $R^2Y = 0.9519$, $Q^2Y = 0.9040$ and $p < 0.05$) achieved complete discrimination as evidenced by the scores plot (Tcv, Figure 4.3B1).

The corresponding coefficient plot (Figure 4.3B2) showed that the MCD diet group animals had elevated levels of citrate, urocanate, guanidinoacetate, methylamine, taurine, formate and FIGLU, and depleted levels of trimethylamine-N-oxide (TMAO) and dimethylamine relative to the control diet animals. A summary of the findings is presented in Table 4.1.

Faecal water metabolic phenotype of the NASH model

O-PLS-DA models were also computed to compare the pre-dose faecal water metabolic profiles of the two diet groups (-12 – -6 and -6 to 0 hours). The two pre-dose time periods in each diet were not statistically significantly different and were therefore grouped together to achieve greater statistical power. The robust model (Figure 4.3; $R^2Y = 0.8429$ $Q^2Y = 0.7533$ and $p < 0.05$) achieved a significant degree of separation in multivariate space (Tcv, Figure 4.3C1). The corresponding coefficient plot revealed that the MCD diet group had higher levels of glucose and fructose and reduced levels of tyrosine, choline, galactose and methionine. A summary of the findings is shown in Table 4.1.

Pathways	Hepatic component	Urine	Faecal water
Choline metabolism		methylamine	
	choline, phosphocholine, trimethylamine	dimethylamine trimethylamine-*N*-oxide	choline
Energy metabolism	fumarate	citrate	glucose, fructose
	glucose, glycogen, lactate, maltose, mannose		galactose
Nucleic acids	inosine, uridine		
Amino acids	FIGLU, glycine	FIGLU, urocanate, guanidinoacetate, taurine	
	glutamate, glutathione, niacinamide, tyrosine		tyrosine, methionine
Other		formate	

Table 4.1: All of the metabolic perturbations shown are relative to the MCD diet group. Red and blue indicate elevation and depletion of the metabolite levels respectively with respect to the control group. A cut-off point of $|R| > 0.5$ was used. FIGLU, formiminoglutamic acid.

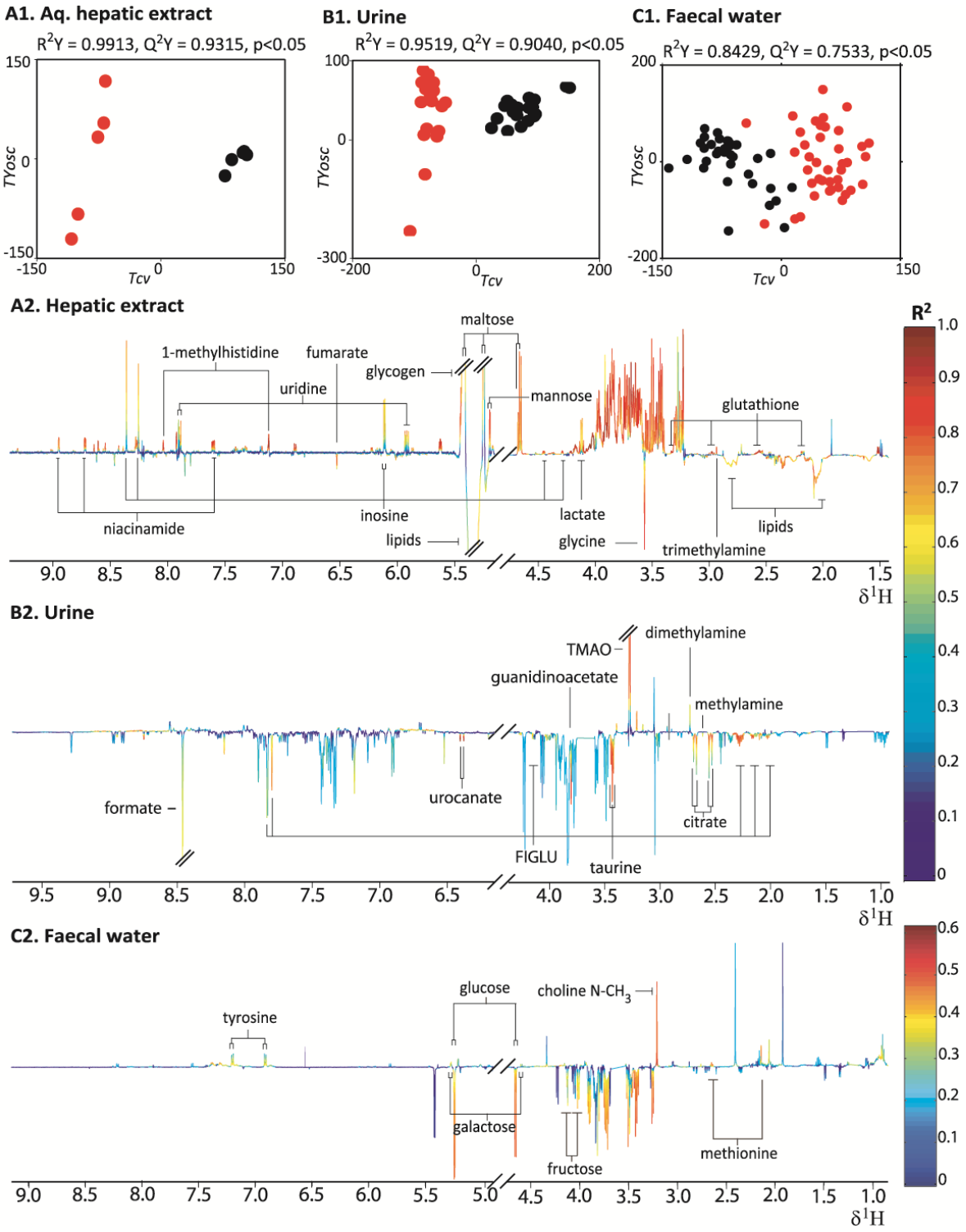


Figure 4.3: The O-PLS-DA models comparing the vehicle group or baseline (0hr) metabolic profiles of the two diets in the hepatic component (A; *n* = 5 per group), urine (B; *n* =22 per diet group) and faecal water (*n* = 36 and *n* = 42 for control and MCD diet respectively; C) are depicted above. The scores plots (A1, B1, C1) reveal the separation in multivariate space between the MCD diet (red) and the control diet (black), while the corresponding coefficient plots (A2, B2, C2) reveal the discriminatory metabolites predicted by each model. Resonances pointing up are higher in the control diet groups and vice versa. The colour scale on the right reveals the Pearson correlation coefficient (R^2) of each data point. TMAO – trimethylamine-*N*-oxide; FIGLU – formiminoglutamic acid.

Discussion

The MCD diet is an important model for the study of the hepatic consequences of fat accumulation, inflammation, fibrogenesis, oxidative stress and altered drug metabolism which are all features of NASH (Kucera and Cervinkova, 2014, Fisher et al., 2009). Despite the extensive existing research on this model, we have a limited understanding concerning the metabolic phenotype of the MCD diet model and why significant inter-species and inter-gender differences are observed in rodents (Kirsch et al., 2003, Kucera and Cervinkova, 2014). Such questions emphasize the importance of improving our understanding of the underlying hepatic pathology induced by the MCD diet in order to further contextualize its use as an animal model of NASH.

Histopathology of the MCD diet baseline

Histopathological analysis revealed that the MCD diet model of NASH was characterized by inflammation, necrosis and lipid accumulation (steatosis), all of which are part of the NASH clinical presentation (Brunt, 2001). The systems level metabolic profiles revealed that the MCD diet induced significant metabolic perturbations, affecting a spectrum of important metabolic pathways, especially methionine, choline and energy metabolism, as well as causing oxidative stress. The MCD diet is linked to the disruption of one carbon metabolism through deficiency of choline and methionine (Figure 4.4), which would lead to a cascade of consequences that would affect the biosynthesis of nucleotides, lipids and proteins (Locasale, 2013).

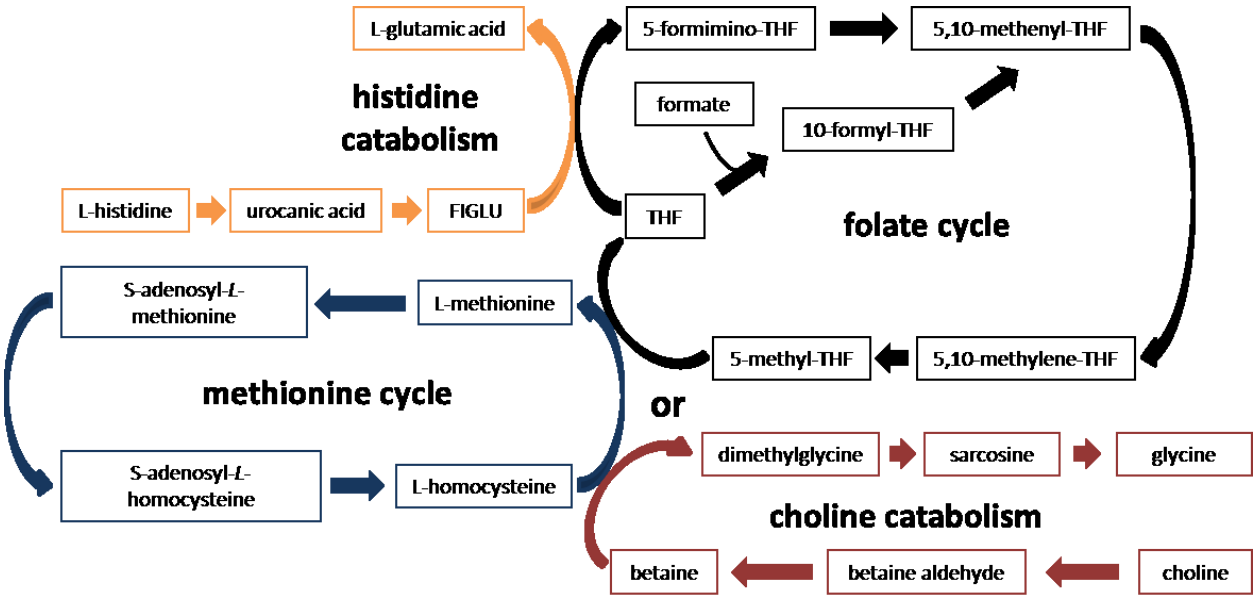


Figure 4.4: A simplified diagrammatic representation of the interaction of the methionine cycle (blue), folate cycle (black), choline catabolism (red) and histidine catabolism (orange) pathways, are depicted above. THF; tetrahydrofolate; FIGLU – formiminoglutamic acid.

Hepatic metabolic phenotype of NASH

Multivariate modelling of the hepatic metabolic profiles revealed the MCD diet induced significant metabolic perturbations affecting amino acid, energy, lipid, choline and nucleoside metabolisms. The observed depletion of hepatic choline, phosphocholine and trimethylamine in the MCD diet relative to the control diet were most likely directly linked to the choline deficient nature of the diet. Glutathione levels, a marker of oxidative stress, was also observed to be at lower levels in the MCD diet group, which could be another direct effect of the methionine deficiency of the diet or linked to the NASH condition itself since it has previously been reported to cause oxidative stress (Musso et al., 2013). The depletion of nicotinamide in the MCD diet group could also be linked to oxidative stress through the upregulation of nicotinamide adenine dinucleotide (NAD) synthesis (Xu and Sauve, 2010).

Interestingly, the elevation of glycine in the MCD diet group seemed to contradict the other observed changes. Glycine is an amino acid that can be synthesized via various metabolic

pathways, the majority of which require choline or tetrahydrofolate (THF) (Wang et al., 2013b); therefore the methionine and choline deficient nature of the diet would have been expected to lead to glycine depletion. Furthermore, a previous study has reported that glycine levels remain unchanged in NASH patients (Dasarathy et al., 2009). The observed elevation could be due to an up-regulation of glycine synthesis to compensate for the aforementioned glutathione depletion or because of a disruption of the mitochondrial glycine cleavage system which is the main pathway of glycine degradation (Wang et al., 2013b).

The observed hepatic depletion of glycogen, lactate, maltose, mannose and glucose in the MCD diet group were suggestive of impairment in hepatic energy metabolism. Energy metabolism dysfunction could be a consequence of a defective mitochondrial respiratory chain which has been reported to be a characteristic of NASH (Perez-Carreras et al., 2003) or the inhibition of SCD-1, an enzyme involved in the regulation of the rate of metabolism (Rizki et al., 2006) and whose inhibition has been previously linked to higher energy expenditure in mice. A potential inhibition of SCD-1 is not likely to be linked to the accumulation of lipids since it has been reported to lead to an up-regulation of genes involved in β-oxidation which results in protection from adiposity (Miyazaki et al., 2004). The accumulation of lipids is believed to be linked to a disruption of cholesterol transport as a result of choline deficiency (Larter and Yeh, 2008).

As previously mentioned, an important effect of the methionine and choline deficiency is the disruption of the folate cycle (Figure 4.4), which would result in an inhibition of THF formation. As Figure 4.4 illustrates, depletion of THF would lead to an inhibition of conversion of FIGLU to glutamate, which would result in higher levels of hepatic FIGLU in the MCD diet group. Furthermore, a disruption of the folate cycle would have a severe effect on nucleotide

biosynthesis and could be linked to the observed higher levels of hepatic nucleosides; inosine and uridine (Crider et al., 2012).

Urinary metabolic phenotype of the MCD diet

The majority of the discriminatory metabolites identified in the urinary baseline metabolic profile of the MCD diet were directly correlated to the observed hepatic metabolic perturbations. The higher levels of TMAO and dimethylamine in the urine of the control diet group could be attributed to the choline deficiency of the MCD diet. Higher levels of formate, urocanate and FIGLU are possibly due to the aforementioned disruption of the folate cycle by the MCD diet (Figure 4.4). Finally, higher levels of guanidinoacetate, a urinary metabolite of glycine, in the MCD diet group are most likely linked to the aforementioned higher levels of hepatic glycine.

Potential perturbation of microbial populations

Metabolic profiling of the faecal water could potentially provide information concerning gastrointestinal or microbial population disturbances. The microbiota are thought to have an important role in the development of NAFLD and NASH (Zhu et al., 2013, Moschen et al., 2013, Abu-Shanab and Quigley, 2010), while lactic acid bacteria in the colon have been reported to be involved in the development of the NASH like disease induced by the MCD diet (Okubo et al., 2013). The lower levels of galactose in the MCD diet group could be linked to a disturbance in the microbial population in the colon since galactose can be derived from the catabolism of dietary fibres or mucin oligosaccharides via bacterial fermentation in the colon (Slomiany et al., 1980). However, further investigations are required to determine the effect of the MCD diet on the gut microbiome of rodents and whether gut microbiota play an important role in the development of the condition induced by this diet.

The lower levels of faecal water methionine and choline in the MCD diet, relative to the control diet group, were most likely due to the deficient nature of the diet. The elevated levels of fructose and glucose could be a sign of malabsorption, which would also be related to the lower levels of glucose identified in the hepatic metabolic profiles. Fructose is a product of sucrose hydrolysis that occurs mainly in the proximal small intestine where it is absorbed with glucose (Dahlqvist and Thomson, 1963). The lower levels of these energy metabolites could therefore be linked with intestinal dysfunction, as previously linked to NAFLD (Volynets et al., 2012).

Other models of non-alcoholic steatohepatitis

Animal models of NASH should not only replicate the pathological pattern of liver injury of the human disease but should ideally model the metabolic syndrome component (Larter and Yeh, 2008). This metabolic syndrome is characterised by insulin resistance, hypertension, low concentration of high density lipoproteins, an altered adipokine profile and obesity (Pagano et al., 2002, Larter et al., 2010). An association of metabolic syndrome and the development of liver steatosis has already been reported but further work is required to elucidate the underlying mechanism (Marceau et al., 1999, Larter, 2007, Larter and Yeh, 2008).

The MCD diet can rapidly induce a condition that is thought to be an accurate reflection of clinical steatohepatitis and is therefore important in the characterisation of NASH pathology. This condition is characterized by neutrophil infiltration, elevated triglyceride content, oxidative stress, macrovesicular steatosis and fibrosis (Rinella et al., 2008, Larter and Yeh, 2008). However the mechanism by which the aforementioned pathological pattern develops, as induced by the depletion of choline and methionine, is understood to be different from the clinical condition. Furthermore, the absence of the metabolic syndrome in rodents fed by the

MCD diet is reflected by the significant weight loss experienced by the rodents after three weeks and this is considered to be the most significant disadvantage of this model (Rinella and Green, 2004, Larter and Yeh, 2008).

Other animal models of NASH can be generally categorized to genetic and dietary models and have been reported to have a varying degree of success in creating an accurate model of NASH. Alternative dietary models such as the high fat diet or the atherogenic diet (contains cholesterol and cholic acid) have been reported to similarly mimic the pathological pattern but not the metabolic syndrome of the clinical condition (Matsuzawa et al., 2007, Larter and Yeh, 2008). Genetic models such as leptin (ob/ob) or leptin receptor (db/db) deficient mice are thought to be poor models of the liver histology of NASH, even though they model the metabolic phenotype associated with the disease (Browning and Horton, 2004). Other animal models, such as the high fat fed foz/foz (*Alms1* mutant) mice (Arsov et al., 2006), which incorporate a genetic and dietary component are thought to be the most accurate models of NASH (Larter and Yeh, 2008). However, it is worth noting that the high fat fed foz/foz mouse model does not induce a rise in FFA levels and is therefore not reflective of our current understanding of the clinical condition (Van Rooyen et al., 2011).

All models will inevitably be associated with a different extent of limitations in their ability to replicate human NASH. These limitations are accentuated by our restricted knowledge concerning the underlying mechanism of NASH development and the use of organisms which will not behave in the same manner due to genotypic differences. Therefore, the use of each specific model should depend on the aim of the investigation, while comparative studies of the different models will be a valuable contribution to our knowledge in this field (Kucera and Cervinkova, 2014).

Study limitations and future work

The observed weight difference between the two diet cohorts at the beginning and end of the study was an important confounding factor which would have a pronounced effect on the metabolic profiles and more specifically on the intermediates of energy metabolism. Even though, it was not possible to determine which metabolic perturbations were induced specifically by the weight loss of the MCD diet, it was nonetheless important to characterize the complete metabolic baseline induced by the MCD diet for a better understanding of this dietary model. It is important to note that the reported pattern of urinary markers linked to caloric restriction was not observed in this study, as further discussed in Chapter 5 (Connor et al., 2004, Szkudelski et al., 2004).

Apart from the limitations associated with the MCD diet as a model of NASH, there were several complications associated with the analytical work which could be further optimized in follow-up studies. In the liver, the high lipid content of the MCD diet group was not sufficiently accounted for with the metabolite extraction protocol and therefore a CPMG pulse sequence had to be used during ^{1}H-NMR spectral acquisition to supress resonances from the lipidic species. There have been several comparisons of metabolic extraction methods but perhaps the use of a bi-layer extraction (methanol and chloroform) would have sufficiently isolated the lipids (Masson et al., 2010). In the faeces, the significant variation in inter-sample consistency could be better addressed through collection of the entire faecal output in a given time period, rather than the extraction of a single pellet.

A future targeted approach using UPLC-MS could be used to study how choline and methionine deficiency can affect folate metabolism through targeted study of intermediate metabolites (Wang et al., 2014). Finally, 16S RNA gene sequencing and a metagenomic

analysis should also be performed to verify whether microbial populations are perturbed by this diet and how relevant these perturbations could be to the actual clinical condition (Janda and Abbott, 2007).

Chapter 5: Systems level metabolic phenotype of methotrexate administration in non-alcoholic steatohepatitis in the rat

The hepatic extract and urine analysis results presented in this chapter have been published (Kyriakides et al., 2014). A copy of the publication is provided in the appendix.

Introduction

Study details and aims

This study was performed in parallel to the investigation detailed in Chapter 4. It characterizes the metabolic effect and disposition of MTX in healthy rats and in the context of NASH, as induced by the MCD diet. The hepatic aqueous-soluble extract, urine and faecal water metabolic profiles were acquired and analysed by ^{1}H-NMR spectroscopy. Similar to the metabolic characterization of the MCD diet presented in Chapter 4, this study provided the novel opportunity to describe the systemic effect of MTX in a healthy and a diseased state. The characterization of the metabolic effect of MTX in the diseased state was hypothesized to provide novel mechanistic insight of potential clinical relevance for further understanding the link between liver pathology and occurrence of ADRs.

Methods

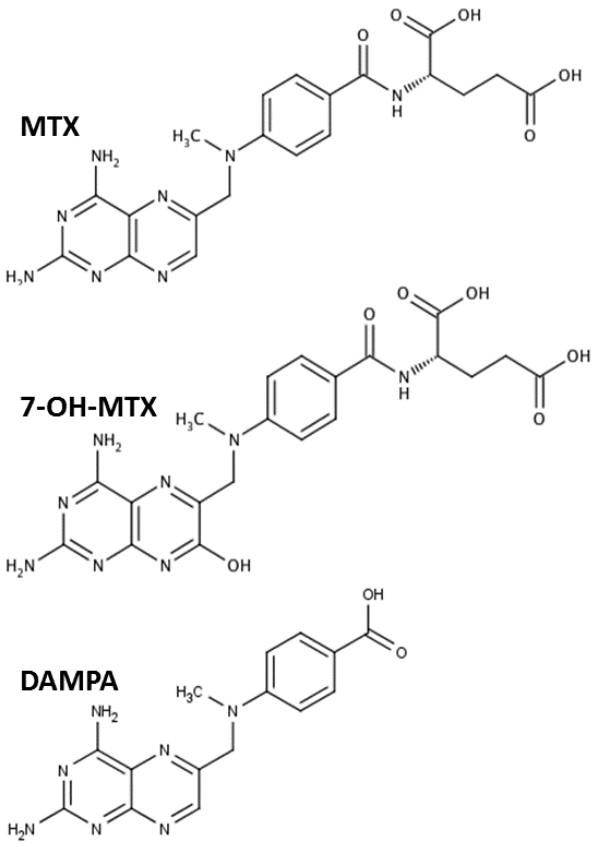
Only the methods not already discussed in Chapter 4 will be presented in this chapter. The time period abbreviations are as follows: -6 to 0 hours (pre-dose; 0hr), 6 – 12 hours (12hr), 18 – 24 hours (24hr) and 36 – 48 hr (48hr).

Dosing of MTX

The doses of MTX used in the current study were designed to reflect low dosage of MTX such as that used to treat inflammatory diseases (10 and 40 mg/kg doses) and high doses such as that used to treat acute lymphoblastic leukemia (100 mg/kg dose). MTX is dosed in patients based on body surface area (1000 mg/m^2). When taking into account the average body surface area of pediatric patients aged 1-10 years and converting to a mg/kg dose, a 100 mg/kg dose in rats falls well under that used clinically (Genestier et al., 2000).

Quantification of urinary excretion of MTX

The urinary excretion of MTX (100 mg/kg) per kg of rat (the weight was measured at the beginning of the study) at 12hr, 24hr and 48hr was quantified in both diet groups. Local baseline correction was performed in TopSpin 3.0 (Bruker) before integrating the resonance of MTX at δ 8.63, whose identity was verified by a spike-in experiment. The TSP resonance, of known concentration from the buffer solution, was used to estimate the quantity of MTX in the sample. The total urine volume collected per rat at each time period was then used to estimate the total amount of excreted MTX per rat per time period. The results were verified independently by LC-MS achieving a correlation (Pearson R value) with the NMR data greater than 0.99. Table 5.1 depicts the assignments of the MTX resonances, as well as the resonances assigned to DAMPA and 7-OH-MTX.



Metabolite	Species	Chemical shift (ppm)	Multiplicity	J-coupling (Hz)
Faecal water				
MTX	H1	7.74	d	8.87
	H2	6.94	d	8.87
	H3	8.63	s	-
	Ha	3.16	s	-
DAMPA	H1	7.78	d	8.92
	H2	6.90	d	8.92
	H3	8.61	s	-
	Ha	3.18	s	-
Urine				
MTX	H1	7.73	s	8.82
	H2	6.93	d	8.82
	H3	8.63	s	-
	Ha	3.19	s	-
7-OH-MTX	H1	7.72	d	8.84
	H2	6.98	d	8.84
	Ha	3.16	s	8.29

Table 5.1: The urinary and hepatic extract assigned resonances of MTX related molecules are depicted above. DAMPA - 2, 4-diamino-N(10)-methylpteroic acid; 7-OH-MTX – MTX hydroxyl conjugate; s – singlet; d – doublet; ppm – parts per million; Hα – N-acetyl resonance.

Statistical analysis

O-PLS-DA models were constructed to model the metabolic effect of MTX in both diet groups with and without the MTX and related resonances in order to ensure that the endogenous metabolic changes were statistically significantly different for both models. PLS regression analysis was also used to characterize the correlation of the hepatic metabolic profiles of both diet groups with each of the biliary hyperplasia and liver fibrosis scores. Univariate testing (Kruskal-Wallis coupled to Dunn's multiple test correction) was used to test for significant differences in the phenylalanine levels in each group per diet (based on the integral of the resonance at δ 7.38). Please note that each diet group was normalized separately due to their distinctly different metabolic profiles and therefore the phenylalanine levels are not directly comparable. Permutation tests (n = 1000) were used to test O-PLS-DA and PLS model validity, while a $p < 0.05$ statistical significance threshold was set throughout.

Results

Histopathology

Histopathological assessment of the control diet group showed that MTX treatment (40 and 100 mg/kg) led to hepatic necrosis (Figure 5.1A). One animal also developed liver inflammation (40 mg/kg) and another biliary hyperplasia following MTX treatment (100 mg/kg respectively; Figure 5.1C and 1E respectively). MTX treatment in the MCD diet group (40 mg/kg) led to a statistically significant reduction in lipid accumulation and liver inflammation (Figure 5.1B and 1C). Minimal liver fibrosis and mild biliary hyperplasia were also detected in the MCD diet group following treatment of MTX at a statistically significant level (100 mg/kg; Figure 5.1D and 1E). Small intestinal histopathology inferred that MTX (100 mg/kg) led to moderate villous atrophy, villous fusion and dilated crypts, as well as minimal apoptosis, inflammation and vacuolization in both groups at similar levels.

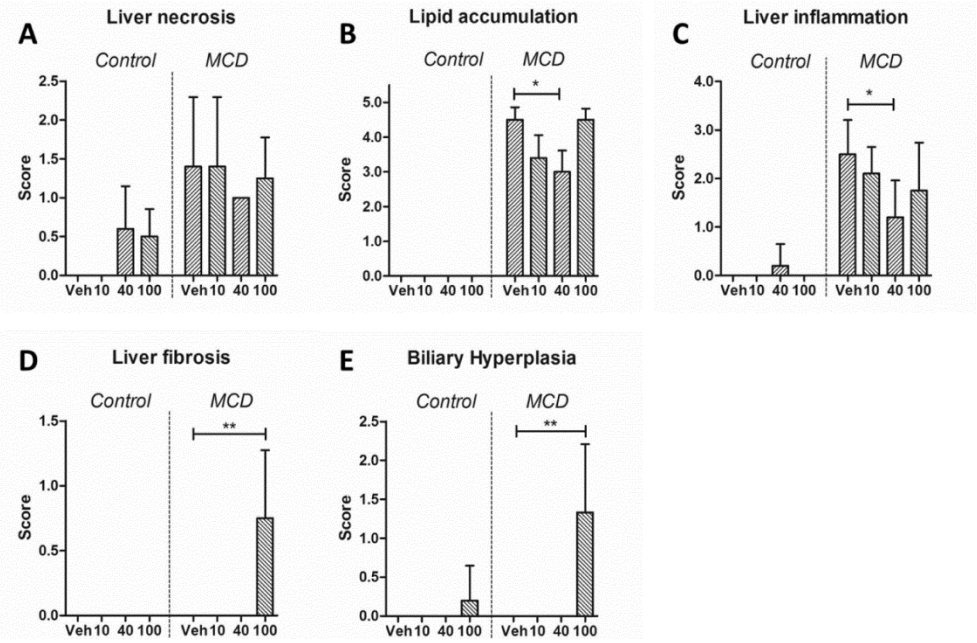


Figure 5.1: The mean and standard deviation of the histopathology scores representing liver necrosis (A), lipid accumulation (B), liver inflammation (C), liver fibrosis (D) and biliary hyperplasia (E) following MTX administration (vehicle, 10, 40 and 100 mg/kg; *n* = 5 for each per diet and *n* = 6 for 100 mg/kg MTX dose in the MCD diet). Statistical significance is indicated by (*) or (**) representing $p < 0.05$ and $p < 0.01$ respectively. The scoring criteria are: 0 = no significant lesions, 1 = minimal, 2 = mild, 3 = moderate, 4 = marked and 5 = severe; Veh – Vehicle.

Animal weight

The body weight of animals was recorded at the beginning (prior to MTX administration) and at the end of the study (post MTX administration, 96 hours). At the beginning of the study, the average weight of the animals was 390 g (STD ± 57 g) in the control diet group and 200 g (STD ± 46 g) in the MCD diet group. The average weight loss observed following administration of MTX in the control diet groups were 7 %, 16 % and 26 % for the groups administered 10, 40 and 100 mg/kg MTX respectively. Weight loss was also observed in the MCD diet group with an average percentage weight loss of 18 %, 20 % and 20 % for the groups administered 10, 40 and 100 mg/kg MTX respectively. The percentage weight loss in each diet relative to the vehicle can be seen below in Figure 5.2.

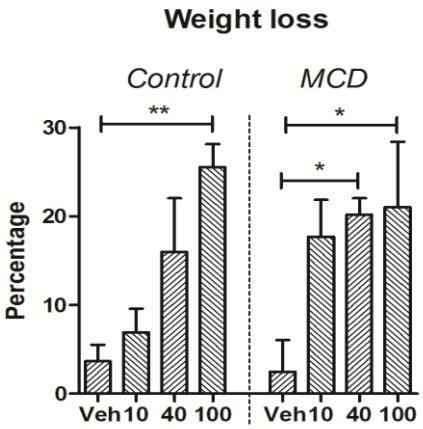


Figure 5.2: The mean percentage body weight loss and standard deviation of all dose groups in both diet groups during the duration of the study is depicted above (*n* = 5 for each per diet and *n* = 6 for 100 mg/kg MTX dose in the MCD diet). Statistical significance at $p < 0.05$ and $p < 0.01$ are indicated by (*) and (**) respectively. The vehicle and three doses of MTX are indicated at the horizontal axis (0, 10, 40 and 100 mg/kg). Veh – Vehicle.

Hepatic metabolic phenotype after MTX administration in the control diet group

The metabolic consequences following MTX administration in the control diet group were characterized by O-PLS-DA pair-wise models, relative to the vehicle group. The statistically

robust O-PLS-DA model describing the effect of 10 mg/kg MTX administration (Figure 5.3A; $R^2Y = 0.9888$, $Q^2Y = 0.5029$ and $p < 0.05$) achieved complete separation between the two groups in the scores plot (Tcv, Figure 5.3A1). The corresponding coefficient plot (Figure 5.3A2) revealed that the MTX treated group had lower levels of lactate, glucose, glycogen, maltose, inosine, betaine, phosphocholine, glutathione and dimethylamine, as well as elevated levels of D-3-hydroxybutyrate, uracil, glutamate, valine, isoleucine and leucine. The statistically robust O-PLS-DA model describing the metabolic effect of 40 mg/kg MTX administration (Figure 5.3B; $R^2Y = 0.9384$, $Q^2Y = 0.7846$ and $p < 0.05$) led to complete separation between the two groups in the scores plot (Tcv, Figure 5.3B1). The corresponding coefficient plot (Figure 5.3B2) revealed depleted levels of glucose, maltose, mannose, glycogen, lactate, betaine, phosphocholine, dimethylamine and glutathione, as well as higher levels of uracil, D-3-hydroxybutrate, glutamate, valine, isoleucine, leucine, choline and glycerophosphocholine (tentatively assigned). Finally, the model computed to characterize the metabolic effect of the highest dose of MTX (100 mg/kg; Figure 5.3C; $R^2Y = 0.9985$, $Q^2Y = 0.8485$ and $p < 0.05$) was also statistically robust and achieved complete separation in the scores plot (Tcv, Figure 5.3C1). The equivalent coefficient plot (Figure 5.3C2) revealed that the administration of 100 mg/kg MTX led to the depletion of lactate, glucose, maltose, mannose, glycogen, betaine, inosine, dimethylamine and glutathione. It also led to the concomitant rise in the levels of valine, glutamate, leucine, isoleucine, glycerophosphocholine (tentatively assigned), D-3-hydroxybutyrate, formate, uracil, hypoxanthine, creatine and choline following MTX administration, relative to the vehicle group. A summary of the hepatic metabolic effects induced by MTX administration at all doses in the control diet group is presented in Figure 5.5A.

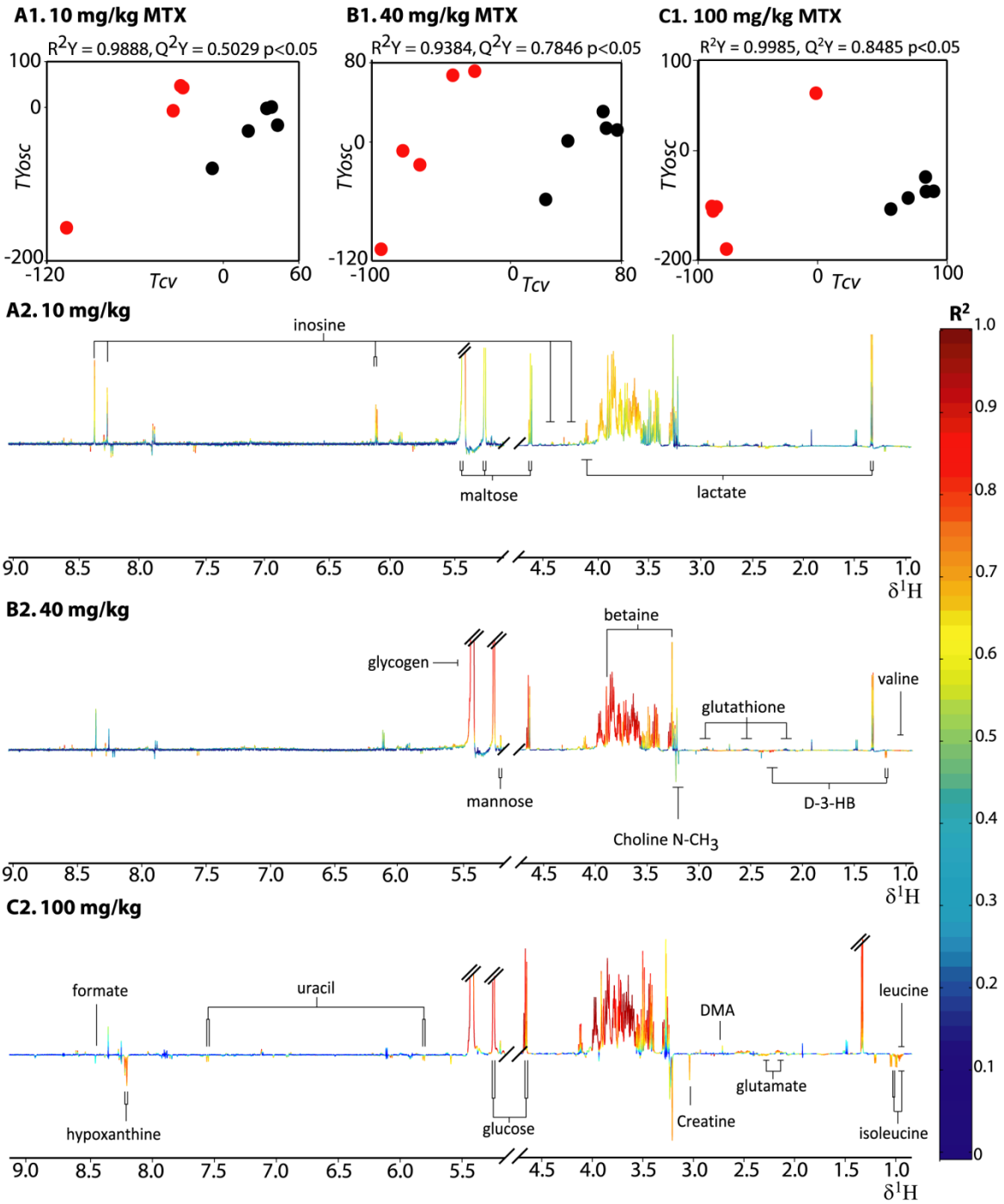


Figure 5.3: Hepatic extract O-PLS-DA models comparing the vehicle groups and 10, 40 and 100 mg/kg MTX administration groups in the control diet at 96hr post-treatment (*n* = 5 per group). The scores plots (A1, B1 and C1) depict the separation of the MTX administered groups (red) and vehicle group (black) in multivariate space. Tcv is the predictive component, whilst TYosc is the orthogonal component. The coefficient plots (A2 and B2) illustrate the discriminatory spectral resonances with the height of spectral peaks representing covariance. The colour-scale corresponds to the coefficient of discrimination (R^2) ranging from low (0; blue) to high (red; 1). Resonances pointing up indicate an increase in that specific resonance in the control group and vice versa. Choline-NCH_3 – N-methyl resonance of choline, phosphocholines and glycerophosphocholines; DMA – dimethylamine; D-3-HB – D-3-hydroxybutyrate; glutathione – oxidized glutathione.

Hepatic metabolic phenotype after MTX administration in the MCD diet group

A complementary O-PLS-DA was used to elucidate the metabolic effect of MTX (10, 40 and 100 mg/kg) relative to the vehicle group in the MCD diet. The statistically robust O-PLS-DA model characterizing the effect of 10 mg/kg MTX (Figure 5.4A; $R^2Y = 0.9949$, $Q^2Y = 0.5491$ and $p < 0.05$) achieved complete separation in the scores plot (Tcv, Figure 5.4A1). The corresponding coefficient plot (Figure 5.4A2) revealed that the MTX treated group had lower levels of inosine, glucose, maltose, glycogen and betaine, as well as higher levels of uracil, D-3-hydroxybutyrate, glutamate, acetate, valine, leucine, urocanate and FIGLU, relative to the vehicle group. The O-PLS-DA model computed to describe the metabolic effect of 40 mg/kg MTX (Figure 5.4B; $R^2Y = 0.9945$, $Q^2Y = 0.7928$ and $p < 0.05$) achieved complete discrimination in the scores plot (Tcv, Figure 5.4B1). The corresponding coefficient plot (Figure 5.4B2) revealed that there was a depletion of glucose, maltose, mannose, glycogen, acetate, betaine and choline, as well as a concomitant elevation of uracil, D-3-hydroxybutyrate, acetate, valine, isoleucine, leucine, phenylalanine, betaine, creatine, FIGLU, niacinamide and formate. Finally, The O-PLS-DA model computed to characterize the effect of the highest dose of MTX (100 mg/kg; Figure 5.4C; $R^2Y = 0.9957$, $Q^2Y = 0.9155$ and $p < 0.05$) achieved complete group separation in the scores plot (Tcv, Figure 5.4C1). The equivalent coefficient plot (Figure 5.4C2) revealed that MTX administration led to the depletion of inosine, maltose, mannose, lactate, glycogen and phosphocholine, as well as the elevation of uracil, D-3-hydroxybutyrate, acetate, glutamate, valine, leucine, phenylalanine, choline, creatine, FIGLU, niacinamide, formate and urocanate. A summary of the hepatic metabolic effects induced by MTX administration at all doses for the MCD diet group is presented in Figure 5.5B.

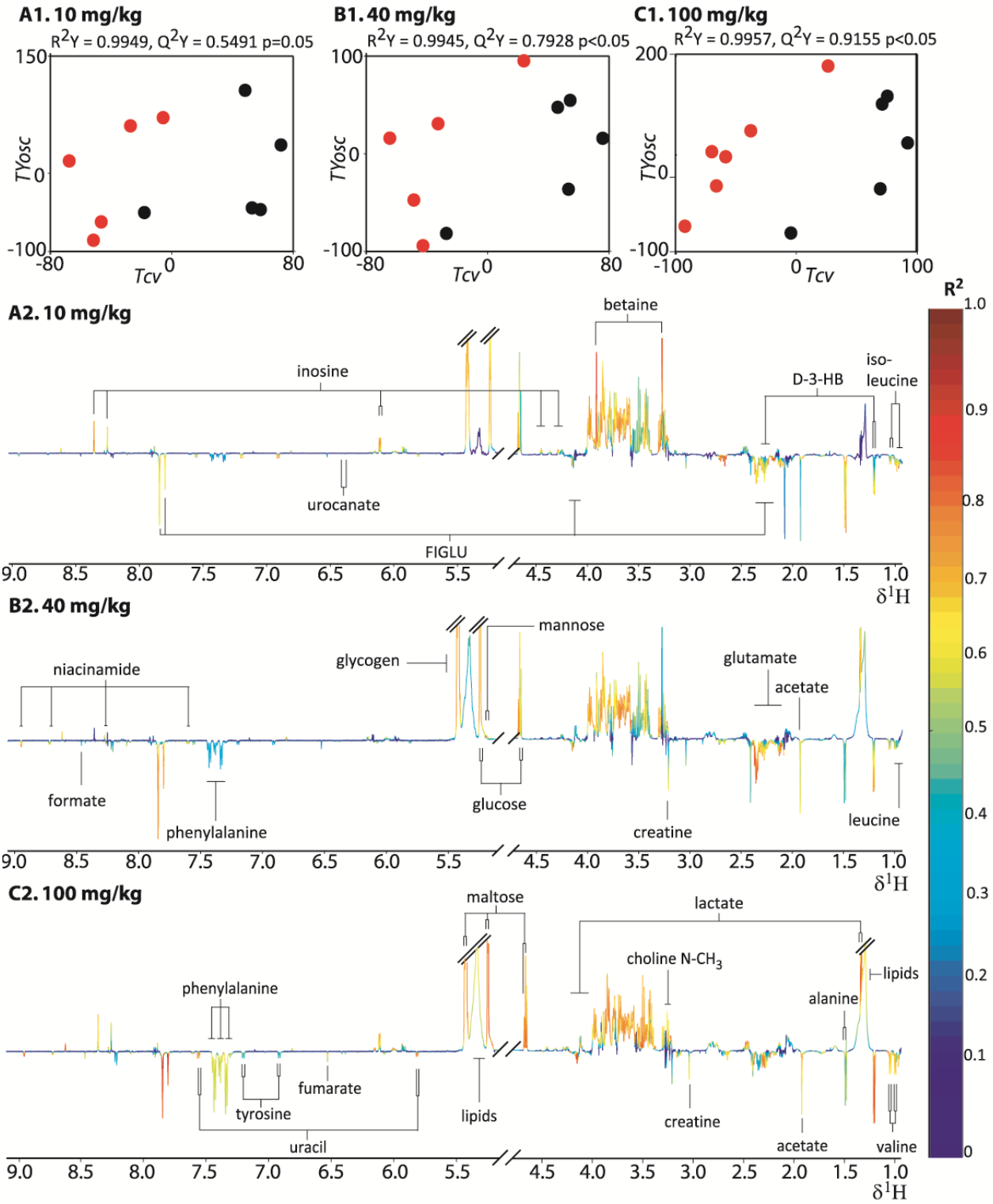


Figure 5.4: The O-PLS-DA models comparing the hepatic metabolic profiles of the vehicle groups (black) and each of the 10, 40 and 100 mg/kg MTX administered groups (red) in the MCD diet at 96hr post-treatment are shown (*n* = 5 for vehicle, 10 and 40 mg/kg doses of MTX, *n* = 6 for 100 mg/kg MTX dose group). The scores plots (A1, B1 and C1) depict the separation of the MTX administered groups (red) and vehicle group (black) in multivariate space. Please see legend of Figure 5.3.

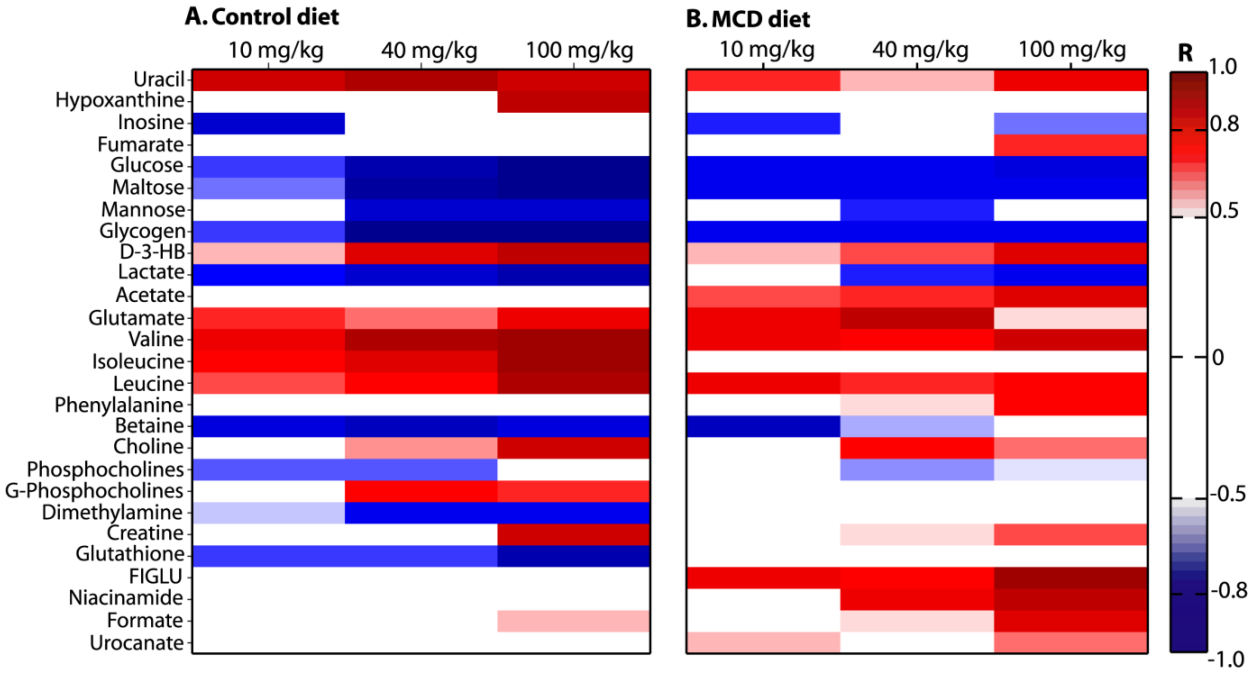


Figure 5.5: The hepatic metabolic effects of MTX administration in the control diet (A) and MCD diet (B) at 96hr are shown. The maximum Pearson correlation coefficient values (R) for each discriminant metabolite from the O-PLS-DA models separating between the metabolic profiles of MTX treated (10, 40, 100 mg/kg) and the vehicle groups are displayed. The scale ranges from -1 (perfect negative correlation; blue) to 1 (perfect positive correlation; red). A cut-off value of |0.5| was set. Please see legends of Figures 5.3 and 5.4.

Phenylalanine elevation

A statistical regression analysis between the biliary hyperplasia and liver fibrosis scores with the hepatic metabolic profiles inferred that phenylalanine was the only endogenous metabolite to be correlated to the development of those conditions ($R^2Y = 0.5218$ and $Q^2Y = 0.2423$, and $R^2Y = 0.5406$ and $Q^2Y = 0.2542$ respectively; Figure 5.6A). Analysis of the phenylalanine resonance integrals at δ 7.38 revealed that the administration of the highest dose of MTX (100 mg/kg) in the MCD diet group led to a statistically significant elevation of phenylalanine relative to the vehicle group of the same diet ($p < 0.05$; Figure 5.6B).

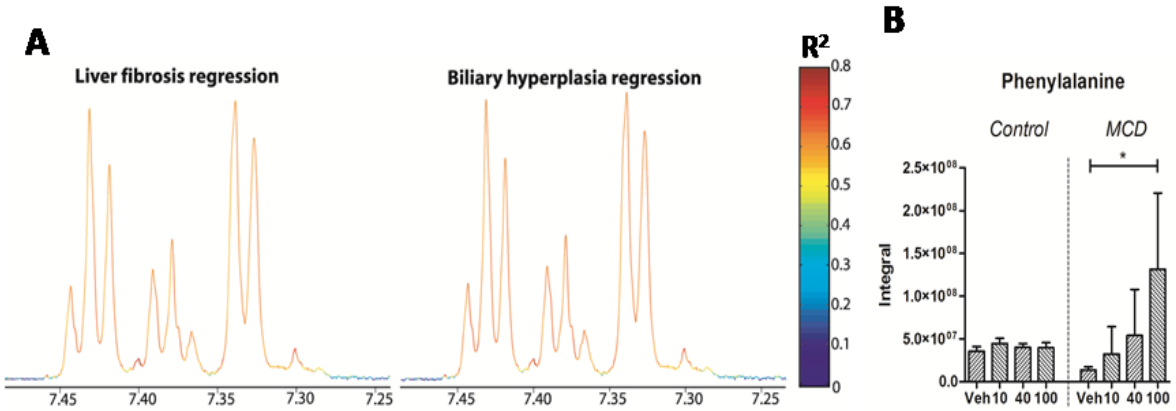


Figure 5.6: Excerpts from the PLS regression coefficient plots of the phenylalanine resonance from the regression analyses are shown (A). The correlation scale ranged from low (0; blue) to high (0.8; red). The integrals (mean and standard deviation) of phenylalanine from the displayed resonance in all dosage groups in both diets at 96hr are shown (B; *n* = 5 for each MTX dosage group per diet and *n* = 6 for 100 mg/kg MTX dose in the MCD diet). Please note that the integrals cannot be directly compared between the two diet groups due to individual separate pre-processing and normalization of each diet group. Statistical significance was set at $p < 0.05$ (*). Veh – Vehicle.

Faecal water metabolic phenotype after MTX administration in the control diet

The collection of faecal samples at sequential time-points enabled the characterization of the temporal metabolic consequences of MTX at each dose level for each diet group. O-PLS-DA pair-wise models were computed to model the metabolic effect of MTX administration at each of the time-points. The comparisons between the pre-dose baseline (0hr time-point) and the 48hr post-dose time-point were the only models that were statistically robust due to sufficient sample numbers. The model discriminating between the 10 mg/kg dose of MTX at 48hr and the baseline group at 0hr ($R^2Y = 0.9552$, $Q^2Y = 0.6297$, $p < 0.05$) achieved complete discrimination in multivariate space between the two groups (Tcv). The corresponding coefficient plot revealed that propionate and acetate were depleted following MTX administration, while succinate, dihydroxyacetone (DHA), valine and sarcosine were elevated. The O-PLS-DA model describing the metabolic effect of 40 mg/kg at 48hr, relative to the baseline ($R^2Y = 0.9821$, $Q^2Y = 0.7191$, $p < 0.05$), achieved complete separation between the

two groups as well (Tcv). The corresponding coefficient plot revealed that MTX administration led to the depletion of tyrosine, propionate and acetate, while DHA, valine, 5-aminovalerate, sarcosine and putrescine were at higher levels. The model discriminating between the highest dose of MTX (100 mg/kg) at 48hr, relative to the baseline, (Figure 5.7A; $R^2Y = 0.9606$, $Q^2Y = 0.7261$, $p < 0.05$) achieved complete discrimination of the two groups in the scores plot as well (Tcv, Figure 5.7A1). The corresponding coefficients plot (Figure 5.7A2) revealed that MTX administration led to higher levels of uracil, galactose, fucose, DHA, valine, 5-aminovalerate and putrescine. A summary of the metabolic effects of MTX at all doses is presented in the form of a heatmap in Figure 5.8A.

Faecal water metabolic phenotype following MTX administration in the MCD diet.

The metabolic effect of MTX administration (10, 40 and 100 mg/kg) in the MCD diet group was also modelled by O-PLS-DA. The comparisons between the pre-dose baseline (0hr time period) and the 48hr post-dose time period were the only models that were statistically robust at all doses of MTX. The model discriminating the metabolic effect of the 40 mg/kg dose at 48hr, relative to the pre-dose baseline, was not statistically robust and was therefore not analyzed further. The model constructed to discriminate the metabolic effect of the 10 mg/kg MTX dose at 48hr relative to the pre-dose baseline (0hr) achieved complete separation in the scores plot ($R^2Y = 0.9674$, $Q^2Y = 0.6389$, $p < 0.05$). The equivalent coefficient plot revealed that acetate and tyrosine were depleted after MTX administration, while uracil, succinate, galactose, DHA, fucose, methionine, sarcosine and putrescine were elevated. Finally, the robust O-PLS-DA model characterizing the metabolic effect of the highest dose of MTX at 48hr, relative to 0hr, (Figure 5.7B, $R^2Y = 0.9627$, $Q^2Y = 0.6492$, $p < 0.05$) achieved complete separation of the two groups in the scores plot (Tcv, Figure 5.7B1). The

corresponding coefficient plot (Figure 5.7B2) revealed that the levels of uracil, galactose, DHA, methionine, 5-aminovalerate, sarcosine and putrescine were elevated after MTX administration. A summary of the metabolic effects of MTX administration (10 and 100 mg/kg) at 48hr is presented in a heatmap in Figure 5.8B.

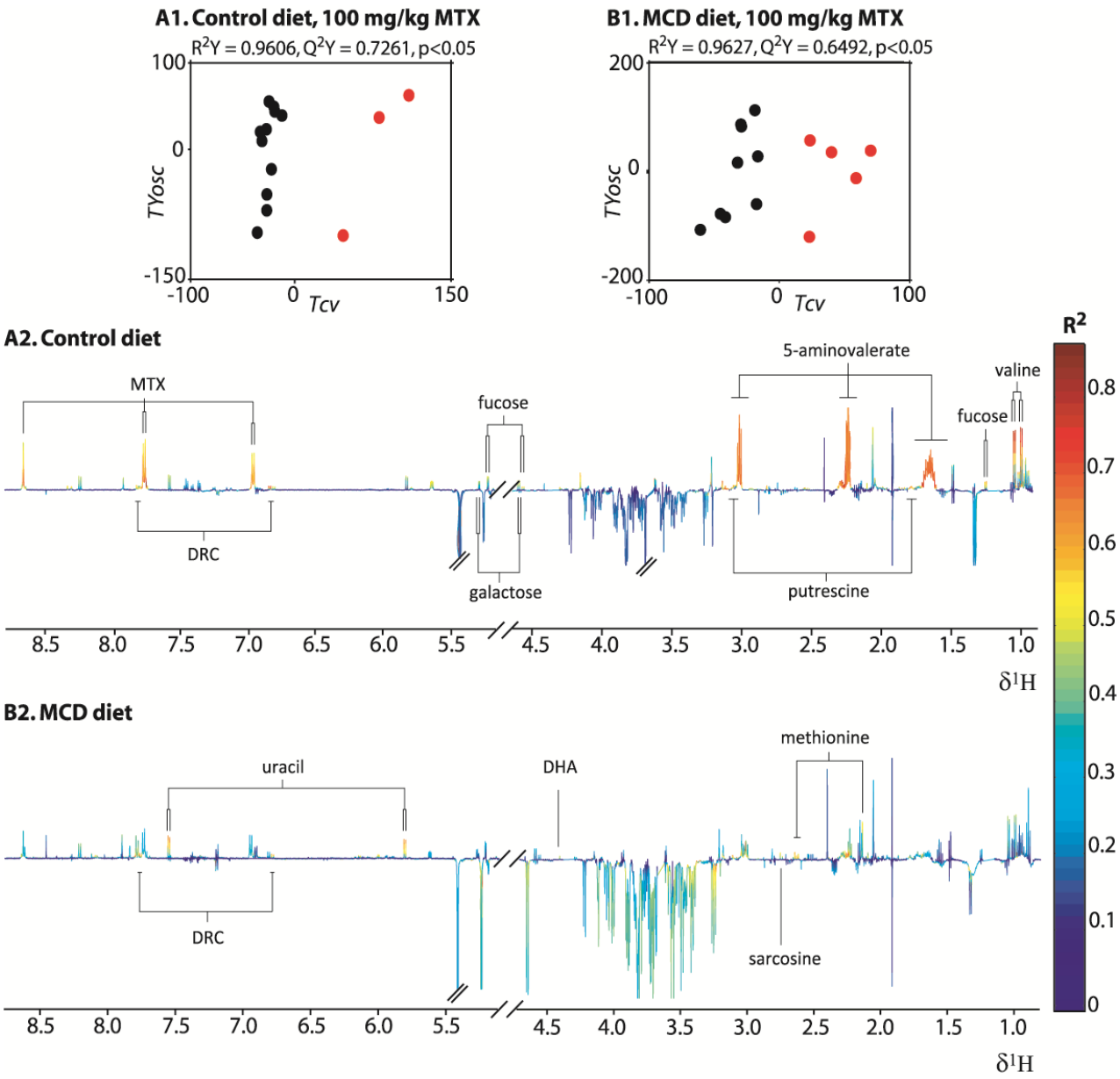


Figure 5.7: Faecal water O-PLS-DA models comparing the pre-dose time period (0hr; black) and 48hr (red) after 100 mg/kg MTX administration in the normal diet (A1 and A2; *n* = 12 and *n* = 3 respectively) and MCD diet (B1 and B2; *n* = 12 and *n* = 5 respectively). DRC – Drug related compound; DHA – dihydroxyacetone (tentatively assigned). Please see legend of Figure 5.3.

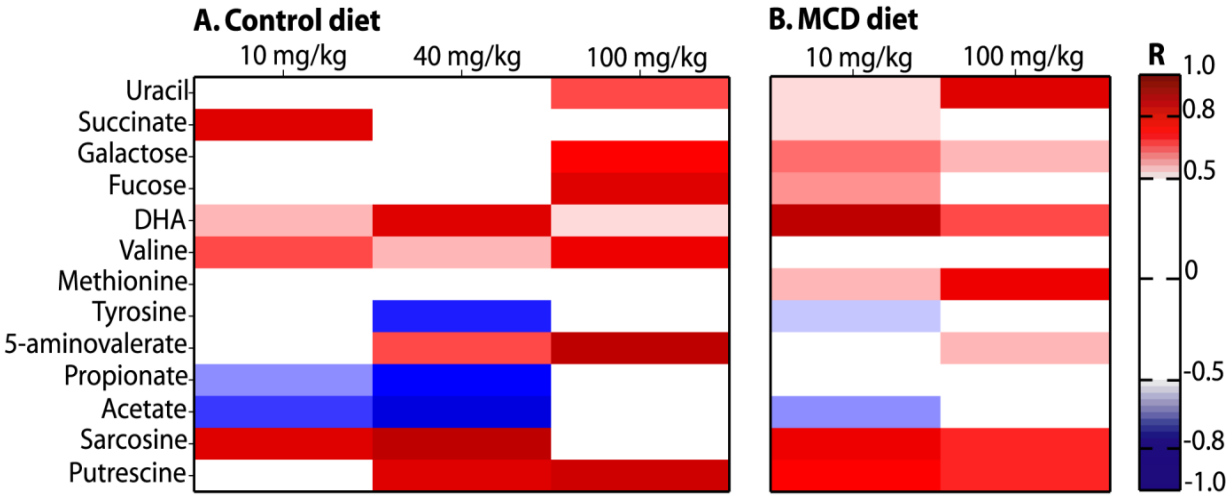


Figure 5.8: Heatmap describing the faecal water metabolic effects of MTX administration in the control diet (A) and MCD diet (B) at 48hr relative to 0hr (pre-dose; 10, 40 and 100 mg/kg in the control diet; 10 and 100 mg/kg in MCD diet). DHA – dihydroxyacetone. Please see legend of Figure 5.5.

Urinary metabolic phenotype following MTX administration in the control diet

The collection of sequential time-point urine samples enabled the characterization of the temporal MTX-induced metabolic effect. O-PLS-DA pair-wise models were used to describe the metabolic effect of MTX at the 12hr, 24hr and 48hr time-periods relative to the pre-dose baseline (0hr). The results of the models that discriminated the high dose (100 mg/kg) group with controls will only be presented since they were consistently statistically robust and had the greatest predictive ability.

The O-PLS-DA models describing the metabolic effect of MTX (100 mg/kg) at 12hr, 24hr and 48hr relative to the pre-dose baseline inferred that MTX had a time-dependent progressive metabolic effect. This is reflected in the statistical parameters of the models for each time-point shown in Table 8.3 in the appendix. The robust O-PLS-DA model discriminating between the metabolic profiles of the control diet 0hr and 48hr time-points after MTX administration (Figure 5.9A; $R^2Y = 0.9865$, $Q^2Y = 0.7581$, $p < 0.05$) achieved complete discrimination between the groups in the scores plot (Tcv; Figure 5.9A1). The corresponding coefficient plot (Figure

5.9A2) showed that the levels of alanine, methylamine, dimethylamine, hippurate, TMAO and 3-indoxylsulphate were depleted, while the levels of levels of succinate, creatine, phenylacetylglycine and formate were elevated.

Urinary metabolic phenotype following MTX administration in the MCD diet

The corresponding O-PLS-DA analysis of the urinary metabolic effect of MTX (100 mg/kg) administration in the MCD diet group also revealed a progressive metabolic effect up to 48hr. The statistically robust O-PLS-DA model characterizing the metabolic effect of the MTX at 48hr relative to the pre-dose baseline (0hr) (Figure 5.9B; $R^2Y = 0.9474$, $Q^2Y = 0.8328$, $p < 0.05$), achieved complete discrimination between the two groups in the scores plot (Tcv, Figure 5.9B1). The corresponding coefficient plot (Figure 5.9B2) revealed that MTX administration led to a rise in the levels of FIGLU and formate, and a depletion of methylamine, alanine and hippurate. The progressive metabolic effect of MTX (100 mg/kg) from 12hr to 48hr revealed a depletion of methylamine and hippurate, and an elevation of formate and FIGLU. The depletion of alanine at 48hr was specific to that time-point, while depletions of other metabolites unique to other time periods were also observed, such as the decreases in the levels of 3-indoxylsulphate and phenylacetylglycine which were specific to 24hr. A summary of the models of each time-point can be seen in Table 8.3 in the appendix.

The elevation of FIGLU and formate at 48hr were also observed after the administration of the lower doses of MTX (10 and 40 mg/kg) in the MCD diet group. Interestingly, the O-PLS-DA models of these lower doses also revealed some metabolic effects at 48hr that were not observed after the administration of 100 mg/kg, including the depletion of methylamine and 3-indoxylsulphate, as well as the elevation of dimethylamine and TMAO.

The comparison of the metabolic effects of the administration of MTX (100 mg/kg) between the two diet groups revealed several diet specific MTX-induced effects. At 48hr, the higher levels of creatine, citrate, succinate and phenylacetylglycine were specific to the control diet group, while the observed MTX-induced elevated levels of FIGLU were specific to the MCD diet group. Figure 5.10 illustrates a summary of the metabolic effect of MTX (100 mg/kg) at the three time-points in both diet groups.

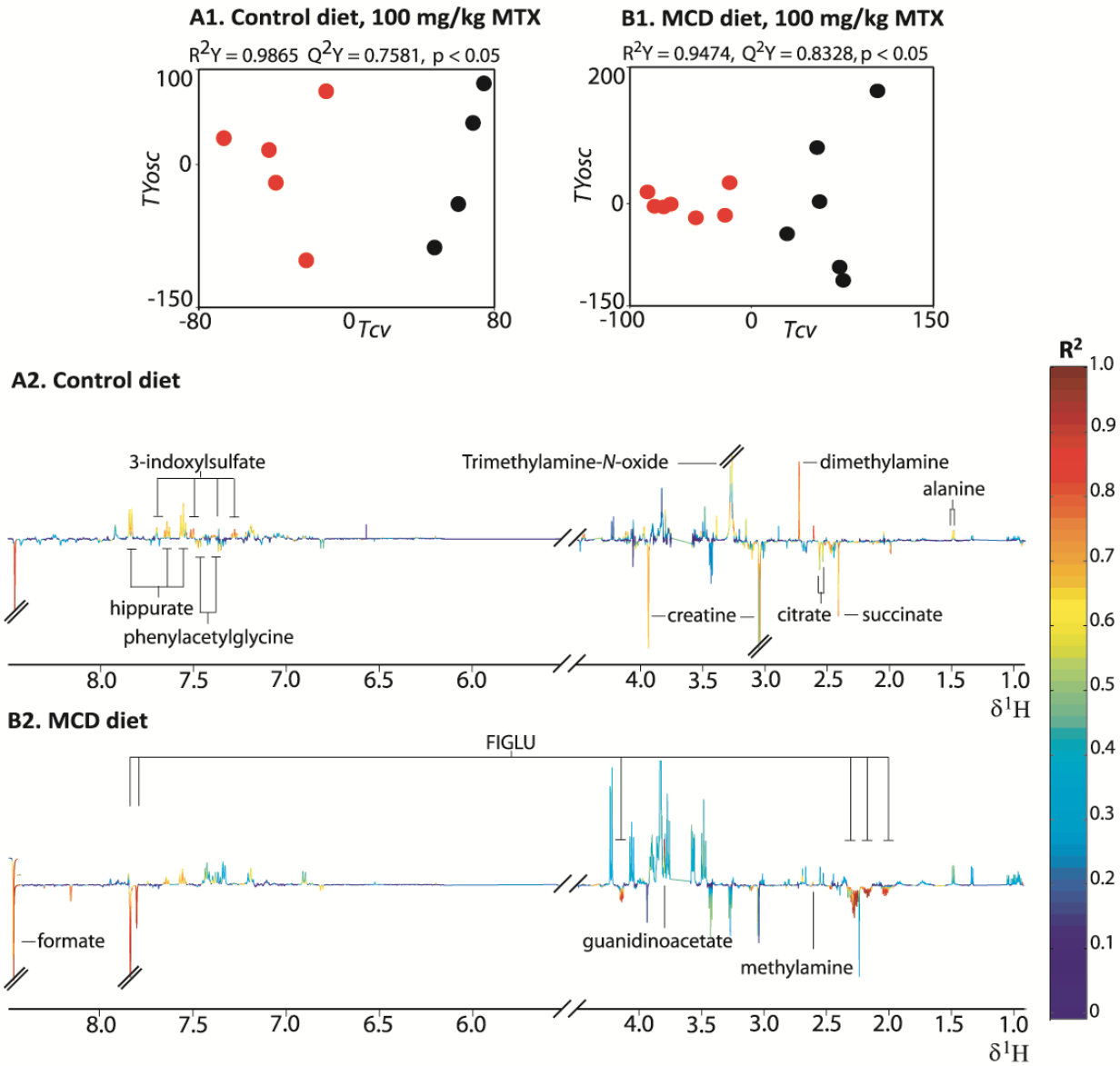


Figure 5.9: Urinary O-PLS-DA models comparing the pre-dose time period (0hr; black) and at 48hr (red) after 100 mg/kg MTX administration in the normal diet (A1 and A2; *n* = 5 and *n* = 4 respectively) and MCD diet (B1 and B2; *n* = 6 for both). See Legend for Figure 5.3.

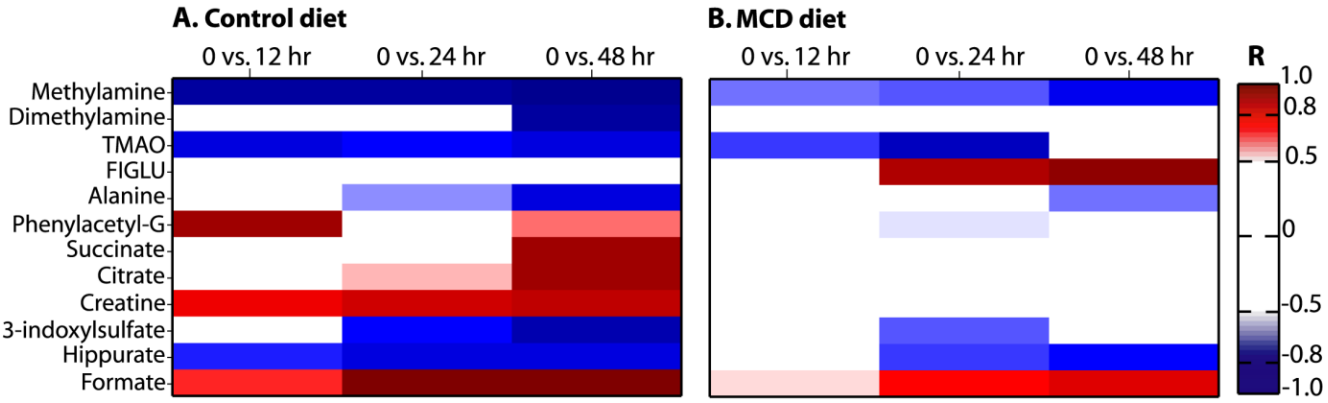


Figure 5.10: A heatmap of the urinary metabolic effects of MTX administration in the control diet (A) and MCD diet (B) from the O-PLS-DA models that discriminated between the metabolic profiles of the post-dose time-periods (12hr, 24hr and 48hr) of MTX administration (100 mg/kg) and the pre-dose time-periods (0hr), in both diets. Phenylacetyl-G phenylacetylglycine; TMAO – trimethylamine-*N*-oxide.

Urinary quantitation of MTX

The quantity (µg) of MTX in the urine of animals from each diet group was also compared at a number of post-dose time-points following administration of the highest dose of MTX (100 mg/kg). The levels of excreted MTX were observed to be higher in the control diet group at all time-periods (Figure 5.11).

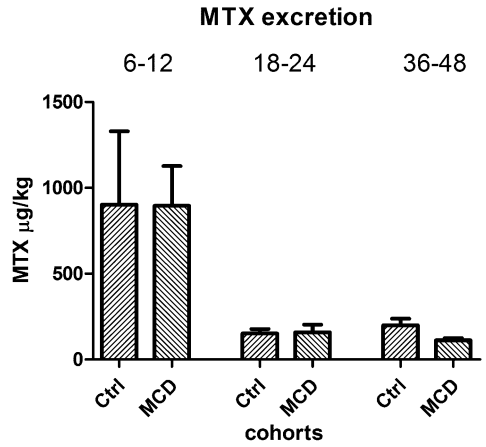


Figure 5.11: Mean and standard deviation of the quantity of urinary MTX (µg) per kg of rat following the administration of 100 mg/kg MTX at 6-12 hours, 18-24 hours and 36-48 hours.

Discussion

The metabolism, toxicity, pharmacokinetics and clinical profile of MTX have been extensively studied since the first report by Farber et al concerning the treatment of children with acute leukaemia (Kremer, 2004, Farber et al., 1956). Despite our existing knowledge, there is a lack of sound understanding concerning the hepatotoxic and multiorgan toxic effects of the drug or its potential to cause ADRs in people with underlying diseases such as NASH. Therefore, an improved understanding of the complexities of MTX metabolism will inevitably lead to safer and more effect therapeutic treatments (Kremer, 2004).

Metabolic and toxic effect of MTX administration in healthy rats

The observed liver necrosis and small intestine toxicity induced by MTX administration (40 and 100 mg/kg and 100 mg/kg respectively) comprise some of the classic ADR symptoms of MTX (Feagan et al., 1995, Lobo and Balthasar, 2003). The ^{1}H-NMR O-PLS-DA models of MTX administration in the three sample matrices characterized the metabolic perturbations associated with these pathophysiological conditions. A general dose-dependent progressive metabolic effect was observed in all three sample matrices while a temporal effect was also observed in the faecal water and urine O-PLS-DA models, where the effect of MTX was becoming more significant over time. The MTX-induced metabolic effect was observed to affect various pathways including those of amino acids, nucleobases, nucleosides, energy metabolites and choline metabolisms.

The metabolic effects pertaining to nucleic acid related molecules are most likely due to the inhibitory properties of MTX on enzymes involved in nucleic acid and folate cycle metabolism. The observed elevation in the levels of hepatic and faecal water uracil after the administration

of the (100 mg/kg) dose is potentially a result of MTX-induced thymidylate synthetase inhibition. The depletion of hepatic inosine (10 and 100 mg/kg MTX) could also be due to the reported MTX-induced inhibition of AICAR transformylase (Genestier et al., 2000). Moreover, the elevation of hypoxanthine observed after the administration of the highest dose of MTX could be linked to the inhibition of xanthine oxidase, an enzyme that forms xanthine from hypoxanthine (Lewis et al., 1984).

The inhibition of DHFR by MTX would lead to a disruption of the folate cycle which would have consequences in a spectrum of metabolic pathways including the aforementioned nucleic acid metabolism (Genestier et al., 2000). Since we could not detect any of the folate cycle intermediates in the ^{1}H-NMR metabolic profiles, the effect of the disruption could be observed via the levels of metabolites that directly interact with folate cycle intermediates. For example, the higher levels of hepatic formate could be due to the lower rate of formyl-THF formation, as a consequence of a drop in THF production. The higher levels of sarcosine after administration of MTX (10 and 40 mg/kg) could also be a consequence of THF depletion since THF is required by sarcosine dehydrogenase for the conversion of glycine to sarcosine (Lu and Mato, 2012). However, it is not clear why this wasn't observed after the administration of the highest dose but it could be due to the variation in faecal content between the individual samples. Furthermore, raised putrescine levels in the faecal water metabolic profiles could be linked to a reduction of S-adenosylmethionine regeneration. Putrescine is converted to spermidine and spermine through a methyl group addition provided by S-adenosylmethionine (Tabor et al., 1958). MTX could affect S-adenosylmethionine regeneration through the disruption of the folate cycle or through the inhibition of S-adenoyltransferase expression, which would reduce the rate of conversion of

methionine to S-adenosylmethionine (Nesher et al., 1991, Wang and Chiang, 2012). Finally, the absence of an elevation of urinary and hepatic FIGLU at any dose of MTX suggests that the disruption of the folate cycle was not absolute (Cooperman and Lopez, 2002).

The observed depletion of energy metabolites including lactate, glucose, glycogen and maltose is associated with the observed weight loss. Weight loss could have occurred due to a reduced dietary intake, intestinal toxicity of MTX (gut absorption dysfunction and mucositis) and a possible MTX-induced inhibition of oxidative phosphorylation, which would lead to a higher utilization of energy metabolites through other metabolic pathways (Yamamoto et al., 1988, Yamamoto et al., 1992, Naruhashi et al., 2000). The elevation of D-3-hydroxybutyrate could also reflect an increased rate of lipid breakdown as a consequence of a general shift in energy metabolism. This conclusion is also supported by the elevated levels of DHA in the faecal water which could also be a sign of lipid breakdown and gluconeogenesis. DHA is a product of glycerol breakdown while its phosphorylated form is an important intermediate of glycolysis and gluconeogenesis (Ouellette et al., 2013, Liu et al., 1995).

Another metabolic consequence linked to dietary intake could be the depletion of metabolites linked to choline metabolism including hepatic phosphocholine and dimethylamine (Figure 5.5) as well as urinary TMAO, methylamine, dimethylamine and trimethylamine (Figure 5.10). However, the observed elevations of hepatic choline and glycerophosphocholine (tentative assignment) are contradictory to the overall pattern and suggest that the levels of these metabolites are not directly indicative of dietary intake. Furthermore, the fluctuation of choline levels is expected to be controlled by multiple factors since choline has many important functions within the body (Zeisel and Blusztajn, 1994).

Finally, other metabolic perturbations that could be linked to the weight loss or reduced dietary intake include the depletions of hepatic glutathione, urinary 3-indoxylsulphate (a tryptophan catabolism intermediate) and hippurate (Szkudelski et al., 2004, Connor et al., 2004). However, the overall pattern of urinary metabolic changes after MTX administration did not reflect the pattern observed in the Wistar Han rat fasting studies by Connor *et al*, while the levels of metabolites such as citrate and succinate were actually elevated in this study, in contrast to that investigation (Connor et al., 2004). Therefore it cannot be assumed that a potential reduced dietary intake is the driving force for the observed aforementioned metabolic changes. A summary of the metabolic effects and histopathology in the control diet after MTX administration is presented below in Figure 5.12.

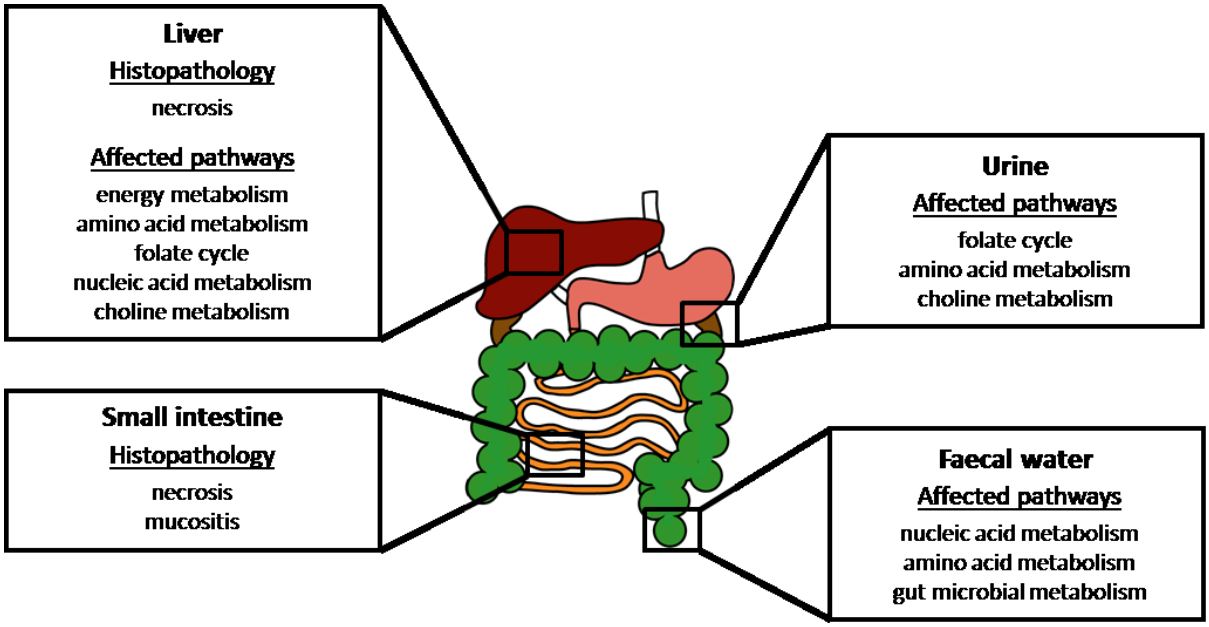


Figure 5.12: A summary of the histopathology and metabolic effects common to both diets after the administration of the highest dose of MTX (100 mg/kg).

The MCD diet affects the disposition and toxicity of MTX

The hypothesis of this investigation was that the MCD diet background, which has been reported to affect drug metabolizing enzymes and hepatic transporters (Fisher et al., 2009,

Hardwick et al., 2011), would alter the metabolic effect of MTX. Hepatic histopathology revealed that administration of MTX (40 mg/kg) in the MCD diet group led to a histomorphologic reduction of liver inflammation and lipid accumulation at a statistically significant level. This reduction could be due to the anti-inflammatory properties of MTX, while it has also been reported to affect cholesterol transport and accumulation (Genestier et al., 2000, Coomes et al., 2011). Administration of the highest dose of MTX (100 mg/kg) led to the development of biliary hyperplasia and liver fibrosis revealing an enhanced MTX toxicity in a NASH background. The lipid accumulation and liver inflammation scores were similar to those of the baseline (vehicle) group after the administration of the highest dose, suggesting that the toxic effects of MTX were outweighing its therapeutic properties at the highest dose.

Differences in the MTX-induced metabolic effect between the two diets were also identified suggesting that the NASH background altered the metabolic consequences of MTX administration. More specifically, the increased levels of FIGLU, urocanate, phenylalanine, acetate, fumarate and niacinamide were only seen in the hepatic extract analysis. Furthermore, the MTX-induced increase of urinary succinate, citrate, creatine and phenylacetylglycine in the control diet group were not observed in the MCD diet group, while the MTX-induced elevation of faecal water methionine was also specific to the MCD diet group.

Phenylalanine was identified as the only endogenous metabolite to be associated with the development of liver fibrosis and biliary hyperplasia by a regression analysis (Figure 5.6). The levels of phenylalanine can be used as a measure of liver function since they are reflective of phenylalanine hydroxylase activity, which converts phenylalanine to tyrosine (Burke et al.,

1997). MTX has also been associated with higher serum phenylalanine levels and it is thought to be through the MTX-induced inhibition of dihydropteridine reductase, an enzyme that produced an essential cofactor for the conversion of phenylalanine to tyrosine (Hilton et al., 1989). Both of these hypotheses would suggest that hepatic tyrosine should be at lower levels in response to the higher levels of phenylalanine but that was not observed throughout the analysis. Therefore there must be another mechanism by which MTX affects phenylalanine levels, which is likely to be closely associated with the development of liver fibrosis and biliary hyperplasia.

The elevations of hepatic metabolites associated with the folate cycle following MTX administration, such as FIGLU and urocanate are signs of a significant disruption of the cycle through the depletion of THF. Furthermore, the MTX-induced higher levels of methionine in the MCD diet group could be linked to the inhibition of methionine S-adenosyltransferase and are indicative of methionine cycle dysfunction (Wang and Chiang, 2012). The absence of these effects in the control diet suggest that the MCD diet and MTX can synergistically disrupt the folate and methionine cycles more severely than MTX on its own. Since NASH has also been reported to affect the methionine cycle through the depletion of glutathione, these are potentially clinically relevant demonstrations of how NASH and MTX can affect folate and methionine metabolism and lead to more severe ADRs (Kalhan et al., 2011a).

The relatively higher levels of MTX excretion in the in the 48hr time period in the control diet, relative to the MCD diet group, was potentially related to the higher excretion of MTX in the MCD diet in the first six hours post-dose (recently published data by our collaborators). The observed higher early urinary excretion in the MCD diet group could be due to a reduced

absorption of MTX from the gastrointestinal tract or through a diminished expression of uptake transporter genes in unhealthy livers ,as reported (Lake et al., 2011).

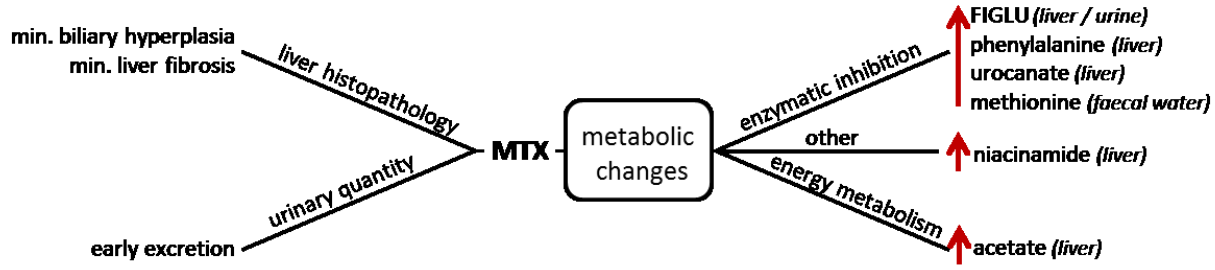


Figure 5.13: Summary of the unique effects of MTX in the MCD diet group.

Effect of MTX on gut microbial co-metabolites

The urinary and faecal water extract metabolic changes after MTX administration are also suggestive that there might be a disturbance of gut microbial populations in both diet groups. MTX has been reported to affect gut microbial composition (Naruhashi et al., 2000), while small intestinal toxicity was also observed in this study after MTX administration in both diet cohorts (100 mg/kg). MTX has been reported to induce intestinal mucositis through the reduction of gut mucin content (Boukhettala et al., 2009). The reduction of mucin levels could be related to the ability of bacteria to degrade mucin to smaller components leading to the higher levels of galactose and fucose that were observed in the faecal water extract of both diets after MTX administration (Hoskins et al., 1992, Chow and Lee, 2008). However, further investigation is required to verify the link between mucositis and an increased excretion of fucose and galactose.

The higher levels of valine and 5-aminovalerate in the faecal water extracts of the MTX administered rats could be reflective of intestinal malabsorption or bacterial overgrowth. Branched chain amino acids such as valine can be released from dietary protein via gut microbial mediated hydrolysis (Romick-Rosendale et al., 2009), while 5-aminovalerate is a

product of lysine degradation (Fothergill and Guest, 1977). In contrast to the suspected bacterial overgrowth in the small intestine, the MTX-induced reduction in the levels of propionate and acetate, two products of colonic fermentation, are indicative of a reduction or a change in the population of gut microbiota in the colon. However, another possible scenario unrelated to a population change of gut microbiota is the possible increased uptake of these gluconeogenesis substrates by the liver in order to produce more energy due to the aforementioned shift in energy metabolism (Tremaroli and Backhed, 2012). Finally, signs of changes in the gut microbial balance were also observed in the urinary metabolic profiles through the depletion of methylamine, TMAO and 3-indoxylsulphate (Nicholson et al., 2012).

Study limitations and future work

The limitations associated with the use of the MCD diet as a model of NASH have been previously discussed in Chapter 1 and 4, while the limitations associated with the analytical procedures that were used in this study have been already discussed in Chapter 4. Furthermore, the faecal water analysis was especially confounded by the low sample numbers per group post-MTX administration (100 mg/kg) in the control diet.

The administration of MTX to animals fed the MCD diet could perhaps induce an exaggerated disruptive effect on the folate cycle. Even though the clinical condition of NASH can also affect the folate cycle, it would be interesting to determine how concomitant folate supplementation would affect the subsequent metabolic and toxic effect of MTX in the context of the MCD diet. Another important limitation associated with the study design is the lack of food intake recording which complicated the interpretation of the metabolic profiling analysis. Induction of toxicity through the administration of MTX would expectedly lead to a reduction in food intake by the animals but it was not possible to quantify the exact effect

since food intake was not recorded. Regression analyses between the hepatic extract metabolic profiles and the percentage weight loss revealed that mostly energy metabolites were correlated to the weight loss, but that was not necessarily due to a reduction in food intake since MTX can also affect gut absorption. It is worth noting that the aforementioned unique hepatic effects of MTX in the MCD diet group were not found to be correlated to weight loss. Finally, it was difficult to infer the exact effect of MTX on gut microbial populations through the induced metabolic changes. The observed changes could be more directly related to the MTX induced gastrointestinal toxicity which would have secondary effects on the gut microbial population.

A future more targeted approach could be employed to investigate the potential mechanisms by which MTX administration can lead to greater toxicity in the MCD diet. More specifically, the underlying mechanism of the elevation of phenylalanine could be determined through the quantification of the expression of genes or proteins relative to phenylalanine catabolism as a first step, in order to obtain an improved mechanistic understanding. In relation to the suspected gut microbial perturbations, metagenomic sequencing could also be performed to decisively conclude whether the administration of MTX affected gut microbial populations (Janda and Abbott, 2007).

Chapter 6: Cross liver metabolic characterization of decompensated cirrhosis, acute on chronic liver failure and acute liver failure

Introduction

Study details and aims

This study employed metabolic profiling to discriminate serum ^{1}H-NMR metabolic profiles from decompensated cirrhotic, ACLF and ALF patients. The metabolic discrimination of the serum reflecting different liver conditions, relative to healthy controls, enabled the determination of metabolic perturbations associated with each disease, with the aim to improve our understanding of the respective underlying mechanisms associated with disease development. In addition, this study incorporated a novel "cross liver" metabolic characterization of serum using ^{1}H-NMR spectroscopy to acquire the metabolic profiles of the hepatic portal vein, hepatic vein and a peripheral artery in the context of differential aetiologies requiring liver transplantation. The comparison of the metabolic profiles from the three blood vessels facilitated the transverse characterization of the metabolic state of the liver during disease.

Methods

The study design, patient selection and sample collection were performed by our collaborators at Kings College Hospital. The "cross liver" sample set was acquired during liver transplantation.

Patient selection and sample collection

A local national research ethics service (NRES) approval was obtained for this study and patients or their nominee provided written informed consent within 24 hours of admission to Kings College Hospital. Patients suffering from decompensated cirrhosis (*n* = 33), ACLF (*n* = 26) and ALF (*n* = 17) were enrolled in the study, while patients suffering from viral diseases such as hepatitis B/C were not included. Nine volunteers were also recruited as healthy controls. For the hepatic disease comparison sample set, blood samples from an artery or vein in the upper limb were collected from each patient during the first day of admission as well as from the nine healthy volunteers. For the "cross liver" sample set, blood samples from the hepatic portal vein, hepatic vein and peripheral artery (usually radial or brachial artery) were collected during liver transplantation (*n* = 14). A mixture of propofol, noradrenaline, alfentanyl or fentanyl was administered to the patients during the surgical procedure. Sera fractions were collected after the incubation of the collected blood samples at room temperature and centrifugation at 4,000 g for 10 minutes at 4^{o}C. All samples were then stored at -80^{o}C.

Clinical and demographic data including, age, sex, BMI, serum biochemistry and physiology are provided, while the 30 day, 90 day and one year survival rates, as well as the hepatic encephalopathy (HE) grade, Child Pugh, sequential organ failure assessment (SOFA) and model for end-stage liver disease (MELD) scores were also calculated and provided per

disease group. The MELD score is used to assess whether a patient requires a liver transplant, while the SOFA score is used to track a patient's status in the intensive care unit. A summary of the patient population of the general disease comparison and "cross liver" sample sets can be seen in Tables 6.1 and 6.2 respectively.

Sample preparation and ^{1}H-NMR spectroscopy of serum

Sera samples were thawed, vortexed for a period of 15 seconds and allowed to stand for 10 minutes. The samples were then mixed with phosphate buffer (1:1, 600 µL total volume; 20 % D_2O, 0.142 M $NaHPO_4$, 2 mM NaN_3, 4 mM TSP) and were centrifuged for 15 minutes at 16,000 g at 4^{o}C. The resulting supernatants were then transferred to 5 mm NMR tubes (SampleJet Tube Z105684; Bruker) for NMR spectral acquisition. A standard one-dimensional solvent suppression pulse sequence and CPMG spin-echo pulse sequence were used to acquire the FID. The acquisition parameters for each pulse sequence can be seen in Table 8.1 in the appendix.

^{1}H-NMR spectral data processing

The NMR spectra were processed in TopSpin 3.0 NMR software (Bruker) and MATLAB (Mathworks) as previously described in Chapter 3. Processing prior to alignment included the removal of the TSP and water resonances, while the data were not normalized prior to statistical analysis. Spectral assignments were performed using STOCSY, spectral databases (in-house, Human Metabolome Database and Biological Magnetic Resonance Bank), Chenomx NMR Suite and previously published assignments (Nicholson et al., 1995).

Statistical analysis

Non-parametric ANOVA (Kruskal-Wallis) coupled to Dunn's multiple test correction was used to compare the baseline characteristics and clinical data of the different disease groups (Tables 6.1 and 6.2).

Hepatic disease comparison sample set: O-PLS-DA in MATLAB (Mathworks, using in-house scripts) was used to discriminate in pair-wise models between the serum metabolic profiles of the healthy volunteers and the three disease groups. PLS analysis in MATLAB (Mathworks, using in-house scripts) was used to identify the correlation between the metabolic profiles of the decompensated cirrhotic and ACLF metabolic profiles with the 30 day, 90 day and 1 year survival rates.

"Cross liver" sample set: Prism 5.0 (Graphpad) was used to conduct non-parametric univariate analysis between the integrals of metabolites from the three blood vessels (Friedman test coupled to Dunn's multiple correction test) and between the chronic liver disease samples (decompensated cirrhotics and ACLF) and the ALF samples, for each blood vessel (Mann-Whitney with Bonferonni multiple test correction). A non-parametric repeated measures ANOVA (Friedman test) was used because intra-individual variance between the blood vessel metabolic profiles of each patient was lower than the inter-individual variance of the metabolic profiles of the blood vessels between different individuals.

All multivariate models were validated by permutation testing ($p < 0.05$, $n = 1000$) and the summary of results are presented in the form of a heatmap presenting the maximum Pearson correlation values for each resonance obtained from models with a cut-off of $R > |0.5|$.

Results

Clinical characteristics of decompensated cirrhosis, ACLF and ALF

The baseline characteristics and clinical data of the decompensated cirrhosis, ACLF and ALF patients who were enrolled in the study are presented in Table 6.1. The clinical data include age of the patient, grade of hepatic encephalopathy (HE) and total bilirubin levels which are part of the King's College criteria (O'Grady et al., 1993), as well as other clinical parameters which are commonly measured in ALF cases, such as lactate, total bilirubin, urea and haemoglobin levels (Polson et al., 2005).

Decompensated cirrhosis patients had a statistically significantly higher age than their ACLF and ALF counterparts, as well as higher levels of haemoglobin relative to ACLF patients. In contrast, bilirubin levels were statistically significantly lower in decompensated cirrhosis patients relative to ACLF patients, while the levels of creatinine were also lower relative to both ACLF and ALF patients. Clinically derived disease scores such as HE grade, Child Pugh, MELD and SOFA scores were statistically significantly higher in ALF and ACLF patients, relative to decompensated cirrhotics. White blood cell count and lactate levels were also statistically significantly elevated in ALF patients relative to decompensated cirrhosis patients. Furthermore, liver enzymes such as aspartate aminotransferase (AST) and ALT were statistically significantly higher in the ALF group, relative to the other two disease groups, while ACLF patients also had higher levels of AST relative to decompensated cirrhosis patients. Finally, ACLF was associated with the lowest survival rate (30 day, 90 day and 1 year), which was statistically significantly lower at all periods relative to decompensated cirrhosis, as well as at 90 day and 1 year relative to ALF patients. Figure 6.1 presents the mean and standard deviation of the aforementioned statistically significantly clinical parameters for each group.

Parameter	Disease			Healthy volunteers
	Decompensated cirrhosis	Acute on chronic liver failure	Acute liver failure	
Number	33	26	17	9
Age	57.0 *(46.0 – 62.0)*	47.5 *(35.5 – 53.5)*	34.0 *(34.0 – 46.0)*	34.0 *(32.0 – 39.0)*
Gender (% female)	39.4	26.9	70.6	44
BMI	26.5 *(21.2 – 28.9)*	22.9 *(20.9 – 23.1)*	21.3 *(20.8 – 23.0)*	-
HE grade	1 *(0 – 1)*	3 *(2 – 4)*	3 *(1 – 4)*	-
Child Pugh score	9.0 *(8.0 – 11.0)*	12.0 *(11.0 – 13.8)*	12.0 *(11.0 – 13.0)*	-
MELD score	12.7 *(10.8 – 23.9)*	35.7 *(29.8 – 39.3)*	42.0 *(35.8 – 50.0)*	-
SOFA score	5.0 *(3.3 – 8.3)*	15.0 *(12.0 – 17.0)*	10.0 *(9.0 – 16.0)*	-
30 day survival (%)	87.9	53.8	82.4	-
90 day survival (%)	84.8	46.2	82.4	-
1 year survival (%)	71.5	32.0	78.6	-
ALT (IU/L)	33.0 *(25.0 – 57.0)*	60.5 *(26.8 – 289.8)*	3734.0 *(1407.0 – 6843.0)*	-
AST (IU/L)	55.0 *(40.0 – 100.0)*	169.0 *(66.8 – 525.3)*	5216.0 *(1840.0 – 9480.0)*	-
GGT (IU/L)	85.0 *(38.0 – 186.0)*	59.0 (36.0 – 172.3)	88.0 *(36.0 – 174.0)*	-
Bilirubin (µM)	54.0 *(29.0 – 172.0)*	186.5 *(95.8 – 331.8)*	96.0 *(57.0 – 177.0)*	-
Serum creatinine (µM)	82.0 *(61.0 – 116.0)*	155.5 *(124.8 – 197.5)*	148.0 *(79.0 – 248.0)*	-
Lactate (mM)	1.7 *(1.4 – 2.3)*	2.3 *(1.4 – 5.1)*	3.1 *(2.6 – 6.2)*	-
Urea (mM)	7.1 *(5.0 – 10.9)*	9.5 *(6.4 – 13.1)*	11.2 *(3.6 – 12.2)*	-
Haemoglobin (g/dL)	109 *(91.0 – 124.0)*	89.5 *(83.3 – 98.3)*	98.0 *(88 – 121.0)*	-
WBC (10^9/L)	6.5 *(4.5 – 9)*	10.2 *(7.0 – 15.7)*	13.3 *(8.7 – 17.8)*	-

Table 6.1: Baseline and clinical parameters of the patients are shown above. The median values and 25%/75% interquartile range values (in brackets) are shown for each parameter where applicable. WBC - white blood cell; ALT – alanine aminotransferase; AST – aspartate aminotransferase; SOFA – sequential organ failure assessment; MELD – model for end-stage liver disease; HE – hepatic encephalopathy; GGT – gamma-glutamyl transferase.

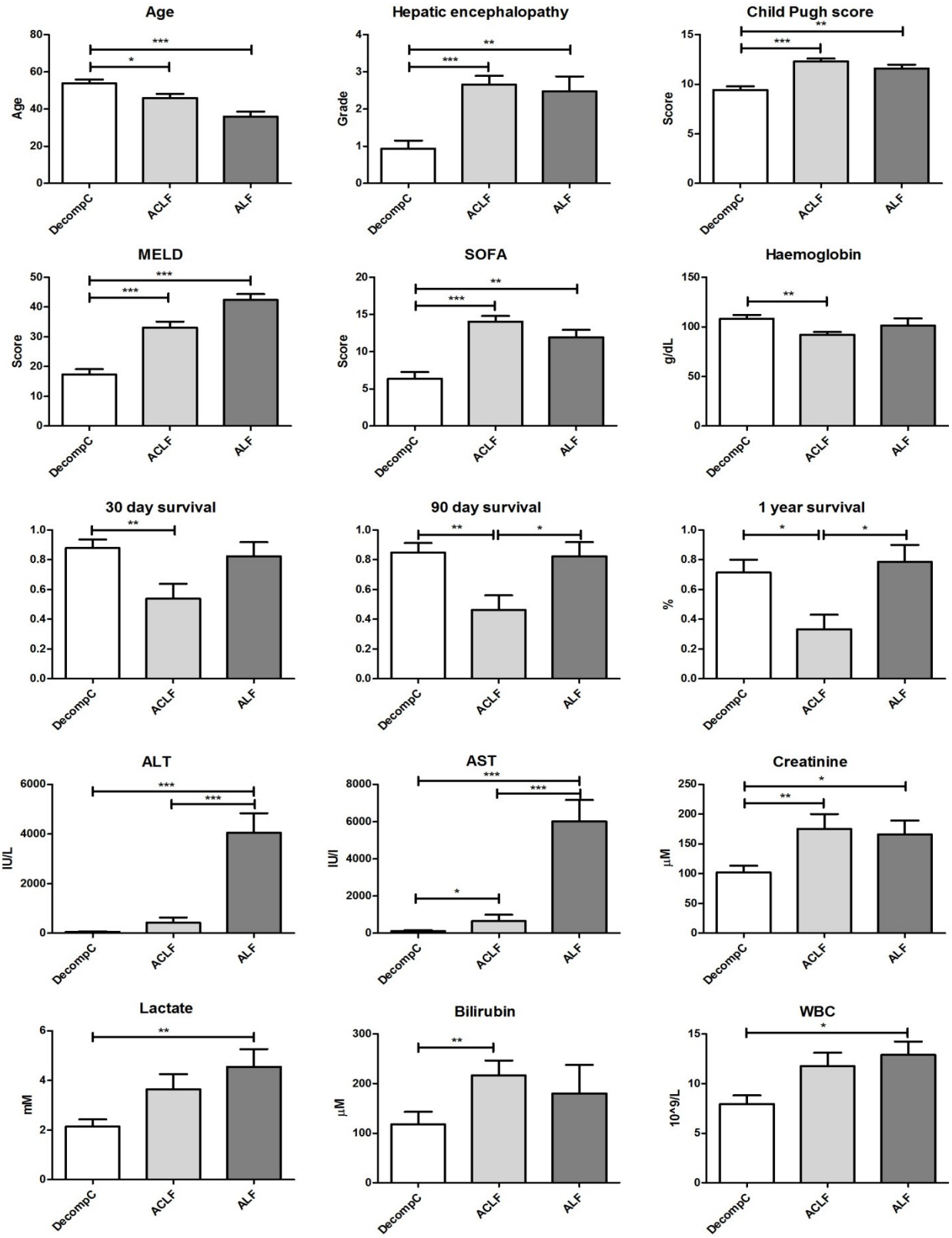


Figure 6.1: The mean and standard deviation are shown for the statistically significantly different parameters between the three disease groups. Kruskal-Wallis coupled to Dunn's multiple test correction was used to test for statistical significance at $p < 0.05$, $p < 0.01$ and $p < 0.001$ which are represented by *, ** and *** respectively. Please see legend of Table 6.1 for more details concerning the subjects.

Serum metabolic phenotype of decompensated cirrhosis, ACLF and ALF

O-PLS-DA models were constructed to identify the discriminatory metabolites in the serum metabolic profiles of decompensated cirrhosis (*n* = 33), ACLF (*n* = 26) and ALF (*n* = 17) relative to those of healthy controls (*n* = 9). The O-PLS-DA model discriminating between the serum metabolic profiles of decompensated cirrhosis from healthy controls (Figure 6.2A; R^2Y = 0.8719 and Q^2Y = 0.6679; $p < 0.05$) achieved complete separation between the two groups in multivariate space (Tcv; Figure 6.2A1). The equivalent coefficient plot (Figure 6.2A2) revealed that the levels of phenylalanine and tyrosine were elevated in the decompensated cirrhotic metabolic profiles, while the levels of lipid fatty acyl chains (resonance at δ 0.89), choline containing phospholipids (resonance at δ 3.23) and valine were depleted, relative to controls. The O-PLS-DA model discriminating between the ACLF and control serum metabolic profiles (Figure 6.2B; R^2Y = 0.8776 and Q^2Y = 0.7517; $p < 0.05$) also achieved complete separation in the scores plot (Tcv; Figure 6.2B1). The corresponding coefficient plot (Figure 6.2B2) showed that the levels of phenylalanine, pyruvate and isobutyrate were elevated in the ACLF patients, while the levels of lipid fatty acyl chains (resonance at δ 0.89) and choline containing phospholipids (resonance at δ 3.23) were depleted. Finally, the O-PLS-DA model discriminating between the ALF and control serum metabolic profiles (Figure 6.2C; R^2Y = 0.9032 and Q^2Y = 0.7970 and; $p < 0.05$) also achieved complete separation in the scores plot (Tcv; Figure 6.2C1). The equivalent coefficient plot (Figure 6.2C2) inferred that lysine, glutamine, phenylalanine, tyrosine, methionine, citrate, fumarate, acetate, glycerol, pyruvate, formate and isobutyrate were elevated in the ALF patients, while the levels of lipid fatty acyl chains (resonance at δ 0.89) and choline containing phospholipids (resonance at δ 3.23) were depleted, relative to control.

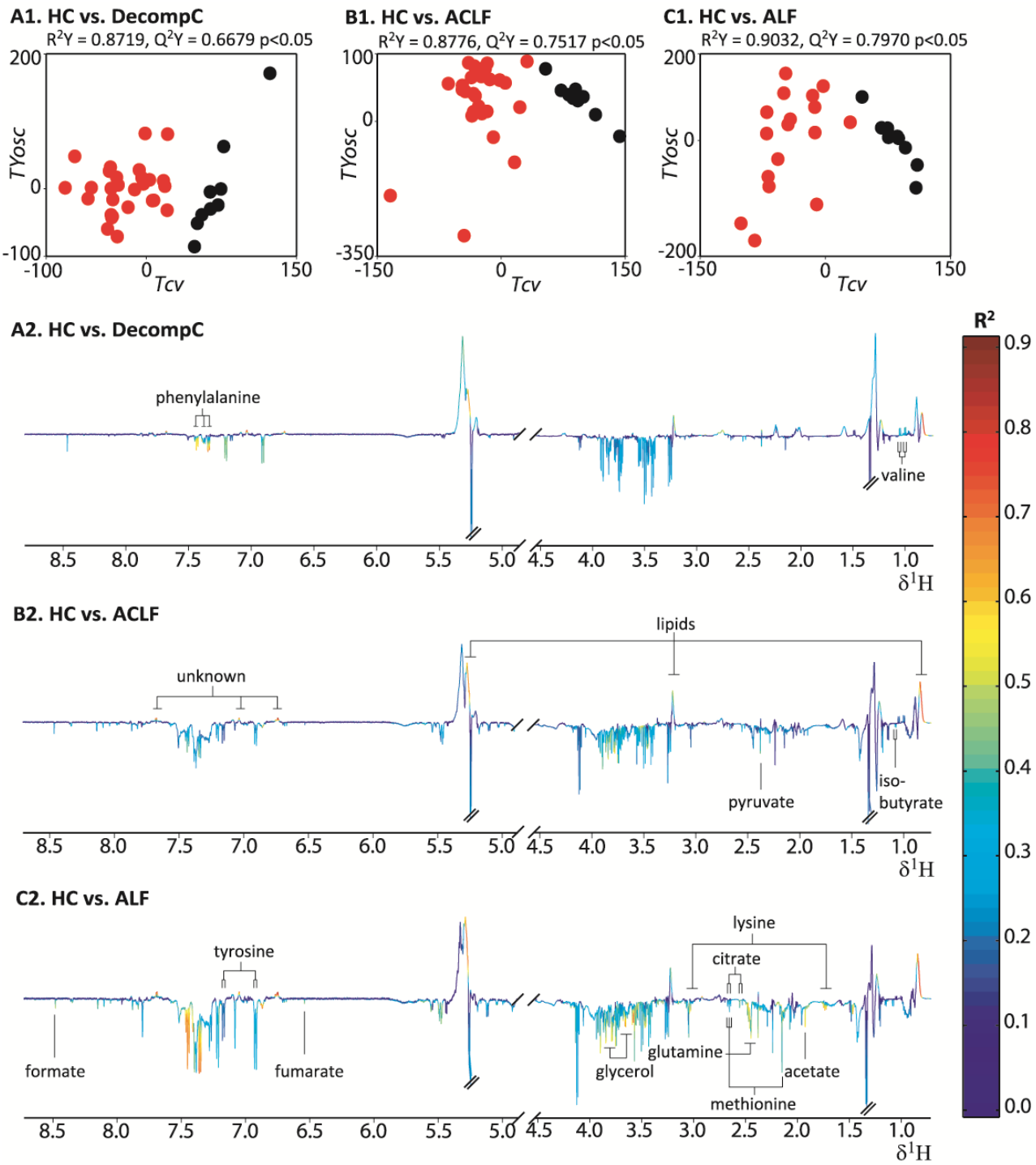


Figure 6.2: Serum O-PLS-DA models comparing the decompensated cirrhotic (*n* = 33; A), ACLF (*n* = 26; B) and ALF (*n* = 17; C) metabolic profiles, relative to those of healthy controls (*n* = 9) are shown above. The scores plots (A1, B1 and C1) depict the separation of each disease group (red) relative to the control group (black) in multivariate space. The coefficient plots (A2, B2 and C2) show the correlated resonances with the height of spectral peaks indicating the covariance. The colour-scale represents the coefficient of Pearson correlation (R^2), ranging from low (0; blue) to high (red; 0.9). Resonances pointing up reveal a positive correlation with the metabolic profiles of healthy controls and vice versa. A permutation test was used to test for model validity at $p < 0.05$. HC – healthy controls; DC – decompensated cirrhosis; ALF – acute liver failure; ACLF – acute on chronic liver failure.

Some metabolic perturbations were consistent across all three diseases, including the elevation of phenylalanine, tyrosine, citrate and pyruvate, as well as the general depletion of lipids. However, ALF was associated with the most extensive metabolic disturbance, in terms of the number of perturbed metabolites. A summary of the discriminatory metabolites from the O-PLS-DA models is presented in the form of a heatmap in Figure 6.3.

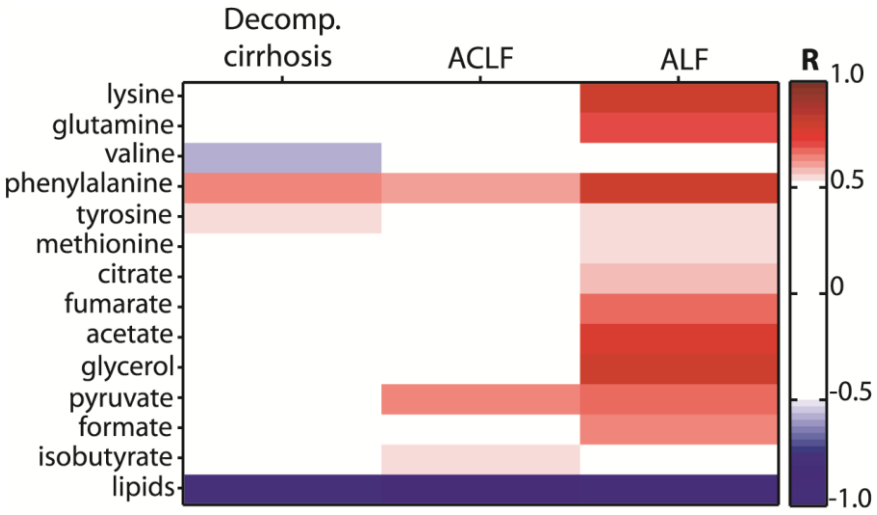


Figure 6.3: The metabolic changes associated with decompensated cirrhosis, ACLF and ALF, relative to healthy controls, are shown above. The maximum Pearson correlation coefficient values (R) for each discriminant metabolite from the O-PLS-DA models are displayed. The scale ranges from -1 (perfect negative correlation; blue) to 1 (perfect positive correlation; red). A cut-off value of |0.5| was set.

Metabolic characterization of APAP-induced ALF

O-PLS-DA was employed to compare the metabolic perturbations associated with APAP-induced ALF and ALF of other aetiologies grouped together, relative to the control group. Other ALF aetiologies included acute Budd-Chiari syndrome, non-APAP induced drug overdose and pregnancy. The O-PLS-DA model discriminating between the non-APAP induced ALF group (n = 9) and healthy controls (n = 9) achieved complete discrimination in the multivariate space (R^2Y = 0.9234 and Q^2Y = 0.7774 and; $p < 0.05$). The corresponding coefficient plot revealed that the non-APAP induced ALF group had higher levels of lysine,

glutamine, tyrosine, phenylalanine, methionine, histidine, fumarate, acetate, glycerol, pyruvate, formate, lactate and isobutyrate, as well as lower levels of lipid fatty acyl chains (resonance at *δ* 0.89) and choline containing phospholipids (resonance at δ 3.23), relative to the control group. The O-PLS-DA model differentiating between the serum metabolic spectra of APAP-induced ALF (*n* = 8) and healthy control (*n* = 9) also achieved complete discrimination of the two groups in multivariate space (R^2Y = 0.9490 and Q^2Y = 0.8303 and; $p < 0.05$). The corresponding coefficient plot revealed that APAP-induced ALF was associated with elevated levels of lysine, glutamine, phenylalanine, tyrosine, methionine, histidine, citrate, fumarate, acetate, glycerol, pyruvate, formate and isobutyrate, as well as the concomitant depletion of lipid fatty acyl chains (resonance at *δ* 0.89) and choline containing phospholipids (resonance at δ 3.23). The majority of the metabolic changes associated with non-APAP induced ALF and APAP-induced ALF were common to both disease groups, albeit at different extents (as determined by the relative correlation values in each model) and the general effect of ALF versus control was observed to be an average of the two sub-groups. The most significant difference in the models of the ALF aetiological sub-groups was the absence of elevated citrate in the non-APAP induced serum metabolic profiles and the absence elevated lactate in the APAP-induced serum metabolic profiles. Furthermore, the levels of tyrosine, methionine, histidine, isobutyrate and formate were significantly more discriminatory in the APAP-induced ALF model. A summary of the discriminatory metabolites from the O-PLS-DA models is presented in Figure 6.4.

Decompensated cirrhosis and ACLF survival PLS analysis

PLS discriminant analysis was employed to characterize the correlation between 30 day, 90 day and 1 year survival rates of the decompensated cirrhosis and ACLF patients with the respective ^{1}H-NMR serum metabolic profiles. The PLS model of the 30 day survival rate (Figure

6.5A; R^2Y =0.2075, Q^2Y = 0.1312, $p < 0.05$) revealed minimal clustering of survivors versus non-survivors in the predictive component of the scores plot (Figure 6.5A1). The corresponding coefficient plot (Figure 6.5A2) showed that alanine, lysine, glycine, histidine, leucine, glutamine, phenylalanine, lactate, pyruvate, isobutyrate and creatine levels were negatively correlated with the 30 day survival rate. The PLS model describing the correlation of the 90 day survival rate with the ^{1}H-NMR serum metabolic profiles (Figure 6.5B; R^2Y = 0.2069, Q^2Y = 0.1263, $p < 0.05$) also revealed minor grouping of survivors versus non-survivors in the scores plot (Figure 6.5B1). The equivalent coefficient plot (Figure 6.5B) showed that the 90 day survival rate was negatively correlated to alanine, lysine, histidine, leucine, glutamine, phenylalanine, lactate, pyruvate, isobutyrate and creatine levels. Finally, the PLS model characterizing the association between the 1 year survival rate and the serum metabolic profiles (Figure 6.5C; R^2Y =0.1563, Q^2Y = 0.0726, $p < 0.05$) showed a higher degree of clustering between the metabolic profiles of survivors versus non-survivors in multivariate space (Figure 6.5C1). The corresponding coefficient plot inferred that lysine, glycine, leucine, glutamine, phenylalanine, lactate, pyruvate, isobutyrate and creatine levels were negatively correlated with the survival rate.

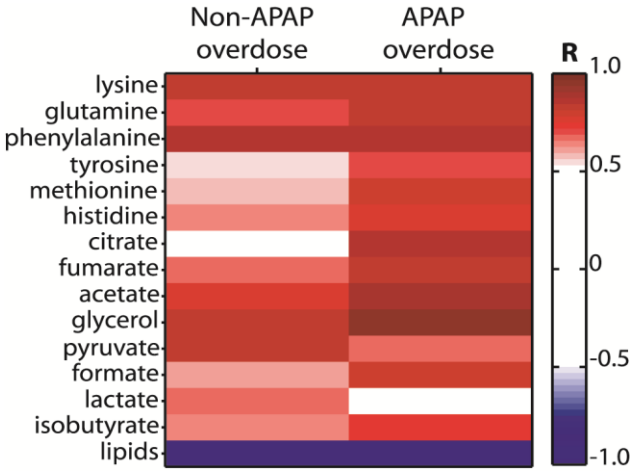


Figure 6.4: The metabolic changes identified by the O-PLS-DA models to be associated with APAP and non-APAP induced ALF, relative to healthy controls, are displayed above. Please see legend of Figure 6.3.

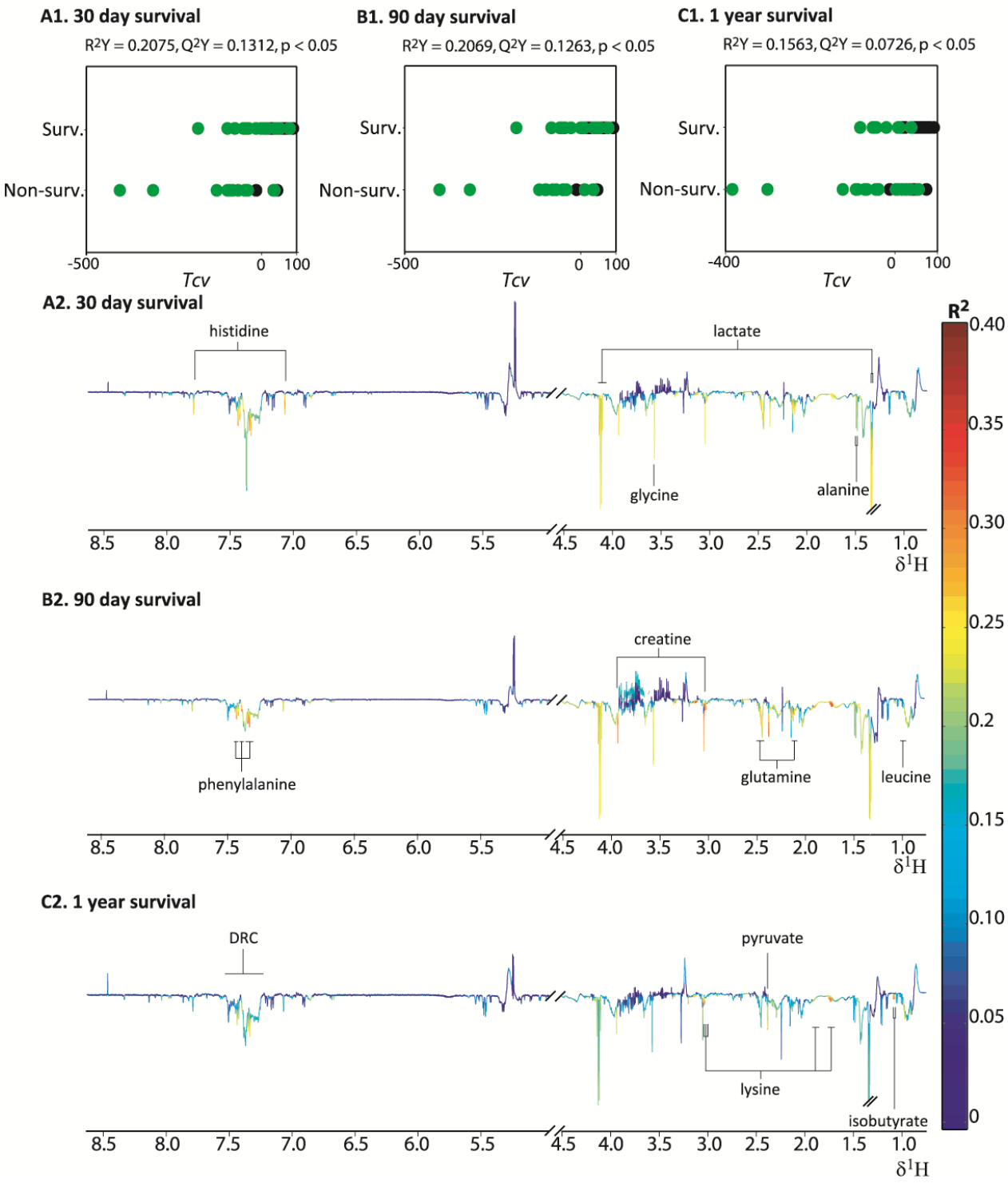


Figure 6.5: The PLS models of the 30, 90 and 1 year survival rates with the ^{1}H-NMR serum metabolic profiles of decompensated cirrhosis black; *n* = 32) and ACLF (green; *n* = 26) patients are shown. The scores plots (A1, B1 and C1) depict the first predictive component (Tcv) and the survivors vs. non-survivors of ACLF (green) and decompensated cirrhosis (black) patients in multivariate space. Resonances pointing upwards reveal a positive correlation with survival and vice versa. Please note that there is extensive overlap of the dots in the scores plot. Please see the legend of Figure 6.2.

The 30 and 90 day PLS analysis had a common pattern of metabolites which were negatively associated with patient survival. A similar pattern was also predicted in the 1 year survival models excluding glutamine, glycine, phenylalanine, histidine and alanine which were not predicted to be negatively correlated with patient survival rate at this time-point. The equivalent PLS analysis which included the ALF patients also showed a similar pattern of negatively correlated metabolites. A summary of the results is presented in the form of a heatmap in Figure 6.6. Please note that the 1 year survival of some patients is still pending, therefore those patients were excluded prior to the PLS analysis.

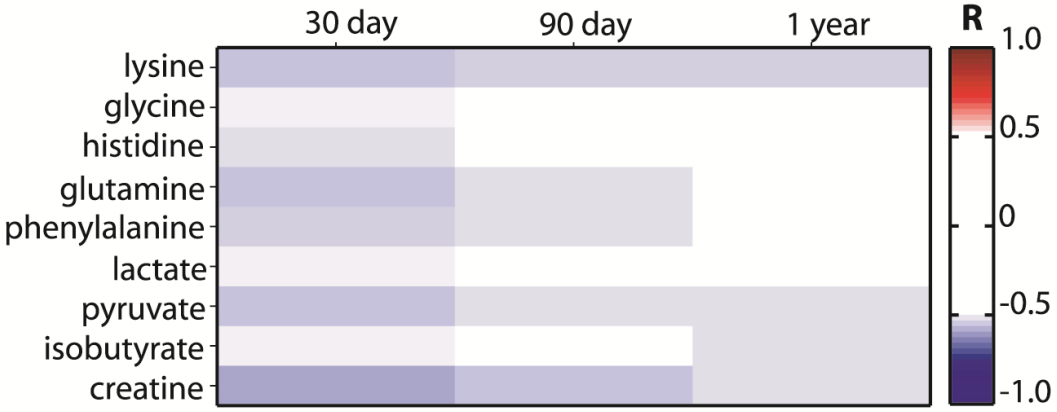


Figure 6.6: The metabolites associated with the 30 day, 90 day and 1 year survival rates of the decompensated cirrhosis and ACLF patients are shown. Please see legend of Figure 6.3.

Clinical characteristics of the "cross liver" sample set

The baseline characteristics and clinical data of the "cross liver" patients obtained on the day of admission are presented in Table 6.2. A statistical comparison (Kruskal-Wallis test coupled to Dunn's multiple test correction) of the clinical data between the different disease groups found that the MELD and SOFA scores, as well as aspartate aminotransferase activity were statistically significantly higher in ALF patients, relative to decompensated cirrhosis patients ($p < 0.05$). The lack of any other differences between the baseline characteristics and clinical data of the different disease groups is potentially due to the very low sample numbers per group.

Parameter	Disease				
	Stable cirrhosis	Decompensated cirrhosis	Seronegative acute liver failure	Acute on chronic liver failure	Acute liver failure
Number	1	4	1	3	5
Age	57.0	51.0 *(51.0 – 54.5)*	49.0	49 *(33.5 – 55.0)*	27.0 *(23.0 – 28.0)*
Gender (% female)	0.0	50.0	100.0	33.3	100.0
BMI	-	25.1 *(23.6 – 26.7)*	20.1	23.1 *(21.8 – 25.0)*	21 *(20.7 – 21.6)*
HE grade	0.0	0.0 (0 – 0.3)	0	1.0 *(0.5 – 2.5)*	4.0 *(3.0 - 4.0)*
Child Pugh score	9.0	9.0 (7.5 – 10.3)	12.0	11.0 *(11.0 – 12.0)*	13.0 *(12.0 – 13.0)*
MELD score	20.8	17.8 (14.5 – 22.4)	30.2	34.3 *(30.4 – 35.0)*	40.0 *(40.0 – 40.0)*
SOFA score	5.0	6.0 (4.8 – 7.5)	7.0	12.0 *(10.0 – 15.5)*	16.0 *(14.0 – 16.0)*
Survival (%, 1 year)	100.0	100.0	100.0	100.0	50.0*
ALT (IU/L)	-	23.0 *(11.5 – 26.5)*	1138.0	91.0 *(45.5 – 253.0)*	2071.00 *(316.3 - 4273.3)*
AST (IU/L)	118.0	47.5 *(39.8 – 60.5)*	307.0	206.0 *(204.0 – 380.5)*	3087.00 *(279.0 - 5216.0)*
GGT (IU/L)	116.0	56 *(41.8 – 92.8)*	215.0	37.0 *(32.0 – 113.0)*	32.0 *(31.0 – 36.0)*
Bilirubin (µM)	234.0	111.0 *(32.8 – 206.8)*	335.0	197.0 *(186.5 – 346.0)*	96.0 *(88.0 – 374.0)*
Serum creatinine (µM)	89.0	72.0 *(66.0 – 9.8)*	115.0	134.0 *(109.5 – 150.0)*	61.0 *(56.0 – 112.0)*
Lactate (mM)	1.8	1.6 *(1.3 – 2.0)*	1.9	1.6 *(1.4 – 1.7)*	4.0 *(2.7 – 4.9)*
Urea (mM)	9.0	5.1 *(4.6 – 14.1)*	4.8	9.6 *(8.2 – 11.5)*	5.0 *(2.5 – 10.6)*
Haemoglobin (g/dL)	133.0	101.1 *(97.5 – 106.3)*	131	93.0 *(86.0 - 95.0)*	111.0 *(88.0 – 121.0)*
WBC (10^9/L)	10.5	5.7 *(3.8 – 6.0)*	10.6	8.2 (6.4 – 15.8)	9.0 *(8.7 – 13.3)*

Table 6.2: Summary of baseline characteristics and clinical data of the patients subjected to a liver transplant. The median values and 25%/75% interquartile range values (in brackets) are shown for each parameter where applicable. Please note that the asterisk indicates that the one year survival rate of the ALF sub-group has not been finalized yet. Please see the legend of Table 6.1.

"Cross liver" metabolic profiling

The "cross liver" disease groups were grouped together to achieve sufficient sample numbers per blood vessel (total $n = 14$) before comparing the metabolite levels in the metabolic profiles of the hepatic portal vein, hepatic vein and peripheral artery by non-parametric repeated measures ANOVA (Friedman test coupled to Dunn's multiple test correction). The analysis revealed that all changes of metabolite levels were relative to the hepatic vein. The levels of histidine, isoleucine, valine, alanine, and lactate were observed to be depleted in the artery relative to the hepatic vein at a statistically significant level ($p < 0.05$), while the levels of an unidentified DRC (aromatic resonances at δ 8.13) were elevated. The levels of glycine, glutamine, lysine, lactate and an N-acetyl resonance (resonance at δ 2.15) were observed to be statistically significantly depleted relative in the hepatic portal vein to the hepatic vein. The integrals of the statistically significant differences are presented in Figure 6.7 and summarized in Table 6.3.

Metabolites	Blood vessel *(relative to hepatic vein)*	
	Artery	Hepatic portal vein
Histidine	**	
Isoleucine	**	
Valine	***	
Alanine	**	
Glycine		*
Glutamine		*
Lysine		*
Lactate	***	***
N-acetyl group		*
DRC	*	

Depleted
Elevated

Table 6.3: Summary of the metabolic differences is presented above. The Friedman test coupled to Dunn's multiple test correction was used to test for statistical significance. Statistical significance is shown by the asterisks *, ** and *** which indicate $p < 0.05$, $p < 0.01$ and $p < 0.001$ respectively. Elevated metabolites are shown in red and vice versa for blue. DRC – drug related compound.

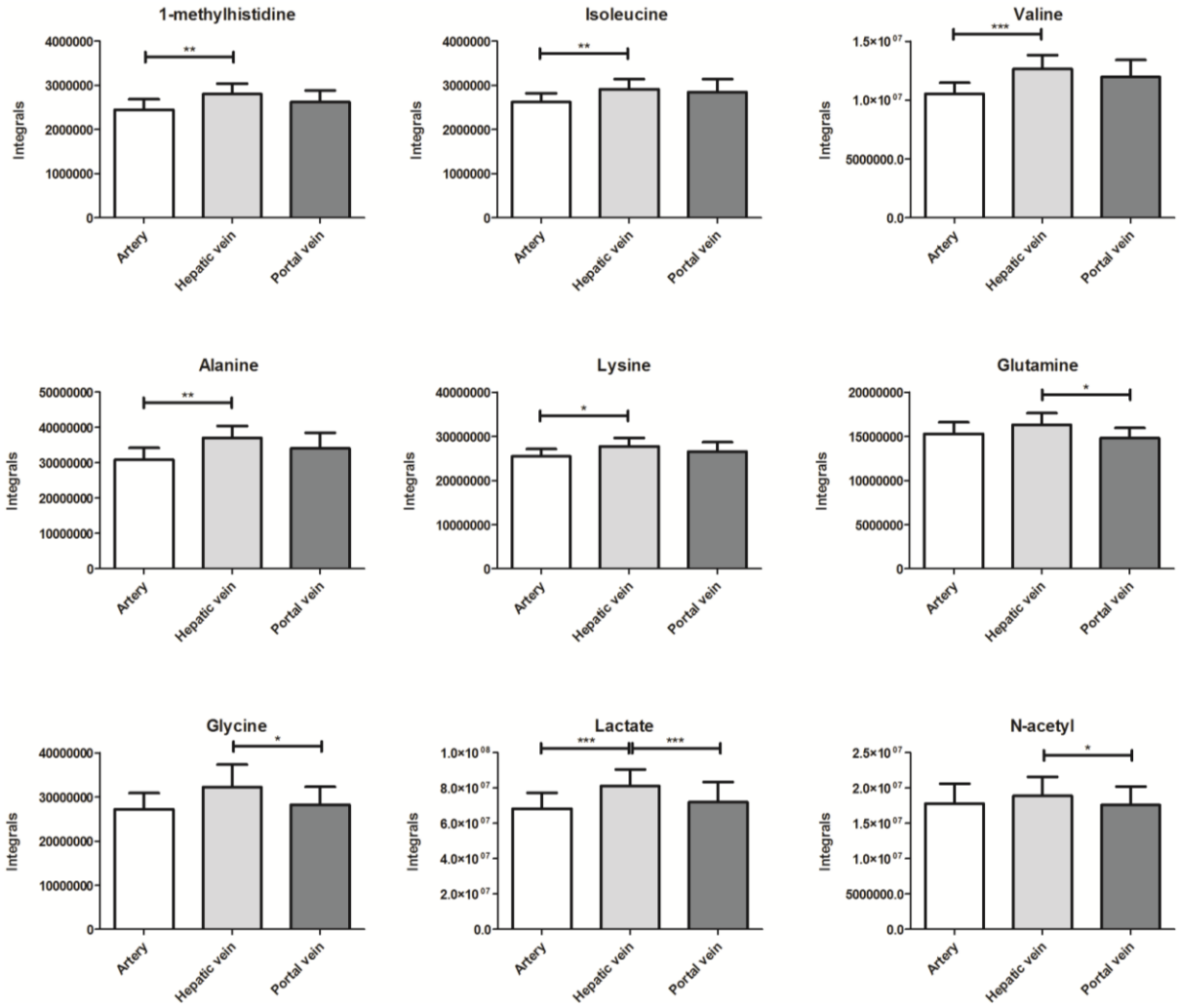


Figure 6.7: The statistically significant metabolic differences between the peripheral artery, hepatic portal vein and hepatic vein are shown above. The Friedman test coupled to Dunn's multiple test correction was used to test for statistical significance. Statistical significance is shown by the asterisks *, ** and *** which indicate $p < 0.05$, $p < 0.01$ and $p < 0.001$ respectively.

"Cross liver" metabolite comparison of decompensated cirrhosis and ACLF relative to ALF in serum metabolic profiles

The levels of metabolites in the decompensated cirrhosis and ACLF patients (n = 7), relative to the ALF patients (n = 5) were contrasted in the peripheral artery, hepatic portal vein and hepatic vein. Non-parametric univariate analysis (Mann-Whitney test) revealed that the levels of histidine, lysine, fumarate, phenylalanine and glycine were elevated in the peripheral artery of the ALF patients. The levels of histidine, lysine and phenylalanine were also higher in the hepatic portal vein of the ALF patients, while the levels of lysine and histidine were

higher in the hepatic vein of the ALF patients. The elevated levels of histidine in all three blood vessels of the ALF patients were the only statistically robust metabolic differences after Bonferonni multiple testing correction was applied. The integrals of the statistically significant endogenous metabolites are presented in Figure 6.8 and Table 6.4 presents a summary of the statistically significant results.

Metabolites	Blood vessel		
	Artery	Hepatic portal vein	Hepatic vein
Histidine	**	**	**
Lysine	*	*	*
Fumarate	*		
Phenylalanine	*	*	
Glycine	*		

Depleted
Elevated

Table 6.4: The summary of the statistically significant metabolic differences between the ACLF/decompensated cirrhosis patients, relative to the ALF patients, is shown above. Statistical significance was tested with the Mann-Whitney test coupled to the Bonferonni multiple correction test and is shown by the asterisks * and **, which indicate $p < 0.05$ and $p < 0.01$ respectively. Histidine was the only metabolic difference that was statistically robust after the Bonferonni test.

It is important to note that the observed metabolic differences between the diseased states are a potential confounder of the metabolite level comparison between the three blood vessels (Table 6.3). The observed differences in the levels of lysine, histidine and glycine were also observed in the blood vessel comparison, indicating that the blood vessel differences might be driven by a specific disease state. However, the presence of unique metabolic differences between the disease states, such as fumarate and phenylalanine, which were not detected between the blood vessels suggest otherwise. Finally, it was not possible to compare the metabolite levels between the individual diseases in each blood vessel separately due to low sample numbers per disease group.

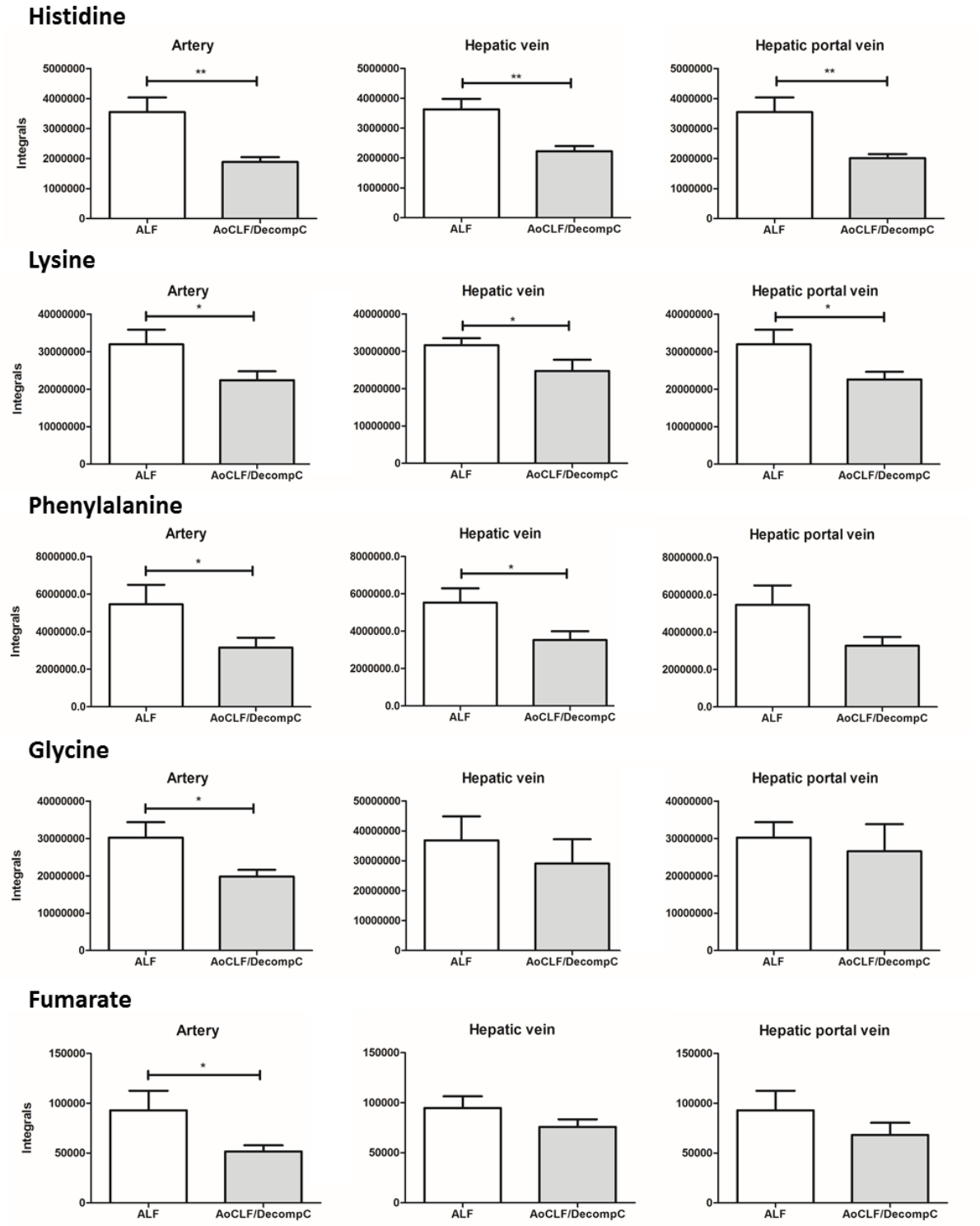


Figure 6.8: The statistically significantly different integrals of metabolites in the peripheral artery, hepatic portal vein and hepatic vein of ALF and decompensated cirrhosis/ACLF (grouped together) patients are shown above. Statistical significance was tested with the Mann-Whitney test coupled to the Bonferonni multiple correction test. Statistical significance is shown by the asterisks * and ** which indicate $p < 0.05$ and $p < 0.01$ respectively. Please note that only the perturbations in histidine levels were statistically robust after the application of the Bonferonni multiple correction test.

Discussion

Pattern of metabolic perturbations associated with decompensated cirrhosis, ACLF and ALF

The metabonomic comparison of the baseline ^{1}H-NMR serum metabolic profiles of decompensated cirrhosis, ACLF and ALF patients relative to healthy controls compared and contrasted the metabolic perturbation pattern associated with each disease. The metabolic profiles of the decompensated cirrhosis patients were observed to have lower levels of the branched chain amino acids valine and isoleucine, relative to healthy controls. The underlying mechanism responsible for lower levels of branched chain amino acids is thought to be linked to insulin, which promotes their breakdown in order to conserve endocellular glucose stores (Leweling et al., 1996, Holecek et al., 1996). Furthermore, malnutrition, which is an important clinical complication in chronic liver disease patients, is also considered to be another contributing factor to the depletion of branched chain amino acids (Mezey, 1982, Silk, 1986) and therefore the administration of branched chain amino acids to chronic liver disease patients is considered beneficial (Khanna and Gopalan, 2007, Plauth and Schutz, 2011). Furthermore, the decompensated cirrhosis group also had elevated levels of the aromatic amino acids tyrosine and phenylalanine relative to control levels. Severe liver diseases such as decompensated cirrhosis and ALF are typically associated with high serum aromatic amino acid levels (tyrosine and phenylalanine) because of a disruption of the hepatic capability to breakdown these amino acids (Soeters and Fischer, 1976). A high serum ratio of aromatic amino acids (phenylalanine and tyrosine) to branched chain amino acids (also known as the Fischer ratio) is linked to a worse prognosis and development of encephalopathy (Soeters and Fischer, 1976, Campollo et al., 1992). Finally, these metabolic perturbations have also been

previously characterized by other metabonomic analyses in cirrhosis and ACLF (Qi et al., 2012, Gao et al., 2009, Amathieu et al., 2014).

A similar metabolic pattern of perturbations was observed in the ACLF patients with the additional elevations of isobutyrate and pyruvate. Isobutyrate is a branched chain fatty acid which is an intermediate of amino acid metabolism and can be produced by bacterial metabolism in the gut (Cummings et al., 1987). Higher levels of pyruvate, a glycolysis end product, have been previously been reported to be associated to decompensated cirrhosis (Gao et al., 2009) and could be a cumulative result of gluconeogenesis inhibition (Record et al., 1975), up-regulation of anaerobic respiration and down-regulation of the Krebs cycle (Lee, 1993, Jeppesen et al., 2013), all of which have been previously associated with severe liver dysfunction. The perturbation of isobutyrate and pyruvate in ACLF in contrast to decompensated cirrhosis, suggest that the acute deterioration of the liver is associated with energy metabolism dysfunction and a change in the role of gut microbial metabolism. A summary of the metabolite perturbations observed in decompensated cirrhosis and ACLF is provided in Figure 6.9.

In contrast to ACLF and decompensated cirrhosis, the ALF metabolic profiles were characterized by additional metabolic perturbations, including higher levels of glutamine relative to healthy controls. Patients suffering from a severe liver disease, such as ALF, have a reduced capacity of urea synthesis which leads to an accumulation of the ammonium ion and a condition known as hyperammonemia (Olde Damink et al., 2002). This is a severe condition which can result to encephalopathy and therefore ammonia is removed from the system through other metabolic pathways, such as the synthesis of glutamine from glutamate

through the addition of a molecule of ammonia (Holecek, 2002). This would result in elevated levels of glutamine, as observed in the serum of the ALF patients relative to control.

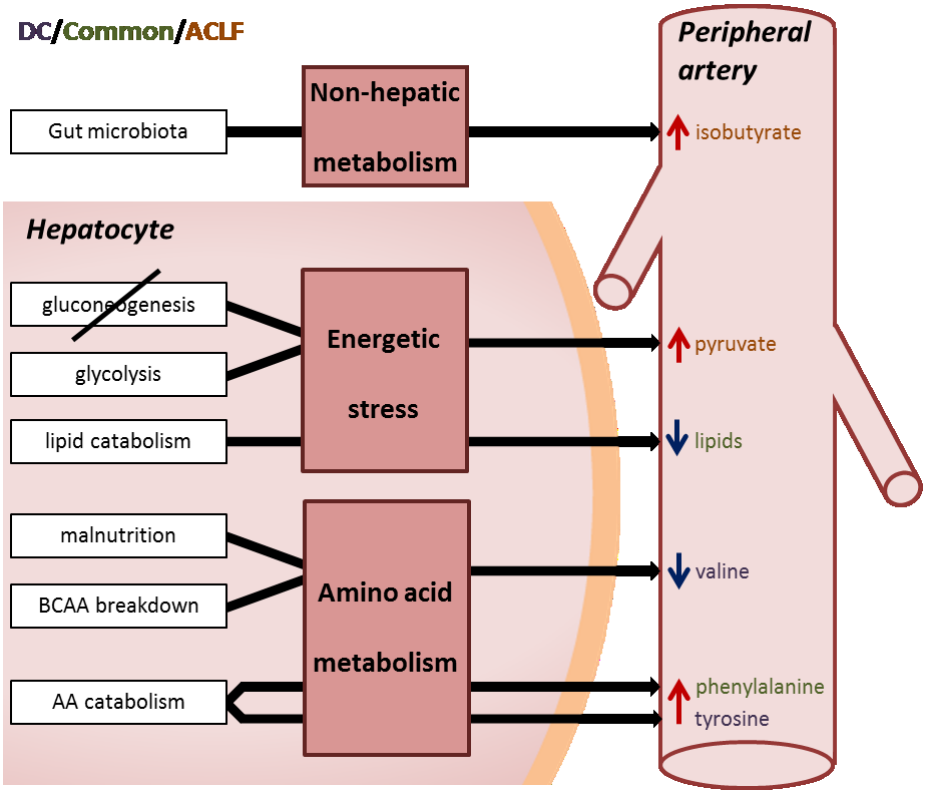


Figure 6.9: A summary of the proposed underlying mechanisms responsible for the observed metabolic effects is shown. Purple, orange and green metabolic changes were associated with decompensated cirrhosis, ACLF or both diseases respectively. Crossed-out metabolic pathways have been reported to be disrupted by ACLF and decompensated cirrhosis. BCAA – branched chain amino acids. DC – decompensated cirrhosis; ACLF – acute on chronic liver failure.

ALF patients also had higher levels of methionine, a condition known as hypermethioninemia, which is considered to be positively correlated with disease severity (Kinsell et al., 1947, Marchesini et al., 1992). Higher levels of methionine are thought to be linked a disruption in the transsulfuration pathway and S-adenosylmethionine synthesis, as well as reduced blood clearance (Horowitz et al., 1981, Marchesini et al., 1992). The transsulfuration pathway is important for the regeneration of glutathione, which is depleted in severe liver diseases (Yamamoto et al., 1998), through the formation of cysteine from homocysteine (Figure 6.10). S-adenosylmethionine, an intermediate in the transsulfuration pathway, has been reported

to be depleted through the attenuation of its synthesis by S-adenosylmethionine synthetase (Cabrero et al., 1988, Martinez-Chantar et al., 2002) due to a modification of the enzyme's sulfhydryl groups (Corrales et al., 1990).

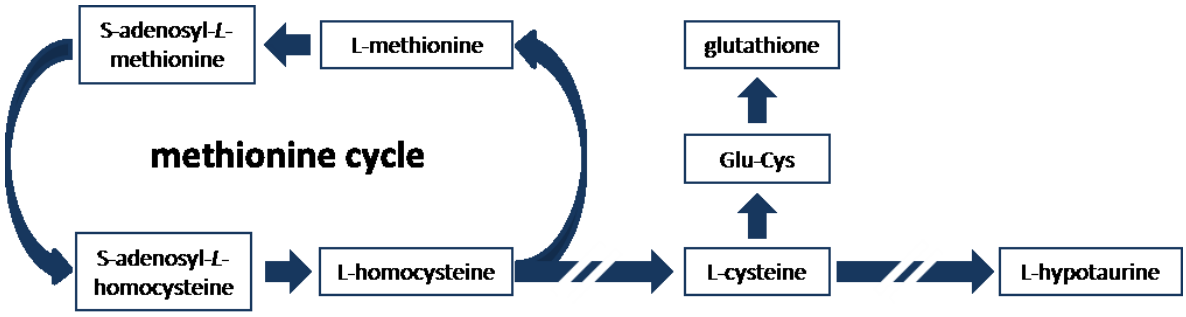


Figure 6:10: Inter-connectivity of methionine and hypotaurine metabolisms with cysteine metabolism.

Other metabolic perturbations unique to ALF, relative to decompensated cirrhosis and ACLF, included higher levels of glycerol and acetate (by-products of lipolysis) (Lind and Lithell, 1994) which have been previously linked to cirrhosis and ACLF (Gao et al., 2009, Amathieu et al., 2014). This observation suggests a greater degree of lipid catabolism in ALF, in comparison to decompensated cirrhosis and ACLF. Finally, higher levels of citrate were also observed which are considered to be a consequence of hepatic citrate metabolism dysfunction and the release of citrate by peripheral organs (Record et al., 1975, Apsner et al., 1997), revealing a greater hepatic dysfunction in ALF.

The role of bacteria in the development and deterioration of liver conditions such as ALF and ACLF is also considered to be very important and is additionally further discussed later on. Higher levels of formate, which can be formed by bacteria through the metabolism of short chain fatty acids (Zhang et al., 2009), were observed in the ^{1}H-NMR metabolic profiles of ALF patients, while elevated isobutyrate was also observed in the ACLF patients. Perturbed levels

of these metabolites could be indicative of a change in the composition of gut bacteria, bacterial translocation or bacterial overgrowth (Antharam et al., 2013).

A summary of the metabolic effects induced by ALF in the serum is shown below in Figure 6.11.

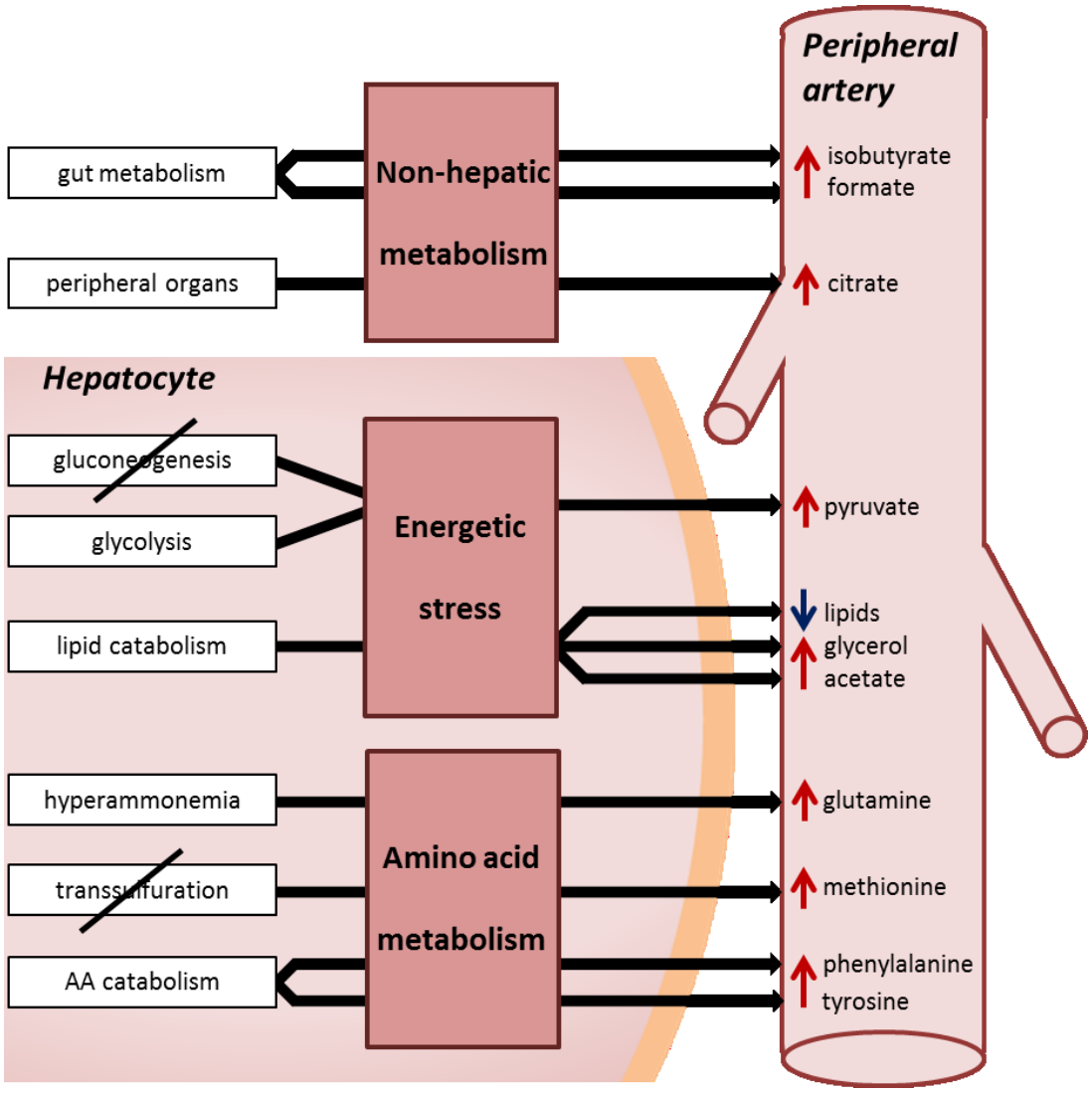


Figure 6.11: A summary of the proposed underlying mechanisms responsible for the observed metabolic perturbations in ALF is shown. Crossed-out metabolic pathways have been reported to be disrupted by ALF. AA – aromatic amino acids.

Overall the metabolic perturbations observed in ALF are indicative of a more severe metabolic imbalance and dysfunction, relative to decompensated cirrhosis and ACLF, where an enhanced disturbance in detoxification mechanisms and energy metabolism was observed.

Finally, there was no sign of depletion in the levels of branched chain amino acids in ACLF and ALF, which suggests that these conditions were more strongly associated with other metabolic perturbations.

APAP-induced ALF

APAP-induced ALF had more marked elevations in the levels of tyrosine, citrate and methionine, relative to the ALF metabolic profiles of other aetiologies. The relatively higher elevation of tyrosine and methionine levels could be reflective of a more advanced ALF condition in the APAP overdose patients. Higher levels of tyrosine and methionine are considered to be correlated with disease severity (Soeters and Fischer, 1976, Kinsell et al., 1947, Marchesini et al., 1992). The higher positive correlation observed in the citrate levels observed in the APAP-induced ALF subgroup could due to an enhanced disruption of citrate metabolism as a result of APAP-induced mitochondrial dysfunction (McGill et al., 2012a, Jaeschke et al., 2012), as well as the higher release of citrate by peripheral organs (Record et al., 1975).

This comparative metabonomic analysis also found that the non-APAP induced ALF sub-group had a greater perturbation of serum lactate levels than the APAP-induced ALF sub-group. Higher levels of lactate lead to a condition known as lactic acidosis (Mizock and Falk, 1992, Bernal et al., 2002) but the exact underlying mechanism responsible for this condition in the liver has not yet been elucidated. Potential mechanisms include a pH-induced or hypoxia mediated up-regulation of glycolysis (Zborowska-Sluis and Dossetor, 1967), as well as a reduced lactate uptake by the liver (Record et al., 1981), but further investigations are required (Bernal et al., 2002). Since APAP is thought to cause the upregulation of glycolysis, as shown in Chapter 3, lactic acidosis would have been an expected clinical feature of APAP

overdose (Shah et al., 2011). It is however, important to clarify that a significant rise in lactate levels was predicted by the O-PLS-DA in the APAP-induced ALF patients but the associated correlation was lower than the arbitrary heatmap cut-off value (set at |0.5|). The difference observed in the correlation levels between the O-PLS-DA models of the two sub-groups could be due to differences in intra-group lactate level variance and it essentially reveals that lactate was more discriminatory in the non-APAP induced ALF model.

Survival rate PLS analysis

The PLS analysis revealed that glutamine, phenylalanine, pyruvate, isobutyrate, lactate, creatine and lysine levels were negatively correlated with short term survival rates (30 and 90 day). As previously explained, higher levels of phenylalanine are potentially linked to impaired aromatic amino acid catabolism, higher levels of pyruvate and lactate are related to energetic stress, isobutyrate levels are linked to bacterial overgrowth and higher levels of glutamine could be indicative of a disruption in the urea cycle. Finally, even though the mechanism by which lysine is elevated in liver cirrhosis has not yet been identified, higher levels have been previously associated with a poor prognosis (Qi et al., 2012).

Blood creatine was not previously detected to be associated with any of the three liver conditions relative to healthy controls, but it was discovered to be negatively correlated with short term survival as well. Creatine is found at high concentrations in muscles and can be produced *de*-novo in the pancreas, kidney and liver by a process which depends on the urea cycle; therefore a disruption in the urea cycle would affect the capability of the liver to synthesize creatine (Brosnan and Brosnan, 2010). Muscle wasting, a condition associated with a poor prognosis in liver cirrhosis (Tessari, 2003), could also lead to a reduced demand and

release of creatine and could therefore be responsible for the relatively higher levels of creatine observed in the patients who did not survive.

The levels of these aforementioned metabolites are directly representative of the extent of disruption of endocellular processes caused by the deteriorating liver. A greater perturbation is indicative of a greater disruption of homeostasis and therefore reveals a greater extent of deterioration, which is ultimately linked to a lower patient survival rate. The levels of glutamine, glycine, phenylalanine, histidine and alanine were not predicted to be correlated as strongly with long term survival which is suggestive that they are not strong predictive markers of the long term state of liver deterioration.

"Cross liver" metabonomic analysis

The metabolic characterization and subsequent comparison of the metabolic profiles of the hepatic portal vein, hepatic vein and peripheral artery provided a rare insight into subtle hepatic metabolic phenotype differences. The metabolic compositions of the hepatic vein and peripheral artery reflect the metabolic state of the liver and system in general respectively, while the hepatic portal vein metabolic profiles show the contribution of the GI tract to the liver, which is thought to be vital in the development and deterioration of liver disease (Ilan, 2012, Schnabl and Brenner, 2014). Intestinal overgrowth of bacteria, changes in bacterial populations (Wu et al., 2012, Bajaj et al., 2012) and a higher rate of bacterial translocation from the GI tract through the alteration of tight junctions between epithelial cells (Ilan, 2012), can lead to the development of sepsis (Wiest and Garcia-Tsao, 2005, Wiest et al., 2014). Furthermore, overgrowth and translocation of bacteria can cause an increase in the systemic levels of lipopolysaccharide (LPS) which can lead to an activation of proinflammatory

signalling cascades and a subsequent “over activation” of the immune system (Wang et al., 2010).

The majority of the metabolic differences of three blood vessels, comprised of elevations of metabolites in the hepatic vein relative to the peripheral artery and hepatic portal vein. The only exception was the higher levels of unidentified DRC molecules in the peripheral artery, relative to the hepatic vein, which could be due to the intra-venous administration of anaesthetic medication during the surgical operation. The fasted state of the patients during the procedure would have affected the metabolic profiles of the hepatic portal vein and could have contributed to the observed pattern of consistently higher levels of endogenous metabolites in the hepatic vein because of the absence of digestion products. Furthermore, the metabolic profiles of the hepatic vein reveal the immediate metabolic perturbations resulting from the metabolism of the most metabolically active organ which could also explain why it was consistently observed to have the highest concentration of metabolites relative to the other two blood vessels. Finally, it is also important to note the potential effect of the administered drugs which could further skew the observed effect. Noradrenaline, has been reported to cause a fasting effect (Froberg et al., 1975), while propofol (general anaesthetic) has been previously linked to affect the mitochondrial function (Cray et al., 1998, Fodale and La Monaca, 2008).

The univariate analysis results revealed that the levels of valine and isoleucine were higher in the serum of the hepatic vein, when compared to the peripheral artery, and are therefore seemingly contradictory to the literature, which suggests that the metabolism of these compounds is impaired during disease. This discrepancy could be explained through the up-regulation of protein breakdown as a response to a fasted state. Fasting would cause the

concomitant down-regulation of insulin and up-regulation of glucagon, which would result in hepatic protein catabolism and higher levels of various essential amino acids, such as lysine, histidine, valine and isoleucine (Bergamini et al., 1995, Tom and Nair, 2006, Holecek, 2002). Furthermore, an *in-vivo* rat study investigating the effect of SIRS on leucine metabolism found that serum branched chain amino acid levels were decreased, but there was an up-regulation of hepatic branched chain amino acid synthesis from the reamination of branched chain ketoacids and the majority of which was excreted by the liver, which would result to higher concentrations in the hepatic vein (Holecek et al., 1998). Therefore, there are many factors which can influence the levels of valine, leucine and isoleucine and it was not possible to estimate the contribution of each factor in the observed cumulative metabolic effect.

Other elevated metabolites in the hepatic vein include lactate and glycine. Higher levels of lactate were observed relative to the hepatic portal vein and peripheral artery revealing lactic acidosis. Higher levels of glycine could be linked to a decrease in the expression of glycine N-methyltransferase, an enzyme which converts glycine to sarcosine, and has been previously associated with the development of severe liver diseases such as hepatocarcinomas (Mato et al., 2008). Finally, N-acetyl and alanine resonances were also observed to be elevated in the hepatic vein relative to the peripheral artery and have been previously described as blood markers of liver deterioration in cirrhosis (Gao et al., 2009, Qi et al., 2012). However, the underlying mechanism has yet to be elucidated therefore the relevance of these results is unclear. A summary of the potential mechanisms affecting the levels of the discriminatory metabolites is shown in Figure 6.12.

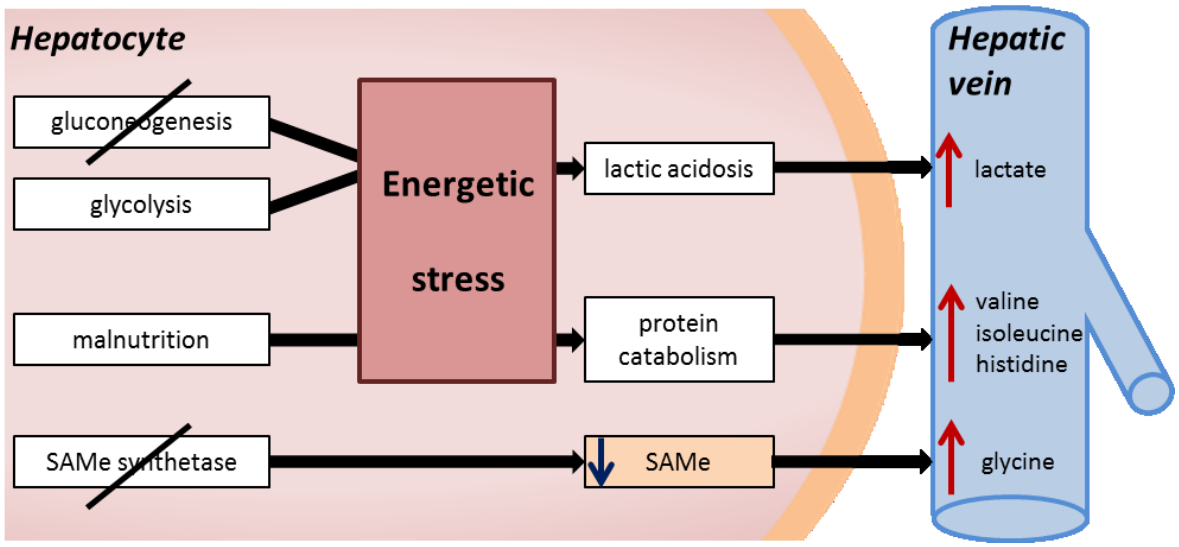


Figure 6.12: A summary of the proposed underlying mechanisms responsible for the observed elevation of some metabolites in the hepatic vein is shown above. Please note that the depletion of S-adenosylmethionine (SAMe) was not observed in the metabonomic analysis.

The univariate comparison of metabolites between decompensated cirrhosis and ACLF with ALF samples in the three blood vessels revealed that histidine and lysine were consistently elevated in the ALF patients in all blood vessels. The decompensated cirrhosis and ACLF patients were grouped together in order to increase group sample numbers and because they are similarly characterized by background cirrhosis (Jalan and Williams, 2002, Schuppan and Afdhal, 2008). The rise of histidine in the ALF patient blood vessels was the only statistically significant result after the Bonferonni multiple test correction and could be indicative of protein breakdown or a general dysfunction of liver metabolism. A previous investigation has reported higher levels of histidine in decompensated cirrhosis patients, relative to compensated cirrhosis, so it could be considered as a marker of liver deterioration and could therefore be even further elevated in ALF (Qi et al., 2012).

Study limitations and future work

Metabonomic studies of clinical samples usually have several limitations associated with a significant genetic variation between individuals, different causes of disease aetiology and

differences in background health/diet/environmental influences/microbiome, but low group numbers are especially problematic. The “cross liver” study was especaially affected by relatively low numbers since it comprised of only fourteen patients due to the difficulty of collecting such samples. Furthermore, the sample numbers per disease group were even smaller which rendered disease comparisons difficult and it was therefore necessary to group the ACLF and decompensated cirrhosis groups together in order to achieve greater sample numbers for that aspect of the analysis. Ideally, a comparison between each disease group and healthy controls would have facilitated the interpretation of the metabolic pattern associated with each disease but that was not possible due to the special circumstances under which these samples are collected. Another complication that affected the “cross liver” analysis was the general anaesthesia medication which led to extensive resonance overlap in the NMR spectra. The quantity and combination of medication varied in each patient, while it was also not possible to account for the potential metabolic effect of each xenobiotic.

The metabonomic comparison of the metabolic profiles of the serum collected from patients on the day of hospital admission was also compromised by several factors. Firstly, the time period between the development of the disease and when the patient was admitted to hospital naturally varied and was not possible to account for. Secondly, the exact aetiology of disease development, such as the exact medication mixture in the development of DILI, was not determined for all cases. This was especially problematic in the separation of the APAP overdose patients who were usually affected by a condition induced by the overdose of APAP and a mixture of other medications, both at variable quantities, and it was therefore difficult to deduce the contribution of each xenobiotic to the subsequent development of ALF.

The proposed future work for this study involves suggested improvements of study design, including sample collection. The continuation of the "cross liver" study should include greater sample numbers which would improve statistical power and permit the direct comparison of different liver diseases. The analysis of liver tissue samples could also complement the serum metabolic profiles and reveal the correlation between the metabolic profiles of the liver and hepatic vein.

In terms of obtaining a more comprehensive picture of the metabolome of decompensated cirrhosis, ACLF and ALF, existing literature suggests that bile acid (Neale et al., 1971, Barnes et al., 1975), lipid (McIntyre, 1978, Reddy and Rao, 2006) and carnitine (Krahenbuhl, 1996) levels are affected in liver disease and should therefore be investigated by a more targeted approach by UPLC-MS. The complementary use of metabolic profiles revealing different classes of metabolites will provide a better overview of the effect of the disease and would be beneficial in our attempts to further understanding the underlying mechanisms of disease development. Furthermore, future work should also involve the measurement of blood miRNA levels (Wang et al., 2012, Szabo and Bala, 2013) and bacterial DNA (Fujita, 2009, Garcia-Alvarez et al., 2012) in order to determine how these markers correlate with the metabolic profiles which could further facilitate the identification of the underlying mechanisms of disease development. Finally, the collection of serum samples at multiple time-points per person would permit the identification of metabolites associated with the improvement or deterioration of each disease.

Chapter 7: Concluding thoughts

Metabonomics can identify either diagnostic panels of metabolites or provide temporal mechanistic insight into a pathological state through the characterization of disease progression or patient recovery. In reality, metabonomics analyses have to deal with vast and complex data, the majority of which is often beyond our understanding. The development of chemometric tools is important for our efforts of dealing with such data but further analytical advancements are required before we can fully take advantage of this approach. It is also important to integrate the data derived from metabonomic analyses with that of other –omics techniques, such as transcriptomics or proteomics. The observed metabolic perturbations are the consequence of a potentially large cascade of endocellular processes that can be further understood through integration with data representing the differential layers of biological organisation. The complementary use of different approaches will facilitate the mechanistic interpretation of the observed metabolic effects and will provide a better understanding of the biological processes associated with disease development.

In-vivo pre-clinical investigations are very important in our efforts to improve our mechanistic understanding of a disease. In the case of DILI investigations, the ability to study hepatic tissue samples in particular is very valuable because it can reveal the immediate effect of drug toxicity on endocellular metabolism. The study presented in Chapter 3 presented novel metabolic evidence which corroborates previous investigations concerning APAP-induced mitochondrial dysfunction and oxidative stress. The metabonomic analysis revealed a previously uncharacterized broad metabolic effect in response to mitochondrial toxicity, including changes in energy metabolites and the up-regulation of glycolysis. These findings are directly translatable to clinical studies since they provide mechanistic clues of the endocellular consequences of energetic and oxidative stress. Furthermore, the study also

revealed that, even at a comparable dose, AMAP-induced toxicity would not have been mediated through mitochondrial dysfunction due to the lack of common effects with APAP.

Chapter 5 presented the second *in-vivo* DILI study which demonstrated the risk of ADR occurrence in the presence of a background liver disease. The previously uncharacterized hepatic and systemic effect of MTX was studied in healthy rats, while the influence of a background disease on the metabolic and toxic effect of MTX was also demonstrated in the NASH model. MTX in the context of NASH resulted in increased liver toxicity and was associated with unique metabolic perturbations in comparison to MTX exposure in the healthy rat, including an elevation in phenylalanine levels in particular. This was an interesting result because phenylalanine metabolism has been extensively reported to be associated with the deterioration of liver function and was consistently observed to be elevated in the serum of the decompensated cirrhosis, ACLF and ALF patients, as shown in Chapter 6. Even though these studies involved different species and were performed under different conditions, the observed similarities reveal a certain degree of translatability inter-species conservation in some metabolic processes or disease related adaptations.

In addition to the investigations of the metabolic perturbations associated with DILI, the study presented in Chapter 4 described the metabolic state of a chronic liver disease, NASH, as modelled by the MCD diet. This novel systemic characterization enables the contextualization of studies performed with this dietary model of NASH, while it also raised questions concerning other models which attempt to mimic the metabolic syndrome. Unfortunately it was not possible to conduct a metabonomic analysis of NASH clinical samples in order to further evaluate the strengths and weaknesses of the MCD diet as a model of clinical NASH.

The three aforementioned *in-vivo* investigations focused at looking at different concepts of liver disease in animal models. Following these studies, the clinical study of Chapter 6 provided the opportunity to characterize three important liver diseases (decompensated cirrhosis, ACLF and ALF), as well as to potentially identify common metabolic perturbations with the animal studies. The preliminary "cross liver" study provided the unique opportunity of studying the local metabolic environment of the liver in a diseased state, as mirrored by the surrounding blood vessels. It had however proven difficult to contextualize the results due to the limitations associated with the special circumstances under which these samples were collected, as well as the low numbers per group. The metabonomic analysis of the three liver conditions (decompensated cirrhosis, ACLF and ALF) revealed both common and unique metabolic perturbations associated with each disease and revealed that the acute nature of ALF was responsible for a greater disturbance of homeostasis. Furthermore, the novel metabolic characterization of the ACLF patients is a valuable step towards an improved biological classification of this condition, while it was also interesting to observe that the pattern of its metabolic perturbations lay in between that of decompensated cirrhosis and ALF. Finally, regressing against the different survival rates was of particular interest because it facilitated the identification of the mechanistic markers which are more closely associated with disease deterioration and patient survival.

Even though the individual studies presented in this thesis involve different species, drugs, and sample collection time-points, and are therefore difficult to directly compare, useful conclusions concerning the translatability of *in-vivo* models to study hepatic dysfunction can still be drawn. At the beginning, any observed metabolic profile changes will be more closely associated with the toxicity mechanism of the inducer. Providing there is a large enough toxic

insult and sample collection was performed after a sufficient time period, the latter metabolic perturbations will be more closely associated with universal liver dysfunction. This hypothesis can be applied to the drug toxicity associated metabolic perturbations identified in the two *in-vivo* animal studies. The hepatic metabolic changes identified after APAP toxicity are more likely to be APAP specific due to the short time-period between dosage and sample collection (1, 3 and 6 hours), while the MTX-induced hepatic metabolic changes could be representative of markers of universal hepatic dysfunction due to the longer time period between dosage and sample collection (96 hours).

Overall, the work presented in this thesis illustrates the power of a metabonomics approach in our efforts to improve our understanding of particular biological conditions such as liver diseases. Although a direct metabolic comparison of the clinical and animal studies was not entirely possible due to the focus of the latter on hepatic tissue analysis, the characterization of animal models of and DILI and NASH led to the elucidation of important mechanistic information concerning hepatic metabolism and adaptation to toxic insults, which was then applied to the clinical study.

References

ABDEL-MISIH, S. R. & BLOOMSTON, M. 2010. Liver anatomy. *Surg Clin North Am,* 90**,** 643-53.

ABU-SHANAB, A. & QUIGLEY, E. M. 2010. The role of the gut microbiota in nonalcoholic fatty liver disease. *Nat Rev Gastroenterol Hepatol,* 7**,** 691-701.

ADAMS, L. A. & ANGULO, P. 2005. Recent concepts in non-alcoholic fatty liver disease. *Diabet Med,* 22**,** 1129-33.

AGARWAL, R., MACMILLAN-CROW, L. A., RAFFERTY, T. M., SABA, H., ROBERTS, D. W., FIFER, E. K., JAMES, L. P. & HINSON, J. A. 2011. Acetaminophen-induced hepatotoxicity in mice occurs with inhibition of activity and nitration of mitochondrial manganese superoxide dismutase. *J Pharmacol Exp Ther,* 337**,** 110-6.

ALI, R. & CUSI, K. 2009. New diagnostic and treatment approaches in non-alcoholic fatty liver disease (NAFLD). *Ann Med,* 41**,** 265-78.

ALLEGRA, C. J., CHABNER, B. A., DRAKE, J. C., LUTZ, R., RODBARD, D. & JOLIVET, J. 1985a. Enhanced inhibition of thymidylate synthase by methotrexate polyglutamates. *J Biol Chem,* 260**,** 9720-6.

ALLEGRA, C. J., DRAKE, J. C., JOLIVET, J. & CHABNER, B. A. 1985b. Inhibition of phosphoribosylaminoimidazolecarboxamide transformylase by methotrexate and dihydrofolic acid polyglutamates. *Proceedings of the National Academy of Sciences of the United States of America,* 82**,** 4881-5.

AMATHIEU, R., TRIBA, M. N., NAHON, P., BOUCHEMAL, N., KAMOUN, W., HAOUACHE, H., TRINCHET, J. C., SAVARIN, P., LE MOYEC, L. & DHONNEUR, G. 2014. Serum 1H-NMR metabolomic fingerprints of acute-on-chronic liver failure in intensive care unit patients with alcoholic cirrhosis. *PLoS One,* 9**,** e89230.

ANDREW, E. R. 1984. A historical review of NMR and its clinical applications. *Br Med Bull,* 40**,** 115-9.

ANTHARAM, V. C., LI, E. C., ISHMAEL, A., SHARMA, A., MAI, V., RAND, K. H. & WANG, G. P. 2013. Intestinal dysbiosis and depletion of butyrogenic bacteria in Clostridium difficile infection and nosocomial diarrhea. *J Clin Microbiol,* 51**,** 2884-92.

ANTOINE, D. J., WILLIAMS, D. P., KIPAR, A., LAVERTY, H. & PARK, B. K. 2010. Diet restriction inhibits apoptosis and HMGB1 oxidation and promotes inflammatory cell recruitment during acetaminophen hepatotoxicity. *Mol Med,* 16**,** 479-90.

ANTONIADES, C. G., BERRY, P. A., WENDON, J. A. & VERGANI, D. 2008. The importance of immune dysfunction in determining outcome in acute liver failure. *J Hepatol,* 49**,** 845-61.

APSNER, R., SCHWARZENHOFER, M., DERFLER, K., ZAUNER, C., RATHEISER, K. & KRANZ, A. 1997. Impairment of citrate metabolism in acute hepatic failure. *Wien Klin Wochenschr,* 109**,** 123-7.

ARSOV, T., LARTER, C. Z., NOLAN, C. J., PETROVSKY, N., GOODNOW, C. C., TEOH, N. C., YEH, M. M. & FARRELL, G. C. 2006. Adaptive failure to high-fat diet characterizes steatohepatitis in Alms1 mutant mice. *Biochem Biophys Res Commun,* 342**,** 1152-9.

ATAIE, G., SAFARIAN, S., DIVSALAR, A., SABOURY, A. A., MOOSAVI-MOVAHEDI, A. A., RANJBAR, B., CRISTALLI, G. & MARDANIAN, S. 2004. Kinetic and structural analysis of the inhibition of adenosine deaminase by acetaminophen. *J Enzyme Inhib Med Chem,* 19**,** 71-8.

AUE, W. P., BARTHOLDI, E. & R., E. R. 1975. Two-dimensional spectroscopy. Application to nuclear magnetic resonance. *The Journal of Chemical Physics,* 64**,** 2229 - 2246.

BAILEY, L. B. 2009. *Folate in Health and Disease, Second Edition,* New York, CRC Press.

BAJAJ, J. S., RIDLON, J. M., HYLEMON, P. B., THACKER, L. R., HEUMAN, D. M., SMITH, S., SIKAROODI, M. & GILLEVET, P. M. 2012. Linkage of gut microbiome with cognition in hepatic encephalopathy. *Am J Physiol Gastrointest Liver Physiol,* 302**,** G168-75.

BAJT, M. L., COVER, C., LEMASTERS, J. J. & JAESCHKE, H. 2006. Nuclear translocation of endonuclease G and apoptosis-inducing factor during acetaminophen-induced liver cell injury. *Toxicol Sci,* 94**,** 217-25.

BALA, L., MEHROTRA, M., MOHINDRA, S., SAXENA, R. & KHETRAPAL, C. L. 2013. Early prognostic markers for fatal fulminant hepatic failure cases with viral hepatitis: proton nuclear magnetic resonance spectroscopic studies of serum. *Dig Liver Dis,* 45**,** 155-63.

BALES, J. R., BELL, J. D., NICHOLSON, J. K., SADLER, P. J., TIMBRELL, J. A., HUGHES, R. D., BENNETT, P. N. & WILLIAMS, R. 1988. Metabolic profiling of body fluids by proton NMR: self-poisoning episodes with paracetamol (acetaminophen). *Magn Reson Med,* 6**,** 300-6.

BALES, J. R., SADLER, P. J., NICHOLSON, J. K. & TIMBRELL, J. A. 1984. Urinary excretion of acetaminophen and its metabolites as studied by proton NMR spectroscopy. *Clin Chem,* 30**,** 1631-6.

BANTEL, H. & SCHULZE-OSTHOFF, K. 2012. Mechanisms of cell death in acute liver failure. *Front Physiol,* 3**,** 79.

BARNES, S., GALLO, G. A., TRASH, D. B. & MORRIS, J. S. 1975. Diagnositic value of serum bile acid estimations in liver disease. *J Clin Pathol,* 28**,** 506-9.

BARR, J., VAZQUEZ-CHANTADA, M., ALONSO, C., PEREZ-CORMENZANA, M., MAYO, R., GALAN, A., CABALLERIA, J., MARTIN-DUCE, A., TRAN, A., WAGNER, C., LUKA, Z., LU, S. C., CASTRO, A., LE MARCHAND-BRUSTEL, Y., MARTINEZ-CHANTAR, M. L., VEYRIE, N., CLEMENT, K., TORDJMAN, J., GUAL, P. & MATO, J. M. 2010. Liquid chromatography-mass spectrometry-based parallel metabolic profiling of human and mouse model serum reveals putative biomarkers associated with the progression of nonalcoholic fatty liver disease. *J Proteome Res,* 9**,** 4501-12.

BARRUECO, J. R., O'LEARY, D. F. & SIROTNAK, F. M. 1992. Metabolic turnover of methotrexate polyglutamates in lysosomes derived from S180 cells. Definition of a two-step process limited by mediated lysosomal permeation of polyglutamates and activating reduced sulfhydryl compounds. *J Biol Chem,* 267**,** 15356-61.

BATEMAN, D. N., DEAR, J. W., THANACOODY, H. K., THOMAS, S. H., EDDLESTON, M., SANDILANDS, E. A., COYLE, J., COOPER, J. G., RODRIGUEZ, A., BUTCHER, I., LEWIS, S. C., VLIEGENTHART, A. D., VEIRAIAH, A., WEBB, D. J. & GRAY, A. 2013. Reduction of adverse effects from intravenous acetylcysteine treatment for paracetamol poisoning: a randomised controlled trial. *Lancet*.

BECKONERT, O., COEN, M., KEUN, H. C., WANG, Y., EBBELS, T. M., HOLMES, E., LINDON, J. C. & NICHOLSON, J. K. 2010. High-resolution magic-angle-spinning NMR spectroscopy for metabolic profiling of intact tissues. *Nat Protoc,* 5**,** 1019-32.

BECKONERT, O., KEUN, H. C., EBBELS, T. M., BUNDY, J., HOLMES, E., LINDON, J. C. & NICHOLSON, J. K. 2007. Metabolic profiling, metabolomic and metabonomic procedures for NMR spectroscopy of urine, plasma, serum and tissue extracts. *Nat Protoc,* 2**,** 2692-703.

BEECHER, C. W. W. 2003. The Human metabolome. *In:* HARRIGAN, G. G. & GOODACRE, R. (eds.) *Metabolic Profiling: Its Role in Biomarker Discovery and Gene Function Analysis: Its Role in Biomarker Discovery and Gene Function Analysis.* Kluwer Academic Publishers.

BEHRENDS, V., TREDWELL, G. D. & BUNDY, J. G. 2011. A software complement to AMDIS for processing GC-MS metabolomic data. *Anal Biochem,* 415**,** 206-8.

BEMEUR, C., VAQUERO, J., DESJARDINS, P. & BUTTERWORTH, R. F. 2010. N-acetylcysteine attenuates cerebral complications of non-acetaminophen-induced acute liver failure in mice: antioxidant and anti-inflammatory mechanisms. *Metab Brain Dis,* 25**,** 241-9.

BERGAMINI, E., BOMBARA, M., DEL ROSO, A., GORI, Z., MASIELLO, P., MASINI, M., POLLERA, M. & VITTORINI, S. 1995. The regulation of liver protein degradation by aminoacids in vivo. Effects of glutamine and leucine. *Arch Physiol Biochem,* 103**,** 512-5.

BERNAL, W., DONALDSON, N., WYNCOLL, D. & WENDON, J. 2002. Blood lactate as an early predictor of outcome in paracetamol-induced acute liver failure: a cohort study. *Lancet,* 359**,** 558-63.

BERNAL, W. & WENDON, J. 2013. Acute liver failure. *N Engl J Med,* 369**,** 2525-34.

BESSEMS, J. G. & VERMEULEN, N. P. 2001. Paracetamol (acetaminophen)-induced toxicity: molecular and biochemical mechanisms, analogues and protective approaches. *Crit Rev Toxicol,* 31**,** 55-138.

BEYER, R. P., FRY, R. C., LASAREV, M. R., MCCONNACHIE, L. A., MEIRA, L. B., PALMER, V. S., POWELL, C. L., ROSS, P. K., BAMMLER, T. K., BRADFORD, B. U., CRANSON, A. B., CUNNINGHAM, M. L., FANNIN, R. D., HIGGINS, G. M., HURBAN, P., KAYTON, R. J., KERR, K. F., KOSYK, O., LOBENHOFER, E. K., SIEBER, S. O., VLIET, P. A., WEIS, B. K., WOLFINGER, R., WOODS, C. G., FREEDMAN, J. H., LINNEY, E., KAUFMANN, W. K., KAVANAGH, T. J., PAULES, R. S., RUSYN, I., SAMSON, L. D., SPENCER, P. S., SUK, W., TENNANT, R. J. & ZARBL, H. 2007. Multicenter study of acetaminophen hepatotoxicity reveals the importance of biological endpoints in genomic analyses. *Toxicol Sci,* 99**,** 326-37.

BEYOGLU, D. & IDLE, J. R. 2013. The metabolomic window into hepatobiliary disease. *J Hepatol,* 59**,** 842-58.

BLAKELY, P. & MCDONALD, B. R. 1995. Acute renal failure due to acetaminophen ingestion: a case report and review of the literature. *J Am Soc Nephrol,* 6**,** 48-53.

BLEIBEL, W., KIM, S., D'SILVA, K. & LEMMER, E. R. 2007. Drug-induced liver injury: review article. *Dig Dis Sci,* 52**,** 2463-71.

BOLLARD, M. E., KEUN, H. C., BECKONERT, O., EBBELS, T. M., ANTTI, H., NICHOLLS, A. W., SHOCKCOR, J. P., CANTOR, G. H., STEVENS, G., LINDON, J. C., HOLMES, E. & NICHOLSON, J. K. 2005. Comparative metabonomics of differential hydrazine toxicity in the rat and mouse. *Toxicol Appl Pharmacol,* 204**,** 135-51.

BORRADAILE, N. M., HAN, X., HARP, J. D., GALE, S. E., ORY, D. S. & SCHAFFER, J. E. 2006. Disruption of endoplasmic reticulum structure and integrity in lipotoxic cell death. *J Lipid Res,* 47**,** 2726-37.

BOTTING, R. M. 2000. Mechanism of action of acetaminophen: is there a cyclooxygenase 3? *Clin Infect Dis,* 31 Suppl 5**,** S202-10.

BOUATRA, S., AZIAT, F., MANDAL, R., GUO, A. C., WILSON, M. R., KNOX, C., BJORNDAHL, T. C., KRISHNAMURTHY, R., SALEEM, F., LIU, P., DAME, Z. T., POELZER, J., HUYNH, J., YALLOU, F. S., PSYCHOGIOS, N., DONG, E., BOGUMIL, R., ROEHRING, C. & WISHART, D. S. 2013. The human urine metabolome. *PLoS One,* 8**,** e73076.

BOUKHETTALA, N., LEBLOND, J., CLAEYSSENS, S., FAURE, M., LE PESSOT, F., BOLE-FEYSOT, C., HASSAN, A., METTRAUX, C., VUICHOUD, J., LAVOINNE, A., BREUILLE, D., DECHELOTTE, P. & COEFFIER, M. 2009. Methotrexate induces intestinal mucositis and alters gut protein metabolism independently of reduced food intake. *Am J Physiol Endocrinol Metab,* 296**,** E182-90.

BREMER, J. 1983. Carnitine--metabolism and functions. *Physiol Rev,* 63**,** 1420-80.

BROSNAN, J. T. & BROSNAN, M. E. 2010. Creatine metabolism and the urea cycle. *Mol Genet Metab,* 100 Suppl 1**,** S49-52.

BROWNING, J. D. & HORTON, J. D. 2004. Molecular mediators of hepatic steatosis and liver injury. *J Clin Invest,* 114**,** 147-52.

BRUNT, E. M. 2001. Nonalcoholic steatohepatitis: definition and pathology. *Semin Liver Dis,* 21**,** 3-16.

BURCHAM, P. C. & HARMAN, A. W. 1991. Acetaminophen toxicity results in site-specific mitochondrial damage in isolated mouse hepatocytes. *J Biol Chem,* 266**,** 5049-54.

BURKE, P. A., STACK, J. A., WAGNER, D., LEWIS, D. W., JENKINS, R. L. & FORSE, R. A. 1997. L-[1-(13)C] Phenylalanine oxidation as a measure of hepatocyte functional capacity in end-stage liver disease. *Am J Surg,* 173**,** 270-3; discussion 273-4.

CABALLERO, F., FERNANDEZ, A., MATIAS, N., MARTINEZ, L., FUCHO, R., ELENA, M., CABALLERIA, J., MORALES, A., FERNANDEZ-CHECA, J. C. & GARCIA-RUIZ, C. 2010. Specific contribution of methionine and choline in nutritional nonalcoholic steatohepatitis: impact on mitochondrial S-adenosyl-L-methionine and glutathione. *J Biol Chem,* 285**,** 18528-36.

CABRERO, C., DUCE, A. M., ORTIZ, P., ALEMANY, S. & MATO, J. M. 1988. Specific loss of the high-molecular-weight form of S-adenosyl-L-methionine synthetase in human liver cirrhosis. *Hepatology,* 8**,** 1530-4.

CAMPOLLO, O., SPRENGERS, D. & MCINTYRE, N. 1992. The BCAA/AAA ratio of plasma amino acids in three different groups of cirrhotics. *Rev Invest Clin,* 44**,** 513-8.

CARR, H. Y. & PURCELL, E. M. 1954. Effects of Diffusion on Free Precession in Nuclear Magnetic Resonance Experiments. *Physical Review* 94**,** 630-638.

CAVUOTO, P. & FENECH, M. F. 2012. A review of methionine dependency and the role of methionine restriction in cancer growth control and life-span extension. *Cancer Treat Rev,* 38**,** 726-36.

CAZANAVE, S. C., MOTT, J. L., ELMI, N. A., BRONK, S. F., WERNEBURG, N. W., AKAZAWA, Y., KAHRAMAN, A., GARRISON, S. P., ZAMBETTI, G. P., CHARLTON, M. R. & GORES, G. J. 2009. JNK1-dependent PUMA expression contributes to hepatocyte lipoapoptosis. *J Biol Chem,* 284**,** 26591-602.

CHEN, C., HENNIG, G. E. & MANAUTOU, J. E. 2003. Hepatobiliary excretion of acetaminophen glutathione conjugate and its derivatives in transport-deficient (TR-) hyperbilirubinemic rats. *Drug Metab Dispos,* 31**,** 798-804.

CHEN, C., KRAUSZ, K. W., SHAH, Y. M., IDLE, J. R. & GONZALEZ, F. J. 2009. Serum metabolomics reveals irreversible inhibition of fatty acid beta-oxidation through the suppression of PPARalpha activation as a contributing mechanism of acetaminophen-induced hepatotoxicity. *Chem Res Toxicol,* 22**,** 699-707.

CHEN, C., KRAUSZ, K.W., SHAH, Y.M., IDLE, J.R. AND GONZALEZ, F.J. 2009. Serum Metabolomics Reveals Irreversible Inhibition of Fatty Acid beta-Oxidation through the Suppression of PPARr Activation as a Contributing Mechanism of Acetaminophen-Induced Hepatotoxicity. *Chem Res Toxicol,* 22**,** 699-707.

CHENG, J., JOYCE, A., YATES, K., AOUIZERAT, B. & SANYAL, A. J. 2012. Metabolomic profiling to identify predictors of response to vitamin E for non-alcoholic steatohepatitis (NASH). *PLoS One,* 7**,** e44106.

CHIANG, H. M., FANG, S. H., WEN, K. C., HSIU, S. L., TSAI, S. Y., HOU, Y. C., CHI, Y. C. & CHAO, P. D. 2005. Life-threatening interaction between the root extract of Pueraria lobata and methotrexate in rats. *Toxicol Appl Pharmacol,* 209**,** 263-8.

CHIMENTI, M. S., TUCCI, P., CANDI, E., PERRICONE, R., MELINO, G. & WILLIS, A. E. 2013. Metabolic profiling of human CD4+ cells following treatment with methotrexate and anti-TNF-alpha infliximab. *Cell Cycle,* 12**,** 3025-36.

CHOW, W. L. & LEE, Y. K. 2008. Free fucose is a danger signal to human intestinal epithelial cells. *Br J Nutr,* 99**,** 449-54.

CLAUS, S. P. & SWANN, J. R. 2013. Nutrimetabonomics:applications for nutritional sciences, with specific reference to gut microbial interactions. *Annu Rev Food Sci Technol,* 4**,** 381-99.

CLAYTON, T. A., BAKER, D., LINDON, J. C., EVERETT, J. R. & NICHOLSON, J. K. 2009. Pharmacometabonomic identification of a significant host-microbiome metabolic interaction affecting human drug metabolism. *Proc Natl Acad Sci U S A,* 106**,** 14728-33.

CLAYTON, T. A., LINDON, J. C., CLOAREC, O., ANTTI, H., CHARUEL, C., HANTON, G., PROVOST, J. P., LE NET, J. L., BAKER, D., WALLEY, R. J., EVERETT, J. R. & NICHOLSON, J. K. 2006. Pharmaco-metabonomic phenotyping and personalized drug treatment. *Nature,* 440**,** 1073-7.

CLOAREC, O., DUMAS, M. E., CRAIG, A., BARTON, R. H., TRYGG, J., HUDSON, J., BLANCHER, C., GAUGUIER, D., LINDON, J. C., HOLMES, E. & NICHOLSON, J. 2005a. Statistical total correlation spectroscopy: an exploratory approach for latent biomarker identification from metabolic 1H NMR data sets. *Anal Chem,* 77**,** 1282-9.

CLOAREC, O., DUMAS, M. E., TRYGG, J., CRAIG, A., BARTON, R. H., LINDON, J. C., NICHOLSON, J. K. & HOLMES, E. 2005b. Evaluation of the orthogonal projection on latent structure model limitations caused by chemical shift variability and improved visualization of biomarker changes in 1H NMR spectroscopic metabonomic studies. *Anal Chem,* 77**,** 517-26.

COEN, M. 2010. A metabonomic approach for mechanistic exploration of pre-clinical toxicology. *Toxicology,* 278**,** 326-40.

COEN, M., HOLMES, E., LINDON, J. C. & NICHOLSON, J. K. 2008. NMR-based metabolic profiling and metabonomic approaches to problems in molecular toxicology. *Chem Res Toxicol,* 21**,** 9-27.

COEN, M., LENZ, E. M., NICHOLSON, J. K., WILSON, I. D., POGNAN, F. & LINDON, J. C. 2003. An integrated metabonomic investigation of acetaminophen toxicity in the mouse using NMR spectroscopy. *Chem Res Toxicol,* 16**,** 295-303.

COEN, M., RUEPP, S. U., LINDON, J. C., NICHOLSON, J. K., POGNAN, F., LENZ, E. M. & WILSON, I. D. 2004. Integrated application of transcriptomics and metabonomics yields new insight into the toxicity due to paracetamol in the mouse. *J Pharm Biomed Anal,* 35**,** 93-105.

COHEN, S. D. & KHAIRALLAH, E. A. 1997. Selective protein arylation and acetaminophen-induced hepatotoxicity. *Drug Metab Rev,* 29**,** 59-77.

CONNOR, S. C., WU, W., SWEATMAN, B. C., MANINI, J., HASELDEN, J. N., CROWTHER, D. J. & WATERFIELD, C. J. 2004. Effects of feeding and body weight loss on the 1H-NMR-based urine metabolic profiles of male Wistar Han rats: implications for biomarker discovery. *Biomarkers,* 9**,** 156-79.

COOMES, E., CHAN, E. S. & REISS, A. B. 2011. Methotrexate in atherogenesis and cholesterol metabolism. *Cholesterol,* 2011**,** 503028.

COOPERMAN, J. M. & LOPEZ, R. 2002. The role of histidine in the anemia of folate deficiency. *Exp Biol Med (Maywood),* 227**,** 998-1000.

CORRALES, F., CABRERO, C., PAJARES, M. A., ORTIZ, P., MARTIN-DUCE, A. & MATO, J. M. 1990. Inactivation and dissociation of S-adenosylmethionine synthetase by modification of sulfhydryl groups and its possible occurrence in cirrhosis. *Hepatology,* 11**,** 216-22.

COVER, C., MANSOURI, A., KNIGHT, T. R., BAJT, M. L., LEMASTERS, J. J., PESSAYRE, D. & JAESCHKE, H. 2005. Peroxynitrite-induced mitochondrial and endonuclease-mediated nuclear DNA damage in acetaminophen hepatotoxicity. *J Pharmacol Exp Ther,* 315**,** 879-87.

CRAY, S. H., ROBINSON, B. H. & COX, P. N. 1998. Lactic acidemia and bradyarrhythmia in a child sedated with propofol. *Crit Care Med,* 26**,** 2087-92.

CRIDER, K. S., YANG, T. P., BERRY, R. J. & BAILEY, L. B. 2012. Folate and DNA methylation: a review of molecular mechanisms and the evidence for folate's role. *Adv Nutr,* 3**,** 21-38.

CUMMINGS, J. H., POMARE, E. W., BRANCH, W. J., NAYLOR, C. P. & MACFARLANE, G. T. 1987. Short chain fatty acids in human large intestine, portal, hepatic and venous blood. *Gut,* 28**,** 1221-7.

DAHLIN, D. C. & NELSON, S. D. 1982. Synthesis, decomposition kinetics, and preliminary toxicological studies of pure N-acetyl-p-benzoquinone imine, a proposed toxic metabolite of acetaminophen. *J Med Chem,* 25**,** 885-6.

DAHLQVIST, A. & THOMSON, D. L. 1963. The digestion and absorption of sucrose by the intact rat. *J Physiol,* 167**,** 193-209.

DAS, V., BOELLE, P. Y., GALBOIS, A., GUIDET, B., MAURY, E., CARBONELL, N., MOREAU, R. & OFFENSTADT, G. 2010. Cirrhotic patients in the medical intensive care unit: early prognosis and long-term survival. *Crit Care Med,* 38**,** 2108-16.

DASARATHY, S., KASUMOV, T., EDMISON, J. M., GRUCA, L. L., BENNETT, C., DUENAS, C., MARCZEWSKI, S., MCCULLOUGH, A. J., HANSON, R. W. & KALHAN, S. C. 2009. Glycine and urea kinetics in nonalcoholic steatohepatitis in human: effect of intralipid infusion. *Am J Physiol Gastrointest Liver Physiol,* 297**,** G567-75.

DAVIDSON, D. G. & EASTHAM, W. N. 1966. Acute liver necrosis following overdose of paracetamol. *Br Med J,* 2**,** 497-9.

DAY, C. P. 2002. Non-alcoholic steatohepatitis (NASH): where are we now and where are we going? *Gut,* 50**,** 585-8.

DAY, C. P. & JAMES, O. F. 1998. Steatohepatitis: a tale of two "hits"? *Gastroenterology,* 114**,** 842-5.

DE HOFFMAN, E., CHARETTE, J. & STROOBANT, V. 1996. *Mass spectrometry: Principles and applications,* New York, Wiley.

DEGUIL, J., PINEAU, L., ROWLAND SNYDER, E. C., DUPONT, S., BENEY, L., GIL, A., FRAPPER, G. & FERREIRA, T. 2011. Modulation of lipid-induced ER stress by fatty acid shape. *Traffic,* 12**,** 349-62.

DETTMER, K., ALMSTETTER, M. F., APPEL, I. J., NURNBERGER, N., SCHLAMBERGER, G., GRONWALD, W., MEYER, H. H. & OEFNER, P. J. 2010. Comparison of serum versus plasma collection in gas chromatography--mass spectrometry-based metabolomics. *Electrophoresis,* 31**,** 2365-73.

DETTMER, K., ARONOV, P. A. & HAMMOCK, B. D. 2007. Mass spectrometry-based metabolomics. *Mass Spectrom Rev,* 26**,** 51-78.

DIETERLE, F., ROSS, A., SCHLOTTERBECK, G. & SENN, H. 2006. Probabilistic quotient normalization as robust method to account for dilution of complex biological mixtures. Application in 1H NMR metabonomics. *Analytical chemistry,* 78**,** 4281-90.

DIETZE, E. C., SCHAFER, A., OMICHINSKI, J. G. & NELSON, S. D. 1997. Inactivation of glyceraldehyde-3-phosphate dehydrogenase by a reactive metabolite of acetaminophen and mass spectral characterization of an arylated active site peptide. *Chem Res Toxicol,* 10**,** 1097-103.

DIXON, M. F. 1984. Histopathological and enzyme changes in paracetamol-induced liver damage. *In:* RAINSFORD, K. D. A. V., G.P. (ed.) *Advances in inflammation research.* New York: Raven press.

DONA, A. C., JIMENEZ, B., SCHAEFER, H., HUMPFER, E., SPRAUL, M., LEWIS, M. R., PEARCE, J. T., HOLMES, E., LINDON, J. C. & NICHOLSON, J. K. 2014. Precision high throughput proton NMR spectroscopy of human urine, serum and plasma for large-scale metabolic phenotyping. *Anal Chem*.

DUNN, W. B., BROADHURST, D., BEGLEY, P., ZELENA, E., FRANCIS-MCINTYRE, S., ANDERSON, N., BROWN, M., KNOWLES, J. D., HALSALL, A., HASELDEN, J. N., NICHOLLS, A. W., WILSON, I. D., KELL, D. B., GOODACRE, R. & HUMAN SERUM METABOLOME, C. 2011. Procedures for large-scale metabolic profiling of serum and plasma using gas chromatography and liquid chromatography coupled to mass spectrometry. *Nat Protoc,* 6**,** 1060-83.

EXTON, J. H. 1972. Gluconeogenesis. *Metabolism,* 21**,** 945-90.

FABRE, G., MATHERLY, L. H., FAVRE, R., CATALIN, J. & CANO, J. P. 1983. In vitro formation of polyglutamyl derivatives of methotrexate and 7-hydroxymethotrexate in human lymphoblastic leukemia cells. *Cancer Res,* 43**,** 4648-52.

FAGERER, S. R., NIELSEN, S., IBANEZ, A. & ZENOBI, R. 2013. Matrix-assisted laser desorption/ionization matrices for negative mode metabolomics. *Eur J Mass Spectrom (Chichester, Eng),* 19**,** 39-47.

FAIRBANKS, L. D., RUCKEMANN, K., QIU, Y., HAWRYLOWICZ, C. M., RICHARDS, D. F., SWAMINATHAN, R., KIRSCHBAUM, B. & SIMMONDS, H. A. 1999. Methotrexate inhibits the first committed step of purine biosynthesis in mitogen-stimulated human T-lymphocytes: a metabolic basis for efficacy in rheumatoid arthritis? *Biochem J,* 342 (Pt 1)**,** 143-52.

FARBER, S., PINKEL, D., SEARS, E. M. & TOCH, R. 1956. Advances in chemotherapy of cancer in man. *Adv Cancer Res,* 4**,** 1-71.

FARRELL, G. C. & LARTER, C. Z. 2006. Nonalcoholic fatty liver disease: from steatosis to cirrhosis. *Hepatology,* 43**,** S99-S112.

FEAGAN, B. G., ROCHON, J., FEDORAK, R. N., IRVINE, E. J., WILD, G., SUTHERLAND, L., STEINHART, A. H., GREENBERG, G. R., GILLIES, R., HOPKINS, M. & ET AL. 1995. Methotrexate for the treatment of Crohn's disease. The North American Crohn's Study Group Investigators. *N Engl J Med,* 332**,** 292-7.

FENG, B., WU, S., LIU, F., GAO, Y., DONG, F. & WEI, L. 2013. Metabonomic analysis of liver tissue from BALB/c mice with D-galactosamine/lipopolysaccharide-induced acute hepatic failure. *BMC Gastroenterol,* 13**,** 73.

FENG, B., WU, S., LV, S., LIU, F., CHEN, H., YAN, X., LI, Y., DONG, F. & WEI, L. 2007. Metabolic profiling analysis of a D-galactosamine/lipopolysaccharide-induced mouse model of fulminant hepatic failure. *J Proteome Res,* 6**,** 2161-7.

FENN, J. B., MANN, M., MENG, C. K., WONG, S. F. & WHITEHOUSE, C. M. 1989. Electrospray ionization for mass spectrometry of large biomolecules. *Science,* 246**,** 64-71.

FERGUSON, R. E., MCKULLOH, K. E. & ROSENSTOCK, H. M. 1965. *Journal of Chemical Physics,* 42.

FIEHN, O. 2008. Extending the breadth of metabolite profiling by gas chromatography coupled to mass spectrometry. *Trends Analyt Chem,* 27**,** 261-269.

FISHER, C. D., LICKTEIG, A. J., AUGUSTINE, L. M., RANGER-MOORE, J., JACKSON, J. P., FERGUSON, S. S. & CHERRINGTON, N. J. 2009. Hepatic cytochrome P450 enzyme alterations in humans with progressive stages of nonalcoholic fatty liver disease. *Drug Metab Dispos,* 37**,** 2087-94.

FLOMBAUM, C. D. & MEYERS, P. A. 1999. High-dose leucovorin as sole therapy for methotrexate toxicity. *J Clin Oncol,* 17**,** 1589-94.

FLOWER, R. J. & VANE, J. R. 1972. Inhibition of prostaglandin synthetase in brain explains the anti-pyretic activity of paracetamol (4-acetamidophenol). *Nature,* 240**,** 410-1.

FODALE, V. & LA MONACA, E. 2008. Propofol infusion syndrome: an overview of a perplexing disease. *Drug Saf,* 31**,** 293-303.

FONVILLE, J. M., RICHARDS, S. E., BARTON, R. H., BOULANGE, C. L., EBBELS, T. M. D., NICHOLSON, J. K., HOLMES, E. & DUMAS, M.-E. 2010. The evolution of partial least squares models and related chemometric approaches in metabonomics and metabolic phenotyping. *Journal of Chemometrics,* 24**,** 636-649.

FORTE, A. J., WILSON, J. M., SLATTERY, J. T. & NELSON, S. D. 1984. The formation and toxicity of catechol metabolites of acetaminophen in mice. *Drug Metab Dispos,* 12**,** 484-91.

FOTHERGILL, J. C. & GUEST, J. R. 1977. Catabolism of L-lysine by Pseudomonas aeruginosa. *J Gen Microbiol,* 99**,** 139-55.

FOUNTOULAKIS, M., BERNDT, P., BOELSTERLI, U. A., CRAMERI, F., WINTER, M., ALBERTINI, S. & SUTER, L. 2000. Two-dimensional database of mouse liver proteins: changes in hepatic protein levels following treatment with acetaminophen or its nontoxic regioisomer 3-acetamidophenol. *Electrophoresis,* 21**,** 2148-61.

FRIEDMAN, L. S. & EMMET, B. K. 1998. *Handbook of Liver Disease,* Philadelphia, Churchill Livingstone.

FROBERG, S. O., HULTMAN, E. & NILSSON, L. H. 1975. Effect of noradrenaline on triglyceride and glycogen concentrations in liver and muscle from man. *Metabolism,* 24**,** 119-26.

FROMENTY, B., ROBIN, M. A., IGOUDJIL, A., MANSOURI, A. & PESSAYRE, D. 2004. The ins and outs of mitochondrial dysfunction in NASH. *Diabetes Metab,* 30**,** 121-38.

FRY, D. W., ANDERSON, L. A., BORST, M. & GOLDMAN, I. D. 1983. Analysis of the role of membrane transport and polyglutamation of methotrexate in gut and the Ehrlich tumor in vivo as factors in drug sensitivity and selectivity. *Cancer Res,* 43**,** 1087-92.

FUJITA, T. 2009. How does bacterial DNA induce liver failure in cirrhosis? *Hepatology,* 49**,** 1393; author reply 1393-4.

FUKUHARA, K., OHNO, A., ANDO, Y., YAMOTO, T. & OKUDA, H. 2011. A 1H NMR-based Metabolomics Approach for Mechanistic Insight into Acetaminophen-induced Hepatotoxicity. *Drug Metabolism and Pharmacokinetics,* 26**,** 399-406.

GALINSKI, M., RACINE, S. X., BOSSARD, A. E., FLEYFEL, M., HAMZA, L., BOUCHEMAL, N., ADNET, F. & LE MOYEC, L. 2014. Detection and follow-up, after partial liver resection, of the urinary paracetamol metabolites by proton NMR spectroscopy. *Pharmacology,* 93**,** 18-23.

GAO, H., LU, Q., LIU, X., CONG, H., ZHAO, L., WANG, H. & LIN, D. 2009. Application of 1H NMR-based metabonomics in the study of metabolic profiling of human hepatocellular carcinoma and liver cirrhosis. *Cancer Sci,* 100**,** 782-5.

GARCIA-ALVAREZ, M., BERENGUER, J., GUZMAN-FULGENCIO, M., ALVAREZ, E., COSIN, J., MICHELOUD, D., JIMENEZ-SOUSA, M. A., FERNANDEZ-RODRIGUEZ, A., ALDAMIZ-ECHEVARRIA, T., CARRERO, A., MIRALLES, P. & RESINO, S. 2012. Bacterial DNA translocation and liver disease severity among HIV-infected patients with chronic hepatitis C. *J Acquir Immune Defic Syndr,* 61**,** 552-6.

GARCIA-TSAO, G., FRIEDMAN, S., IREDALE, J. & PINZANI, M. 2010. Now there are many (stages) where before there was one: In search of a pathophysiological classification of cirrhosis. *Hepatology,* 51**,** 1445-9.

GARDNER, C. R., HECK, D. E., YANG, C. S., THOMAS, P. E., ZHANG, X. J., DEGEORGE, G. L., LASKIN, J. D. & LASKIN, D. L. 1998. Role of nitric oxide in acetaminophen-induced hepatotoxicity in the rat. *Hepatology,* 27**,** 748-54.

GENESTIER, L., PAILLOT, R., QUEMENEUR, L., IZERADJENE, K. & REVILLARD, J. P. 2000. Mechanisms of action of methotrexate. *Immunopharmacology,* 47**,** 247-57.

GHAURI, F. Y., MCLEAN, A. E., BEALES, D., WILSON, I. D. & NICHOLSON, J. K. 1993. Induction of 5-oxoprolinuria in the rat following chronic feeding with N-acetyl 4-aminophenol (paracetamol). *Biochem Pharmacol,* 46**,** 953-7.

GIBELLINI, F. & SMITH, T. K. 2010. The Kennedy pathway--De novo synthesis of phosphatidylethanolamine and phosphatidylcholine. *IUBMB Life,* 62**,** 414-28.

GIBSON, J. D., PUMFORD, N. R., SAMOKYSZYN, V. M. & HINSON, J. A. 1996. Mechanism of acetaminophen-induced hepatotoxicity: covalent binding versus oxidative stress. *Chem Res Toxicol,* 9**,** 580-5.

GODEJOHANN, M., TSENG, L. H., BRAUMANN, U., FUCHSER, J. & SPRAUL, M. 2004. Characterization of a paracetamol metabolite using on-line LC-SPE-NMR-MS and a cryogenic NMR probe. *J Chromatogr A,* 1058**,** 191-6.

GOLDMAN, I. D. & MATHERLY, L. H. 1985. The cellular pharmacology of methotrexate. *Pharmacol Ther,* 28**,** 77-102.

GUJRAL, J. S., KNIGHT, T. R., FARHOOD, A., BAJT, M. L. & JAESCHKE, H. 2002. Mode of cell death after acetaminophen overdose in mice: apoptosis or oncotic necrosis? *Toxicol Sci,* 67**,** 322-8.

GUTOWSKY, H. S. 1954. Nuclear Magnetic Resonance. *Annual Reviews of Physical Chemistry***,** 333-356.

HADI, M., DRAGOVIC, S., VAN SWELM, R., HERPERS, B., VAN DE WATER, B., RUSSEL, F. G., COMMANDEUR, J. N. & GROOTHUIS, G. M. 2012. AMAP, the alleged non-toxic isomer of acetaminophen, is toxic in rat and human liver. *Arch Toxicol*.

HADI, M., DRAGOVIC, S., VAN SWELM, R., HERPERS, B., VAN DE WATER, B., RUSSEL, F. G., COMMANDEUR, J. N. & GROOTHUIS, G. M. 2013. AMAP, the alleged non-toxic isomer of acetaminophen, is toxic in rat and human liver. *Arch Toxicol,* 87**,** 155-65.

HAHN, E. L. 1950. Spin Echoes. *Phys. Rev.,* 80**,** 580 - 594.

HALMES, N. C., HINSON, J. A., MARTIN, B. M. & PUMFORD, N. R. 1996. Glutamate dehydrogenase covalently binds to a reactive metabolite of acetaminophen. *Chem Res Toxicol,* 9**,** 541-6.

HALMES, N. C., SAMOKYSZYN, V. M., HINTON, T. W., HINSON, J. A. & PUMFORD, N. R. 1998. The acetaminophen regioisomer 3'-hydroxyacetanilide inhibits and covalently binds to cytochrome P450 2E1. *Toxicol Lett,* 94**,** 65-71.

HAMILTON, M. & KISSINGER, P. T. 1986. The metabolism of 2- and 3-hydroxyacetanilide. Determination of metabolic products by liquid chromatography/electrochemistry. *Drug Metab Dispos,* 14**,** 5-12.

HARDWICK, R. N., FERREIRA, D. W., MORE, V. R., LAKE, A. D., LU, Z., MANAUTOU, J. E., SLITT, A. L. & CHERRINGTON, N. J. 2013. Altered UDP-glucuronosyltransferase and sulfotransferase expression and function during progressive stages of human nonalcoholic fatty liver disease. *Drug Metab Dispos,* 41**,** 554-61.

HARDWICK, R. N., FISHER, C. D., CANET, M. J., LAKE, A. D. & CHERRINGTON, N. J. 2010. Diversity in antioxidant response enzymes in progressive stages of human nonalcoholic fatty liver disease. *Drug Metab Dispos,* 38**,** 2293-301.

HARDWICK, R. N., FISHER, C. D., CANET, M. J., SCHEFFER, G. L. & CHERRINGTON, N. J. 2011. Variations in ATP-binding cassette transporter regulation during the progression of human nonalcoholic fatty liver disease. *Drug Metab Dispos,* 39**,** 2395-402.

HENKEL, A. S., DEWEY, A. M., ANDERSON, K. A., OLIVARES, S. & GREEN, R. M. 2012. Reducing endoplasmic reticulum stress does not improve steatohepatitis in mice fed a methionine- and choline-deficient diet. *Am J Physiol Gastrointest Liver Physiol,* 303**,** G54-9.

HILLENKAMP, F., KARAS, M., INGENDOH, A. & STAHL, B. 1990. Matrix Assisted UV-Laser DEsorption Ionization: a New Approach to Mass Spectrometry of Large Molecules. *Biological Mass Spectrometry*.

HILTON, M. A., BERTOLONE, S. & PATEL, C. C. 1989. Daily profiles of plasma phenylalanine and tyrosine in patients with osteogenic sarcoma during treatment with high-dose methotrexate-citrovorum rescue. *Med Pediatr Oncol,* 17**,** 265-70.

HINSON, J. A., ROBERTS, D. W., HALMES, N. C., GIBSON, J. D. & PUMFORD, N. R. 1996. Immunochemical detection of drug-protein adducts in acetaminophen hepatotoxicity. *Adv Exp Med Biol,* 387**,** 47-55.

HINSON, J. A., ROBERTS, D. W. & JAMES, L. P. 2010. Mechanisms of acetaminophen-induced liver necrosis. *Handbook of experimental pharmacology***,** 369-405.

HINZ, B., CHEREMINA, O. & BRUNE, K. 2008. Acetaminophen (paracetamol) is a selective cyclooxygenase-2 inhibitor in man. *FASEB J,* 22**,** 383-90.

HOLECEK, M. 2002. Relation between glutamine, branched-chain amino acids, and protein metabolism. *Nutrition,* 18**,** 130-3.

HOLECEK, M., SPRONGL, L., TICHY, M. & PECKA, M. 1998. Leucine metabolism in rat liver after a bolus injection of endotoxin. *Metabolism,* 47**,** 681-5.

HOLECEK, M., TILSER, I., SKOPEC, F. & SPRONGL, L. 1996. Leucine metabolism in rats with cirrhosis. *J Hepatol,* 24**,** 209-16.

HOLME, J. A., HONGSLO, J. K., BJORGE, C. & NELSON, S. D. 1991. Comparative cytotoxic effects of acetaminophen (N-acetyl-p-aminophenol), a non-hepatotoxic regioisomer acetyl-m-aminophenol and their postulated reactive hydroquinone and quinone metabolites in monolayer cultures of mouse hepatocytes. *Biochem Pharmacol,* 42**,** 1137-42.

HOLMES, E., LOO, R. L., CLOAREC, O., COEN, M., TANG, H., MAIBAUM, E., BRUCE, S., CHAN, Q., ELLIOTT, P., STAMLER, J., WILSON, I. D., LINDON, J. C. & NICHOLSON, J. K. 2007. Detection of urinary drug metabolite (xenometabolome) signatures in molecular epidemiology studies via statistical total correlation (NMR) spectroscopy. *Anal Chem,* 79**,** 2629-40.

HOLTZMAN, J. L. 1995. The role of covalent binding to microsomal proteins in the hepatotoxicity of acetaminophen. *Drug Metab Rev,* 27**,** 277-97.

HONGSLO, J. K., SMITH, C. V., BRUNBORG, G., SODERLUND, E. J. & HOLME, J. A. 1994. Genotoxicity of paracetamol in mice and rats. *Mutagenesis,* 9**,** 93-100.

HORE, P. J. 2011. *Nuclear Magnetic Resonance,* Oxford, Oxford University Press.

HORNE, D. W. 1989. Effects of nitrous oxide inactivation of vitamin B12 and of methionine on folate coenzyme metabolism in rat liver, kidney, brain, small intestine and bone marrow. *Biofactors,* 2**,** 65-8.

HOROWITZ, J. H., RYPINS, E. B., HENDERSON, J. M., HEYMSFIELD, S. B., MOFFITT, S. D., BAIN, R. P., CHAWLA, R. K., BLEIER, J. C. & RUDMAN, D. 1981. Evidence for impairment of transsulfuration pathway in cirrhosis. *Gastroenterology,* 81**,** 668-75.

HOSKINS, L. C., BOULDING, E. T., GERKEN, T. A., HAROUNY, V. R. & KRIARIS, M. S. 1992. Mucin Glycoprotein Degradation by Mucin Oligosaccharide-degradng STrains of Human Faecal Bacteria. Characterisation of Saccharide Cleavage Products and their Potential Role in Nutritional Support of Larger Faecal Bacterial Populations. *Microbial Ecology,* 5**,** 193-207.

HOWELL, B. A., SILER, S. Q. & WATKINS, P. B. 2014. Use of a systems model of drug-induced liver injury (DILIsym((R))) to elucidate the mechanistic differences between acetaminophen and its less-toxic isomer, AMAP, in mice. *Toxicol Lett,* 226**,** 163-72.

HOWIE, D., ADRIAENSSENS, P. I. & PRESCOTT, L. F. 1977. Paracetamol metabolism following overdosage: application of high performance liquid chromatography. *J Pharm Pharmacol,* 29**,** 235-7.

HU, B. & COLLETTI, L. M. 2010. CXC receptor-2 knockout genotype increases X-linked inhibitor of apoptosis protein and protects mice from acetaminophen hepatotoxicity. *Hepatology,* 52**,** 691-702.

HU, J. J., LEE, M. J., VAPIWALA, M., REUHL, K., THOMAS, P. E. & YANG, C. S. 1993. Sex-related differences in mouse renal metabolism and toxicity of acetaminophen. *Toxicol Appl Pharmacol,* 122**,** 16-26.

IKEDA, S., KANEKO, M., NISHIYA, S. & NISHIMURA, C. 1990. Restoration of hematopoietic activity by lipid A analogue GLA-60 in cyclophosphamide-treated immunosuppressed mice. *J Clin Lab Immunol,* 32**,** 189-93.

ILAN, Y. 2012. Leaky gut and the liver: a role for bacterial translocation in nonalcoholic steatohepatitis. *World J Gastroenterol,* 18**,** 2609-18.

JACOBS, S. A., STOLLER, R. G., CHABNER, B. A. & JOHNS, D. G. 1976. 7-Hydroxymethotrexate as a urinary metabolite in human subjects and rhesus monkeys receiving high dose methotrexate. *J Clin Invest,* 57**,** 534-8.

JAESCHKE, H. 2008. Innate immunity and acetaminophen-induced liver injury: why so many controversies? *Hepatology,* 48**,** 699-701.

JAESCHKE, H., MCGILL, M. R. & RAMACHANDRAN, A. 2012. Oxidant stress, mitochondria, and cell death mechanisms in drug-induced liver injury: lessons learned from acetaminophen hepatotoxicity. *Drug Metab Rev,* 44**,** 88-106.

JALAN, R., GINES, P., OLSON, J. C., MOOKERJEE, R. P., MOREAU, R., GARCIA-TSAO, G., ARROYO, V. & KAMATH, P. S. 2012. Acute-on chronic liver failure. *J Hepatol,* 57**,** 1336-48.

JALAN, R. & WILLIAMS, R. 2002. Acute-on-chronic liver failure: pathophysiological basis of therapeutic options. *Blood Purif,* 20**,** 252-61.

JANDA, J. M. & ABBOTT, S. L. 2007. 16S rRNA gene sequencing for bacterial identification in the diagnostic laboratory: pluses, perils, and pitfalls. *J Clin Microbiol,* 45**,** 2761-4.

JANSEN, G., WESTERHOF, G. R., JARMUSZEWSKI, M. J., KATHMANN, I., RIJKSEN, G. & SCHORNAGEL, J. H. 1990. Methotrexate transport in variant human CCRF-CEM leukemia cells with elevated levels of the reduced folate carrier. Selective effect on carrier-mediated transport of physiological concentrations of reduced folates. *J Biol Chem,* 265**,** 18272-7.

JEENER, J., MEIER, B. H., BACHMANN, P. & ERSNT, R. R. 1979. Investigation of exchange processes by twodimensional NMR spectroscopy. *The Journal of Chemical Physics,* 71**,** 4546 - 4553.

JEFFERY, E. H., ARNDT, K. & HASCHEK, W. M. 1988. Mechanism of inhibition of hepatic bioactivation of paracetamol by dimethyl sulfoxide. *Drug Metabol Drug Interact,* 6**,** 413-24.

JEPPESEN, J. B., MORTENSEN, C., BENDTSEN, F. & MOLLER, S. 2013. Lactate metabolism in chronic liver disease. *Scand J Clin Lab Invest*.

JIMBA, S., NAKAGAMI, T., TAKAHASHI, M., WAKAMATSU, T., HIROTA, Y., IWAMOTO, Y. & WASADA, T. 2005. Prevalence of non-alcoholic fatty liver disease and its association with impaired glucose metabolism in Japanese adults. *Diabet Med,* 22**,** 1141-5.

JORDAN, C. G., RASHIDI, M. R., LALJEE, H., CLARKE, S. E., BROWN, J. E. & BEEDHAM, C. 1999. Aldehyde oxidase-catalysed oxidation of methotrexate in the liver of guinea-pig, rabbit and man. *J Pharm Pharmacol,* 51**,** 411-8.

JUNG, Y. S., KIM, S. J., KWON DO, Y., JUN, D. S. & KIM, Y. C. 2013. Significance of alterations in the metabolomics of sulfur-containing amino acids during liver regeneration. *Biochimie,* 95**,** 1605-10.

KALHAN, S. C., EDMISON, J., MARCZEWSKI, S., DASARATHY, S., GRUCA, L. L., BENNETT, C., DUENAS, C. & LOPEZ, R. 2011a. Methionine and protein metabolism in non-alcoholic steatohepatitis: evidence for lower rate of transmethylation of methionine. *Clin Sci (Lond),* 121**,** 179-89.

KALHAN, S. C., GUO, L., EDMISON, J., DASARATHY, S., MCCULLOUGH, A. J., HANSON, R. W. & MILBURN, M. 2011b. Plasma metabolomic profile in nonalcoholic fatty liver disease. *Metabolism,* 60**,** 404-13.

KAMADA, Y., MATSUMOTO, H., TAMURA, S., FUKUSHIMA, J., KISO, S., FUKUI, K., IGURA, T., MAEDA, N., KIHARA, S., FUNAHASHI, T., MATSUZAWA, Y., SHIMOMURA, I. & HAYASHI, N. 2007. Hypoadiponectinemia accelerates hepatic tumor formation in a nonalcoholic steatohepatitis mouse model. *J Hepatol,* 47**,** 556-64.

KAPLOWITZ, N. 2004. Drug Induced Liver Injury. *Infectious Diseases Society of America,* 38**,** 844-848.

KASIM, N. A., WHITEHOUSE, M., RAMACHANDRAN, C., BERMEJO, M., LENNERNAS, H., HUSSAIN, A. S., JUNGINGER, H. E., STAVCHANSKY, S. A., MIDHA, K. K., SHAH, V. P. & AMIDON, G. L. 2004. Molecular properties of WHO essential drugs and provisional biopharmaceutical classification. *Mol Pharm,* 1**,** 85-96.

KATYARE, S. S. & SATAV, J. G. 1989. Impaired mitochondrial oxidative energy metabolism following paracetamol-induced hepatotoxicity in the rat. *Br J Pharmacol,* 96**,** 51-8.

KAWAHARA, H., FUKURA, M., TSUCHISHIMA, M. & TAKASE, S. 2007. Mutation of mitochondrial DNA in livers from patients with alcoholic hepatitis and nonalcoholic steatohepatitis. *Alcohol Clin Exp Res,* 31**,** S54-60.

KHAN, Z. A., TRIPATHI, R. & MISHRA, B. 2012. Methotrexate: a detailed review on drug delivery and clinical aspects. *Expert Opin Drug Deliv,* 9**,** 151-69.

KHANNA, S. & GOPALAN, S. 2007. Role of branched-chain amino acids in liver disease: the evidence for and against. *Curr Opin Clin Nutr Metab Care,* 10**,** 297-303.

KIND, T., WOHLGEMUTH, G., LEE DO, Y., LU, Y., PALAZOGLU, M., SHAHBAZ, S. & FIEHN, O. 2009. FiehnLib: mass spectral and retention index libraries for metabolomics based on quadrupole and time-of-flight gas chromatography/mass spectrometry. *Analytical chemistry,* 81**,** 10038-48.

KINSELL, L. W., HARPER, H. A., BARTON, H. C., MICHAELS, G. D. & WEISS, H. A. 1947. Rate of Disappearance From Plasma of Intravenously Administered Methionine in Patients With Liver Damage. *Science,* 106**,** 589-90.

KIRSCH, R., CLARKSON, V., SHEPHARD, E. G., MARAIS, D. A., JAFFER, M. A., WOODBURNE, V. E., KIRSCH, R. E. & HALL PDE, L. 2003. Rodent nutritional model of non-alcoholic steatohepatitis: species, strain and sex difference studies. *J Gastroenterol Hepatol,* 18**,** 1272-82.

KNIGHT, T. R., HO, Y. S., FARHOOD, A. & JAESCHKE, H. 2002. Peroxynitrite is a critical mediator of acetaminophen hepatotoxicity in murine livers: protection by glutathione. *J Pharmacol Exp Ther,* 303**,** 468-75.

KOYMANS, L., VAN LENTHE, J. H., VAN DE STRAAT, R., DONNE-OP DEN KELDER, G. M. & VERMEULEN, N. P. 1989. A theoretical study on the metabolic activation of paracetamol by cytochrome P-450: indications for a uniform oxidation mechanism. *Chem Res Toxicol,* 2**,** 60-6.

KRAHENBUHL, S. 1996. Carnitine metabolism in chronic liver disease. *Life Sci,* 59**,** 1579-99.

KREMER, J. M. 2004. Toward a better understanding of methotrexate. *Arthritis Rheum,* 50**,** 1370-82.

KRENZELOK, E. P. 2009. The FDA Acetaminophen Advisory Committee Meeting - what is the future of acetaminophen in the United States? The perspective of a committee member. *Clin Toxicol (Phila),* 47**,** 784-9.

KUCERA, O. & CERVINKOVA, Z. 2014. Experimental models of non-alcoholic fatty liver disease in rats. *World J Gastroenterol,* 20**,** 8364-8376.

KUHL, C., TAUTENHAHN, R., BOTTCHER, C., LARSON, T. R. & NEUMANN, S. 2012. CAMERA: an integrated strategy for compound spectra extraction and annotation of liquid chromatography/mass spectrometry data sets. *Anal Chem,* 84**,** 283-9.

KUMAR, B. S., CHUNG, B. C., KWON, O. S. & JUNG, B. H. 2012. Discovery of common urinary biomarkers for hepatotoxicity induced by carbon tetrachloride, acetaminophen and methotrexate by mass spectrometry-based metabolomics. *J Appl Toxicol,* 32**,** 505-20.

KYRIAKIDES, M., HARDWICK, R. N., JIN, Z., GOEDKEN, M. J., HOLMES, E., CHERRINGTON, N. J. & COEN, M. 2014. Systems Level Metabolic Phenotype Of Methotrexate Administration In The Context Of Non-Alcoholic Steatohepatitis In The Rat. *Toxicol Sci*.

LADEP, N. G., DONA, A. C., LEWIS, M. R., CROSSEY, M. M., LEMOINE, M., OKEKE, E., SHIMAKAWA, Y., DUGURU, M., NJAI, H. F., FYE, H. K., TAAL, M., CHETWOOD, J., KASSTAN, B., KHAN, S. A., GARSIDE, D. A., WIJEYESEKERA, A., THILLAINAYAGAM, A. V., BANWAT, E., THURSZ, M. R., NICHOLSON, J. K., NJIE, R., HOLMES, E. & TAYLOR-ROBINSON, S. D. 2014. Discovery and validation of urinary metabotypes for the diagnosis of hepatocellular carcinoma in West Africans. *Hepatology*.

LAI, W. K. 2004. Management of acute liver failure. *Continuing Education in Anaesthesia, Critical Care & Pain,* 4**,** 40-43.

LAKE, A. D., NOVAK, P., FISHER, C. D., JACKSON, J. P., HARDWICK, R. N., BILLHEIMER, D. D., KLIMECKI, W. T. & CHERRINGTON, N. J. 2011. Analysis of global and absorption, distribution, metabolism, and elimination gene expression in the progressive stages of human nonalcoholic fatty liver disease. *Drug Metab Dispos,* 39**,** 1954-60.

LANDAU, L. & LIFSHITZ, E. M. 1935. Theory of the dispersion of magnetic permeability in ferromagnetic bodies. *Physikalische Zeitschrift der Sowjetunion,* 8**,** 977-979.

LANDIN, J. S., COHEN, S. D. & KHAIRALLAH, E. A. 1996. Identification of a 54-kDa mitochondrial acetaminophen-binding protein as aldehyde dehydrogenase. *Toxicol Appl Pharmacol,* 141**,** 299-307.

LANGMAN, G., HALL, P. M. & TODD, G. 2001. Role of non-alcoholic steatohepatitis in methotrexate-induced liver injury. *J Gastroenterol Hepatol,* 16**,** 1395-401.

LARTER, C. Z. 2007. Not all models of fatty liver are created equal: understanding mechanisms of steatosis development is important. *J Gastroenterol Hepatol,* 22**,** 1353-4.

LARTER, C. Z., CHITTURI, S., HEYDET, D. & FARRELL, G. C. 2010. A fresh look at NASH pathogenesis. Part 1: the metabolic movers. *J Gastroenterol Hepatol,* 25**,** 672-90.

LARTER, C. Z. & YEH, M. M. 2008. Animal models of NASH: getting both pathology and metabolic context right. *J Gastroenterol Hepatol,* 23**,** 1635-48.

LEAMY, A. K., EGNATCHIK, R. A. & YOUNG, J. D. 2013. Molecular mechanisms and the role of saturated fatty acids in the progression of non-alcoholic fatty liver disease. *Prog Lipid Res,* 52**,** 165-74.

LEE, J. K., ABE, K., BRIDGES, A. S., PATEL, N. J., RAUB, T. J., POLLACK, G. M. & BROUWER, K. L. 2009. Sex-dependent disposition of acetaminophen sulphate and glucuronide in the in situ perfused mouse liver. *Drug Metab Dispos,* 37**,** 1916-21.

LEE, W. M. 1993. Acute liver failure. *The New England Journal Of Medicine,* 329**,** 1862-1871.

LEE, W. M. 2012a. Acute liver failure. *Semin Respir Crit Care Med,* 33**,** 36-45.

LEE, W. M. 2012b. Recent developments in acute liver failure. *Best Pract Res Clin Gastroenterol,* 26**,** 3-16.

LEWELING, H., BREITKREUTZ, R., BEHNE, F., STAEDT, U., STRIEBEL, J. P. & HOLM, E. 1996. Hyperammonemia-induced depletion of glutamate and branched-chain amino acids in muscle and plasma. *J Hepatol,* 25**,** 756-62.

LEWIS, A. S., MURPHY, L., MCCALLA, C., FLEARY, M. & PURCELL, S. 1984. Inhibition of mammalian xanthine oxidase by folate compounds and amethopterin. *J Biol Chem,* 259**,** 12-5.

LI, H., WANG, L., YAN, X., LIU, Q., YU, C., WEI, H., LI, Y., ZHANG, X., HE, F. & JIANG, Y. 2011. A proton nuclear magnetic resonance metabonomics approach for biomarker discovery in nonalcoholic fatty liver disease. *J Proteome Res,* 10**,** 2797-806.

LI, Z. Z., BERK, M., MCINTYRE, T. M. & FELDSTEIN, A. E. 2009. Hepatic lipid partitioning and liver damage in nonalcoholic fatty liver disease: role of stearoyl-CoA desaturase. *J Biol Chem,* 284**,** 5637-44.

LIND, L. & LITHELL, H. 1994. Impaired glucose and lipid metabolism seen in intensive care patients is related to severity of illness and survival. *Clin Intensive Care,* 5**,** 100-5.

LINDON, J. C., HOLMES, E. & NICHOLSON, J. K. 2006. Metabonomics techniques and applications to pharmaceutical research & development. *Pharm Res,* 23**,** 1075-88.

LINDON, J. C. & NICHOLSON, J. K. 2014. The emergent role of metabolic phenotyping in dynamic patient stratification. *Expert Opin Drug Metab Toxicol,* 10**,** 915-9.

LINDON, J. C., NICHOLSON, J. K., HOLMES, E., ANTTI, H., BOLLARD, M. E., KEUN, H., BECKONERT, O., EBBELS, T. M., REILY, M. D., ROBERTSON, D., STEVENS, G. J., LUKE, P., BREAU, A. P., CANTOR, G. H., BIBLE, R. H., NIEDERHAUSER, U., SENN, H., SCHLOTTERBECK, G., SIDELMANN, U. G., LAURSEN, S. M., TYMIAK, A., CAR, B. D., LEHMAN-MCKEEMAN, L., COLET, J. M., LOUKACI, A. & THOMAS, C. 2003. Contemporary issues in toxicology the role of metabonomics in toxicology and its evaluation by the COMET project. *Toxicol Appl Pharmacol,* 187**,** 137-46.

LIU, K. J., DRUCKER, Y. & JARAD, J. 1995. Hepatic glycerol metabolism in tumorous rats: a 13C nuclear magnetic resonance study. *Cancer Res,* 55**,** 761-6.

LOBO, E. D. & BALTHASAR, J. P. 2003. Pharmacokinetic-pharmacodynamic modeling of methotrexate-induced toxicity in mice. *J Pharm Sci,* 92**,** 1654-64.

LOCASALE, J. W. 2013. Serine, glycine and one-carbon units: cancer metabolism in full circle. *Nat Rev Cancer,* 13**,** 572-83.

LOO, R. L., CHAN, Q., BROWN, I. J., ROBERTSON, C. E., STAMLER, J., NICHOLSON, J. K., HOLMES, E. & ELLIOTT, P. 2012. A comparison of self-reported analgesic use and detection of urinary ibuprofen and acetaminophen metabolites by means of metabonomics: the INTERMAP Study. *Am J Epidemiol,* 175**,** 348-58.

LU, S. C. 1999. Regulation of hepatic glutathione synthesis: current concepts and controversies. *FASEB J,* 13**,** 1169-83.

LU, S. C. & MATO, J. M. 2012. S-adenosylmethionine in liver health, injury, and cancer. *Physiol Rev,* 92**,** 1515-42.

LUBEK, B. M., AVARIA, M., BASU, P. K. & WELLS, P. G. 1988. Pharmacological studies on the in vivo cataractogenicity of acetaminophen in mice and rabbits. *Fundam Appl Toxicol,* 10**,** 596-606.

LUDWIG, J., VIGGIANO, T. R., MCGILL, D. B. & OH, B. J. 1980. Nonalcoholic steatohepatitis: Mayo Clinic experiences with a hitherto unnamed disease. *Mayo Clin Proc,* 55**,** 434-8.

MARCEAU, P., BIRON, S., HOULD, F. S., MARCEAU, S., SIMARD, S., THUNG, S. N. & KRAL, J. G. 1999. Liver pathology and the metabolic syndrome X in severe obesity. *J Clin Endocrinol Metab,* 84**,** 1513-7.

MARCHESINI, G., BUGIANESI, E., BIANCHI, G., FABBRI, A., MARCHI, E., ZOLI, M. & PISI, E. 1992. Defective methionine metabolism in cirrhosis: relation to severity of liver disease. *Hepatology,* 16**,** 149-55.

MARION, D. 2013. An introduction to biological NMR spectroscopy. *Mol Cell Proteomics,* 12**,** 3006-25.

MARTINEZ-CHANTAR, M. L., GARCIA-TREVIJANO, E. R., LATASA, M. U., PEREZ-MATO, I., SANCHEZ DEL PINO, M. M., CORRALES, F. J., AVILA, M. A. & MATO, J. M. 2002. Importance of a deficiency in S-adenosyl-L-methionine synthesis in the pathogenesis of liver injury. *Am J Clin Nutr,* 76**,** 1177S-82S.

MASSON, P., ALVES, A. C., EBBELS, T. M., NICHOLSON, J. K. & WANT, E. J. 2010. Optimization and evaluation of metabolite extraction protocols for untargeted metabolic profiling of liver samples by UPLC-MS. *Anal Chem,* 82**,** 7779-86.

MASUBUCHI, Y., SUDA, C. & HORIE, T. 2005. Involvement of mitochondrial permeability transition in acetaminophen-induced liver injury in mice. *J Hepatol,* 42**,** 110-6.

MATO, J. M., MARTINEZ-CHANTAR, M. L. & LU, S. C. 2008. Methionine metabolism and liver disease. *Annu Rev Nutr,* 28**,** 273-93.

MATSUZAWA, N., TAKAMURA, T., KURITA, S., MISU, H., OTA, T., ANDO, H., YOKOYAMA, M., HONDA, M., ZEN, Y., NAKANUMA, Y., MIYAMOTO, K. & KANEKO, S. 2007. Lipid-induced oxidative stress causes steatohepatitis in mice fed an atherogenic diet. *Hepatology,* 46**,** 1392-403.

MATTAMAL, M. B., ZENSER, T.V., BROWN, W.W., HERMAN, C.A. AND DAVIS B.B. 1979. Mechanisms of inhibition of renal prostaglandin production by acetaminophen. *J Pharmacol Exp Ther,* 8**,** 405-409.

MCCULLOUGH, A. J. 2007. The Epidemiology and Risk Factors of NASH. *Fatty Liver Disease.* Blackwell Publishing Ltd.

MCGILL, M. R. & JAESCHKE, H. 2013. Metabolism and Disposition of Acetaminophen: Recent Advances in Relation to Hepatotoxicity and Diagnosis. *Pharm Res*.

MCGILL, M. R., LI, F., SHARPE, M. R., WILLIAMS, C. D., CURRY, S. C., MA, X. & JAESCHKE, H. 2014a. Circulating acylcarnitines as biomarkers of mitochondrial dysfunction after acetaminophen overdose in mice and humans. *Arch Toxicol,* 88**,** 391-401.

MCGILL, M. R., SHARPE, M. R., WILLIAMS, C. D., TAHA, M., CURRY, S. C. & JAESCHKE, H. 2012a. The mechanism underlying acetaminophen-induced hepatotoxicity in humans and mice involves mitochondrial damage and nuclear DNA fragmentation. *J Clin Invest,* 122**,** 1574-83.

MCGILL, M. R., STAGGS, V. S., SHARPE, M. R., LEE, W. M., JAESCHKE, H. & ACUTE LIVER FAILURE STUDY, G. 2014b. Serum mitochondrial biomarkers and damage-associated molecular patterns are higher in acetaminophen overdose patients with poor outcome. *Hepatology*.

MCGILL, M. R., WILLIAMS, C. D., XIE, Y., RAMACHANDRAN, A. & JAESCHKE, H. 2012b. Acetaminophen-induced liver injury in rats and mice: comparison of protein adducts, mitochondrial dysfunction, and oxidative stress in the mechanism of toxicity. *Toxicol Appl Pharmacol,* 264**,** 387-94.

MCINTYRE, N. 1978. Plasma lipids and lipoproteins in liver disease. *Gut,* 19**,** 526-30.

MCKAY, R. T. 2011. How the 1D-NOESY suppresses solvent signal in metabonomics NMR spectroscopy: An examination of the pulse sequence components and evolution. *Concepts Magn. Reson.,* 38A**,** 197-220.

MEIBOOM, S. & GILL, D. 1958. Modified SpinEcho Method for Measuring Nuclear Relaxation Times. *The Review of Scientific Instruments,* 29**,** 688-691.

MEYER, L. M., MILLER, F. R., ROWEN, M. J., BOCK, G. & RUTZKY, J. 1950. Treatment of acute leukemia with amethopterin (4-amino, 10-methyl pteroyl glutamic acid). *Acta Haematol,* 4**,** 157-67.

MEYERS, L. L., BEIERSCHMITT, W. P., KHAIRALLAH, E. A. & COHEN, S. D. 1988. Acetaminophen-induced inhibition of hepatic mitochondrial respiration in mice. *Toxicol Appl Pharmacol,* 93**,** 378-87.

MEZEY, E. 1982. Liver disease and protein needs. *Annu Rev Nutr,* 2**,** 21-50.

MICHAEL, B. J., BALL, J. G., WRIGHT, M. S., VAN METER, S. & VALENTOVIC, M. A. 2012. Novel protective mechanisms for S-adenosyl-L-methionine against acetaminophen hepatotoxicity: improvement of key antioxidant enzymatic function. *Toxicol Lett,* 212**,** 320-8.

MIELE, L., MARRONE, G., LAURITANO, C., CEFALO, C., GASBARRINI, A., DAY, C. & GRIECO, A. 2013. Gut-liver axis and microbiota in NAFLD: insight pathophysiology for novel therapeutic target. *Curr Pharm Des,* 19**,** 5314-24.

MILLER, R. A., BUEHNER, G., CHANG, Y., HARPER, J. M., SIGLER, R. & SMITH-WHEELOCK, M. 2005. Methionine-deficient diet extends mouse lifespan, slows immune and lens aging, alters glucose, T4, IGF-I and insulin levels, and increases hepatocyte MIF levels and stress resistance. *Aging Cell,* 4**,** 119-25.

MINER, D. J. & KISSINGER, P. T. 1979. Evidence for the involvement of N-acetyl-p- quinoneimine in acetaminophen metabolism. *Biochem Pharmacol,* 28**,** 3285-90.

MITCHELL, J. R., JOLLOW, D. J., POTTER, W. Z., DAVIS, D. C., GILLETTE, J. R. & BRODIE, B. B. 1973. Acetaminophen-induced hepatic necrosis. I. Role of drug metabolism. *J Pharmacol Exp Ther,* 187**,** 185-94.

MITKA, M. 2014. FDA asks physicians to stop prescribing high-dose acetaminophen products. *JAMA,* 311**,** 563.

MIYAZAKI, M., DOBRZYN, A., SAMPATH, H., LEE, S. H., MAN, W. C., CHU, K., PETERS, J. M., GONZALEZ, F. J. & NTAMBI, J. M. 2004. Reduced adiposity and liver steatosis by stearoyl-CoA desaturase deficiency are independent of peroxisome proliferator-activated receptor-alpha. *J Biol Chem,* 279**,** 35017-24.

MIYAZAKI, M., KIM, Y. C. & NTAMBI, J. M. 2001. A lipogenic diet in mice with a disruption of the stearoyl-CoA desaturase 1 gene reveals a stringent requirement of endogenous monounsaturated fatty acids for triglyceride synthesis. *J Lipid Res,* 42**,** 1018-24.

MIZOCK, B. A. & FALK, J. L. 1992. Lactic acidosis in critical illness. *Crit Care Med,* 20**,** 80-93.

MOHANDAS, J., DUGGIN, G. G., HORVATH, J. S. & TILLER, D. J. 1981. Regional differences in peroxidatic activation of paracetamol (acetaminophen) mediated by cytochrome P450 and prostaglandin endoperoxide synthetase in rabbit kidney. *Res Commun Chem Pathol Pharmacol,* 34**,** 69-80.

MOISA, A., FRITZ, P., BENZ, D. & WEHNER, H. D. 2006. Iatrogenically-related, fatal methotrexate intoxication: a series of four cases. *Forensic Sci Int,* 156**,** 154-7.

MOREAU, R., JALAN, R., GINES, P., PAVESI, M., ANGELI, P., CORDOBA, J., DURAND, F., GUSTOT, T., SALIBA, F., DOMENICALI, M., GERBES, A., WENDON, J., ALESSANDRIA, C., LALEMAN, W., ZEUZEM, S., TREBICKA, J., BERNARDI, M., ARROYO, V. & CONSORTIUM, C. S. I. O. T. E.-C. 2013. Acute-on-chronic liver failure is a distinct syndrome that develops in patients with acute decompensation of cirrhosis. *Gastroenterology,* 144**,** 1426-37, 1437 e1-9.

MORIYASU, A., SUGIHARA, K., NAKATANI, K., OHTA, S. & KITAMURA, S. 2006. In vivo-in vitro relationship of methotrexate 7-hydroxylation by aldehyde oxidase in four different strain rats. *Drug Metab Pharmacokinet,* 21**,** 485-91.

MOSCHEN, A. R., KASER, S. & TILG, H. 2013. Non-alcoholic steatohepatitis: a microbiota-driven disease. *Trends Endocrinol Metab,* 24**,** 537-45.

MOURELLE, M., BEALES, D. & MCLEAN, A. E. 1990. Electron transport and protection of liver slices in the late stage of paracetamol injury. *Biochem Pharmacol,* 40**,** 2023-8.

MU, Y. P., OGAWA, T. & KAWADA, N. 2010. Reversibility of fibrosis, inflammation, and endoplasmic reticulum stress in the liver of rats fed a methionine-choline-deficient diet. *Lab Invest,* 90**,** 245-56.

MU, Y. P., OGAWA, T. & KWADA, N. 2012. [Mechanism of hepatocyte apoptosis in rats with liver fibrosis induced by lipogenic methionine-choline-deficient diet]. *Zhonghua Bing Li Xue Za Zhi,* 41**,** 112-8.

MUSSO, G., GAMBINO, R. & CASSADER, M. 2013. Cholesterol metabolism and the pathogenesis of non-alcoholic steatohepatitis. *Prog Lipid Res,* 52**,** 175-91.

MYERS, T. G., DIETZ, E. C., ANDERSON, N. L., KHAIRALLAH, E. A., COHEN, S. D. & NELSON, S. D. 1995. A comparative study of mouse liver proteins arylated by reactive metabolites of acetaminophen and its nonhepatotoxic regioisomer, 3'-hydroxyacetanilide. *Chem Res Toxicol,* 8**,** 403-13.

NARUHASHI, K., NADAI, M., NAKAO, M., SUZUKI, N., NABESHIMA, T. & HASEGAWA, T. 2000. Changes in absorptive function of rat intestine injured by methotrexate. *Clin Exp Pharmacol Physiol,* 27**,** 980-6.

NEALE, G., LEWIS, B., WEAVER, V. & PANVELIWALLA, D. 1971. Serum bile acids in liver disease. *Gut,* 12**,** 145-52.

NELSON, E. B. 1980. The pharmacology and toxicology of meta-substituted acetanilide I: acute toxicity of 3-hydroxyacetanilide in mice. *Res Commun Chem Pathol Pharmacol,* 28**,** 447-56.

NELSON, S. D. 1995. Mechanisms of the formation and disposition of reactive metabolites that can cause acute liver injury. *Drug Metab Rev,* 27**,** 147-77.

NESHER, G., MOORE, T. L. & DORNER, R. W. 1991. In vitro effects of methotrexate on peripheral blood monocytes: modulation by folinic acid and S-adenosylmethionine. *Ann Rheum Dis,* 50**,** 637-41.

NEWTON, J. F., HOEFLE, D., GEMBORYS, M. W., MUDGE, G. H. & HOOK, J. B. 1986. Metabolism and excretion of a glutathione conjugate of acetaminophen in the isolated perfused rat kidney. *J Pharmacol Exp Ther,* 237**,** 519-24.

NICHOLLS, A. W., CADDICK, S., WILSON, I. D., FARRANT, R. D., LINDON, J. C. & NICHOLSON, J. K. 1995. High resolution NMR spectroscopic studies on the metabolism and futile deacetylation of 4-hydroxyacetanilide (paracetamol) in the rat. *Biochem Pharmacol,* 49**,** 1155-64.

NICHOLLS, A. W., FARRANT, R. D., SHOCKCOR, J. P., UNGER, S. E., WILSON, I. D., LINDON, J. C. & NICHOLSON, J. K. 1997. NMR and HPLC-NMR spectroscopic studies of futile deacetylation in paracetamol metabolites in rat and man. *J Pharm Biomed Anal,* 15**,** 901-10.

NICHOLLS, A. W., WILSON, I. D., GODEJOHANN, M., NICHOLSON, J. K. & SHOCKCOR, J. P. 2006. Identification of phenacetin metabolites in human urine after administration of phenacetin-C2H3: measurement of futile metabolic deacetylation via HPLC/MS-SPE-NMR and HPLC-ToF MS. *Xenobiotica,* 36**,** 615-29.

NICHOLSON, J. K., CONNELLY, J., LINDON, J. C. & HOLMES, E. 2002. Metabonomics: a platform for studying drug toxicity and gene function. *Nat Rev Drug Discov,* 1**,** 153-61.

NICHOLSON, J. K., FOXALL, P. J., SPRAUL, M., FARRANT, R. D. & LINDON, J. C. 1995. 750 MHz 1H and 1H-13C NMR spectroscopy of human blood plasma. *Analytical chemistry,* 67**,** 793-811.

NICHOLSON, J. K., HOLMES, E., KINROSS, J., BURCELIN, R., GIBSON, G., JIA, W. & PETTERSSON, S. 2012. Host-gut microbiota metabolic interactions. *Science,* 336**,** 1262-7.

NICHOLSON, J. K. & LINDON, J. C. 2008. Systems biology: Metabonomics. *Nature,* 455**,** 1054-6.

NICHOLSON, J. K., LINDON, J. C. & HOLMES, E. 1999. 'Metabonomics': understanding the metabolic responses of living systems to pathophysiological stimuli via multivariate statistical analysis of biological NMR spectroscopic data. *Xenobiotica,* 29**,** 1181-9.

NICHOLSON, J. K., O'FLYNN, M. P., SADLER, P. J., MACLEOD, A. F., JUUL, S. M. & SONKSEN, P. H. 1984. Proton-nuclear-magnetic-resonance studies of serum, plasma and urine from fasting normal and diabetic subjects. *Biochem J,* 217**,** 365-75.

NIE, C. Y., HAN, T., ZHANG, L., LI, Y., LIU, H., XIAO, S. X., LI, Y., KANG, H. & LIU, S. Y. 2014. Cross-sectional and dynamic change of serum metabolite profiling for Hepatitis B-related acute-on-chronic liver failure by UPLC/MS. *J Viral Hepat,* 21**,** 53-63.

NIER, A. O. 1947. *Review of Scientific Instruments,* 18.

NOWACZYK, M. J., WHELAN, D., HILL, R. E., CLARKE, J. T. & POLLITT, R. J. 2000. Long-chain hydroxydicarboxylic aciduria, carnitine depletion and acetaminophen exposure. *J Inherit Metab Dis,* 23**,** 188-9.

NSEIR, W. & MAHAMID, M. 2013. Statins in nonalcoholic fatty liver disease and steatohepatitis: updated review. *Curr Atheroscler Rep,* 15**,** 305.

O'GRADY, J. G., SCHALM, S. W. & WILLIAMS, R. 1993. Acute liver failure: redefining the syndromes. *Lancet,* 342**,** 273-5.

OHNISHI, H., SUGIHARA, J., MORIWAKI, H. & MUTO, Y. 1995. [Acute-on-chronic liver failure]. *Ryoikibetsu Shokogun Shirizu***,** 217-9.

OKUBO, H., SAKODA, H., KUSHIYAMA, A., FUJISHIRO, M., NAKATSU, Y., FUKUSHIMA, T., MATSUNAGA, Y., KAMATA, H., ASAHARA, T., YOSHIDA, Y., CHONAN, O., IWASHITA, M., NISHIMURA, F. & ASANO, T. 2013. Lactobacillus casei strain Shirota protects against nonalcoholic steatohepatitis development in a rodent model. *Am J Physiol Gastrointest Liver Physiol,* 305**,** G911-8.

OLDE DAMINK, S. W., DEUTZ, N. E., DEJONG, C. H., SOETERS, P. B. & JALAN, R. 2002. Interorgan ammonia metabolism in liver failure. *Neurochem Int,* 41**,** 177-88.

OMIECINSKI, C. J., REMMEL, R. P. & HOSAGRAHARA, V. P. 1999. Concise review of the cytochrome P450s and their roles in toxicology. *Toxicol Sci,* 48**,** 151-6.

OUELLETTE, M., MAKKAY, A. M. & PAPKE, R. T. 2013. Dihydroxyacetone metabolism in Haloferax volcanii. *Front Microbiol,* 4**,** 376.

PAGANO, G., PACINI, G., MUSSO, G., GAMBINO, R., MECCA, F., DEPETRIS, N., CASSADER, M., DAVID, E., CAVALLO-PERIN, P. & RIZZETTO, M. 2002. Nonalcoholic steatohepatitis, insulin resistance, and metabolic syndrome: further evidence for an etiologic association. *Hepatology,* 35**,** 367-72.

PANAYIOTIDIS, M. I., STABLER, S. P., ALLEN, R. H., PAPPA, A. & WHITE, C. W. 2009. Oxidative stress-induced regulation of the methionine metabolic pathway in human lung epithelial-like (A549) cells. *Mutat Res,* 674**,** 23-30.

PELZ, S., STOCK, P., BRUCKNER, S. & CHRIST, B. 2012. A methionine-choline-deficient diet elicits NASH in the immunodeficient mouse featuring a model for hepatic cell transplantation. *Exp Cell Res,* 318**,** 276-87.

PEREZ-CARRERAS, M., DEL HOYO, P., MARTIN, M. A., RUBIO, J. C., MARTIN, A., CASTELLANO, G., COLINA, F., ARENAS, J. & SOLIS-HERRUZO, J. A. 2003. Defective hepatic mitochondrial respiratory chain in patients with nonalcoholic steatohepatitis. *Hepatology,* 38**,** 999-1007.

PESSAYRE, D. & FROMENTY, B. 2005. NASH: a mitochondrial disease. *J Hepatol,* 42**,** 928-40.

PHAM, T. V., LU, S. AND KAPLOWITZ, N. 1997. Acetaminophen hepatotoxicity. *In:* TAYLOR, M. B. (ed.) *Gastrointestinal emergencies.* Baltimore: Williams & Wilkins.

PINZANI, M., ROSSELLI, M. & ZUCKERMANN, M. 2011. Liver cirrhosis. *Best Pract Res Clin Gastroenterol,* 25**,** 281-90.

PLACKE, M. E., GINSBERG, G. L., WYAND, D. S. & COHEN, S. D. 1987. Ultrastructural changes during acute acetaminophen-induced hepatotoxicity in the mouse: a time and dose study. *Toxicol Pathol,* 15**,** 431-8.

PLAUTH, M. & SCHUTZ, T. 2011. Branched-chain amino acids in liver disease: new aspects of long known phenomena. *Curr Opin Clin Nutr Metab Care,* 14**,** 61-6.

POLSON, J., LEE, W. M. & AMERICAN ASSOCIATION FOR THE STUDY OF LIVER, D. 2005. AASLD position paper: the management of acute liver failure. *Hepatology,* 41**,** 1179-97.

POMFRET, E. A., DACOSTA, K. A. & ZEISEL, S. H. 1990. Effects of choline deficiency and methotrexate treatment upon rat liver. *J Nutr Biochem,* 1**,** 533-41.

POTTER, W. Z., THORGEIRSSON, S. S., JOLLOW, D. J. & MITCHELL, J. R. 1974. Acetaminophen-induced hepatic necrosis. V. Correlation of hepatic necrosis, covalent binding and glutathione depletion in hamsters. *Pharmacology,* 12**,** 129-43.

PRATT, S. & IOANNIDES, C. 1985. Mechanism of the protective action of n-acetylcysteine and methionine against paracetamol toxicity in the hamster. *Arch Toxicol,* 57**,** 173-7.

PRESCOTT, L. F. 1980. Kinetics and metabolism of paracetamol and phenacetin. *Br J Clin Pharmacol,* 10 Suppl 2**,** 291S-298S.

PRIYADARSINY, P., KHATTAR, S. K., MALIK, R., UDUPA, V., SESHAIAH, A., RAHMAN, S., SHINGATGERI, V. M., BORA, R. S. & SAINI, K. S. 2008. Differential gene expression analysis of a known hepatotoxin, N-acetyl-p-amino-phenol (APAP) as compared to its non-toxic analog, N-acetyl-m-amino-phenol (AMAP) in mouse liver. *J Toxicol Sci,* 33**,** 163-73.

PUMFORD, N. R. & HALMES, N. C. 1997. Protein targets of xenobiotic reactive intermediates. *Annu Rev Pharmacol Toxicol,* 37**,** 91-117.

PURI, P., WIEST, M. M., CHEUNG, O., MIRSHAHI, F., SARGEANT, C., MIN, H. K., CONTOS, M. J., STERLING, R. K., FUCHS, M., ZHOU, H., WATKINS, S. M. & SANYAL, A. J. 2009. The plasma lipidomic signature of nonalcoholic steatohepatitis. *Hepatology,* 50**,** 1827-38.

QI, S. W., TU, Z. G., PENG, W. J., WANG, L. X., OU-YANG, X., CAI, A. J. & DAI, Y. 2012. (1)H NMR-based serum metabolic profiling in compensated and decompensated cirrhosis. *World J Gastroenterol,* 18**,** 285-90.

QIU, Y., BENET, L. Z. & BURLINGAME, A. L. 1998. Identification of the hepatic protein targets of reactive metabolites of acetaminophen in vivo in mice using two-dimensional gel electrophoresis and mass spectrometry. *J Biol Chem,* 273**,** 17940-53.

RADI, R., PELUFFO, G., ALVAREZ, M. N., NAVILIAT, M. & CAYOTA, A. 2001. Unraveling peroxynitrite formation in biological systems. *Free Radic Biol Med,* 30**,** 463-88.

RAMSAY, R. R., RASHED, M. S. & NELSON, S. D. 1989. In vitro effects of acetaminophen metabolites and analogs on the respiration of mouse liver mitochondria. *Arch Biochem Biophys,* 273**,** 449-57.

RASHED, M. S., MYERS, T. G. & NELSON, S. D. 1990. Hepatic protein arylation, glutathione depletion, and metabolite profiles of acetaminophen and a non-hepatotoxic regioisomer, 3'-hydroxyacetanilide, in the mouse. *Drug Metab Dispos,* 18**,** 765-70.

RASHED, M. S. & NELSON, S. D. 1989a. Characterization of glutathione conjugates of reactive metabolites of 3'-hydroxyacetanilide, a nonhepatotoxic positional isomer of acetaminophen. *Chem Res Toxicol,* 2**,** 41-5.

RASHED, M. S. & NELSON, S. D. 1989b. Use of thermospray liquid chromatography-mass spectrometry for characterization of reactive metabolites of 3'-hydroxyacetanilide, a non-hepatotoxic regioisomer of acetaminophen. *J Chromatogr,* 474**,** 209-22.

RAY, S. D., MUMAW, V. R., RAJE, R. R. & FARISS, M. W. 1996. Protection of acetaminophen-induced hepatocellular apoptosis and necrosis by cholesteryl hemisuccinate pretreatment. *J Pharmacol Exp Ther,* 279**,** 1470-83.

RECORD, C. O., CHASE, R. A., WILLIAMS, R. & APPLETON, D. 1981. Disturbances of lactate metabolism in patients with liver damage due to paracetamol overdose. *Metabolism,* 30**,** 638-43.

RECORD, C. O., ILES, R. A., COHEN, R. D. & WILLIAMS, R. 1975. Acid-base and metabolic disturbances in fulminant hepatic failure. *Gut,* 16**,** 144-9.

REDDY, J. K. & RAO, M. S. 2006. Lipid metabolism and liver inflammation. II. Fatty liver disease and fatty acid oxidation. *Am J Physiol Gastrointest Liver Physiol,* 290**,** G852-8.

REICH, S. D., BACHUR, N. R., GOEBEL, R. H. & BERMAN, M. 1977. A pharmacokinetic model for high-dose methotrexate infusions in man. *J Pharmacokinet Biopharm,* 5**,** 421-33.

RIES, F. & KLASTERSKY, J. 1986. Nephrotoxicity induced by cancer chemotherapy with special emphasis on cisplatin toxicity. *Am J Kidney Dis,* 8**,** 368-79.

RINELLA, M. E., ELIAS, M. S., SMOLAK, R. R., FU, T., BORENSZTAJN, J. & GREEN, R. M. 2008. Mechanisms of hepatic steatosis in mice fed a lipogenic methionine choline-deficient diet. *J Lipid Res,* 49**,** 1068-76.

RINELLA, M. E. & GREEN, R. M. 2004. The methionine-choline deficient dietary model of steatohepatitis does not exhibit insulin resistance. *J Hepatol,* 40**,** 47-51.

RIZKI, G., ARNABOLDI, L., GABRIELLI, B., YAN, J., LEE, G. S., NG, R. K., TURNER, S. M., BADGER, T. M., PITAS, R. E. & MAHER, J. J. 2006. Mice fed a lipogenic methionine-choline-deficient diet develop hypermetabolism coincident with hepatic suppression of SCD-1. *J Lipid Res,* 47**,** 2280-90.

ROBERTS, S. A., PRICE, V. F. & JOLLOW, D. J. 1990. Acetaminophen structure-toxicity studies: in vivo covalent binding of a nonhepatotoxic analog, 3-hydroxyacetanilide. *Toxicol Appl Pharmacol,* 105**,** 195-208.

ROBERTS, S. A. A. J., D.J. 1978. Acetaminophen structure-toxicity relationships: Why is 3-Hydroxyacetanilide not hepatotoxic. *Pharmacologist,* 20.

ROBERTSON, D. G. 2005. Metabonomics in toxicology: a review. *Toxicol Sci,* 85**,** 809-22.

ROBERTSON, D. G., WATKINS, P. B. & REILY, M. D. 2011. Metabolomics in toxicology: preclinical and clinical applications. *Toxicol Sci,* 120 Suppl 1**,** S146-70.

ROBINETTE, S. L., VESELKOV, K. A., BOHUS, E., COEN, M., KEUN, H. C., EBBELS, T. M. D., BECKONERT, O., HOLMES, E. C., LINDON, J. C. & NICHOLSON, J. K. 2009. Cluster Analysis Statistical Spectroscopy Using Nuclear Magnetic Resonance Generated Metabolic Data Sets from Perturbed Biological Systems. *Analytical chemistry,* 81**,** 6581-6589.

ROENIGK, H. H., JR., AUERBACH, R., MAIBACH, H. I. & WEINSTEIN, G. D. 1982. Methotrexate guidelines--revised. *J Am Acad Dermatol,* 6**,** 145-55.

ROLANDO, N., WADE, J., DAVALOS, M., WENDON, J., PHILPOTT-HOWARD, J. & WILLIAMS, R. 2000. The systemic inflammatory response syndrome in acute liver failure. *Hepatology,* 32**,** 734-9.

ROMESTAING, C., PIQUET, M. A., BEDU, E., ROULEAU, V., DAUTRESME, M., HOURMAND-OLLIVIER, I., FILIPPI, C., DUCHAMP, C. & SIBILLE, B. 2007. Long term highly saturated fat diet does not induce NASH in Wistar rats. *Nutr Metab (Lond),* 4**,** 4.

ROMICK-ROSENDALE, L. E., GOODPASTER, A. M., HANWRIGHT, P. J., PATEL, N. B., WHEELER, E. T., CHONA, D. L. & KENNEDY, M. A. 2009. NMR-based metabonomics analysis of mouse urine and fecal extracts following oral treatment with the broad-spectrum antibiotic enrofloxacin (Baytril). *Magn Reson Chem,* 47 Suppl 1**,** S36-46.

ROSENBERG, P., URWITZ, H., JOHANNESSON, A., ROS, A. M., LINDHOLM, J., KINNMAN, N. & HULTCRANTZ, R. 2007. Psoriasis patients with diabetes type 2 are at high risk of developing liver fibrosis during methotrexate treatment. *J Hepatol,* 46**,** 1111-8.

RUBIO, A., GURUCEAGA, E., VAZQUEZ-CHANTADA, M., SANDOVAL, J., MARTINEZ-CRUZ, L. A., SEGURA, V., SEVILLA, J. L., PODHORSKI, A., CORRALES, F. J., TORRES, L., RODRIGUEZ, M., AILLET, F., ARIZ, U., ARRIETA, F. M., CABALLERIA, J., MARTIN-DUCE, A., LU, S. C., MARTINEZ-CHANTAR, M. L. & MATO, J. M. 2007. Identification of a gene-pathway associated with non-alcoholic steatohepatitis. *J Hepatol,* 46**,** 708-18.

RUSSMANN, S., KULLAK-UBLICK, G. A. & GRATTAGLIANO, I. 2009. Current concepts of mechanisms in drug-induced hepatotoxicity. *Curr Med Chem,* 16**,** 3041-53.

RUUD, L. E., WILHELMS, D. B., ESKILSSON, A., VASILACHE, A. M., ELANDER, L., ENGBLOM, D. & BLOMQVIST, A. 2013. Acetaminophen reduces lipopolysaccharide-induced fever by inhibiting cyclooxygenase-2. *Neuropharmacology*.

SAITO, C., LEMASTERS, J. J. & JAESCHKE, H. 2010a. c-Jun N-terminal kinase modulates oxidant stress and peroxynitrite formation independent of inducible nitric oxide synthase in acetaminophen hepatotoxicity. *Toxicol Appl Pharmacol,* 246**,** 8-17.

SAITO, C., ZWINGMANN, C. & JAESCHKE, H. 2010b. Novel mechanisms of protection against acetaminophen hepatotoxicity in mice by glutathione and N-acetylcysteine. *Hepatology,* 51**,** 246-54.

SALMINEN, W. F., JR., VOELLMY, R. & ROBERTS, S. M. 1997. Differential heat shock protein induction by acetaminophen and a nonhepatotoxic regioisomer, 3'-hydroxyacetanilide, in mouse liver. *J Pharmacol Exp Ther,* 282**,** 1533-40.

SANYAL, A. J. & AMERICAN GASTROENTEROLOGICAL, A. 2002. AGA technical review on nonalcoholic fatty liver disease. *Gastroenterology,* 123**,** 1705-25.

SANYAL, A. J., CAMPBELL-SARGENT, C., MIRSHAHI, F., RIZZO, W. B., CONTOS, M. J., STERLING, R. K., LUKETIC, V. A., SHIFFMAN, M. L. & CLORE, J. N. 2001. Nonalcoholic steatohepatitis: association of insulin resistance and mitochondrial abnormalities. *Gastroenterology,* 120**,** 1183-92.

SARIC, J., WANG, Y., LI, J., COEN, M., UTZINGER, J., MARCHESI, J. R., KEISER, J., VESELKOV, K., LINDON, J. C., NICHOLSON, J. K. & HOLMES, E. 2008. Species variation in the fecal metabolome gives insight into differential gastrointestinal function. *J Proteome Res,* 7**,** 352-60.

SARIN, S. K., KUMAR, A., ALMEIDA, J. A., CHAWLA, Y. K., FAN, S. T., GARG, H., DE SILVA, H. J., HAMID, S. S., JALAN, R., KOMOLMIT, P., LAU, G. K., LIU, Q., MADAN, K., MOHAMED, R., NING, Q., RAHMAN, S., RASTOGI, A., RIORDAN, S. M., SAKHUJA, P., SAMUEL, D., SHAH, S., SHARMA, B. C., SHARMA, P., TAKIKAWA, Y., THAPA, B. R., WAI, C. T. & YUEN, M. F. 2009. Acute-on-chronic liver failure: consensus recommendations of the Asian Pacific Association for the study of the liver (APASL). *Hepatol Int,* 3**,** 269-82.

SAVIDES, M. C., OEHME, F. W., NASH, S. L. & LEIPOLD, H. W. 1984. The toxicity and biotransformation of single doses of acetaminophen in dogs and cats. *Toxicol Appl Pharmacol,* 74**,** 26-34.

SAXENA, V., GUPTA, A., NAGANA GOWDA, G. A., SAXENA, R., YACHHA, S. K. & KHETRAPAL, C. L. 2006. 1H NMR spectroscopy for the prediction of therapeutic outcome in patients with fulminant hepatic failure. *NMR Biomed,* 19**,** 521-6.

SCHAFFER, J. E. 2003. Lipotoxicity: when tissues overeat. *Curr Opin Lipidol,* 14**,** 281-7.

SCHNABL, B. & BRENNER, D. A. 2014. Interactions between the intestinal microbiome and liver diseases. *Gastroenterology,* 146**,** 1513-24.

SCHRODER, O. 2003. Low dose methotrexate in inflammatory bowel disease: current status and future directions. *The American Journal of Gastroenterology,* 98**,** 530-537.

SCHULZE-OSTHOFF, K. & BANTEL, H. 2011. Necrosis versus apoptosis in acetaminophen-induced hepatotoxicity. *Hepatology,* 53**,** 1070.

SCHUPPAN, D. & AFDHAL, N. H. 2008. Liver cirrhosis. *Lancet,* 371**,** 838-51.

SELHUB, J., SEYOUM, E., POMFRET, E. A. & ZEISEL, S. H. 1991. Effects of choline deficiency and methotrexate treatment upon liver folate content and distribution. *Cancer Res,* 51**,** 16-21.

SHAH, A. D., WOOD, D. M. & DARGAN, P. I. 2011. Understanding lactic acidosis in paracetamol (acetaminophen) poisoning. *Br J Clin Pharmacol,* 71**,** 20-8.

SHARMA, N. K., DAS, S. K., MONDAL, A. K., HACKNEY, O. G., CHU, W. S., KERN, P. A., RASOULI, N., SPENCER, H. J., YAO-BORENGASSER, A. & ELBEIN, S. C. 2008. Endoplasmic reticulum stress markers are associated with obesity in nondiabetic subjects. *J Clin Endocrinol Metab,* 93**,** 4532-41.

SHOCKCOR, J. P., UNGER, S. E., WILSON, I. D., FOXALL, P. J., NICHOLSON, J. K. & LINDON, J. C. 1996. Combined HPLC, NMR spectroscopy, and ion-trap mass spectrometry with application to the detection and characterization of xenobiotic and endogenous metabolites in human urine. *Anal Chem,* 68**,** 4431-5.

SILK, D. B. 1986. Branched chain amino acids in liver disease: fact or fantasy? *Gut,* 27 Suppl 1**,** 103-10.

SKORPEN, F., ALM, B., SKJELBRED, C., AAS, P. A. & KROKAN, H. E. 1998. Paracetamol increases sensitivity to ultraviolet (UV) irradiation, delays repair of the UNG-gene and recovery of RNA synthesis in HaCaT cells. *Chem Biol Interact,* 110**,** 123-36.

SLOMIANY, B. L., MURTY, V. L. & SLOMIANY, A. 1980. Isolation and characterization of oligosaccharides from rat colonic mucus glycoprotein. *J Biol Chem,* 255**,** 9719-23.

SNEADER, W. 2005. *Drug Discovery: A History,* Chichester, John Wiley & Sons.

SOETERS, P. B. & FISCHER, J. E. 1976. Insulin, glucagon, aminoacid imbalance, and hepatic encephalopathy. *Lancet,* 2**,** 880-2.

SOGA, T., BARAN, R., SUEMATSU, M., UENO, Y., IKEDA, S., SAKURAKAWA, T., KAKAZU, Y., ISHIKAWA, T., ROBERT, M., NISHIOKA, T. & TOMITA, M. 2006. Differential metabolomics reveals ophthalmic acid as an oxidative stress biomarker indicating hepatic glutathione consumption. *J Biol Chem,* 281**,** 16768-76.

SPAGOU, K., WILSON, I. D., MASSON, P., THEODORIDIS, G., RAIKOS, N., COEN, M., HOLMES, E., LINDON, J. C., PLUMB, R. S., NICHOLSON, J. K. & WANT, E. J. 2011. HILIC-UPLC-MS for exploratory urinary metabolic profiling in toxicological studies. *Anal Chem,* 83**,** 382-90.

SPRAUL, M., HOFMANN, M., LINDON, J. C., FARRANT, R. D., SEDDON, M. J., NICHOLSON, J. K. & WILSON, I. D. 1994. Evaluation of liquid chromatography coupled with high-field 1H NMR spectroscopy for drug metabolite detection and characterization: the identification of paracetamol metabolites in urine and bile. *NMR Biomed,* 7**,** 295-303.

SPURWAY, T. D., GARTLAND, K. P., WARRANDER, A., PICKFORD, R., NICHOLSON, J. K. & WILSON, I. D. 1990. Proton nuclear magnetic resonance of urine and bile from paracetamol dosed rats. *J Pharm Biomed Anal,* 8**,** 969-73.

STAMPER, B. D., BAMMLER, T. K., BEYER, R. P., FARIN, F. M. & NELSON, S. D. 2010. Differential regulation of mitogen-activated protein kinase pathways by acetaminophen and its nonhepatotoxic regioisomer 3'-hydroxyacetanilide in TAMH cells. *Toxicol Sci,* 116**,** 164-73.

STRAVITZ, R. T. & KRAMER, D. J. 2009. Management of acute liver failure. *Nat Rev Gastroenterol Hepatol,* 6**,** 542-53.

STREETER, A. J., BJORGE, S. M., AXWORTHY, D. B., NELSON, S. D. & BAILLIE, T. A. 1984. The microsomal metabolism and site of covalent binding to protein of 3'-hydroxyacetanilide, a nonhepatotoxic positional isomer of acetaminophen. *Drug Metab Dispos,* 12**,** 565-76.

SZABO, G. & BALA, S. 2013. MicroRNAs in liver disease. *Nat Rev Gastroenterol Hepatol,* 10**,** 542-52.

SZKUDELSKI, T., OKULICZ, M., BIALIK, I. & SZKUDELSKA, K. 2004. The influence of fasting on liver sulfhydryl groups, glutathione peroxidase and glutathione-S-transferase activities in the rat. *J Physiol Biochem,* 60**,** 1-6.

TABOR, H., ROSENTHAL, S. M. & TABOR, C. W. 1958. The biosynthesis of spermidine and spermine from putrescine and methionine. *J Biol Chem,* 233**,** 907-14.

TANAKA, N., MATSUBARA, T., KRAUSZ, K. W., PATTERSON, A. D. & GONZALEZ, F. J. 2012. Disruption of phospholipid and bile acid homeostasis in mice with nonalcoholic steatohepatitis. *Hepatology,* 56**,** 118-29.

TANG, B., MUSTAFA, A., GUPTA, S., MELNYK, S., JAMES, S. J. & KRUGER, W. D. 2010. Methionine-deficient diet induces post-transcriptional downregulation of cystathionine beta-synthase. *Nutrition,* 26**,** 1170-5.

TATE, S. S. 1980. *Enzymes of mercapturic acid formation,* New york, Academic Press.

TESSARI, P. 2003. Protein metabolism in liver cirrhosis: from albumin to muscle myofibrils. *Curr Opin Clin Nutr Metab Care,* 6**,** 79-85.

THOOLEN, B., MARONPOT, R. R., HARADA, T., NYSKA, A., ROUSSEAUX, C., NOLTE, T., MALARKEY, D. E., KAUFMANN, W., KUTTLER, K., DESCHL, U., NAKAE, D., GREGSON, R., VINLOVE, M. P., BRIX, A. E., SINGH, B., BELPOGGI, F. & WARD, J. M. 2010. Proliferative and nonproliferative lesions of the rat and mouse hepatobiliary system. *Toxicol Pathol,* 38**,** 5S-81S.

THUMMEL, K. E., LEE, C. A., KUNZE, K. L., NELSON, S. D. & SLATTERY, J. T. 1993. Oxidation of acetaminophen to N-acetyl-p-aminobenzoquinone imine by human CYP3A4. *Biochem Pharmacol,* 45**,** 1563-9.

TILG, H. & DIEHL, A. M. 2000. Cytokines in alcoholic and nonalcoholic steatohepatitis. *N Engl J Med,* 343**,** 1467-76.

TIRMENSTEIN, M. A. & NELSON, S. D. 1989. Subcellular binding and effects on calcium homeostasis produced by acetaminophen and a nonhepatotoxic regioisomer, 3'-hydroxyacetanilide, in mouse liver. *J Biol Chem,* 264**,** 9814-9.

TIRMENSTEIN, M. A. & NELSON, S. D. 1990. Acetaminophen-induced oxidation of protein thiols. Contribution of impaired thiol-metabolizing enzymes and the breakdown of adenine nucleotides. *J Biol Chem,* 265**,** 3059-65.

TIRMENSTEIN, M. A. & NELSON, S. D. 1991. Hepatotoxicity after 3'-hydroxyacetanilide administration to buthionine sulfoximine pretreated mice. *Chem Res Toxicol,* 4**,** 214-7.

TOLSTIKOV, V. V. & FIEHN, O. 2002. Analysis of highly polar compounds of plant origin: combination of hydrophilic interaction chromatography and electrospray ion trap mass spectrometry. *Anal Biochem,* 301**,** 298-307.

TOM, A. & NAIR, K. S. 2006. Assessment of branched-chain amino Acid status and potential for biomarkers. *J Nutr,* 136**,** 324S-30S.

TONE, Y., KAWAMATA, K., MURAKAMI, T., HIGASHI, Y. & YATA, N. 1990. Dose-dependent pharmacokinetics and first-pass metabolism of acetaminophen in rats. *J Pharmacobiodyn,* 13**,** 327-35.

TREMAROLI, V. & BACKHED, F. 2012. Functional interactions between the gut microbiota and host metabolism. *Nature,* 489**,** 242-9.

TRYGG, J. & WOLD, S. 2002. Orthogonal projections to latent structures (O-PLS). *Journal of Chemometrics,* 16**,** 119-128.

UCAR, F., YAVUZ TASLIPINAR, M., ALP, B. F., AYDIN, I., AYDIN, F. N., AGILLI, M., TOYGAR, M., OZKAN, E., MACIT, E., OZTOSUN, M., CAYCI, T. & OZCAN, A. 2013. The Effects of N-Acetylcysteine and Ozone Therapy on Oxidative Stress and Inflammation in Acetaminophen-Induced Nephrotoxicity Model. *Ren Fail*.

UETRECHT, J. 2007. Idiosyncratic drug reactions: current understanding. *Annu Rev Pharmacol Toxicol,* 47**,** 513-39.

URBAN, T. J., SHEN, Y., STOLZ, A., CHALASANI, N., FONTANA, R. J., ROCHON, J., GE, D., SHIANNA, K. V., DALY, A. K., LUCENA, M. I., NELSON, M. R., MOLOKHIA, M., AITHAL, G. P., FLORATOS, A.,

PE'ER, I., SERRANO, J., BONKOVSKY, H., DAVERN, T. J., LEE, W. M., NAVARRO, V. J., TALWALKAR, J. A., GOLDSTEIN, D. B., WATKINS, P. B., DRUG-INDUCED LIVER INJURY, N., DILIGEN, EUDRAGENE, SPANISH, D. R. & INTERNATIONAL SERIOUS ADVERSE EVENTS, C. 2012. Limited contribution of common genetic variants to risk for liver injury due to a variety of drugs. *Pharmacogenet Genomics,* 22**,** 784-95.

VALERINO, D. M., JOHNS, D. G., ZAHARKO, D. S. & OLIVERIO, V. T. 1972. Studies of the metabolism of methotrexate by intestinal flora. I. Identification and study of biological properties of the metabolite 4-amino-4-deoxy-N 10 -methylpteroic acid. *Biochem Pharmacol,* 21**,** 821-31.

VAN ROOYEN, D. M., LARTER, C. Z., HAIGH, W. G., YEH, M. M., IOANNOU, G., KUVER, R., LEE, S. P., TEOH, N. C. & FARRELL, G. C. 2011. Hepatic free cholesterol accumulates in obese, diabetic mice and causes nonalcoholic steatohepatitis. *Gastroenterology,* 141**,** 1393-403, 1403 e1-5.

VANCE, J. E. & VANCE, D. E. 1985. The role of phosphatidylcholine biosynthesis in the secretion of lipoproteins from hepatocytes. *Can J Biochem Cell Biol,* 63**,** 870-81.

VIANT, M. R., ROSENBLUM, E. S. & TIEERDEMA, R. S. 2003. NMR-based metabolomics: a powerful approach for characterizing the effects of environmental stressors on organism health. *Environ Sci Technol,* 37**,** 4982-9.

VOLYNETS, V., KUPER, M. A., STRAHL, S., MAIER, I. B., SPRUSS, A., WAGNERBERGER, S., KONIGSRAINER, A., BISCHOFF, S. C. & BERGHEIM, I. 2012. Nutrition, intestinal permeability, and blood ethanol levels are altered in patients with nonalcoholic fatty liver disease (NAFLD). *Dig Dis Sci,* 57**,** 1932-41.

WANG, H. J., ZAKHARI, S. & JUNG, M. K. 2010. Alcohol, inflammation, and gut-liver-brain interactions in tissue damage and disease development. *World J Gastroenterol,* 16**,** 1304-13.

WANG, S. Y., KUO, C. H. & TSENG, Y. J. 2013a. Batch Normalizer: a fast total abundance regression calibration method to simultaneously adjust batch and injection order effects in liquid chromatography/time-of-flight mass spectrometry-based metabolomics data and comparison with current calibration methods. *Anal Chem,* 85**,** 1037-46.

WANG, W., WU, Z., DAI, Z., YANG, Y., WANG, J. & WU, G. 2013b. Glycine metabolism in animals and humans: implications for nutrition and health. *Amino Acids,* 45**,** 463-77.

WANG, X., ZHANG, T., ZHAO, X., GUAN, Z., WANG, Z., ZHU, Z., XIE, Q., WANG, J. & NIU, B. 2014. Quantification of folate metabolites in serum using ultraperformance liquid chromatography tandem mass spectrometry. *J Chromatogr B Analyt Technol Biomed Life Sci,* 962C**,** 9-13.

WANG, X. W., HEEGAARD, N. H. & ORUM, H. 2012. MicroRNAs in liver disease. *Gastroenterology,* 142**,** 1431-43.

WANG, Y. C. & CHIANG, E. P. 2012. Low-dose methotrexate inhibits methionine S-adenosyltransferase in vitro and in vivo. *Mol Med,* 18**,** 423-32.

WANG, Z., CHEN, Z., YANG, S., WANG, Y., YU, L., ZHANG, B., RAO, Z., GAO, J. AND TU, S. 2012. 1H NMR-based metabolomic analysis for identifying serum biomarkers to evaluate methotrexate treatment in patients with early rheumatoid arthritis. *Experimental and Therapeutic medicine,* 4**,** 165-171.

WANG, Z., ZHOU, Q., KRUH, G. D. & GALLO, J. M. 2011. Dose-dependent disposition of methotrexate in Abcc2 and Abcc3 gene knockout murine models. *Drug Metab Dispos,* 39**,** 2155-61.

WANT, E. J., COEN, M., MASSON, P., KEUN, H. C., PEARCE, J. T., REILY, M. D., ROBERTSON, D. G., ROHDE, C. M., HOLMES, E., LINDON, J. C., PLUMB, R. S. & NICHOLSON, J. K. 2010. Ultra performance liquid chromatography-mass spectrometry profiling of bile acid metabolites in biofluids: application to experimental toxicology studies. *Analytical chemistry,* 82**,** 5282-9.

WARNER, T. D., VOJNOVIC, I., GIULIANO, F., JIMENEZ, R., BISHOP-BAILEY, D. & MITCHELL, J. A. 2004. Cyclooxygenases 1, 2, and 3 and the production of prostaglandin I2: investigating the activities of acetaminophen and cyclooxygenase-2-selective inhibitors in rat tissues. *J Pharmacol Exp Ther,* 310**,** 642-7.

WATERS, N. J., WATERFIELD, C. J., FARRANT, R. D., HOLMES, E. & NICHOLSON, J. K. 2005. Metabonomic deconvolution of embedded toxicity: application to thioacetamide hepato- and nephrotoxicity. *Chem Res Toxicol,* 18**,** 639-54.

WATKINS, P. B., SELIGMAN, P. J., PEARS, J. S., AVIGAN, M. I. & SENIOR, J. R. 2008. Using controlled clinical trials to learn more about acute drug-induced liver injury. *Hepatology,* 48**,** 1680-9.

WELTMAN, M. D., FARRELL, G. C. & LIDDLE, C. 1996. Increased hepatocyte CYP2E1 expression in a rat nutritional model of hepatic steatosis with inflammation. *Gastroenterology,* 111**,** 1645-53.

WENDEL, A. & CIKRYT, P. 1981. Binding of paracetamol metabolites to mouse liver glutathione S-transferases. *Res Commun Chem Pathol Pharmacol,* 33**,** 463-73.

WIDEMANN, B. C., SUNG, E., ANDERSON, L., SALZER, W. L., BALIS, F. M., MONITJO, K. S., MCCULLY, C., HAWKINS, M. & ADAMSON, P. C. 2000. Pharmacokinetics and metabolism of the methotrexate metabolite 2, 4-diamino-N(10)-methylpteroic acid. *J Pharmacol Exp Ther,* 294**,** 894-901.

WIEST, R. & GARCIA-TSAO, G. 2005. Bacterial translocation (BT) in cirrhosis. *Hepatology,* 41**,** 422-33.

WIEST, R., LAWSON, M. & GEUKING, M. 2014. Pathological bacterial translocation in liver cirrhosis. *J Hepatol,* 60**,** 197-209.

WILEY, W. C. & MCLAREN, I. H. 1955. Time-of-Flight Mass Spectrometer with Improved Resolution. *Review of Scientific Instruments,* 26.

WILSON, I. D., NICHOLSON, J. K., CASTRO-PEREZ, J., GRANGER, J. H., JOHNSON, K. A., SMITH, B. W. & PLUMB, R. S. 2005. High resolution "ultra performance" liquid chromatography coupled to oa-TOF mass spectrometry as a tool for differential metabolic pathway profiling in functional genomic studies. *J Proteome Res,* 4**,** 591-8.

WINNIKE, J. H., LI, Z., WRIGHT, F. A., MACDONALD, J. M., O'CONNELL, T. M. & WATKINS, P. B. 2010. Use of pharmaco-metabonomics for early prediction of acetaminophen-induced hepatotoxicity in humans. *Clin Pharmacol Ther,* 88**,** 45-51.

WOLD, S., ESBENSEN, K. & GELADI, P. 1987. Principal Component Analysis. *Chemometrics and Intelligent Laboratory Systems,* 2**,** 37-52.

WOOTEN, J. M. 2010. Adverse drug reactions: Part I. *South Med J,* 103**,** 1025-8; quiz 1029.

WRIGHTON, S. A. & STEVENS, J. C. 1992. The human hepatic cytochromes P450 involved in drug metabolism. *Crit Rev Toxicol,* 22**,** 1-21.

WU, Z. W., LU, H. F., WU, J., ZUO, J., CHEN, P., SHENG, J. F., ZHENG, S. S. & LI, L. J. 2012. Assessment of the fecal lactobacilli population in patients with hepatitis B virus-related decompensated cirrhosis and hepatitis B cirrhosis treated with liver transplant. *Microb Ecol,* 63**,** 929-37.

XU, P. & SAUVE, A. A. 2010. Vitamin B3, the nicotinamide adenine dinucleotides and aging. *Mech Ageing Dev,* 131**,** 287-98.

XU, Z. J., FAN, J. G., DING, X. D., QIAO, L. & WANG, G. L. 2010. Characterization of high-fat, diet-induced, non-alcoholic steatohepatitis with fibrosis in rats. *Dig Dis Sci,* 55**,** 931-40.

YAMAGUCHI, M., MIYASHITA, Y., KUMAGAI, Y. & KOJO, S. 2004. Change in liver and plasma ceramides during D-galactosamine-induced acute hepatic injury by LC-MS/MS. *Bioorg Med Chem Lett,* 14**,** 4061-4.

YAMAMOTO, N., OLIVEIRA, M. B., CAMPELLO ADE, P., LOPES, L. C. & KLUPPEL, M. L. 1988. Methotrexate: studies on the cellular metabolism. I. Effect on mitochondrial oxygen uptake and oxidative phosphorylation. *Cell Biochem Funct,* 6**,** 61-6.

YAMAMOTO, N. S., ISHII-IWAMOTO, E. L. & BRACHT, A. 1992. Activation of glycogenolysis by methotrexate. Influence of calcium and inhibitors of hormone action. *Biochem Pharmacol,* 44**,** 761-7.

YAMAMOTO, Y., YAMASHITA, S., FUJISAWA, A., KOKURA, S. & YOSHIKAWA, T. 1998. Oxidative stress in patients with hepatitis, cirrhosis, and hepatoma evaluated by plasma antioxidants. *Biochem Biophys Res Commun,* 247**,** 166-70.

YAMAZAKI, M., MIYAKE, M., SATO, H., MASUTOMI, N., TSUTSUI, N., ADAM, K. P., ALEXANDER, D. C., LAWTON, K. A., MILBURN, M. V., RYALS, J. A., WULFF, J. E. & GUO, L. 2013. Perturbation of

bile acid homeostasis is an early pathogenesis event of drug induced liver injury in rats. *Toxicol Appl Pharmacol,* 268**,** 79-89.

YAO, Z. M. & VANCE, D. E. 1988. The active synthesis of phosphatidylcholine is required for very low density lipoprotein secretion from rat hepatocytes. *J Biol Chem,* 263**,** 2998-3004.

YAPAR, K., KART, A., KARAPEHLIVAN, M., ATAKISI, O., TUNCA, R., ERGINSOY, S. & CITIL, M. 2007. Hepatoprotective effect of L-carnitine against acute acetaminophen toxicity in mice. *Exp Toxicol Pathol,* 59**,** 121-8.

YOSHIHIKO, T., NISHIUMI, S., MINAMI, A., KAWANO, Y., HOSHI, N., AZUMA, T. & YOSHIDA, M. 2014. Metabolomics-based search for therapeutic agents for non-alcoholic steatohepatitis. *Arch Biochem Biophys*.

YOUNES, M., CORNELIUS, S. & SIEGERS, C. P. 1986. Ferrous ion supported in vivo lipid peroxidation induced by paracetamol--its relation to hepatotoxicity. *Res Commun Chem Pathol Pharmacol,* 51**,** 89-99.

YOUNOSSI, Z. M., BARANOVA, A., ZIEGLER, K., DEL GIACCO, L., SCHLAUCH, K., BORN, T. L., ELARINY, H., GORRETA, F., VANMETER, A., YOUNOSZAI, A., ONG, J. P., GOODMAN, Z. & CHANDHOKE, V. 2005. A genomic and proteomic study of the spectrum of nonalcoholic fatty liver disease. *Hepatology,* 42**,** 665-74.

ZBOROWSKA-SLUIS, D. T. & DOSSETOR, J. B. 1967. Hyperlactatemia of hyperventilation. *J Appl Physiol,* 22**,** 746-55.

ZEISEL, S. H. 2004. Nutritional importance of choline for brain development. *J Am Coll Nutr,* 23**,** 621S-626S.

ZEISEL, S. H. & BLUSZTAJN, J. K. 1994. Choline and human nutrition. *Annu Rev Nutr,* 14**,** 269-96.

ZHANG, H., DIBAISE, J. K., ZUCCOLO, A., KUDRNA, D., BRAIDOTTI, M., YU, Y., PARAMESWARAN, P., CROWELL, M. D., WING, R., RITTMANN, B. E. & KRAJMALNIK-BROWN, R. 2009. Human gut microbiota in obesity and after gastric bypass. *Proc Natl Acad Sci U S A,* 106**,** 2365-70.

ZHU, L., BAKER, S. S., GILL, C., LIU, W., ALKHOURI, R., BAKER, R. D. & GILL, S. R. 2013. Characterization of gut microbiomes in nonalcoholic steatohepatitis (NASH) patients: a connection between endogenous alcohol and NASH. *Hepatology,* 57**,** 601-9.

ZWINGMANN, C. & BILODEAU, M. 2006. Metabolic insights into the hepatoprotective role of N-acetylcysteine in mouse liver. *Hepatology,* 43**,** 454-63.

Chapter 8: Appendix

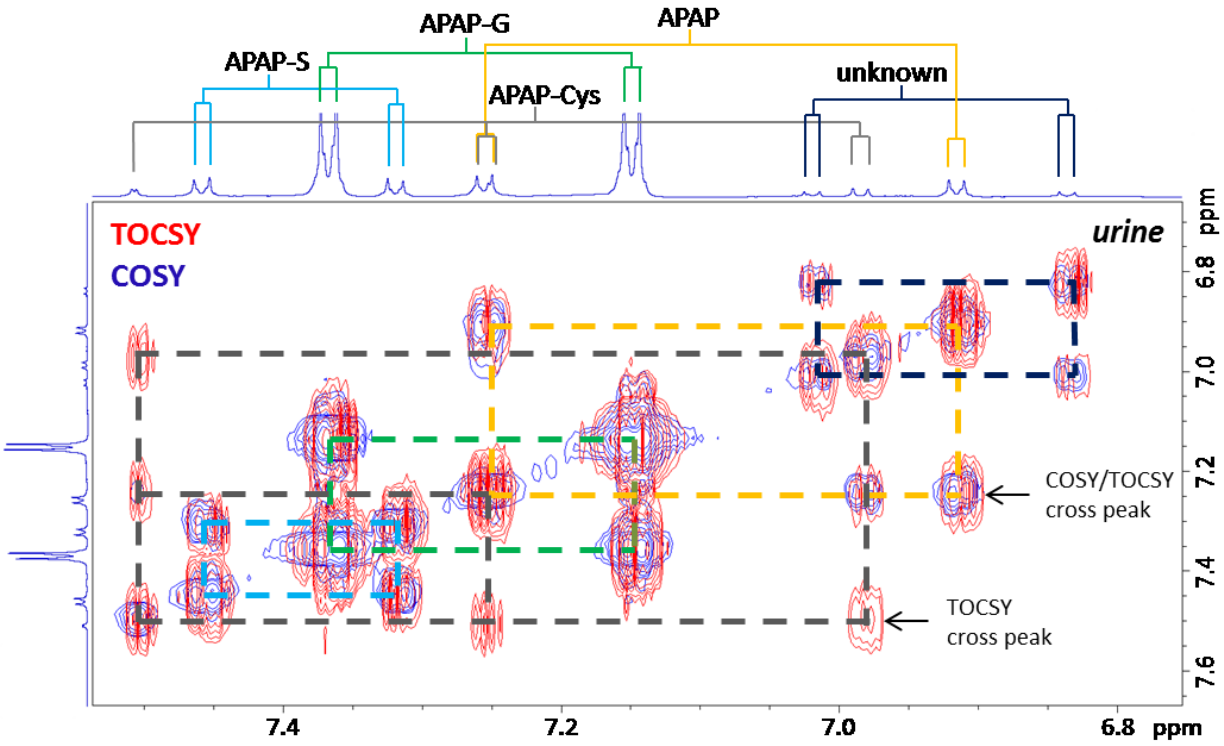


Figure 8.1: TOCSY and COSY of urine spectra post-APAP administration. The TOCSY and COSY spectra are superimposed. The dotted lines reveal the correlated peaks, while the assignments of the metabolites can be seen in the 1D spectrum at the top. APAP-G – APAP glucuronide conjugate; APAP-S – APAP sulphate conjugate; APAP-Cys – APAP cysteinyl conjugate;

		Chapter 3			**Chapter 4 & 5**			**Chapter 6**
		Sample matrix						
	NMR parameters	**Liver**	**Urine**	**Serum**	**Liver**	**Urine**	**Faeces**	**Serum**
standard 1D solvent suppression pulse sequence	Scans	256	256	158	64	320	128	128
	Spectral width (kHz)	12	12	12	12	12	12	12
	Data-points (k)	64	64	64	64	64	64	74
	Acquisition time (s)	4.56	4.56	2.72	2.72	2.72	3.06	3.06
	Relaxation delay (s)	4.0	4.00	2.00	4.00	4.00	4.00	4.00
	Mixing time (ms)	100	100	100	100	100	100	100
	Line broadening (Hz)	0.3						
	Temperature (K)	300						310
CPMG	Scans			158	384		128	128
	Spectral width (kHz)			12	12		12	12
	Data-points (k)			64	64		74	74
	Acquisition time (s)			2.72	2.72		3.06	3.06
	Relaxation delay (µs)			2.00	4.00		4.00	4.00
	CPMG delay (µs)			160	400		300	300
	Number of loops			200	300		128	128
	Line broadening (Hz)	0.3						
	Temperature (K)	300						310

Table 8.1: Summary of ^{1}H-NMR experiment acquisition parameters. Please note that all experiments were performed at a frequency of 600 MHz.

^{1}H shift (δ)	multiplicity	molecule	Sample matrix	Method of ID
0.93	t	isoleucine	urine, liver, serum, faeces	literature[1]
0.95	d	leucine	urine, liver, **serum**, faeces	spike-in
0.97	d	leucine	urine, liver, **serum**, faeces	spike-in
0.97	d	valine	**urine**, liver, serum, faeces	spike-in
1.00	d	isoleucine	urine, liver, serum, faeces	literature[1]
1.02	d	valine	**urine**, liver, serum, faeces	spike-in
1.06	t	propionate	**faeces**	spike-in
1.13	d	isobutyrate	serum	literature[1]
1.19	t	ethanol	urine	software
1.20	d	3-hydroxybutyrate	urine, serum, liver	literature[1]
1.21	d	fucose	**urine**, serum, faeces	spike-in
1.25	d	fucose	**urine**, serum, faeces	spike-in
1.29	s	3-hydroxyisovalerate	**urine**	spike-in
1.32	d	threonine	urine, liver, serum	literature[1]
1.33	d	lactate	urine, liver, serum, faeces	literature[1]
1.36	s	2-hydroxyisobutyrate	**urine**	spike-in
1.48	d	alanine	urine, liver, serum, faeces	literature[1]
1.48	m	lysine	**urine**, serum, faeces	spike-in
1.66	m	5-aminovalerate	**faeces**	spike-in
1.75	m	lysine	**urine**, serum, faeces	spike-in
1.78	m	putrescine	**urine**, faeces	spike-in
1.91	m	lysine	**urine**, serum, faeces	spike-in
1.92	s	acetate	urine, liver, serum, faeces	literature[1]
2.00	m	glutamate	urine, liver, serum, faeces	literature[1]
2.00	m	proline	**serum**	spike-in
2.01	s	glycoprotein	serum	literature[1]
2.07	m	proline	**serum**	spike-in
2.08	m	glutamine	urine, serum, liver, faeces	literature[1]
2.13	s	methionine	**serum**, faeces	spike-in
2.15	m	glutamate	urine, liver, serum, faeces	iterature[1]
2.17	m	reduced glutathione	**liver**	spike-in
2.19	q	propionate	**faeces**	spike-in
2.23	t	2-aminoadipate	**urine, faeces**	spike-in
2.24	t	5-aminovalerate	**faeces**	spike-in
2.31	m	3-hydroxybutyrate	urine, serum, liver	literature[1]
2.35	m	proline	**serum**	spike-in
2.36	m	glutamate	urine, liver, serum, faeces	literature[1]
2.37	s	pyruvate	serum	literature[1]
2.38	m	3-hydroxybutyrate	urine, serum, liver	literature[1]
2.39	s	3-hydroxyisovalerate	**urine**	spike-in
2.40	s	succinate	urine, **liver**, serum, faeces	spike-in
2.41	m	glutamine	urine, serum, liver, faeces	literature[1]
2.52	d	citrate	urine, liver, serum, faeces	literature[1]/software
2.54	s	methylamine	**urine**, liver	spike-in
2.54	m	oxidized glutathione	liver	database
2.56	m	reduced glutathione	**liver**	spike-in
2.65	t	methionine	**serum**, faeces	spike-in
2.69	d	citrate	urine, liver, serum, faeces	literature[1]/software
2.71	s	sarcosine	urine, **faeces**	spike-in

^{1}H shift (δ)	multiplicity	molecule	Sample matrix	Method of ID
2.72	d	dimethylamine	**urine**, **liver**	spike-in
2.83	s	trimethylamine	**urine**	spike-in
2.97	dd	reduced glutathione	**liver**	spike-in
2.98	m	oxidized glutathione	liver	database
3.01	t	5-aminovalerate	**faeces**	spike-in
3.04	s	creatine	**urine**, liver, serum, faeces	spike-in
3.05	s	creatinine	**urine**, serum	spike-in
3.05	t	lysine	**urine**, serum, faeces	spike-in
3.06	t	putrescine	**urine**, faeces	spike-in
3.13	dd	phenylalanine	liver, **serum**	spike-in
3.21	s	choline	**liver**, serum, faeces	spike-in
3.22	s	phosphocholine	**liver**, serum, faeces	spike-in
3.23	s	G-phosphocholine	liver, serum, faeces	software
3.24	dd	β-glucose	urine, liver, serum, faeces	literature[1]/software
3.25	t	taurine	**urine**	spike-in
3.25	s	betaine	serum	software/database
3.26	s	TMAO	**urine**, liver	spike-in
3.29	dd	maltose	**liver**	spike-in
3.32	dd	oxidized glutathione	liver	database
3.35	m	proline	**serum**	spike-in
3.36	s	methanol	urine, liver, **serum**, faeces	literature[1]/software
3.40	t	β-glucose	urine, liver, serum, faeces	literature[1]/software
3.41	t	taurine	**urine**	spike-in
3.42	t	α-glucose	urine, liver, serum, faeces	literature[1]/software
3.45	m	proline	**serum**	spike-in
3.47	ddd	β-glucose	urine, liver, serum, faeces	literature[1]/software
3.48	t	β-glucose	urine, liver, serum, faeces	literature[1]/software
3.54	dd	α-glucose	urine, liver, serum, faeces	literature[1]/software
3.56	s	glycine	**liver**, **serum**, faeces	spike-in
3.57	m	fructose	**faeces**	spike-in
3.59	s	sarcosine	urine, **faeces**	spike-in
3.61	d	threonine	urine, liver, serum	literature[1]
3.65	q	ethanol	urine	software
3.69	s	phenylacetylglycine	**urine**	spike-in
3.70	m	fructose	**faeces**	spike-in
3.71	t	α-glucose	urine, liver, serum, faeces	literature[1]/software
3.72	dd	α-glucose	urine, liver, serum, faeces	literature[1]/software
3.75	m	phenylacetylglycine	**urine**	spike-in
3.76	m	α-glucose	urine, liver, serum, faeces	literature[1]/software
3.78	m	glutathione	**liver**	spike-in
3.79	s	guanidinoacetate	**urine**	spike-in
3.81	m	fructose	**faeces**	spike-in
3.86	ddd	α-glucose	urine, liver, serum, faeces	literature[1]/software
3.87	m	α-glucose	urine, liver, serum, faeces	literature[1]/software
3.90	s	betaine	serum	software/database
3.90	dd	β-glucose	urine, liver, serum, faeces	literature[1]/software
3.90	dd	fructose	**faeces**	spike-in
3.94	s	creatine	**urine**	spike-in
4.01	m	fructose	**faeces**	spike-in

^{1}H shift (δ)	multiplicity	molecule	Sample matrix	Method of ID
4.01	dd	AMP	**liver**	spike-in
4.02	dd	fructose	**faeces**	spike-in
4.02	s	creatinine	**urine**, serum	spike-in
4.11	q	lactate	urine, liver, serum, faeces	literature[1]/software
4.11	dd	glucosan	**urine**, liver	spike-in
4.12	m	proline	**serum**	spike-in
4.12	m	fructose	**faeces**	spike-in
4.14	m	formiminoglutamate	liver, urine	database
4.25	t	uridine	**liver**	spike-in
4.26	m	threonine	liver, serum	literature[1]/software
4.29	m	inosine	**liver**	spike-in
4.34	s	tartrate	**urine**, liver, serum, faeces	spike-in
4.37	t	uridine	**liver**	spike-in
4.37	m	AMP	**liver**	spike-in
4.41	s	1,3-Dihydroxyacetone	faeces	software
4.45	dd	inosine	**liver**	spike-in
4.51	dd	AMP	**liver**	spike-in
4.56	m	reduced glutathione	**liver**	spike-in
4.64	d	β-glucose	urine, liver, serum, faeces	literature[1]/software
4.64	m	glucosan	**urine**, liver	spike-in
4.67	d	maltose	**liver**	spike-in
5.19	d	mannose	**liver**	spike-in
5.23	d	α-glucose	urine, liver, serum, faeces	literature[1]/software
5.23	d	maltose	**liver**	spike-in
5.41	d	maltose	**liver**	spike-in
5.42	m	glycogen	liver	software
5.47	s	glucosan	**urine**, liver	spike-in
5.79	s	urea	urine	software
5.89	d	uracil	urine, **liver**, faeces	spike-in
5.90	d	uridine	**liver**	spike-in
5.93	d	uridine	**liver**	spike-in
6.11	d	inosine	**liver**	spike-in
6.15	d	AMP	**liver**	spike-in
6.39	d	urocanate	urine, liver, faeces	literature[2]/software
6.53	s	fumarate	urine, liver, serum, faeces	software
6.94	d	tyrosine	urine, liver, serum, faeces	literature[1]/software
7.08	s	histidine	liver, **serum**	spike-n
7.19	d	tyrosine	urine, liver, serum, faeces	literature[1]/software
7.20	ddd	3-indoxylsulphate	**urine**	spike-in
7.28	ddd	3-indoxylsulphate	**urine**	spike-in
7.34	m	phenylalanine	liver, **serum**, faeces	spike-in
7.36	s	3-indoxylsulphate	**urine**	spike-in
7.37	m	phenylacetylglycine	**urine**	spike-in
7.38	m	phenylalanine	liver, **serum**, faeces	spike-in
7.42	m	phenylacetylglycine	**urine**	spike-in
7.44	m	phenylalanine	liver, **serum**, faeces	spike-in
7.50	d	3-indoxylsulphate	**urine**	spike-in
7.56	t	hippurate	urine	software
7.60	d	uracil	urine, **liver**, faeces	spike-in

^{1}H shift (δ)	multiplicity	molecule	Sample matrix	Method of ID
7.61	dd	niacinamide	liver	software/database
7.65	t	hippurate	urine	software
7.70	d	3-indoxylsulphate	**urine**	spike-in
7.79	s	histidine	liver, **serum**	spike-in
7.80	s	formiminoglutamate	liver, urine	database
7.84	s	formiminoglutamate	liver, urine	database
7.84	d	hippurate	urine	software
7.89	d	uridine	**liver**	spike-in
8.02	s	phenylacetylglycine	**urine**	spike-in
8.20	t	1-methylnicotinamide	urine	software/database
8.21	s	hypoxanthine	urine, **liver**, faeces	spike-in
8.22	s	hypoxanthine	urine, **liver**, faeces	spike-in
8.25	s	inosine	**liver**	spike-in
8.26	dd	niacinamide	liver	software/database
8.27	s	AMP	**liver**	spike-in
8.36	s	inosine	**liver**	spike-in
8.45	s	formate	urine, liver, serum, faeces	literature[1]/software
8.61	s	AMP	**liver**	spike-in
8.72	dd	niacinamide	liver	software/database
8.90	d	1-methylnicotinamide	urine	software/database
8.95	s	niacinamide	liver	software/database
8.97	d	1-methylnicotinamide	urine	software/database
9.28	s	1-methylnicotinamide	urine	software/database

Table 8.2: The assigned compounds from the ^{1}H-NMR spectra in all sample matrices, excluding APAP, AMAP and methotrexate resonances, are listed above. Bold letters reveal the sample matrix in which the spike-in experiment of the compound was performed. Please note that serum refers to both plasma and serum. The database used was the human metabolome database (www.hmdb.ca). The software used for Chenomx NMR Suite by Chenomx. AMP – adenosine monophosphate. TMAO – trimethylamine-*N*-oxide. s – singlet; d – doublet; ss – split singlet; d – double doublet; ddd – double double doublet; t- triplet; m – multiplet; ppm – parts per million.

literature[1] – Nicholson, J.K. and Foxall, P.J.D. (1995) 750 MHz ^{1}H and ^{1}H-^{13}C NMR Spectroscopy of Human Blood Plasma. *Analytical Chemistry*

literature[2] – Saric, J., Wang, Y., Li, J. et al. (2007) Species Variation in the Fecal Metabolome Gives Insight into Differential Gastrointestinal Function. *Journal of proteome research*

Diet	Comparison	R^2Y	Q^2Y	Statistical significance
Control	0 vs 12 hours	0.9879	0.7963	$p < 0.05$
	0 vs 24 hours	0.9968	0.7222	$p < 0.05$
	0 vs 48 hours	0.8863	0.6925	$p < 0.05$
MCD diet	0 vs 12 hours	0.9371	0.6008	$p > 0.05$
	0 vs 24 hours	0.9508	0.7566	$p < 0.05$
	0 vs 48 hours	0.9469	0.8012	$p < 0.05$

Table 8.3: Summary of O-PLS-DA model parameters derived from the comparison of the metabolic profiles post MTX administration (100 mg/kg) at 12 hours, 24 hours and 48 hours, relative to the pre-dose baseline (0 hour) in both diets.

Publication

Systems level metabolic phenotype of methotrexate administration in the context of non-alcoholic steatohepatitis in the rat

Michael Kyriakides[*,¶], Rhiannon N. Hardwick[†,||], Zhaosheng Jin[‡,|||], Michael J. Goedken[§,||||], Elaine Holmes[*,#], Nathan J. Cherrington[†,**] and Muireann Coen[*,††]

* Biomolecular Medicine, Division of Computational Systems Medicine, Department of Surgery and Cancer, Imperial College London, London, SW7 2AZ, UK

† Department of Pharmacology and Toxicology, University of Arizona, Tucson, Arizona, AZ 85721, USA

‡ Faculty of Medicine, Imperial College London, London, SW7 2AZ, UK

§ Department of Pharmacology and Toxicology, Rutgers University, Piscataway, New Jersey, NJ 08854, USA

¶ michael.kyriakides07@imperial.ac.uk

|| rhardwic@email.unc.edu

||| zhaosheng.jin08@imperial.ac.uk

|||| michael.goedken@gmail.com

elaine.holmes@imperial.ac.uk

** cherrington@pharmacy.arizona.edu

†† m.coen@imperial.ac.uk

Corresponding author

Dr Muireann Coen

Computational and Systems Medicine

Department of Surgery and Cancer

Faculty of Medicine

Imperial College London

SW7 2AZ

m.coen@imperial.ac.uk

+44 207 594 1179

Running title: Metabolic phenotype of methotrexate and NASH

Abstract

Adverse drug reactions (ADRs) represent a significant clinical challenge with respect to patient morbidity and mortality. We investigated the hepatotoxicity and systems level metabolic phenotype of methotrexate (MTX) in the context of a prevalent liver disease; non-alcoholic steatohepatitis (NASH). An NMR spectroscopic based metabonomic approach was employed to analyze the metabolic consequences of MTX (0, 10, 40, 100 mg/kg) in urine and liver of healthy rats (control diet) and in a model of NASH (methionine-choline deficient diet).

Histopathological analysis confirmed baseline (0 mg/kg) liver necrosis, liver inflammation and lipid accumulation in the NASH model. Administration of MTX (40 and 100 mg/kg) led to liver necrosis in the control cohort, whilst the NASH cohort also displayed biliary hyperplasia and liver fibrosis (100 mg/kg), providing evidence of the synergistic effect of MTX and NASH. The complementary hepatic and urinary metabolic phenotypes of the NASH model, at baseline, revealed perturbation of multiple metabolites associated with oxidative and energetic stress, and folate homeostasis. Administration of MTX in both diet cohorts showed dose-dependent metabolic consequences affecting gut microbial, energy, nucleobase, nucleoside and folate metabolism. Furthermore, a unique panel of metabolic changes reflective of the synergistic effect of MTX and NASH were identified, including the elevation of hepatic phenylalanine, urocanate, acetate and both urinary and hepatic formiminoglutamic acid. This systems level metabonomic analysis of the hepatotoxicity of MTX in the context of NASH provided novel mechanistic insight of potential wider clinical relevance for further understanding the role of liver pathology as a risk factor for ADRs.

Keywords

Methionine-choline deficient diet, Liver toxicity, Methotrexate, Metabonomics, Nuclear Magnetic Resonance spectroscopy, Non-alcoholic steatohepatitis

Introduction

Adverse drug reactions (ADRs) are estimated to be responsible for approximately 7 % of hospital admissions in the USA and UK (Lazarou et al., 1998; Pirmohamed et al., 2004). Methotrexate (MTX), a folate analogue originally designed to inhibit dihydrofolate reductase for leukaemia treatment (Farber et al., 1956), can cause ADRs including nephrotoxicity and hepatotoxicity (West, 1997; Widemann and Adamson, 2006). The risk of MTX-induced hepatotoxicity has been shown to increase in the presence of conditions such as diabetes mellitus or non-alcoholic steatohepatitis, with MTX alone also reported to cause a NASH-like injury (Langman et al., 2001; Rosenberg et al., 2007).

NASH is an advanced form of non-alcoholic fatty liver disease characterized by inflammation, macrovesicular steatosis, oxidative stress and insulin resistance (Brunt, 2004). It is estimated to affect approximately 12 % of USA adults, and approximately 20 % of NASH sufferers develop liver cirrhosis (Williams et al., 2011). The development of NASH is believed to involve a first hit, which is the result of imbalanced fat metabolism, and a second hit that involves metabolic and oxidative stress (Day and James, 1998). NASH has also been shown to influence hepatic drug metabolism by affecting CYP 450 enzyme activity (Fisher et al., 2009) and ATP-binding cassette transporters (Hardwick et al., 2011) and could therefore increase the risk of ADR occurrence.

NASH is modelled in-vivo using several methods that include the use of specific diets or genetic models (Larter and Yeh, 2008). The methionine-choline deficient (MCD) diet has been widely employed to model NASH as it leads to a condition characterized by steatosis, mitochondrial dysfunction, inflammation and oxidative stress (Rinella et al., 2008; Rizki et al., 2006). Moreover, increased CYP 2E1 expression (Leclercq et al., 2000) and down-regulation of stearoyl-CoA desaturase-1 (SCD-1) (Rizki, et al., 2006) have also been reported, all of which reflect the clinical NASH phenotype. However, the MCD model fails to recapitulate the metabolic syndrome component of NASH as it does not induce obesity, insulin resistance or hyperglycaemia (Larter and Yeh, 2008).

Metabonomics is a top-down untargeted systems approach that has been widely applied to characterize metabolic profiles of biofluids or tissues in disease states or in response to toxic interventions (Nicholson et al., 1999). Metabonomic analysis typically relies on nuclear magnetic resonance (NMR) spectroscopy and mass spectrometry to generate high-resolution metabolic profiles. Statistical pattern recognition tools including principal components analysis (PCA) and orthogonal partial least squares discriminant analysis (O-PLS-DA) are applied to model the multivariate data (Fonville et al., 2010). Metabonomics has been previously employed to investigate the serum metabolic effects of MTX in rheumatoid arthritis patients, where endogenous metabolic markers capable of predicting response to MTX treatment were identified, which included amino acids, taurine and uracil (Wang et al., 2012). It has also been applied to characterize the clinical NASH lipidomic plasma signature (Puri et al., 2009), together with the serum metabolic phenotype of the MCD model of NASH in mice (Tanaka et al., 2012), which found disruption of phospholipid and bile acid homeostasis.

In the present study we employed a metabonomic approach to investigate the dose and time-dependent systemic endogenous and xenobiotic metabolic phenotype of MTX in the urine and liver of healthy animals and in the context of NASH, as modelled by the MCD diet.

Materials and Methods

Animal Husbandry and MTX administration

This study was approved by the Institutional Animal Care and Use Committee (IACUC) at the University of Arizona, and is in accordance with NIH guidelines for the care and use of experimental animals. Male Sprague-Dawley rats (weighing 200-250 g prior to induction of NASH, ca. 8-weeks old, *n* = 44, Harlan Laboratories; Indianapolis, IN) were rats were split randomly into two groups (*n* = 22), which were either fed ad libitum a choline sufficient and amino-acid defined diet or the equivalent methionine-choline deficient diet (Dyets Inc; Bethlehem, PA), and tap water, for a period of 8 weeks. The rats were acclimated to 12-hour light and dark cycles in an AAALAC-accredited animal facility for one week prior to the initiation of experiments. The rats in each diet group were then randomly assigned to be administered 10, 40 and 100 mg/kg of MTX dissolved in 0.3 M sodium bicarbonate (Toronto Chemicals; Toronto, Canada) or vehicle (0.3 M sodium bicarbonate) via a single intra-peritoneal injection.

Sample collection

Urine samples were collected at 0 hours (pre-dose, -6 to 0 hour collection; 0hr) and across the following time periods 6-12 (12hr), 18-24 (24hr) and 36-48 (48hr) hours post-dose via metabolism cages into 50 mL tubes on ice containing sodium azide (1 mL, 1% w/v in water). At each time-point the urine was transferred to a clean 50 mL conical tube and immediately

stored at -80 °C. At 96 hours post-dose (96hr), animals were euthanized via CO2 asphyxiation and livers were immediately snap-frozen in liquid nitrogen and stored at -80 °C until analysis.

Liver histopathology and imaging

Liver tissue for histomorphologic examination was taken from the medial lobe of each animal, fixed in 10% neutral-buffered formalin for 24 hours then placed in 70% ethanol until paraffin embedding and hematoxylin and eosin (H&E) staining. Masson Trichrome staining was also performed using the Masson Trichrome Kit from Sigma-Aldrich (St. Louis, MO) per manufacturer's instructions. All slides were imaged with a Leica DM4000B microscope, DFC450 camera, and Leica Application Suite software (Leica Microsystems, Wetzlar, Germany). Sections were examined by light microscopy by a board certified blinded veterinary pathologist (Burkhardt et al., 2011). Liver necrosis, inflammation, fibrosis, lipid accumulation and biliary hyperplasia were scored. The scoring criteria were as follows: 0 (no lesion), 1 (<10% lesion; minimal), 2 (10-25 % lesion; mild), 3 (25-40 % lesion; moderate), 4 (40-50 % lesion; marked) and 5 (>50 % lesion; severe). Representative histology images were acquired with a Leica DM4000B microscope, DFC450 camera, and Leica Application Suite software (Leica Microsystems; Wetzlar, Germany).

Sample preparation and ^{1}H-NMR spectroscopy of hepatic aqueous-soluble extracts

Liver metabolite extraction and ^{1}H-NMR spectroscopy of the hepatic aqueous-soluble extracts was performed as previously described (Beckonert et al., 2007). Briefly, liver tissue samples (mean 52.5 mg, STD ± 0.73) were added to acetonitrile/water (1.5 mL, 1:1). The samples were homogenized with zirconia beads in a homogenizer (Qiagen Tissue Lyser, Retsch GmBH, Haan, Germany) at 6500 Hz for two 45 seconds periods, with an intermediate 5 minute cooling

period on dry ice. The samples were then kept on ice for 45 minutes prior to centrifugation at 17,000 g for 15 minutes at 4 oC. The supernatants were concentrated and dried overnight in a centrifugal evaporator (SpeedVac, Thermoscientific, Waltham, Massachusetts, United States) at room temperature. The dried supernatants were reconstituted in phosphate buffer (600 µL of a 0.2 M solution) containing 100% D2O, sodium azide (NaN3, 3 mM) and 3-(trimethylsilyl)-[2,2,3,3-2H4]-propionic acid sodium salt (TSP; 1mM)), vortexed for 30 seconds and then centrifuged at 17,000 g for 15 minutes at 4 oC. The supernatants (550 µL) were transferred to 5 mm NMR tubes (NMR Precision tube 507-HP-7, Norell, Landisville, New Jersey, United States). NMR spectral data were acquired on a Bruker Avance-600 spectrometer (Bruker Biopsin, Rheinstetten, Germany) operating at 600.13 MHz (14.1 T) 1H frequency and at a temperature of 300 K, using a Bruker TXI probe and an automated sample handling carousel (Bruker). A standard one-dimensional solvent suppression pulse sequence was used to acquire the FID (relaxation delay - 90° pulse- 4 µs delay - 90° pulse - mixing time - 90° pulse - acquire FID) (Beckonert, et al., 2007). For each experiment, 64 transients were collected into 64k data points using a spectral width of 12 000 Hz, with a relaxation delay of 4 seconds, an acquisition time of 2.7 seconds and a mixing time of 100 ms. A Carr-Purcell-Meiboom-Gill (CPMG) spin-echo pulse sequence, with a fixed spin-spin relaxation delay 2nτ of 240 ms (n = 300, τ = 400 µs), was also used to acquire the FID (relaxation delay - 90° pulse - (t - 180° - t)n – acquire FID).(Beckonert, et al., 2007) The CPMG pulse sequence is used to attenuate signals from large macromolecules such as lipids and proteins. 384 transients were collected into 64k data points using a spectral width of 12 000 Hz, with a relaxation delay of 4 seconds and an acquisition time of 2.7 seconds. The D2O present in the buffer provided a field frequency lock, whilst TSP served as the chemical shift reference. A line-broadening factor of 0.3 Hz was applied to all spectra prior to Fourier Transformation (FT).

^{1}H-NMR spectroscopy of urine

^{1}H-NMR spectroscopy of urine was performed as previously described (Beckonert, et al., 2007). Briefly, urine was mixed with phosphate buffer (2:1; 600 µL total volume; 0.2 M as above) and vortexed for 1 minute. The samples were then centrifuged at 17,000 g for 15 minutes at 4 oC. The resulting supernatants (550 µL) were then transferred to 5 mm NMR tubes (507-HP-7). NMR spectral data were acquired on a Bruker Avance-600 spectrometer operating at 600.13 MHz (14.1 T) 1H frequency and at a temperature of 300 K using a Bruker TXI probe and an automated sample handling carousel (Bruker). A standard one-dimensional solvent suppression pulse sequence was used to acquire the FID as described above. For each experiment, 320 transients were collected into 64k data points using a spectral width of 12 000 Hz, with a relaxation delay of 4 seconds, an acquisition time of 2.7 seconds and mixing time of 100 ms. A line-broadening factor of 0.3 Hz was applied to all spectra prior to FT.

The NMR spectra were initially processed using TopSpin 3.0 NMR software (Bruker), where they were manually phased, baseline adjusted and referenced to the TSP resonance at 0 ppm. Full-resolution NMR data were imported into MATLAB (R2012, Mathworks Inc, Natick, Massachusetts, United States), using an in-house script, for further processing. This included the removal of the TSP, MTX related and water resonances in the hepatic aqueous-soluble component spectra and the TSP, MTX related, urea and water resonances from the urine spectra. Probabilistic quotient normalization and spectral alignment were performed in each diet cohort dataset separately, apart from when performing the diet baseline comparison (using an in-house script developed by Dr. Kirill Veselkov) (Dieterle et al., 2006). Spectral assignments were performed using Statistical TOtal Correlation Spectroscopy (STOCSY) (Cloarec et al., 2005), spectral databases (in-house, Human Metabolome Database and

Biological Magnetic Resonance Bank), Chenomx NMR Suite (Chenomx, Edmonton, Alberta, Canada) and previously published assignments (Nicholson et al., 1995; Waters et al., 2005). The assignments of uracil, hypoxanthine, inosine, uridine, maltose, mannose, choline, phosphocholine and glycine in the hepatic aqueous-soluble extracts and dimethylamine, methylamine, phenylacetylglycine, putrescine, 3-indoxylsulphate, tartrate, glucosan and taurine in the urine were confirmed by addition of the pure standard compounds. Please note that glutathione refers to total glutathione (sum of oxidized and reduced glutathione). The CPMG spectra of the hepatic aqueous-soluble extracts were acquired and modelled in order to minimize the contribution from lipids that arose from the MCD diet cohort.

The urinary excretion of MTX following administration of 100 mg/kg in both diet cohorts was calculated by performing local baseline correction prior to integration of the MTX resonance at 8.63 ppm in TopSpin. The integral of TSP (which was of known concentration) and the excreted urine volumes per rat at each time-point were used to calculate the urinary amount of MTX (in micrograms). The results were verified independently by mass spectrometry ($R > 0.99$).

Statistical analysis

Multivariate statistical tools were employed to analyze the 1H-NMR data from both the urine and hepatic extracts. PCA was initially applied to investigate the baseline diet comparison and the effect of MTX by characterizing the inherent clustering of the data and the presence of potential outliers (Fonville, et al., 2010). O-PLS-DA was subsequently performed, which discriminated the pre-dose and post-dose groups. O-PLS-DA filters out variation that is orthogonal to class membership and hence improves model interpretability. In order to avoid over-fitting the data, a 7-fold cross-validation was used and statistical parameters (R2Y and

Q2Y representing the goodness of fit and predictive ability) were calculated (Fonville, et al., 2010). Permutation tests (*n* = 1000 permutations of the class membership) were also used to test the validity of each model. Heatmaps based on the Pearson correlation coefficient values (R) of the identified discriminatory resonances from the O-PLS-DA models were also constructed with a cut off R value of |0.5|. Prism 5.0 (Graphpad; La Jolla, CA) was used for non-parametric univariate analysis (Kruskal-Wallis with Dunn's multiple correction test). A significance threshold value of $p < 0.05$ was set throughout.

Results

Liver histopathology

Histopathological assessment of the control diet cohort revealed hepatic necrosis following MTX treatment (40 and 100 mg/kg; Figure 1A, Figure 2). In the control diet cohort, one animal also developed liver inflammation and another biliary hyperplasia following MTX treatment (40 and 100 mg/kg respectively, Figure 1C and 1E respectively). In contrast, the MCD diet cohort had a background (vehicle group) characterized by liver necrosis, lipid accumulation and liver inflammation (Figure 1A-C respectively, Figure 2). Following treatment of the MCD diet cohort with MTX (40 mg/kg), a statistically significant reduction in lipid accumulation and liver inflammation was observed (Figure 1B and 1C respectively, Figure 2). The MCD diet cohort rats also developed minimal liver fibrosis and mild biliary hyperplasia (black arrow, Figure 2) following treatment with the highest dose of MTX (100 mg/kg; Figure 1D and 1E respectively).

Body weight was monitored at the beginning and end of the study. The average baseline weight of the control diet cohort animals was 390 g (± 57 g) whereas that of the MCD diet

cohort was 200 g (± 46 g). In the control diet cohort, weight loss was observed following administration of MTX with an average percentage weight loss of 7 %, 16 % and 26 % for the cohorts administered 10, 40 and 100 mg/kg MTX respectively. The MCD diet cohort also experienced weight loss with an average percentage weight loss of 18 %, 20 % and 20 % for the cohorts administered 10, 40 and 100 mg/kg MTX respectively (Figure S1).

Hepatic and urinary metabolic phenotype of the NASH model (MCD diet cohort baseline)

Pair-wise O-PLS-DA models were computed to identify the discriminatory metabolites between the two diet cohorts for each biological matrix. A robust O-PLS-DA model (Figure 3A; R2Y = 0.9913, Q2Y = 0.9315 and p = 0.009) revealed complete differentiation between the hepatic aqueous-soluble extract baseline (vehicle) metabolic profiles of the two diet cohorts as evidenced from the cross-validated predictive component of the scores plot (Tcv, cross-validated predictive scores, Figure 3A1). The corresponding coefficient plot (Figure 3A2) showed that the metabolic signature of the MCD diet cohort included depleted levels of glucose, glycogen, mannose, maltose, glutathione, lactate, niacinamide, choline, phosphocholine, trimethylamine, tyrosine, 1-methylhistidine, inosine and uridine, together with elevated levels of glycine, lipids, fumarate and formiminoglutamic acid (FIGLU), with respect to the baseline control diet cohort.

The O-PLS-DA model comparing the urinary baseline (pre-dose, 0hr) metabolic profiles of the two diet cohorts (Figure 3B; R2Y = 0.9519, Q2Y = 0.9040 and p = 0.001) indicated complete discrimination as evidenced from the scores plot (Tcv, Figure 3B1). The corresponding coefficient plot (Figure 3B2) indicated that, relative to the control diet, the MCD diet cohorts had elevated levels of citrate, urocanate, guanidinoacetate, methylamine, taurine, formate and FIGLU, and depleted levels of trimethylamine-N-oxide (TMAO) and dimethylamine.

Hepatic metabolic phenotype following MTX administration in the control diet cohort

O-PLS-DA pair-wise models were employed to characterize the metabolic consequences of MTX administration on the hepatic aqueous-soluble extract metabolic profiles of the control diet cohort, relative to the vehicle cohort. The statistically robust O-PLS-DA model characterizing the effect of 100 mg/kg MTX administration (Figure 4A; R2Y = 0.9985, Q2Y = 0.8485 and p = 0.009) achieved complete separation between the two groups in the scores plot (Tcv, Figure 4A1). The corresponding coefficient plot (Figure 4A2) found that the administration of 100 mg/kg MTX led to the depletion of lactate, glucose, maltose, mannose, glycogen, betaine, inosine, dimethylamine and glutathione. It also led to the concomitant rise in the levels of valine, glutamate, leucine, isoleucine, glycerophosphocholine, D-3-hydroxybutyrate, formate, uracil, hypoxanthine, creatine and choline following MTX administration relative to the vehicle cohort.

The O-PLS-DA models comparing the hepatic metabolic profiles of the vehicle with the 10 and 40 mg/kg MTX administration groups (Figure S2) were statistically robust and identified a panel of discriminatory metabolites for each dose group, including an elevation of glutamate, valine, isoleucine, leucine and uracil, together with depletion of betaine, glutathione, dimethylamine, glycogen and glucose, relative to the control cohort. The scale of metabolic perturbations induced by MTX administration was progressive and was maximal at the highest dose (100 mg/kg). Hepatic changes reflective of a dose response included elevation of valine, isoleucine, leucine and depletion of glucose, dimethylamine, glycogen and glutathione. Furthermore, a number of unique metabolic changes were observed specific to the administration of 100 mg/kg MTX relative to the vehicle, which included increased levels of hypoxanthine, formate and creatine. A summary of the hepatic metabolic effects induced

by MTX administration at all doses in the control diet cohort is presented in Figure 5A in the form of a heatmap, which displays the given Pearson correlation coefficient (R) for each discriminatory metabolite obtained from the O-PLS-DA coefficients.

Hepatic metabolic phenotype following MTX administration in the MCD diet cohort

O-PLS-DA pair-wise models were computed to identify the discriminatory metabolites related to the effect of MTX administration at each dose level (10 mg/kg, 40 mg/kg and 100 mg/kg) relative to the vehicle group in the MCD diet cohort. The statistically robust O-PLS-DA model of the vehicle and 100 mg/kg MTX administration group of the MCD diet cohort (Figure 4B1; R2Y = 0.9957, Q2Y = 0.9155 and p = 0.001) differentiated completely between the two groups (Tcv, Figure 4B1). The corresponding coefficient plot (Figure 4B2) indicated that the administration of 100 mg/kg MTX led to the rise of the levels of uracil, fumarate, D-3-hydroxybutyrate, valine, leucine, phenylalanine, glutamate, creatine, choline, urocanate, FIGLU, formate and niacinamide while inosine, phosphocholine, lactate, glycogen, maltose and glucose were depleted. The increase in fumarate was unique to the model characterizing the effect of high dose MTX administration (100 mg/kg) in the MCD diet cohort.

Significant hepatic metabolic perturbations were also identified following administration of both 10 and 40 mg/kg MTX including the depletion of glucose, maltose and glycogen, and the elevation of leucine, isoleucine, glutamate, uracil and FIGLU. The scale of metabolic change was reflective of the dose response with respect to an increase in phenylalanine, acetate, glutamate and FIGLU and decrease in lactate levels. A summary of the hepatic metabolic effects induced by MTX administration at all doses for the MCD diet cohort is presented in Figure 5B.

Elevation of phenylalanine was also observed to be statistically significant in a regression analysis of the hepatic aqueous-soluble extract metabolic profiles from both diet cohorts with the biliary hyperplasia and fibrosis scores (R2Y = 0.5218, Q2Y = 0.2423 and p = 0.020, and R2Y = 0.5406, Q2Y = 0.2542 and p = 0.014 respectively). Integration of the phenylalanine resonance showed a statistically significant elevation following administration of 100 mg/kg MTX in the MCD diet cohort, when compared to the vehicle cohort, confirming the O-PLS regression results (p = 0.02; Figure S3).

Urinary metabolic phenotype following MTX administration in the control diet

The collection of urine samples at sequential time-points facilitated the characterization of the temporal metabolic consequences of MTX at each dose level for each diet cohort. O-PLS-DA pair-wise models were constructed to investigate the differentiation of pre-dose urinary baseline metabolic profiles (0hr) and post-treatment metabolic profiles (12hr, 24hr and 48hr). The O-PLS-DA models that discriminated the metabolic effect of the 100 mg/kg dose of MTX from baseline had the highest statistical significance and greatest predictive ability and will be further discussed.

The O-PLS-DA models characterizing the comparison of the urine pre-dose (0hr) metabolic profiles with each of the post-dose (100mg/kg MTX) time-points (12hr, 24hr and 48hr) in the control diet cohort showed that as time progressed, the effect of MTX became more pronounced (for a summary of the statistical parameters for each model please see Table S1). The statistically robust model comparing the metabolic profiles of the control diet 0hr and 48hr time-points (Figure 6A; R2Y = 0.9859, Q2Y = 0.7608, p = 0.034) achieved complete separation between the two groups in the scores plot (Tcv; Figure 6A1). The corresponding coefficient plot (Figure 6A2) reported a depletion of alanine, methylamine, dimethylamine,

hippurate, TMAO and 3-indoxylsulphate, together with an elevation of the levels of succinate, creatine, phenylacetylglycine and formate.

Urinary metabolic phenotype following MTX administration in the MCD diet

The corresponding urinary analysis of the metabolic effect of MTX administration (100 mg/kg) in the MCD diet cohort also indicated a time-dependent progressive effect of MTX that was maximal at 48hr post-treatment (Table S1 provides a summary of the statistical parameters of the models). The statistically robust model comparing the metabolic profiles of the MCD diet 0hr and 48hr time-points (Figure 6B; R2Y = 0.9985, Q2Y = 0.8485, p = 0.001) achieved complete differentiation between the two groups in the scores plot (Tcv, Figure 6B1). The coefficient plot (Figure 6B2) indicated that MTX administration led to an elevation in the levels of FIGLU and formate, and the depletion of methylamine, alanine and hippurate.

Following administration of MTX (100 mg/kg) the urinary metabolic phenotype showed a progressive depletion from 12hr to 48hr of methylamine and hippurate and elevation of formate and FIGLU. The depletion of alanine at 48hr was a unique metabolic effect that was specific for this time-point. Depletions in the levels of 3-indoxylsulphate and phenylacetylglycine were also observed but these were restricted to the 24hr time-point, whilst TMAO was depleted in both 12hr and 24hr but had returned to baseline levels by 48hr. With respect to the models characterizing the metabolic effect of the 10 mg/kg and 40 mg/kg doses of MTX, elevation of FIGLU and formate was also observed at 48hr post-dose. However, at that time-point, both of the lower doses of MTX also led to the depletion of methylamine and 3-indoxylsulphate, together with the elevation of dimethylamine, all of which were not observed at the corresponding time-point after 100 mg/kg MTX administration.

The comparison of the effects of administration of MTX (100 mg/kg) in the two diet cohorts showed several diet specific MTX-induced metabolic effects. At 48hr post-dose, elevations of phenylacetylglycine, creatine, citrate and succinate were specific only to the control diet cohort, whilst elevated levels of FIGLU were specific only to the MCD diet cohort (Figure 7 illustrates a heatmap summary of the urinary metabolic effect of MTX administration (100mg/kg) in both diet cohorts).

Finally, temporal urinary levels of the MTX parent compound following administration of the 100 mg/kg dose were also compared between the two diet cohorts at the 12hr, 24hr and 48hr time-points. The levels of MTX were greater in the control diet cohort than the MCD cohort at all time-points, reaching statistical significance at the 48hr time-point ($p = 0.0025$, Figure S4).

Discussion

Characterization of the MCD diet model of NASH

The MCD diet had liver histopathology consistent with a phenotype reflective of clinical NASH (Brunt, 2004). Metabonomic analysis of the hepatic extracts and urine from the MCD diet cohort indicated a general impairment of energy and choline metabolism, coupled with glutathione depletion. The depletion of energy metabolites such as hepatic glucose and glycogen, relative to the control diet cohort, is indicative of energetic stress and could be related to the previously reported NASH-induced mitochondrial stress (Perez-Carreras et al., 2003) or the inhibition of stearoyl-CoA desaturase-1 (Rizki, et al., 2006). Glutathione depletion is a marker of oxidative stress which is also characteristic of the NASH background (Merrell and Cherrington, 2011). Its hepatic depletion was also potentially exacerbated by the

methionine deficient nature of the MCD diet. Finally, the choline deficient nature of the diet was also likely to be directly linked to the depletion of choline related metabolites such as hepatic trimethylamine and choline and urinary TMAO.

The choline and methionine deficient nature of this dietary model would have also directly impaired the folate cycle and one-carbon metabolism (Figure 8). Impairment of the folate cycle would lead to reduced tetrahydrofolate (THF) production, which may explain the observed accumulation of urinary and hepatic FIGLU and urocanate and urinary formate. THF is required for the conversion of FIGLU to glutamate and FIGLU is a previously described urinary marker of folate deficiency (Rabinowitz and Tabor, 1958). Accumulation of urinary formate would arise from THF depletion and the subsequent impairment of formyl-THF production. Finally, the depleted levels of hepatic inosine and the elevated levels of hepatic glycine and urinary guanidinoacetate (a glycine metabolite) may also be linked to a general inhibition of the folate cycle (Fowler, 2001).

It is important to be aware of the limitations associated with the MCD diet as a model of NASH. Creation of a model that accurately reflects the clinical condition of NASH has proven difficult, since it would require replication of both the liver pathology and the systemic metabolic environment (Larter and Yeh, 2008). The MCD diet is believed to induce steatohepatitis and oxidative stress through the inhibition of phosphatidylcholine synthesis and impairment of hepatic lipid transport (Rinella, et al., 2008), but it is not thought to be an accurate reflection of the metabolic syndrome component of NASH since it does not induce obesity, insulin resistance or hyperglycaemia. Furthermore, the MCD diet induces significant weight loss as was also observed in our study (Larter and Yeh, 2008; Rinella, et al., 2008).

Effect of MTX in the context of the control diet cohort

Minimal liver necrosis was observed following administration of MTX (40 and 100 mg/kg) in the control diet cohort. Metabonomic analysis showed dose-related metabolic consequences in both sample matrices, together with a temporal effect in the case of urinary metabolic profiles.

The MTX-induced elevation of the levels of hepatic uracil, is potentially due to the inhibition of thymidylate synthetase, while the observed depletion of hepatic inosine could result from the inhibition of phosphoribosylaminoimidazolecarboxamide formyltransferase (Genestier et al., 2000). MTX could also affect the levels of nucleobases and nucleosides indirectly through the disruption of the folate cycle and its inhibition of THF formation, which could have other down-stream consequences such as the observed elevation of urinary formate.

The observed effect of MTX, consistent at all doses, on hepatic energy metabolism, including the depletion of lactate, glucose and glycogen could be attributed to the previously reported inhibition of oxidative phosphorylation, which would lead to a higher utilization of glucose through other pathways (Yamamoto et al., 1988). Furthermore, the depletion of the aforementioned metabolites could lead to lipid breakdown, as indicated by the elevated levels of hepatic D-3-hydroxybutyrate. This observed disturbance of energy metabolism could also be linked to a reduced caloric intake through the previously reported MTX-induced weight loss, which is linked to a disruption of gut absorption and mucositis (Naruhashi et al., 2000). A reduction of caloric intake could also be linked to the observed depletion of hepatic glutathione (Szkudelski et al., 2004) and choline related moieties, such as hepatic phosphocholine and dimethylamine. However, a previous metabolic profiling investigation of caloric restriction observed a different panel of discriminatory urinary metabolites to that of our investigation (Connor et al., 2004). Nevertheless, it is recommended that future studies

should also record food consumption and employ an experimental design that would incorporate a pair feeding system in order to be able to easily identify any metabolic changes linked to fasting.

Effect of MTX in the context of the NASH background (MCD diet model)

We hypothesized that the presence of the NASH background, which can induce changes in drug metabolizing enzymes and hepatic transporters (Fisher, et al., 2009; Hardwick, et al., 2011), would alter MTX-induced metabolic consequences and toxic outcome. The administration of MTX (40 mg/kg) in the context of NASH resulted in a statistically significant histomorphologic reduction of lipid accumulation and inflammation. These observed reductions are suggestive of a protective effect due to the anti-inflammatory properties of MTX, while MTX has previously been reported to affect cholesterol transport (Coomes et al., 2011). However, administration of the highest dose caused minimal liver fibrosis and biliary hyperplasia suggesting enhanced toxicity of MTX in the context of NASH.

Metabonomic analysis of the hepatic aqueous-soluble extracts found that, in part, the metabolic effect of MTX in the NASH model had a similar progressive pattern to the control diet cohort. Interestingly, MTX-induced metabolic effects specific to the NASH model were also observed, suggesting that the NASH baseline influenced the metabolic consequences of MTX administration. These included increased levels of hepatic FIGLU, urocanate, phenylalanine, acetate, niacinamide and fumarate. The progressive dose-dependent elevations of fumarate, phenylalanine and niacinamide did not follow the same pattern as the observed weight loss in the MCD diet cohort and therefore are more likely to be mechanistically indicative of MTX toxicity and not a direct consequence of either MTX or MCD-diet induced weight loss. The elevations of hepatic metabolites associated with the

folate cycle, such as FIGLU and urocanate, following MTX administration in the NASH model are signs of a significant inhibition of the folate cycle, greater than that observed in the MCD diet at baseline and greater than that observed after MTX administration in the control diet cohort. This combined effect of MTX and NASH, coupled to previous clinical reports of NASH induced methionine cycle disruption triggered through glutathione depletion (Kalhan et al., 2011), suggest a clinically relevant synergistic effect of NASH and MTX on folate metabolism (Figure 8).

Hepatic phenylalanine was also identified by regression analyses as the sole endogenous metabolite associated with the development of biliary hyperplasia and liver fibrosis. Levels of hepatic phenylalanine are used as a liver function test because they are related to the activity of the phenylalanine hydroxylase enzyme, an important enzyme for phenylalanine degradation (Burke et al., 1997). Higher levels of serum phenylalanine have been previously reported clinically following treatment with MTX and were linked to the inhibition of dihydropteridine reductase (Hilton et al., 1989). However, the observed elevation of hepatic phenylalanine in our study is likely to be influenced by additional mechanisms since the levels of hepatic tyrosine remained unperturbed. Furthermore the levels of urinary phenylacetylglycine following administration of 100 mg/kg MTX in the MCD diet cohort were largerly unperturbed during the time-course of the study.

The parallel study of the xenobiotic metabolic profile enabled characterization of the effect of NASH on the disposition of MTX and showed increased urinary excretion of MTX in the control cohort at the 12hr, 24hr and 48hr time-points. This is explained by the greater urinary excretion of MTX that was observed for the MCD diet cohort relative to the control diet cohort within the first six hours post-dose (Hardwick et al., recently submitted for publication). The

observed higher early urinary excretion of MTX in the MCD diet cohort could be due to the reported downregulation of canalicular transporters in the NASH model, and the relatively lower quantity of MTX in the feces, which indicate a shift in the excretion pathway of MTX, towards urinary excretion (Hardwick et al., recently submitted for publication). Furthermore, a previous study has also reported the down–regulation of uptake transporter genes in disease–compromised livers as a hepatoprotective mechanism, indicating another potential mechanism behind the observed difference of urinary MTX excretion (Lake et al., 2011).

Effect of MTX on gut microbial co-metabolites

High dose MTX can cause intestinal toxicity and it has also been shown to affect the intestinal microbial composition (Naruhashi, et al., 2000). Both MTX (100 mg/kg) diet cohorts displayed mild inflammation and minimal apoptosis in the small intestine (Hardwick et al., recently submitted for publication). Metabonomic analysis indicated that gut microbial co-metabolites, including urinary methylamine, TMAO and 3-indoxylsulphate, were depleted in both diet cohorts following administration of 100 mg/kg MTX suggesting a potential perturbation of the gut microfloral balance (Nicholson et al., 2012).

Summary

This systems level data analysis provided enhanced mechanistic phenotyping of a widely used model of NASH, revealing a metabolic phenotype characterized by energetic and oxidative stress, and further contextualized its application in experimental studies. Metabolic profiling of the hepatic and urinary dose and temporal response to MTX administration revealed a wide panel of metabolic consequences that provided novel mechanistic insight. Finally, the administration of MTX (100 mg/kg) in the context of NASH led to enhanced hepatotoxicity

and the identification of a unique panel of metabolites which reflected this synergistic effect, providing mechanistic insight of potential translatable relevance for the clinical setting.

Supplementary data description

The figures displaying the percentage weight loss and phenylalanine integrals of each diet/dose cohort (Figure S1 and Figure S3), the O-PLS-DA models of the hepatic aqueous-soluble extract metabolic profiles after the administration of 10 and 40 mg/kg MTX in both diet cohorts (Figure S2) and the temporal quantity of urinary excreted MTX after the administration of 100 mg/kg MTX are provided in the supplementary data (Figure S4). Furthermore, a summary of the statistical parameters of the urine O-PLS-DA models of the metabolic effects after the administration of 100 mg/kg MTX in both diet cohorts is also provided (Table S1).

Funding information

This work was supported by the National Institute of Health, which is gratefully acknowledged for the financial support to N.J.C (grant numbers HD062489, ES006694 and AI083927) and the MRC Integrative Toxicology Training Partnership (ITTP), which is gratefully acknowledged for providing financial support to M.K in the form of a studentship grant and to M.C in the form of a career development fellowship.

References

Beckonert, O., Keun, H. C., Ebbels, T. M., Bundy, J., Holmes, E., Lindon, J. C., and Nicholson, J. K. (2007). Metabolic profiling, metabolomic and metabonomic procedures for NMR spectroscopy of urine, plasma, serum and tissue extracts. Nature protocols 2(11), 2692-703, 10.1038/nprot.2007.376.

Brunt, E. M. (2004). Nonalcoholic steatohepatitis. Seminars in liver disease 24(1), 3-20, 10.1055/s-2004-823098.

Burke, P. A., Stack, J. A., Wagner, D., Lewis, D. W., Jenkins, R. L., and Forse, R. A. (1997). L-[1-(13)C] Phenylalanine oxidation as a measure of hepatocyte functional capacity in end-stage liver disease. American journal of surgery 173(4), 270-3; discussion 273-4, 10.1016/S0002-9610(96)00392-3.

Burkhardt, J. E., Pandher, K., Solter, P. F., Troth, S. P., Boyce, R. W., Zabka, T. S., and Ennulat, D. (2011). Recommendations for the evaluation of pathology data in nonclinical safety biomarker qualification studies. Toxicologic pathology 39(7), 1129-37, 10.1177/0192623311422082.

Cloarec, O., Dumas, M. E., Craig, A., Barton, R. H., Trygg, J., Hudson, J., Blancher, C., Gauguier, D., Lindon, J. C., Holmes, E., and Nicholson, J. (2005). Statistical total correlation spectroscopy: an exploratory approach for latent biomarker identification from metabolic 1H NMR data sets. Anal Chem 77(5), 1282-9, 10.1021/ac048630x.

Connor, S. C., Wu, W., Sweatman, B. C., Manini, J., Haselden, J. N., Crowther, D. J., and Waterfield, C. J. (2004). Effects of feeding and body weight loss on the 1H-NMR-based urine

metabolic profiles of male Wistar Han rats: implications for biomarker discovery. Biomarkers 9(2), 156-79, 10.1080/13547500410001720767.

Coomes, E., Chan, E. S., and Reiss, A. B. (2011). Methotrexate in atherogenesis and cholesterol metabolism. Cholesterol 2011, 503028, 10.1155/2011/503028.

Day, C. P., and James, O. F. (1998). Steatohepatitis: a tale of two "hits"? Gastroenterology 114(4), 842-5.

Dieterle, F., Ross, A., Schlotterbeck, G., and Senn, H. (2006). Probabilistic quotient normalization as robust method to account for dilution of complex biological mixtures. Application in 1H NMR metabonomics. Anal Chem 78(13), 4281-90, 10.1021/ac051632c.

Farber, S., Pinkel, D., Sears, E. M., and Toch, R. (1956). Advances in chemotherapy of cancer in man. Adv Cancer Res 4, 1-71.

Fisher, C. D., Lickteig, A. J., Augustine, L. M., Ranger-Moore, J., Jackson, J. P., Ferguson, S. S., and Cherrington, N. J. (2009). Hepatic cytochrome P450 enzyme alterations in humans with progressive stages of nonalcoholic fatty liver disease. Drug metabolism and disposition: the biological fate of chemicals 37(10), 2087-94, 10.1124/dmd.109.027466.

Fonville, J. M., Richards, S. E., Barton, R. H., Boulange, C. L., Ebbels, T. M. D., Nicholson, J. K., Holmes, E., and Dumas, M.-E. (2010). The evolution of partial least squares models and related chemometric approaches in metabonomics and metabolic phenotyping. Journal of Chemometrics 24(11-12), 636-649, 10.1002/cem.1359.

Fowler, B. (2001). The folate cycle and disease in humans. Kidney international. Supplement 78, S221-9.

Genestier, L., Paillot, R., Quemeneur, L., Izeradjene, K., and Revillard, J. P. (2000). Mechanisms of action of methotrexate. Immunopharmacology 47(2-3), 247-57.

Hardwick, R. N., Fisher, C. D., Canet, M. J., Scheffer, G. L., and Cherrington, N. J. (2011). Variations in ATP-binding cassette transporter regulation during the progression of human nonalcoholic fatty liver disease. Drug metabolism and disposition: the biological fate of chemicals 39(12), 2395-402, 10.1124/dmd.111.041012.

Hilton, M. A., Bertolone, S., and Patel, C. C. (1989). Daily profiles of plasma phenylalanine and tyrosine in patients with osteogenic sarcoma during treatment with high-dose methotrexate-citrovorum rescue. Medical and pediatric oncology 17(4), 265-70.

Kalhan, S. C., Edmison, J., Marczewski, S., Dasarathy, S., Gruca, L. L., Bennett, C., Duenas, C., and Lopez, R. (2011). Methionine and protein metabolism in non-alcoholic steatohepatitis: evidence for lower rate of transmethylation of methionine. Clinical science 121(4), 179-89, 10.1042/CS20110060.

Lake, A. D., Novak, P., Fisher, C. D., Jackson, J. P., Hardwick, R. N., Billheimer, D. D., Klimecki, W. T., and Cherrington, N. J. (2011). Analysis of global and absorption, distribution, metabolism, and elimination gene expression in the progressive stages of human nonalcoholic fatty liver disease. Drug metabolism and disposition: the biological fate of chemicals 39(10), 1954-60, 10.1124/dmd.111.040592.

Langman, G., Hall, P. M., and Todd, G. (2001). Role of non-alcoholic steatohepatitis in methotrexate-induced liver injury. Journal of gastroenterology and hepatology 16(12), 1395-401.

Larter, C. Z., and Yeh, M. M. (2008). Animal models of NASH: getting both pathology and metabolic context right. Journal of gastroenterology and hepatology 23(11), 1635-48, 10.1111/j.1440-1746.2008.05543.x.

Lazarou, J., Pomeranz, B. H., and Corey, P. N. (1998). Incidence of adverse drug reactions in hospitalized patients: a meta-analysis of prospective studies. JAMA : the journal of the American Medical Association 279(15), 1200-5.

Leclercq, I. A., Farrell, G. C., Field, J., Bell, D. R., Gonzalez, F. J., and Robertson, G. R. (2000). CYP2E1 and CYP4A as microsomal catalysts of lipid peroxides in murine nonalcoholic steatohepatitis. The Journal of clinical investigation 105(8), 1067-75, 10.1172/JCI8814.

Merrell, M. D., and Cherrington, N. J. (2011). Drug metabolism alterations in nonalcoholic fatty liver disease. Drug metabolism reviews 43(3), 317-34, 10.3109/03602532.2011.577781.

Naruhashi, K., Nadai, M., Nakao, M., Suzuki, N., Nabeshima, T., and Hasegawa, T. (2000). Changes in absorptive function of rat intestine injured by methotrexate. Clinical and experimental pharmacology & physiology 27(12), 980-6.

Nicholson, J. K., Foxall, P. J., Spraul, M., Farrant, R. D., and Lindon, J. C. (1995). 750 MHz 1H and 1H-13C NMR spectroscopy of human blood plasma. Anal Chem 67(5), 793-811.

Nicholson, J. K., Holmes, E., Kinross, J., Burcelin, R., Gibson, G., Jia, W., and Pettersson, S. (2012). Host-gut microbiota metabolic interactions. Science 336(6086), 1262-7, 10.1126/science.1223813.

Nicholson, J. K., Lindon, J. C., and Holmes, E. (1999). 'Metabonomics': understanding the metabolic responses of living systems to pathophysiological stimuli via multivariate statistical

analysis of biological NMR spectroscopic data. Xenobiotica; the fate of foreign compounds in biological systems 29(11), 1181-9, 10.1080/004982599238047.

Perez-Carreras, M., Del Hoyo, P., Martin, M. A., Rubio, J. C., Martin, A., Castellano, G., Colina, F., Arenas, J., and Solis-Herruzo, J. A. (2003). Defective hepatic mitochondrial respiratory chain in patients with nonalcoholic steatohepatitis. Hepatology 38(4), 999-1007, 10.1053/jhep.2003.50398.

Pirmohamed, M., James, S., Meakin, S., Green, C., Scott, A. K., Walley, T. J., Farrar, K., Park, B. K., and Breckenridge, A. M. (2004). Adverse drug reactions as cause of admission to hospital: prospective analysis of 18 820 patients. Bmj 329(7456), 15-9, 10.1136/bmj.329.7456.15.

Puri, P., Wiest, M. M., Cheung, O., Mirshahi, F., Sargeant, C., Min, H. K., Contos, M. J., Sterling, R. K., Fuchs, M., Zhou, H., Watkins, S. M., and Sanyal, A. J. (2009). The plasma lipidomic signature of nonalcoholic steatohepatitis. Hepatology 50(6), 1827-38, 10.1002/hep.23229.

Rabinowitz, J. C., and Tabor, H. (1958). The urinary excretion of formic acid and formiminoglutamic acid in folic acid deficiency. The Journal of biological chemistry 233(1), 252-5.

Rinella, M. E., Elias, M. S., Smolak, R. R., Fu, T., Borensztajn, J., and Green, R. M. (2008). Mechanisms of hepatic steatosis in mice fed a lipogenic methionine choline-deficient diet. Journal of lipid research 49(5), 1068-76, 10.1194/jlr.M800042-JLR200.

Rizki, G., Arnaboldi, L., Gabrielli, B., Yan, J., Lee, G. S., Ng, R. K., Turner, S. M., Badger, T. M., Pitas, R. E., and Maher, J. J. (2006). Mice fed a lipogenic methionine-choline-deficient diet develop hypermetabolism coincident with hepatic suppression of SCD-1. Journal of lipid research 47(10), 2280-90, 10.1194/jlr.M600198-JLR200.

Rosenberg, P., Urwitz, H., Johannesson, A., Ros, A. M., Lindholm, J., Kinnman, N., and Hultcrantz, R. (2007). Psoriasis patients with diabetes type 2 are at high risk of developing liver fibrosis during methotrexate treatment. Journal of hepatology 46(6), 1111-8, 10.1016/j.jhep.2007.01.024.

Szkudelski, T., Okulicz, M., Bialik, I., and Szkudelska, K. (2004). The influence of fasting on liver sulfhydryl groups, glutathione peroxidase and glutathione-S-transferase activities in the rat. Journal of physiology and biochemistry 60(1), 1-6.

Tanaka, N., Matsubara, T., Krausz, K. W., Patterson, A. D., and Gonzalez, F. J. (2012). Disruption of phospholipid and bile acid homeostasis in mice with nonalcoholic steatohepatitis. Hepatology 56(1), 118-29, 10.1002/hep.25630.

Wang, Z., Chen, Z., Yang, S., Wang, Y., Yu, L., Zhang, B., Rao, Z., Gao, J., and Tu, S. (2012). (1)H NMR-based metabolomic analysis for identifying serum biomarkers to evaluate methotrexate treatment in patients with early rheumatoid arthritis. Exp Ther Med 4(1), 165-171, 10.3892/etm.2012.567.

Waters, N. J., Waterfield, C. J., Farrant, R. D., Holmes, E., and Nicholson, J. K. (2005). Metabonomic deconvolution of embedded toxicity: application to thioacetamide hepato- and nephrotoxicity. Chemical research in toxicology 18(4), 639-54, 10.1021/tx049869b.

West, S. G. (1997). Methotrexate hepatotoxicity. Rheumatic diseases clinics of North America 23(4), 883-915.

Widemann, B. C., and Adamson, P. C. (2006). Understanding and managing methotrexate nephrotoxicity. The oncologist 11(6), 694-703, 10.1634/theoncologist.11-6-694.

Williams, C. D., Stengel, J., Asike, M. I., Torres, D. M., Shaw, J., Contreras, M., Landt, C. L., and Harrison, S. A. (2011). Prevalence of nonalcoholic fatty liver disease and nonalcoholic steatohepatitis among a largely middle-aged population utilizing ultrasound and liver biopsy: a prospective study. Gastroenterology 140(1), 124-31, 10.1053/j.gastro.2010.09.038.

Yamamoto, N., Oliveira, M. B., Campello Ade, P., Lopes, L. C., and Kluppel, M. L. (1988). Methotrexate: studies on the cellular metabolism. I. Effect on mitochondrial oxygen uptake and oxidative phosphorylation. Cell biochemistry and function 6(1), 61-6, 10.1002/cbf.290060110.

Figures

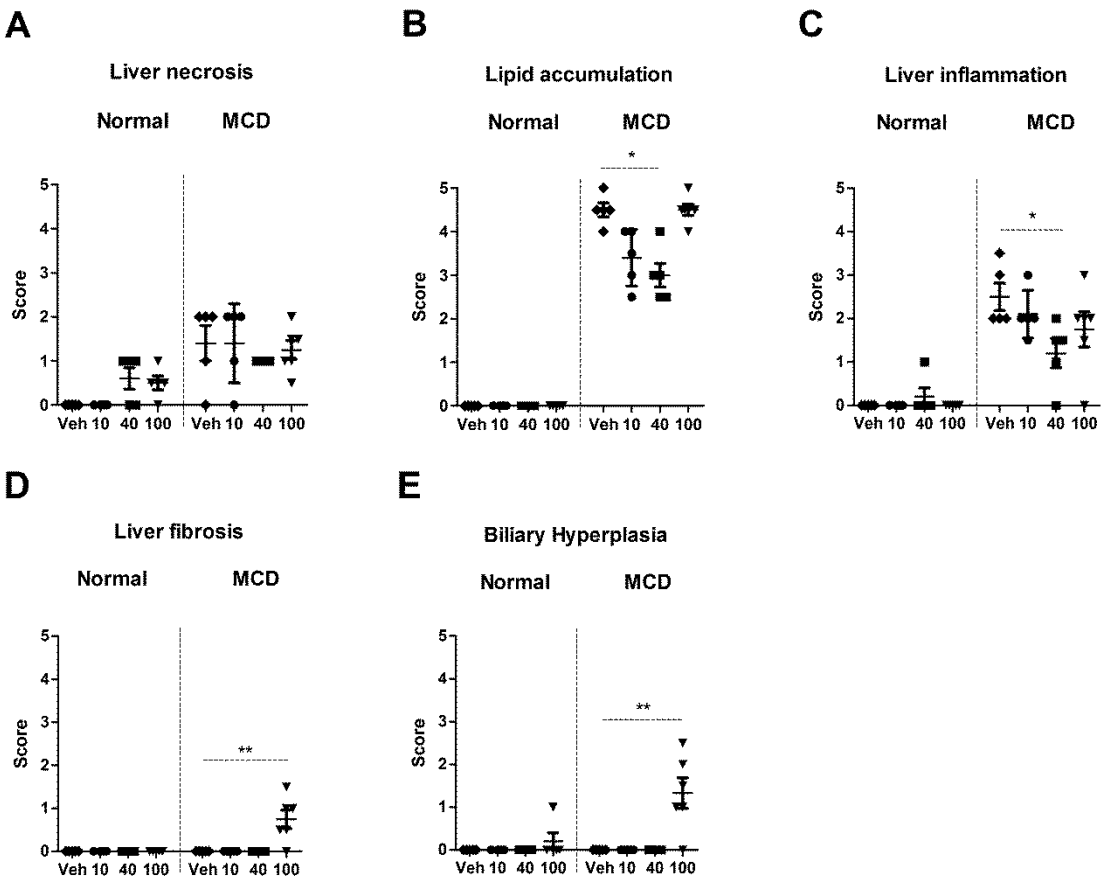


Figure 1: Histopathology scores representing liver necrosis (A), lipid accumulation (B), liver inflammation (C), liver fibrosis (D) and biliary hyperplasia (E) (mean and standard deviation) following administration of MTX (vehicle, 10, 40 and 100 mg/kg) in both the control and MCD diet cohorts. Statistical significance is indicated by one or two asterisks representing $p < 0.05$ and $p < 0.01$ respectively. There are five animals per group apart from the 100 mg/kg dose in the MCD diet cohort which has six. The scoring criteria are: 0 = no significant lesions, 1 = minimal, 2 = mild, 3 = moderate, 4 = marked and 5 = severe. Veh – Vehicle

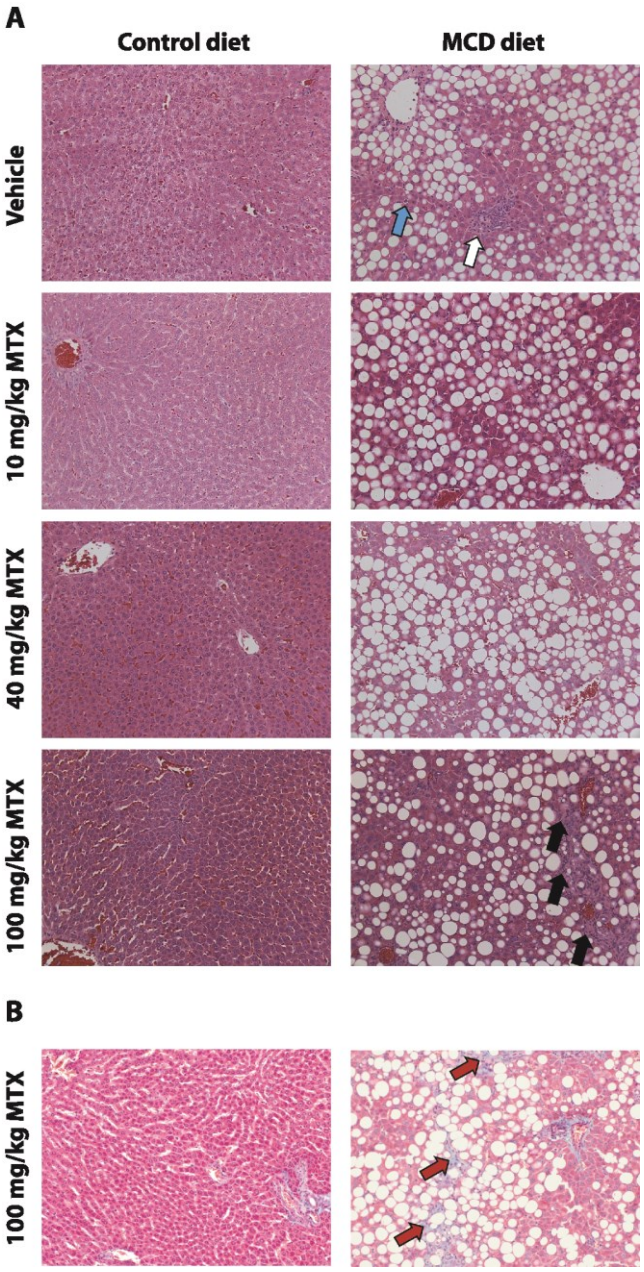


Figure 2: (A) Representative histology images of H&E-stained control and MCD liver sections following vehicle or 10, 40, or 100 mg/kg MTX and (B) Masson Trichrome stained liver sections following 100 mg/kg administration in both diets (20X magnification). White and cyan arrows indicate inflammation and single cell necrosis respectively in the MCD diet cohort baseline. Black and red arrows indicate biliary hyperplasia and liver fibrosis respectively in the MCD cohort following administration of MTX (100 mg/kg).

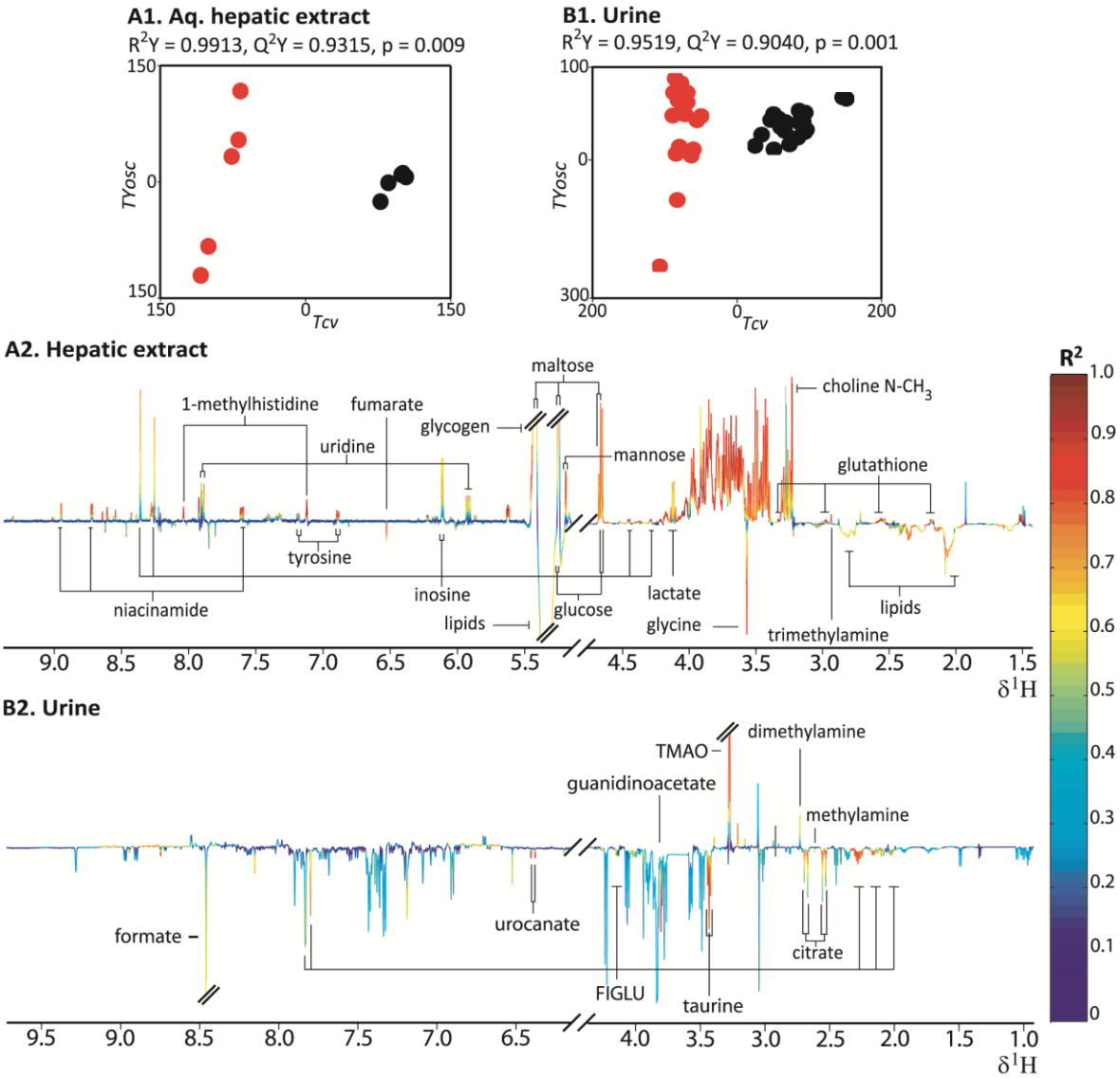


Figure 3: Hepatic aqueous-soluble extracts (A1, A2) and urinary (B1, B2) O-PLS-DA models distinguishing between the baseline of the control and MCD diet cohort. The scores plots (A1 and B1) depict the separation of the MCD (red; *n* = 5 in the liver and *n* = 20 in the urine) and control diet cohort (black; *n* = 5 in the liver and *n* = 20 in the urine) in multivariate space. Tcv is the predictive component, whilst TYosc is the orthogonal component. The loadings coefficient plots (A2 and B2) illustrate the discriminatory spectral resonances with the height of spectral peaks representing covariance. The color-scale corresponds to the coefficient of determination (R^2) ranging from low (0; blue) to high (red; 1). Resonances pointing upwards indicate an increase in that specific resonance in the control cohort and vice versa. FIGLU – formiminoglutamic acid; Choline-NMe_3 – NMe3 resonance of choline, phosphocholines and glycerophosphocholines; TMAO – trimethylamine-*N*-oxide.

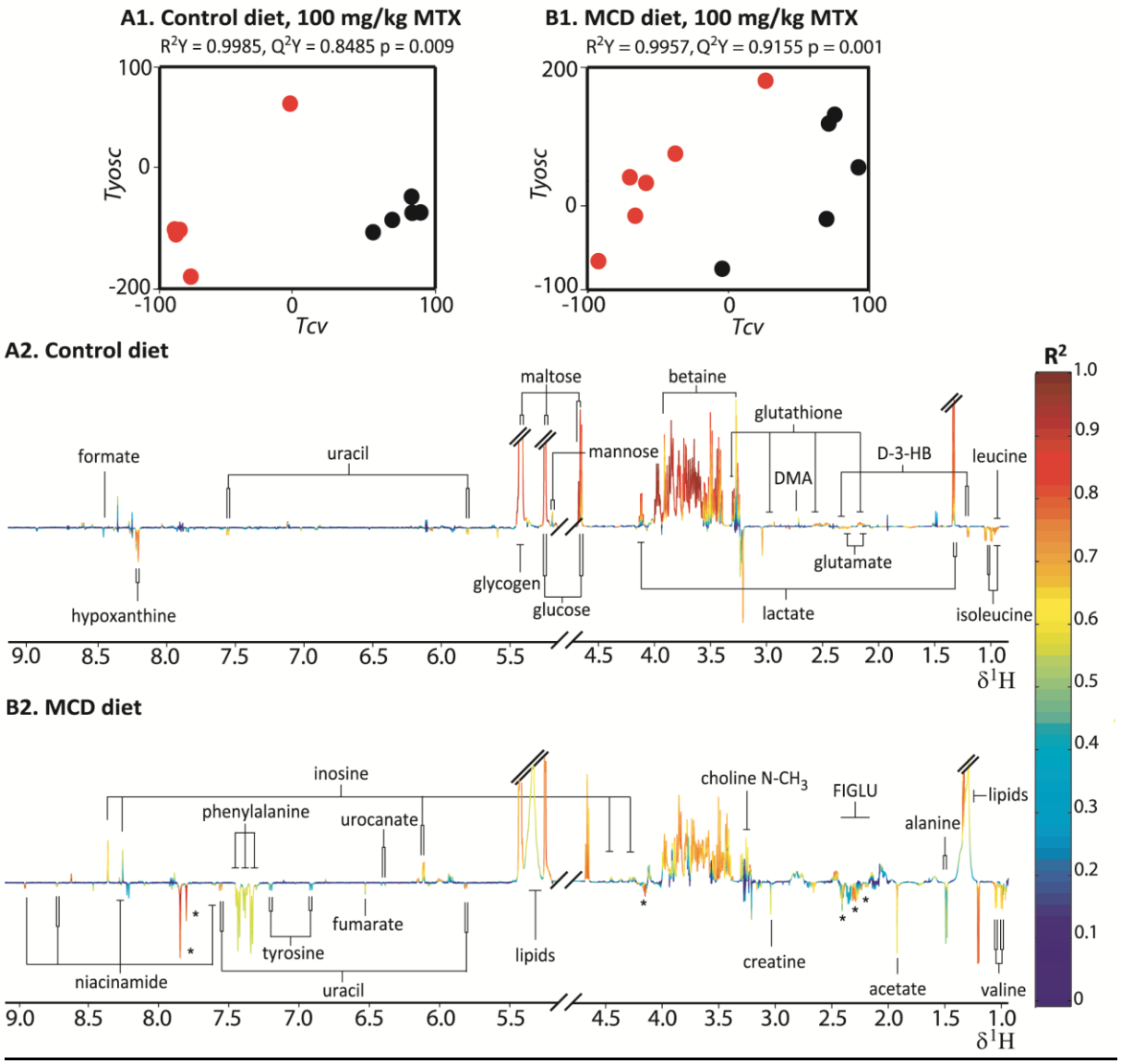


Figure 4: Hepatic extract O-PLS-DA models comparing the vehicle cohorts and 100 mg/kg MTX administration cohorts in the control diet (A1 and A2; *n* = 5 for the vehicle group and *n* = 5 for the MTX dosed group) and MCD diet (B1 and B2; *n* = 5 for the vehicle group and *n* = 6 for the MTX doses group). The scores plots (A1 and B1) depict the separation of the MTX dose (red) and vehicle (black) cohorts in multivariate space. See Legend for Figure 3. Asterisks - formiminoglutamic acid (FIGLU); DMA – dimethylamine; D-3-HB – D-3-hydroxybutyrate.

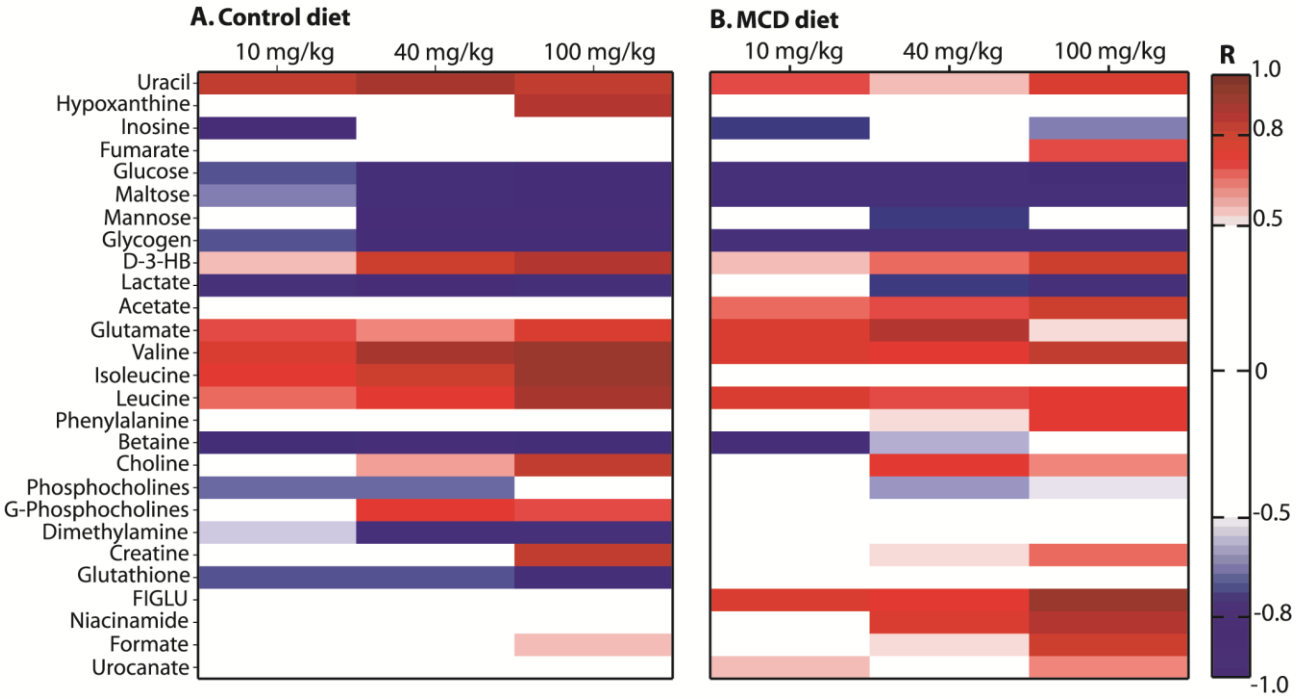


Figure 5: Heatmap describing the hepatic metabolic effects of MTX administration in the control diet (A) and MCD diet (B). The heatmap was constructed using the maximum Pearson correlation coefficient values (R) for each metabolite from the hepatic extract O-PLS-DA models distinguishing the metabolic profiles of MTX treated (10, 40, 100 mg/kg) and the vehicle cohort, in the control diet (A) and MCD diet (B). The scale shown on the right has a range from -1 (perfect negative correlation; blue colour) to 1 perfect positive correlation; red colour), whilst a cut-off value of |0.5| was set. Key: see legend above.

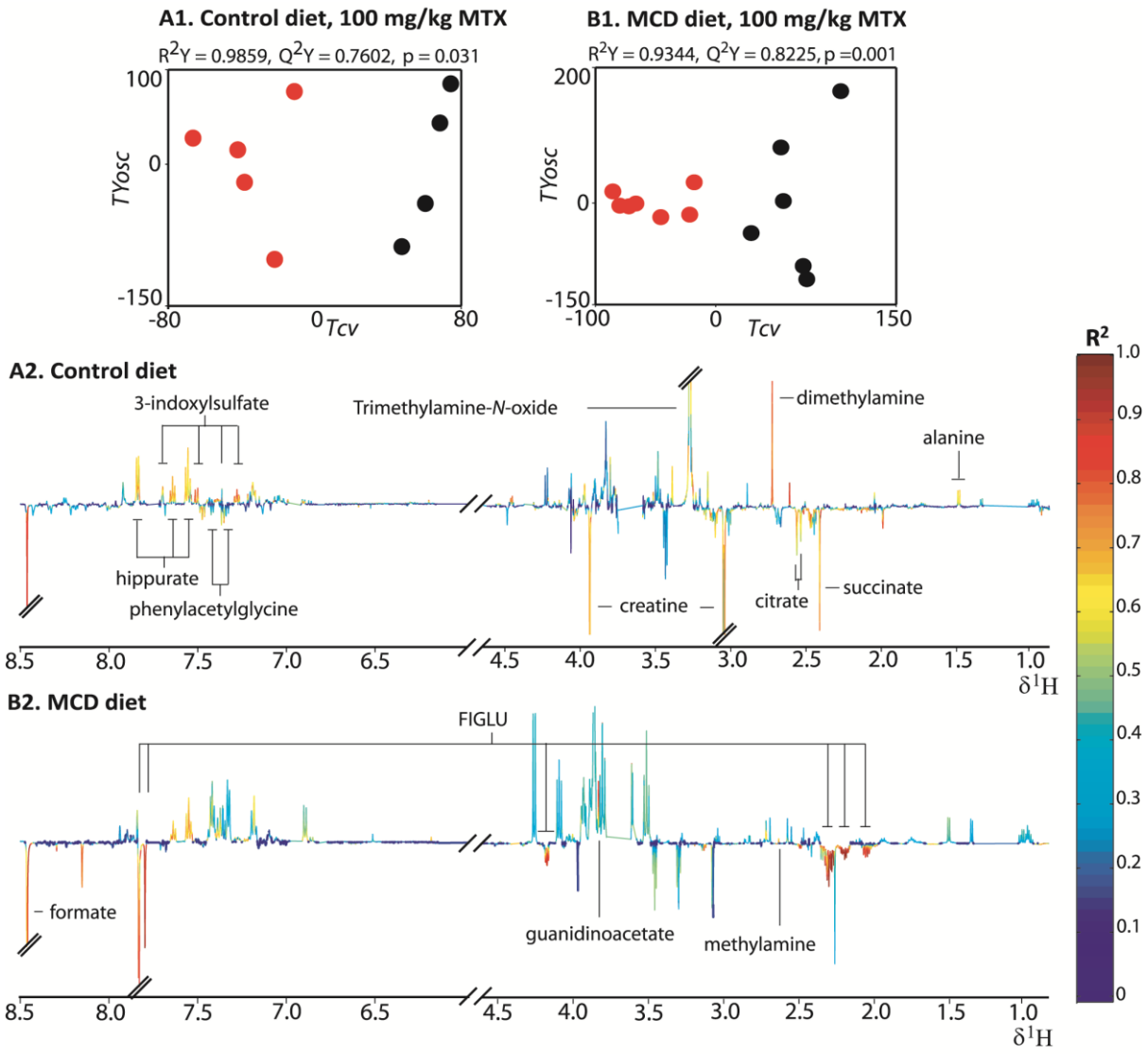


Figure 6: Urinary O-PLS-DA models comparing the pre-dose time point and the 48 hour post-dose time-point after 100 mg/kg MTX administration in the normal diet (A1 and A2; *n* = 4 at 0hr and *n* = 5 at 48hr) and MCD diet (B1 and B2; *n* = 6 at 0hr and *n* = 7 at 48hr). See Legend for Figure 3.

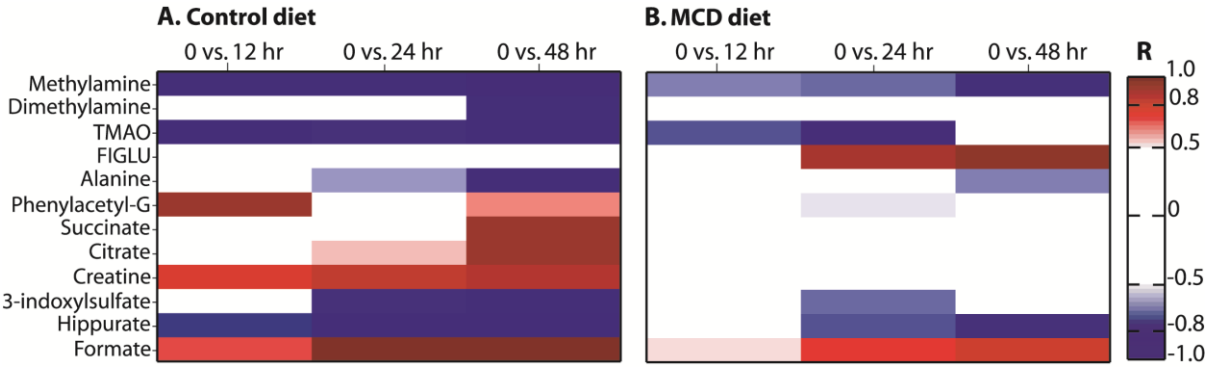


Figure 7: Heatmap describing the urinary metabolic effects of MTX administration in the control diet (A) and MCD diet (B) . Based on O-PLS-DA models that discriminated between the metabolic profiles of the post-dose time-points (12hr, 24hr and 48hr) of MTX administration (100 mg/kg) and the pre-dose time-point (0hr), in both diets. Phenylacetyl-G – phenylacetylglycine.

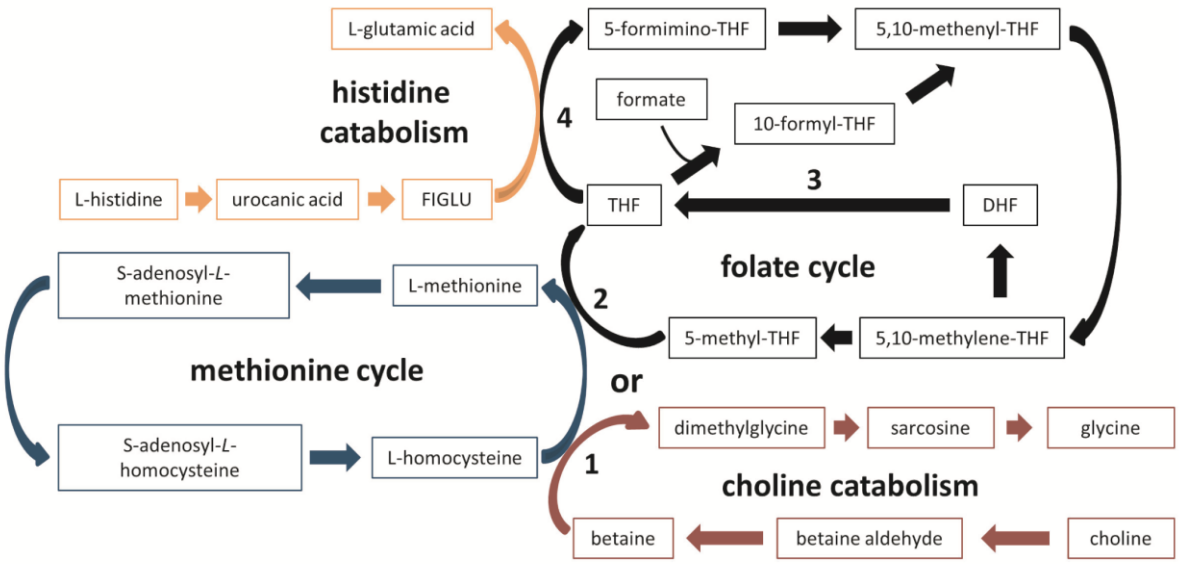
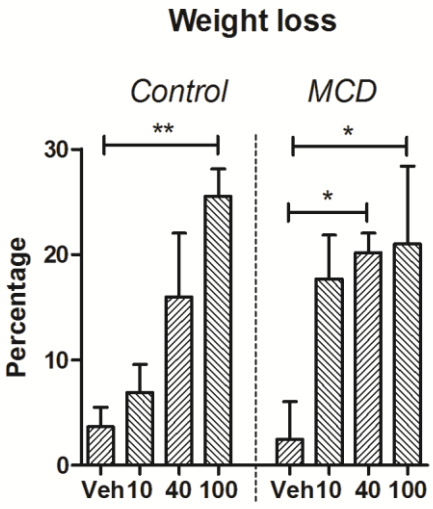
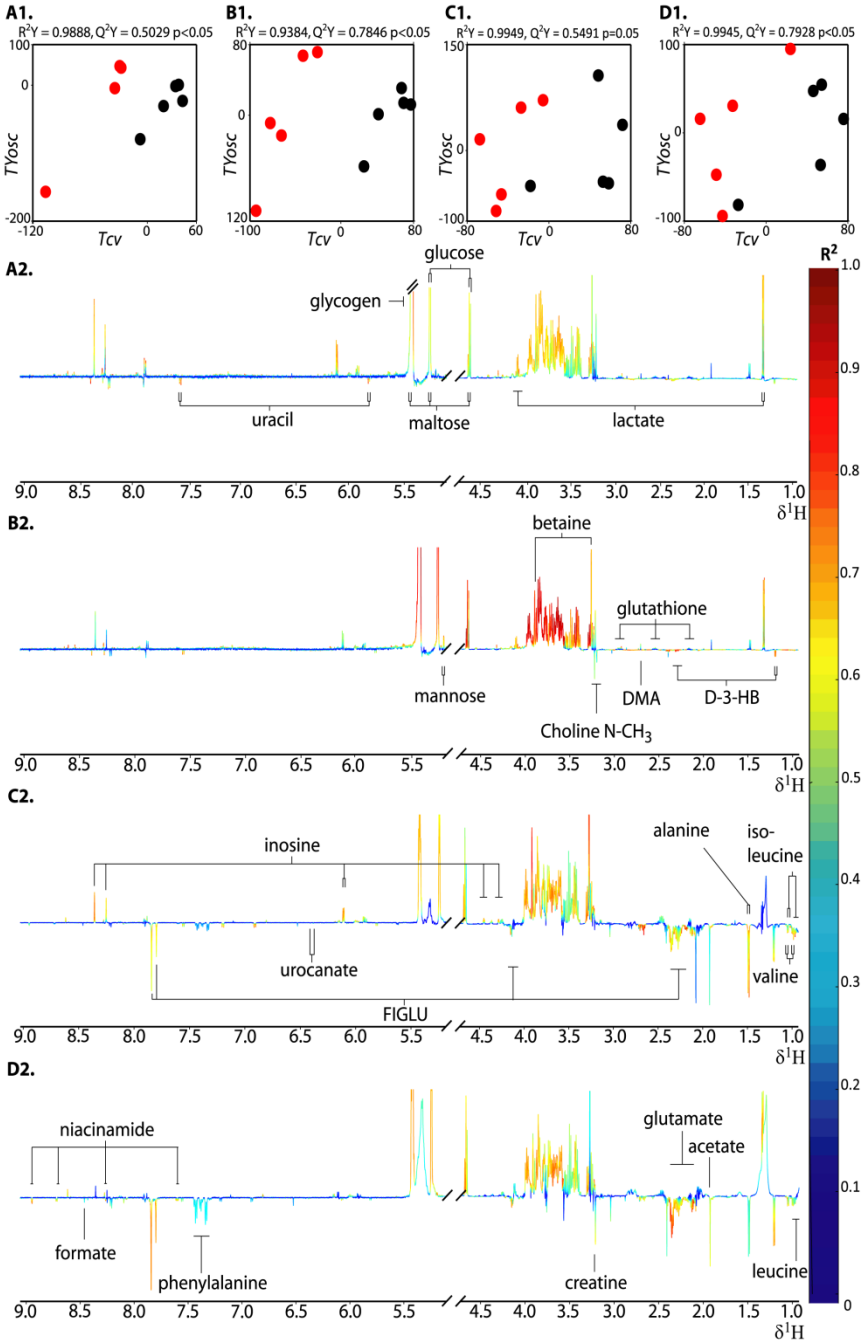


Figure 8: A simplified diagrammatic representation of the interaction of the methionine cycle (blue), folate cycle (black), choline catabolism (red) and histidine catabolism (orange) pathways, are depicted above. (1) reveals where the choline catabolism pathway interacts with the methionine cycle, (2) indicates the point at which the methionine and folate cycles interact, (3) shows the metabolic reaction inhibited by methotrexate and (4) indicates how the folate cycle can directly influence the histidine catabolism pathway. THF; tetrahydroflate; DHF – dihydrofolate; FIGLU – formiminoglutamic acid.

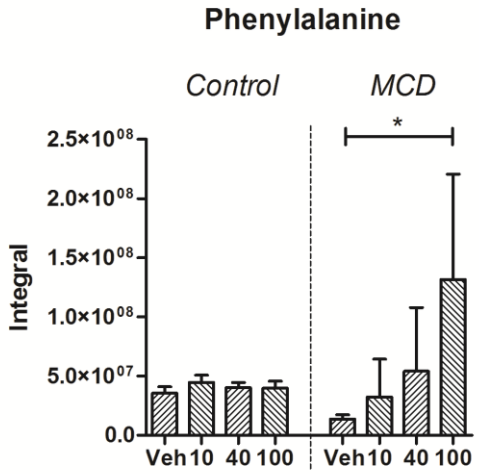
Supplementary information



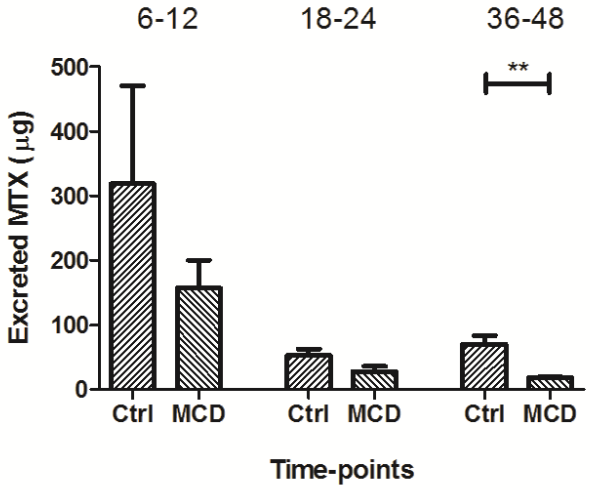
Supplementary figure 1: Average percentage body weight loss and standard deviation (as calculated from the body weights at the beginning and end of the study) of all dose groups in both diet groups is depicted above. Statistical significant at $p < 0.05$ and $p < 0.01$ are indicated by a single asterisk (*) and double asterisk (**) respectively. The vehicle and three doses of MTX are indicated at the horizontal axis (Veh, 10, 40 and 100). Veh – Vehicle



Supplementary figure 2: Aqueous liver extract O-PLS-DA discriminating the vehicle cohort and MTX administration (10 mg/kg) in the normal diet (A1 and A2) and MCD diet (C1 and C2), and between the vehicle cohort and 40 mg/kg MTX administration cohorts in the normal diet (B1 and B2) and MCD diet (D1 and D2). The scores plots (A1, B1, C1 and D1) depict the separation of the MTX dose (red) and vehicle (black) cohorts in multivariate space and the loadings coefficient plots (A2, B2, C2 and D2) illustrate the spectral comparison between control and treated. FIGLU – formiminoglutamic acid; DMA – dimethylamine; D-3-HB - D-3-Hydroxybutyrate.



Supplementary figure 3: Hepatic extract phenylalanine relative integrals of all the dosage groups in both diet groups. Please note that the integrals cannot be directly compared between the two diet cohorts due to individual pre-processing of each diet cohort which included normalisation. Statistical significance was set at $p < 0.05$ and is indicated by the asterisk.



Supplementary figure 4: Quantity of urinary MTX (μg) following the administration of 100 mg/kg MTX at 6-12 hours, 18-24 hours and 36-48 hours. Statistical significance is indicated by the asterisks, indicating $p < 0.01$.

MTX dose	Comparison (model)	R^2Y	Q^2Y	Statistical sig.
100 mg/kg	0 vs. 12 hours (control diet)	0.9011	0.5907	$p < 0.05$
	0 vs. 24 hours (control diet)	0.9404	0.7675	$p < 0.05$
	0 vs. 48 hours (control diet)	0.9344	0.8225	$p < 0.05$
100 mg/kg	0 vs. 12 hours (MCD diet)	0.9833	0.8135	$p < 0.05$
	0 vs. 24 hours (MCD diet)	0.9958	0.7317	$p < 0.05$
	0 vs. 48 hours (MCD diet)	0.9859	0.7602	$p < 0.05$

Supplementary table 1: Summary of urinary O-PLS-DA models following administration of MTX (100 mg/kg) in both diet cohorts at the defined time collection periods.